

GEOLOGY AND GEOCHEMISTRY OF THE PROTEROZOIC AGE ALDER GROUP,  
CENTRAL MAZATZAL MOUNTAINS,  
ARIZONA

by

James Robert Reed

Submitted in partial fulfillment of the requirements for  
the degree of Master of Science in Geochemistry

New Mexico Institute of Mining and Technology  
Socorro, New Mexico

May, 1988

## TABLE OF CONTENTS

Table of Contents.....	i
List of Figures.....	iv
List of Tables.....	vii
Abstract.....	ix
Acknowledgments.....	xiii
INTRODUCTION.....	1
Purpose.....	1
Location.....	3
Methods.....	4
Previous Studies.....	5
PRECAMBRIAN GEOLOGY OF THE CENTRAL MAZATZAL MOUNTAINS.....	6
Stratigraphy.....	6
Structure.....	9
Metamorphism.....	10
METASEDIMENTARY ROCKS.....	13
Introduction.....	13
Quartz Arenites and Quartz Wackes.....	13
Lithic Wackes.....	14
Matrix-rich Quartz Wackes.....	15
Geochemistry of the Metasediments.....	32
Provenance of the Metasediments.....	42

Lithofacies and Environmental Interpretation of the Metasediments.....	54
IGNEOUS ROCKS.....	61
Pyroclastic Rocks.....	61
Mafic Igneous Rocks.....	61
Intermediate and Felsic Rocks.....	64
Geochemistry of Igneous Rocks.....	65
Introduction.....	65
Igneous Rock Classification.....	66
Tectono-Magmatic Diagrams for Mafic Rocks.....	76
Mantle Source.....	92
Tectono-Magmatic Diagrams for Intermediate and Felsic Rocks.....	112
Fractional Crystallization Models.....	118
DISCUSSION.....	139
Interpretation of the Metasedimentary Rocks.....	139
Interpretation of the Mafic Igneous Rocks.....	141
Interpretation of the Intermediate and Felsic Igneous Rocks.....	142
Interpretation of the Structure and Stratigraphy.....	145
SUMMARY AND CONCLUSIONS.....	152
Evolution of the Alder Basin.....	152
Proposed Tectonic Setting.....	153
Scope for Future Studies.....	159
Appendix A: Instrumental Neutron Activation Analysis.....	160
Appendix B: X-Ray Fluorescence Spectrometry (XRF).....	162
Appendix C: Accuracy and Precision of Geochemical Data.....	163

Appendix D: Parameters and Constraints of Modal Analyses.....	171
Appendix E: Chemical Approach to Matrix Recalculation in Sandstones.....	173
Appendix F: Paleocurrent Analysis.....	179
Appendix G: Petrologic Major Element Mixing Calculations.....	183
Appendix H: Equations used in Trace Element Geochemical Modeling...	194
Appendix I: Alteration.....	196
References: .....	204



## LIST OF FIGURES

Figure 1:	Geochronologic Boundary zone in Central Arizona.....	2
Figure 2:	Stratigraphic Column for the Alder and Red Rock Groups.....	8
Figure 3:	Generalized Geologic Map of the Central Mazatzal Mountains (after Ludwig, 1974).....	11
Figure 4:	$Al_2O_3/SiO_2$ vs $Fe_2O_3T + MgO$ Tectonic Discriminant Diagram..	33
Figure 5:	Th-Co-Zr/10 Tectonic Discriminant Diagram.....	34
Figure 6:	Th-Sc-Zr/10 Tectonic Discriminant Diagram.....	36
Figure 7:	Ti/Zr vs La/Sc Tectonic Discriminant Diagram.....	37
Figure 8:	La/Sc vs Zr/Sc Companion Diagram to Figure 8.....	38
Figure 9:	$K_2O/Na_2O$ vs $SiO_2$ Tectonic Discriminant Diagram.....	39
Figure 10:	Chondrite Normalized REE Patterns for the Alder Pelites and NASC.....	40
Figure 11:	Th-Hf-Co Diagram for Shales.....	41
Figure 12:	QFL Diagram of Preserved Detrital Modes.....	43
Figure 13:	$QmFL_t$ Diagram of Preserved Detrital Modes.....	44
Figure 14:	QFL Diagram of Corrected Modes for the Quartz Arenites and the Quartz Wackes.....	46
Figure 15:	$QmFlt$ Diagram of Corrected Modes for the Quartz Arenites and the Quartz Wackes.....	47
Figure 16:	QFL Diagram of Corrected Modes for the Lithic Wackes.....	49
Figure 17:	$QmFlt$ Diagram of Corrected Modes for the Lithic Wackes....	50
Figure 18:	QFL Diagram of Corrected Modes for the Matrix-rich Quartz Wackes.....	52
Figure 19:	$QmFlt$ Diagram of Corrected Modes for the Matrix-rich Quartz Wackes.....	53
Figure 20:	$Al_3O_3$ 1Cz0- $SiO_2/100-MgO/10$ Alteration Screen.....	67

Figure 21: Symbols used in Geochemical Diagrams.....	68
Figure 22: Zr/TiO <sub>2</sub> vs Nb/Y Diagram for Volcanic Rock Classification.....	77
Figure 23: SiO <sub>2</sub> vs Nb/Y Diagram for Volcanic Rock Classification.....	78
Figure 24: Jensen Cation Diagram for Igneous Rock Classification.....	79
Figure 25: Ti/Zr vs Zr/Y Tectonic Discriminant Diagram.....	81
Figure 26: Zr vs TiO <sub>2</sub> Tectonic Discriminant Diagram.....	82
Figure 27: Th vs Hf Tectonic Discriminant Diagram.....	84
Figure 28: Ti-Y-Zr Tectonic Discriminant Diagram.....	85
Figure 29: V vs TiO <sub>2</sub> Tectonic Discriminant Diagram.....	86
Figure 30: MORB normalized Diagram which shows Typical Patterns of Basalts from Different Tectonic Settings.....	88
Figure 31: MORB normalized Diagram which shows the Patterns of the Alder Volcanics.....	89
Figure 32: MORB normalized Diagram which shows the Patterns of the Alder Intrusives.....	90
Figure 33: Zr/y vs Zr Tectonic Discriminant Diagram.....	91
Figure 34: Y vs Hf Diagram for the Geochemical Modeling of Mafic Rocks.....	93
Figure 35: Nb vs Yb Diagram for the Geochemical Modeling of Mafic Rocks.....	94
Figure 36: Zr/Y vs Zr Diagram which shows the Geochemical Model for the Mafic Igneous Rocks.....	101
Figure 37: Zr vs Ni Diagram which shows the Geochemical Model for the Mafic Igneous Rocks.....	102
Figure 38: Zr vs TiO <sub>2</sub> Diagram which shows the Geochemical Model for the Mafic Igneous Rocks.....	103
Figure 39: Th vs Hf Diagram which shows the Geochemical Model for the Mafic Igneous Rocks.....	104
Figure 40: TiO <sub>2</sub> vs Zr Tectonic Discriminant Diagram for Felsic Rocks.....	115
Figure 41: MORB normalized Diagram for the Alder Felsic Samples.....	116
Figure 42: MORB normalized Patterns of Typical Felsic Rocks from Different Tectonic Settings.....	117

Figure 43: Generalized Geologic Map of the Central Mazatzal Mountains which shows the Interpretation of this study.....	146
Figure 44: Stratigraphic Columns for the Alder and Red Rock Groups.....	147
Figure 45: Schematic Diagrams which show the Tectonic Settings in Alder and Red Rock Times.....	157
Figure F-1: Wulff Net Showing the Procedure used in Recalculating aleocurrent Directions in Sandstones.....	181

## LIST OF TABLES

Table 1:	Chemical Compositions of Sedimentary Samples.....	17
Table 2:	Modal Compositions of Sedimentary Samples.....	29
Table 3:	Chemical Compositions of Mafic Igneous Rocks.....	69
Table 4:	Chemical Compositions of Enriched, Undepleted, and Depleted Mantles and the Minerologic Composition of the Mantle Source used in Figures 34 and 35.....	95
Table 5a:	Chemical Compositions of the Calculated Primary Mantle Melt, Calculated Mantle Source, and Undepleted Mantle.....	98
Table 5b:	FXL Assemblage Used to Model the Evolution of Mafic Samples.....	99
Table 6:	Chemical Compositions of Intermediate Igneous Rocks.....	106
Table 7:	Chemical Compositions of Felsic Igneous Rocks.....	109
Table 8:	Results of Various Tectono-Magmatic Diagrams for the Alder Andesite Samples.....	113
Table 9:	Results of Various Tectono-Magmatic Diagrams for the Alder Felsic Samples.....	114
Table 10a:	Parameters and Results of a Geochemical Model which Relates TC-16 to TC-18.....	120
Table 10b:	FXL Assemblage which is used to Relate TC-16 to TC-18.....	121
Table 11a:	Parameters and Results of a Geochemical Model which Relates MTO-14 to MTO-16.....	124
Table 11b:	FXL Assemblage which is Used to Relate MTO-14 to MTO-16.....	125
Table 12a:	Parameters and Results of a Geochemical Model which Relates MW-D to a Calculated Parent Liquid.....	127
Table 12b:	FXL Assemblage which is Used to Relate MW-D to a Calculated Parent Liquid.....	128
Table 13a:	Parameters and Results of a Geochemical Model which Relates WF-1 to a Calculated Parent Liquid.....	129

Table 13b:	FXL Assemblage Used to Relate WF-1 to a Calculated Parent Liquid.....	130
Table 14a:	Parameters and Results of a Petrogenetic Model for the Red Rock Rhyolite which involves the Partial Melting of Lower Crust.....	133
Table 14b:	Assumed Modal and Melting Proportions of Lower Crust.....	134
Table 15a:	Parameters and Results of a Petrogenetic Model for the Red Rock Rhyolite which Involves Fractional Crystallization.....	137
Table 15b:	FXL Assemblage which is used to Model the Red Rock Rhyolite.....	138
Table C-1.	Period of Time which NAA was Acquired for each sample....	164
Table C-2.	Precision of the Analyses of MTO-16.....	166
Table C-3.	Standards Used in Computing Accuracy and Precision.....	167
Table C-4.	Accuracy and Precision of Chemical Data.....	169
Table E-1.	Modal and Chemical Compositions of TC-13.....	175
Table E-2.	Chemical Compositions of Rock and Mineral Fragments Used in Geochemical Matrix Recalculation.....	176
Table E-3.	Determination of Contributions of Al <sub>2</sub> O <sub>3</sub> from the Preserved Detrital Grains.....	177
Table F-1.	Strikes and Dips of Unrestored Cross-Bedding and Bedding, and Dispersal Direction Indicated by Restored Cross-Bedding.....	182
Table G-1.	Compositions of Mafic Mineral Phases Used in Major Element Mixing Calculations.....	192
Table G-2.	Compositions of Felsic Mineral Phases Used in Major Element Mixing Calculations.....	193
Table I-1.	Possible Effects of Hydrothermal Alteration on the Andesitic Samples MTO-B and WF-5.....	200
Table I-2.	Alteration Trends of the Pine Mountain Porphyry.....	202

## ABSTRACT

The Alder Group in the central Mazatzal Mountains of Arizona represents a eugeosynclinal supracrustal succession which is part of the 1680-1700 Ma supracrustal terrane (Condie, 1987). The succession has undergone greenschist facies metamorphism, and primary structures have been preserved; therefore, a clear distinction can be made between meta-igneous and metasedimentary rocks. The Alder Group is composed dominantly of metamorphosed pyroclastic rocks and volcanoclastic sediments (40-60%). Metavolcanic flows ranging from basalt to dacite and metasedimentary rocks ranging from graywackes to quartz arenites each comprise 20-30% of the section. The Alder Group is overlain by a thick (~1000m) felsic volcanic unit which is included in the Red Rock Group of central Arizona (Conway and Silver, 1986). Mafic to andesitic dikes and sills which mainly intrude the youngest Alder rocks and the Red Rock Group comprises ~5% of the total succession. A felsic quartz, feldspar porphyry (the Pine Mountain Porphyry) intrudes subconcordantly at various intervals of the Alder Group and comprises approximately 10% of the sequence.

The Proterozoic rocks in the Mazatzal Mountains strike NE-SW and have been deformed by NW-SE directed compression (Karlstrom and Conway, 1986) associated with a Precambrian orogenic event named the Mazatzal Orogeny (Wilson, 1939). The Alder Group in the central Mazatzal Mountains was considered to be exposed on the limbs of a syncline which is cored by the Red Rock Group (Ludwig, 1974). Because of the disparity of the respective rock associations northwest and southeast of the Red Rock Group, it is proposed that a fault is

(x)

present near the northwestern contact of the Red Rock and Alder Groups, and it is assumed that the northwestern area is older than the southeastern one.

There appears to be a bimodal distribution of igneous rocks in the Proterozoic succession of the Mazatzal Mountains. The Alder igneous rocks are dominantly basalts and basaltic andesites; however, the Pine Mountain Porphyry is a rhyodacite. The Red Rock Group is rhyolitic. All of the Alder igneous rocks are subalkaline in nature. Mafic and andesitic intrusives show tholeiitic affinities while the Alder volcanics, the Red Rock Group, and the Pine Mountain Porphyry are calc-alkaline. Mafic and andesitic intrusives are enriched in incompatible elements relative to the mafic and andesitic volcanics. The Alder igneous rocks are geochemically similar to rocks from continental island arcs, active continental margins, or incipient back arc rifts along active margins.

The mafic igneous rocks can be related, by variable degrees of batch melting, to a garnet lherzolite source which is similar to primordial mantle with respect to the high field strength and heavy rare earth elements. Both chemical and mineralogic source variations are called for in explaining the chemical variations in the igneous rocks. In general, the mafic intrusives appear to have been derived from a source which was chemically enriched and which had a smaller proportion of garnet. Rocks of intermediate composition can be explained by open or closed system fractional crystallization of mafic rocks. The Pine Mountain Porphyry is geochemically modeled by closed system fractional crystallization of a mafic parent. 10% batch

melting of arc derived crust is called for in the generation of the Red Rock Group.

The sandstone types of the Alder Group range from quartz arenites to lithic wackes. Three populations of sandstones are defined petrographically and chemically. A complete gradation between quartz wackes and quartz arenites is observed in the sedimentary sequences southeast of the Red Rock Group exposure; therefore, these rock types are considered to be one sediment population. Lithic wackes are found both northwest and southeast of the Red Rock Group. This population represents volcanoclastic sediments. Quartz wackes which are composed of  $\leq 70\%$  matrix are identified as matrix rich quartz wackes, and this population of sediments is only found northwest of the Red Rock Group.

The quartz arenite and quartz wacke sediments appear to be derived from a recycled orogen and are chemically similar to passive margin sediments. Lithic wackes and matrix rich quartz wackes are interpreted to be primary and reworked arc sediments, respectively. The chemical data from the sediments suggest that a variable amount of mixing occurred between the passive margin and arc sediment types.

Basin analysis suggests that the rocks northwest of the Red Rock Group were deposited in an abyssal plain environment. The succession and distribution of lithofacies in the area southeast of the Red Rock Group seem to represent the development and southwestward progradation of a tidal shelf. The association of sediment types seems to indicate that the basin was areally restricted and was affected by tectonic uplift at its margin.

The association of mature recycled orogen sediments and arc-derived material in the Alder depositional sequence suggests that the



Alder basin represents a remnant ocean basin which formed as an arc collided with a cratonic margin. The enriched nature and the tholeiitic tendencies of the mafic and andesitic intrusives are believed to have resulted from processes related to the collision event. More specifically, it is proposed that the collision slowed subduction beneath the island arc, and this resulted in lower oxygen fugacities in arc magmas and consequently, a change from calc-alkaline to tholeiitic differentiation. It is proposed that the collision of the arc and the continent to the northeast of the Alder basin of deposition resulted in the partial melting of arc derived crust. It is invoked that these partial melts contaminated the arc magmas and enriched the magmas in incompatible elements. The Red Rock Group represents the eruption of this partial melt.

ACKNOWLEDGMENTS

Most of the thanks for this study have to go to my parents. The quality of this work would have been greatly compromised without the unquestioned financial and moral support that my parents provided over the last three years. The funding provided by the apportionment of NSF grant EAR-8313735 to K.C. Condie has been used for field work, chemical analyses, and thin section preparation. Sandia National Laboratory is thanked for the use of the core reactor in neutron activation analysis.

I thank Dr. Condie for the direction and assistance which he provided over the course of this study. I also thank Dr. Budding for help with thin section analyses and for his insight into the understanding of metamorphic and structural information. Dr. Robertson is thanked for his concise, constructive criticism which greatly improved the quality and organization of this work.

The entire group of graduate students working with Dr. Condie have been very helpful in the discussion and formulation of ideas. In particular, I thank Mike Knoper for sharing his insight into problems relating to geology and geochemistry. I also thank Pat Bowling for helping me learn how to use the different computer programs related to "data crunching". I thank Connie Thompson for the typing of this thesis and for working through the deadlines with me. Finally, I thank my grandparents, my sister, and Kelly Fry for their emotional and moral support throughout the duration of this study.

## INTRODUCTION

Central Arizona represents the overlap of two crustal age provinces (Figure 1). The northernmost province is 1760-1800 Ma while the southern province is 1680-1700 Ma. The older terrane contains graywackes, pillow volcanics, and calc-alkaline volcanics (Condie, 1986). This succession is called the Yavapai Group (Conway and Silver, 1987). The younger terrane is represented by a eugeosynclinal succession, a silicic volcanic succession, and a miogeosynclinal succession. These successions are subdivided into the Alder, Red Rock, and Mazatzal Groups, respectively (Conway, and Silver, 1987).

The Alder Group is composed of metapyroclastics (40-60%), metavolcanics (20-30%), and metasediments (20-30%); the Red Rock Group is characterized by felsic flows and felsic pyroclastics; and the Mazatzal Quartzite comprises mature quartzose sediments.

The aforementioned rock successions from both age provinces have been deformed by a Precambrian orogenic event which is named the Mazatzal orogeny (Wilson, 1939). Folding, thrusting, and reverse faulting, which formed as a result of northwest to southeast compression characterize the event (Puls and Karlstrom, 1986). The effects of the Mazatzal orogeny extend across the state of Arizona into California (Silver, 1977).

## Purpose

The aim of this study is to chemically analyze a representative suite of rocks from two Early Proterozoic successions called the Alder

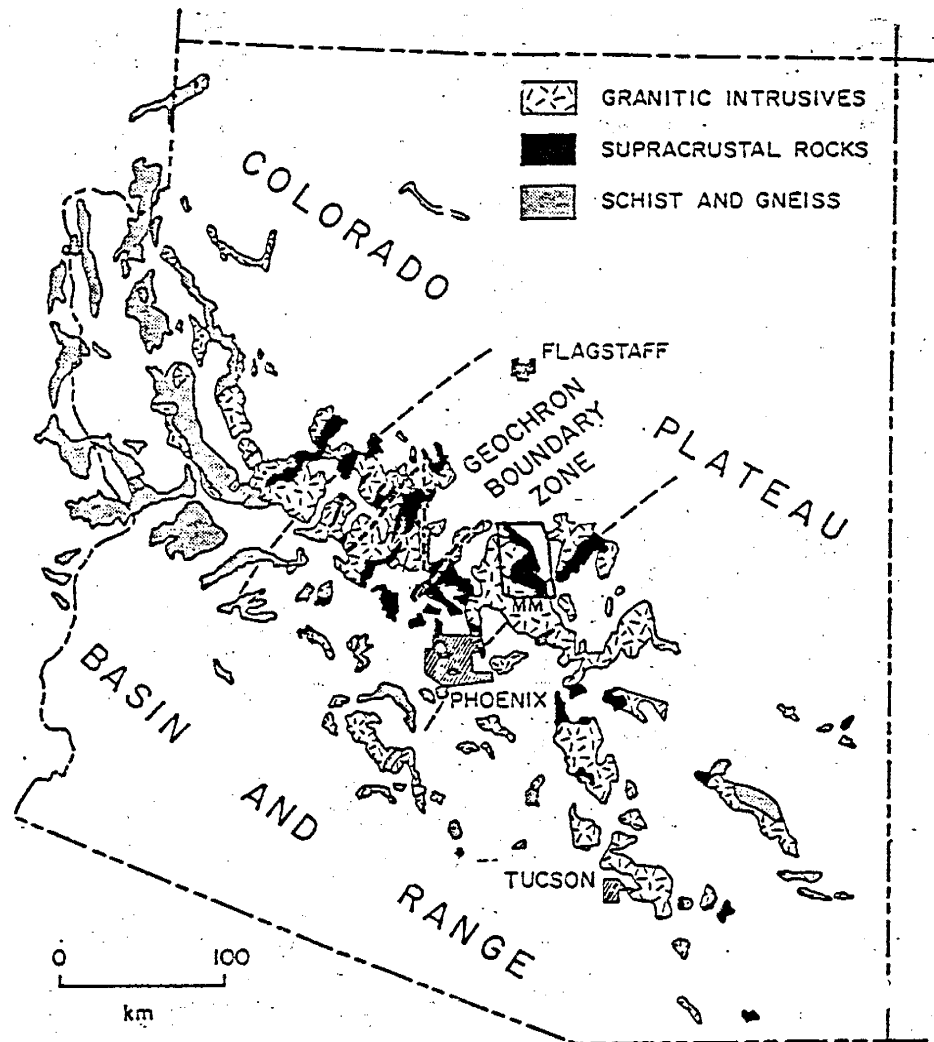


Figure 1. Map of Arizona which shows the distribution of major Precambrian outcrops and a geochronologic boundary zone which represents the overlap of two crustal provinces (see text for explanation). The area of study is outlined by a rectangle which is marked as MM. (after Karlstrom and Conway, 1986).

Group and the Red Rock Group (Conway and Silver, 1987) that are exposed in the central Mazatzal Mountains (Figure 1). The meta-igneous rocks are geochemically modeled to determine the nature of either the mantle source or the parent liquids. These rocks are also geochemically compared to modern rocks in order to identify the tectonic setting in which they formed. Metasedimentary rocks are analyzed by both petrographic and chemical means in order to determine provenance and tectonic setting.

#### Location

In this study, the Alder and Red Rock Groups are examined in the central Mazatzal Mountains of central Arizona. The only younger stratified rocks in the study area are of Tertiary or younger age (Ludwig, 1974).

The Mazatzal Mountains are located near the southwestern margin of the Colorado Plateau. The range trends N 30° W from the Salt River on the south to the East Verde River on the north. It lies between the valley of Tonto Creek on the east and the Verde River on the west, and is roughly 50 miles long and 12-18 miles wide.

The field area is located about 30 miles south of Payson and 50 miles north of Phoenix. This area lies in Maricopa and Gila Counties. The entire field area spans from longitude 111° 37'30"W to 111°22'30"W, and from latitude 33°55'N to 34°00'N; however, most of the work for this thesis involves the area within longitude 111°30'W and 111°22'30"W. Figure 1 shows the location of the Mazatzal Mountains and the field area.

## Methods

In the central Mazatzal Mountains, the Alder Group consists of a succession of metasedimentary and metavolcanic rocks. These rocks have undergone only low degrees of metamorphism (greenschists facies) and primary structures are well preserved. As a result, metasedimentary and meta-igneous rocks are referred to as sedimentary and igneous rocks, respectively, in future discussion. Primary structures and field relationships are described and are used to assess the environments of deposition.

Triplicate samples which are representative of the different rock types have been collected and have been used for hand specimens, thin sections, and chemical analyses. Petrographically determined mineral assemblages are used to confirm the greenschist grade of metamorphism identified by Ludwig (1974). Petrographic analyses also entail modal point counts of sedimentary rocks (Appendix D). These counts are chemically corrected for matrix recrystallization (Appendix E) and the corrected and uncorrected modes are used to interpret the provenance of the sediments. Sediment classification is adapted from Pettijohn, Potter, and Siever (1972).

Chemical analyses are made by x-ray fluorescence (XRF) and neutron activation (NAA). The NAA and the XRF procedures are described in Appendices A and B, respectively. The chemical data are used to classify the igneous rocks and to model potential source rocks or liquids. Tectonic interpretations of the igneous rocks and the sedimentary rocks are drawn from geochemical discriminant diagrams which are based on rocks from modern tectonic settings.

### Previous Studies

Because of all of the research that has been conducted on the Precambrian of Arizona, different stratigraphic nomenclature has been proposed by different investigators. Conway and Silver (1987) have correlated early Proterozoic rocks in central to southeast Arizona; thus they have greatly reduced the stratigraphic discrepancies. Their nomenclature is used in this study. They have identified an Alder Group which has been further subdivided into various formations. The Red Rock Group and the Mazatzal Group stratigraphically overlie the Alder Group.

The Alder Group was first identified by Wilson (1939). He names the succession the Alder Series, described its general lithologies, and estimated the thickness of the succession to be more than 5000 ft. He included the Alder Series with the older Yeager Greenstone and the Red Rock Rhyolite in the Yavapai Group. Conway and Silver (1987) have changed the name of the Yeager Greenstone to the Yavapai Group.

The Red Rock Rhyolite has been included in the Red Rock Group along with other felsic successions of similar age in central Arizona. There is a controversy over the age relationships of the Alder Group and the Red Rock Rhyolite. Wilson (1939) believed that the Alder Group was younger than the Red Rock Rhyolite because of rhyolite clasts in the Alder conglomerates. He proposed that there was a fault contact between the units and that displacement along the fault has moved the younger Alder beneath the older Red Rock Rhyolite. Ludwig (1974) ascertained that the Red Rock Rhyolite is indeed younger than the Alder Group as he identified a conformable contact between the

units instead of a fault contact. This latter opinion is the general consensus today, and it is supported by geochronology. Karlstrom, Bowring, and Conway (1986) have referred to an U-Pb zircon date of  $1710 \pm 20$  Ma for a formation in the upper Alder Group while the Red Rock has been dated as  $1695 \pm 15$  Ma (Conway, 1973).

In addition to determining the age relationships between the Alder Group and the Red Rock Rhyolite in the central Mazatzal Mountains, Ludwig (1974) divided the Alder Group into several stratigraphic units which have been extensively described and mapped. Units have also been sampled for petrographic work and some igneous rocks have been sampled for major element chemical analysis.

## PRECAMBRIAN GEOLOGY OF THE CENTRAL MAZATZAL MOUNTAINS

### Stratigraphy

Pyroclastic rocks and volcanoclastic sediments are the most abundant rock types in the Alder Group of the central Mazatzal Mountains (40-60%). Metavolcanic flows ranging from basalt to dacite and metasedimentary rocks ranging from graywackes to quartz arenites each compose 20-30% of the section. The overlying felsic volcanic flows and pyroclastics of the Red Rock Rhyolite make up  $\sim 15\%$  of the succession. Mafic to andesitic dikes and sills which mainly intrude the youngest Alder rocks and the Red Rock Group compose  $\sim 5\%$  of the total Proterozoic sequence in the central Mazatzal Mountains. A felsic quartz, feldspar porphyry (the Pine Mountain Porphyry) intrudes

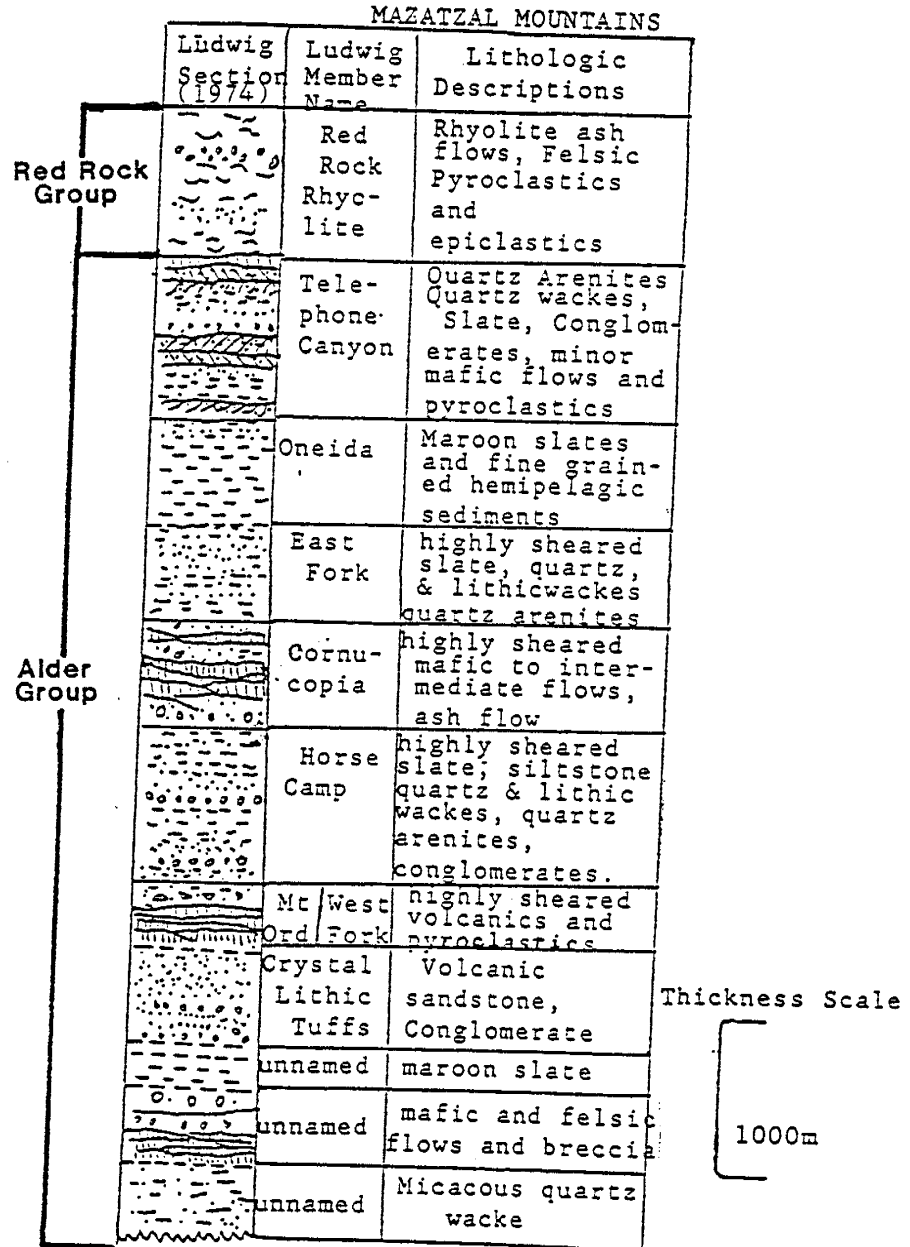


subconcordantly at various intervals of the Alder Group and composes ~10% of the sequence.

The stratigraphy of the Alder and Red Rock Groups as defined by Ludwig (1974) and Conway (personal communication) is shown in Figure 2. The sequence is characterized by alternating volcanic and sedimentary units. The lower three unnamed members in the stratigraphic column have been mapped and identified by Conway, C.M. (personal communication) in the Lion Mountain Quadrangle. The other members are those which have been identified by Ludwig (1974) in the Reno Pass Quadrangle.

Two member names (Mt. Ord and West Fork) are given to the same stratigraphic level in Ludwig's section because of dramatic differences in the rock types on opposite limbs of the syncline. The Mt. Ord member which Ludwig (1974) identified on the southeastern limb of the syncline comprises mafic to andesitic flows, ash flow tuffs, volcanic breccias, and tuffaceous sediments. The equivalent West Fork member on the northwestern limb comprises maroon slates and phyllites. There are also other units in Ludwig's stratigraphy which are dissimilar on opposite sides of the synclinal axis. The southeastern exposure of the Horse Camp member is composed of slates, quartz wackes, lithic wackes, quartz arenites, and conglomerate while the northwestern exposure comprises graded and ungraded volcanoclastic lithic wackes, ash flow tuffs, and tuffaceous sediments. Similarly, the rock types of the southeastern Telephone Canyon and Oneida members are not recognized on the northwestern limb of the syncline. The southeastern exposure of the Telephone Canyon member is composed of quartz arenites, quartz wackes, and minor volcanics, and the

Figure 2. Stratigraphic column, which is proposed by Ludwig (1974), for the Proterozoic Rocks in the central Mazatzal Mountains. The lower three unnamed units have been mapped and identified by Conway (personal communication) in the Lion Mountain Quadrangle.



southeastern exposure of the Oneida member comprises maroon slates and fine grained sediments. Ludwig ambiguously divides a sequence of highly sheared volcanic breccias and tuffs with minor interbeds of quartz arenites and quartz wackes in an attempt to correlate the exposures of the Telephone Canyon and Oneida members on the southeastern limb across the synclinal axis. Ludwig (1974) attributed all of these lithologic variations across the axis of the syncline to dramatic facies changes within the basin of deposition.

Ludwig interpreted the environment of accumulation of the Alder Group as a eugeosynclinal basin for the following reasons: 1) its relatively great thickness (~6000m); 2) the abundance of extrusive volcanics; 3) the presence of thick sections of volcanoclastic sediments; and 4) the overall trend towards more mature, shallow-water lithofacies at the top of the Alder section. Ludwig claimed that the basin evolved from deep water to shallow water deposition with time. He also proposed that the eruption of the Red Rock Rhyolite marked the end of the Alder depositional basin. The overlying Mazatzal group was interpreted to show a continued period of continental deposition in the late Proterozoic.

#### Structure

The rocks of the Alder and Red Rock Groups strike NE-SW. Ludwig (1974) concluded that the Alder Group is exposed on the limbs of a syncline in which the axis trends northeast to southwest. The axis was proposed to run through the Red Rock Rhyolite which has been folded along with the units of the Alder Group. Ludwig reached his

conclusion from strikes and dips taken on each side of the axis and from structures in the supracrustal units which indicate younging directions towards the proposed axis. The geologic interpretation of the Alder Group in the Reno Pass Quadrangle of the central Mazatzal Mountains, as proposed by Ludwig (1974) and Karlstrom and Conway (1986), is shown in Figure 3. A shear zone named the Slate Creek shear zone has been identified on the southeastern limb of the syncline (Karlstrom and Conway, 1986). Because of the similarities of rock successions in the shear zone with those described along strike by Gastil (1958) in the relatively undeformed Tonto Basin area, it is assumed that the shear zone has not greatly disrupted the stratigraphy of the Alder Group in the Mazatzal Mountains.

Conway, C.M. (personal communication) has mapped the Alder Group in the Lion Mountain Quadrangle to the west of the area which has been mapped by Ludwig (Reno Pass Quadrangle; Figure 3). Conway has assumed that the syncline mapped by Ludwig extends to the northwest into the Lion Mountain Quadrangle. This assumption implies that similar rock types have been deposited at different intervals of the Alder deposition. More specifically, at least two successive sequences of volcanic sandstones, pelites, and volcanic flows and pyroclastics have been deposited in the Alder basin if the structure and stratigraphy (next section) of Ludwig and Conway are assumed to be correct.

#### Metamorphism

The level of metamorphism in the Alder sequence is appraised petrographically by mineral associations. The lithologies which have

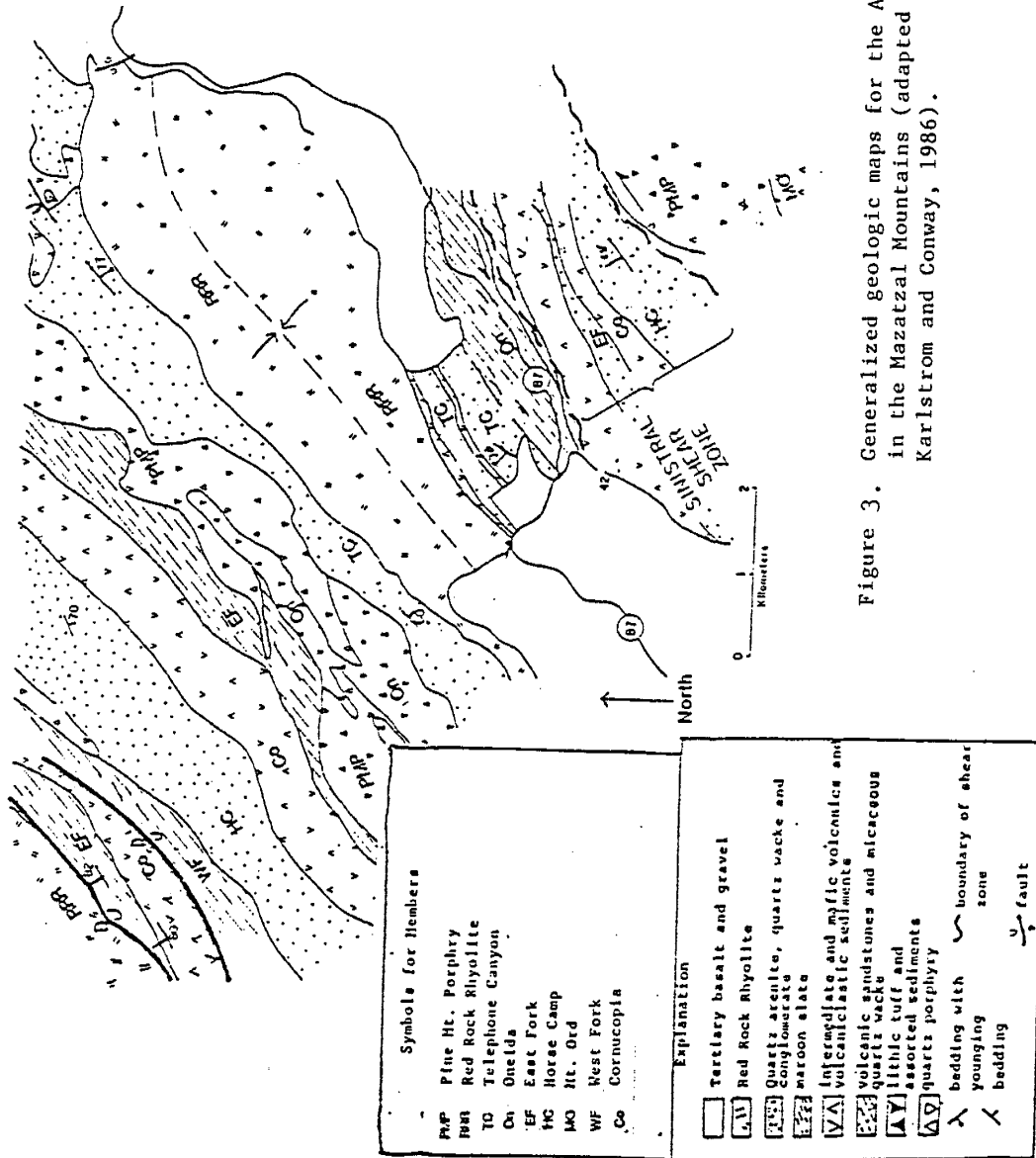


Figure 3. Generalized geologic maps for the Alder and Red Rock Groups in the Mazatzal Mountains (adapted from Ludwig, 1974; and Karlstrom and Conway, 1986).

been examined in thin section are mafic to andesitic intrusives and extrusives, felsic volcanics, quartz arenites, quartz wackes, and volcanoclastic lithic wackes. The different lithologies show mineral assemblages that are characteristic of the greenschist facies of the Barrovian type of metamorphism.

The minerals, which are listed in order of decreasing abundance, are as follows: mafic to andesitic intrusives and extrusives have chlorite + quartz + epidote ± albite ± calcite ± hornblende ± sericite ± apatite; volcanoclastic sediments have chlorite + quartz ± calcite ± albite ± sericite; quartz arenites and quartz wackes have quartz + sericite + albite ± chlorite ± epidote ± biotite; and felsic volcanics have quartz + sericite + albite ± epidote. One thin section of a metadiabase shows relict phenocrysts of diopside which are partly or totally replaced by actinolite.

One thin section of a volcanoclastic sediment (WF-12; Tables 1 and 2) which shows well defined twinning in plagioclase grains has been used to determine plagioclase composition by the Michel-Levy method. The extinction angles of ten feldspar grains which have the (010) plane nearly perpendicular to the thin section have been averaged. The maximum extinction angle was  $-15^\circ$ . This corresponds to a plagioclase composition of  $Ab_{94}$  which is consistent with the greenschist facies of metamorphism.

## METASEDIMENTARY ROCKS

## Introduction

Three general groups of sandstones can be defined in the Alder succession. These groupings are based on petrographic, field, and geochemical evidence. The groups are referred to as the following: 1) quartz arenites and quartz wackes; 2) matrix rich (>70%) quartz wackes; and 3) lithic wackes.

Representative samples from each group have been analyzed petrographically and chemically. Tables 1 and 2 lists the chemical and modal characteristics, respectively, of these samples. The geologic map (Plate I) shows the location of each sample which has been analyzed. The primary structures associated with these sediments are discussed in the section on the sedimentary lithofacies of the Alder Group.

## Quartz Arenites and Quartz Wackes

The sediments of the quartz arenite and quartz wacke population (QAW) are typically fine to medium grained ( $\leq 1\text{mm}$ ). These lithologies vary from poorly to well sorted. Grain shape ranges from angular to rounded using the roundness scale of Powers (1953), and most of the grains are subangular. The fabric and relict texture of these rocks show a weak to strong foliation.

The QAW sediments range in matrix abundance from <5% to >50%. Typically, they have <30% matrix. The matrix of these sediments is

composed of subequal amounts of quartz and sericite. Minor amounts of chlorite, feldspar, and opaques are also present within the matrix. Sericite makes up 5-20% of these rocks. Quartz grains make up 65-90% of the detrital component in the sediments. Both monocrystalline and polycrystalline quartz grains are present; however, monocrystalline quartz is typically twice as abundant as polycrystalline quartz. Irregular-shaped plagioclase grains and rock fragments which are variably altered to sericite and chlorite, respectively, each compose <5% of the QAW sediments. The rock fragments often have oval shapes due to metamorphic deformation. Pelitic, volcanic, and silty-sandy rock fragments are found in these lithologies. Opaques are present in trace amounts.

The QAW population is found only on the southeastern limb of the syncline in the Horse Camp and Telephone Canyon members. The arenites and wackes are grouped together because they are interbedded in the respective units, and a complete gradation is present between the end members. Petrographic and geochemical studies suggest the entire range of sediments is genetically related. The quartz arenites are more common in the Telephone Canyon member relative to the Horse Camp member; however, in both members, quartz wackes are the most common rock type.

#### Lithic Wackes

These rocks contain coarse quartz grains ( $\leq 2\text{mm}$ ); however, most of the sediments are fine grained. The lithic wackes are poorly sorted,



and they are typically well foliated. The grains range from angular to subrounded, and most grains are subangular.

These rocks typically have at least 30% matrix, which is composed predominantly of chlorite + calcite ± sericite. Plagioclase grains which are sericitized and saussuritized compose up to 15% of the rocks. Volcanic rock fragments make up as much as 20% of the sediments. Rock fragments are chloritized and sericitized to varying degrees. Sericite and chlorite make up 5 to 20% and 10 to 60% of the rocks, respectively. Calcite variably replaces matrix, feldspar, and rock fragments, and it composes as much as 20% of the sediments. Opaques make up less than 10% of the rocks. The lithic wackes are volcanoclastics. They often show crude bedding, and they occasionally grade into ash flow units. This sediment type can be observed in the Mt. Ord, Cornucopia, and Telephone Canyon members on the southeastern limb of the syncline and in the Oneida, East Fork, and Horse Camp members of the northwestern limb.

#### Matrix-rich Quartz Wackes

The most notable feature of the matrix-rich quartz wackes is the paucity of large detrital grains. The rocks which are observed in thin section have silt-sized to fine grain size; however, coarse ( $\leq 5\text{mm}$ ) grained graded quartz wackes are occasionally interbedded with these sediments in the field. The thickness of these coarse interbeds ranges from 5 to 10 cm. The grains range from round to angular and most grains are subrounded. The rocks show moderate foliation.

The matrix-rich quartz-wackes have more than 70% matrix. The matrix is composed predominantly of chlorite with minor amounts of sericite and quartz. These rocks contain 15 to 30% quartz; however; Quartz comprises 90-95% of the large detrital grains. Monocrystalline quartz is at least three times more abundant than polycrystalline quartz grains. Sericite composes up to 30% of these sediments while opaques are present in abundances of 5 to 10%.

The matrix-rich quartz wackes occur in two volcanoclastic-sedimentary units which lie to the northwest of the Red Rock Rhyolite. In these units, the matrix-rich quartz wackes overlie poorly bedded chloritized volcanic sandstones and breccias. This latter rock type has been identified as a crystal lithic tuff by Ludwig (1974); however, bedding has been observed in these rocks in the Lion Mountain Quadrangle (Conway, C.M.; personal communication); therefore, Conway's interpretation of this rock type as a volcanic sandstone is assumed to be correct. The detrital composition of the matrix-rich quartz wackes are significantly different from the quartz wackes which are sampled southeast of the RRR. The rocks correspond to the Ta-b layers in the Bouma sequence.

Table 1. Chemical compositions of sedimentary lithologies. Major elements are in %, and trace elements are in ppm.

sample	MTO - 18	TC - 17	TC - 5	TC - 13	MTO - 19
sediment type	quartz wacke	quartz wacke	quartz wacke	quartz wacke	quartz wacke
SiO <sub>2</sub>	91.38	85.90	92.42	84.26	88.18
TiO <sub>2</sub>	0.16	0.21	0.08	0.23	0.35
Al <sub>2</sub> O <sub>3</sub>	3.50	7.32	4.26	8.41	6.82
Fe <sub>2</sub> O <sub>3t</sub>	3.91	2.57	1.98	2.49	2.49
MgO	0.08	0.12	0.05	0.24	--
CaO	0.03	0.20	0.05	0.14	--
Na <sub>2</sub> O	0.15	0.84	0.11	2.21	--
K <sub>2</sub> O	0.70	1.57	1.01	1.74	1.33
MnO	--	0.01	0.01	0.01	--
P <sub>2</sub> O <sub>5</sub>	0.04	0.06	0.03	0.01	0.03
LOI	0.63	1.41	0.51	0.72	1.01
TOTAL	100.58	100.21	100.51	100.46	100.21

Table 1 Continued.

sample sediment type	MTO - 18		TC - 17		TC - 5		TC - 13		MTO - 19	
	quartz wacke		quartz wacke		quartz wacke		quartz wacke		quartz wacke	
Rb	24.6		61.5		38.1		41.8		43.4	
Ba	146.		426.		267.		424.		289.	
Cs	1.6		3.6		1.0		1.5		2.6	
Sr	66.		43.		38.		57.		124.	
Pb	10.1		12.4		8.3		5.1		17.0	
Th	3.8		5.2		2.4		3.7		4.2	
U	2.11		1.40		0.73		1.53		1.40	
Sc	3.0		4.9		2.8		2.8		4.0	
V	87.		34.		25.		46.		64.	
Cr	16.1		27.8		13.7		15.8		1.5	
Co	1.		8.		1.		2.		2.	
Ni	9.		16.		7.		9.		--	

Table 1 Continued.

sample	MTO - 18		TC - 17		TC - 5		TC - 13		MTO - 19	
	quartz wacke		quartz wacke		quartz wacke		quartz wacke		quartz wacke	
Y	24.7		15.5		8.9		13.3		21.9	
Zr	87.3		96.8		43.3		94.6		125.6	
Nb	6.2		3.6		2.2		7.6		4.7	
Hf	2.6		2.9		1.1		2.1		3.7	
Ta	0.3		0.38		0.20		0.28		0.50	
La	19.3		18.5		11.3		17.7		17.8	
Ce	39.2		42.0		25.7		31.4		33.6	
Sm	3.9		3.1		2.2		2.9		3.5	
Eu	0.66		0.80		0.41		0.62		0.81	
Tb	0.66		0.54		0.40		0.51		0.56	
Yb	2.72		1.31		0.70		1.06		1.87	
Lu	0.40		0.18		0.82		0.16		0.34	

Table 1 Continued.

sample	WF - 12	TC - 9	WF - 2	WFT - 2	WF - 11
sediment type	lithic wacke	lithic wacke	lithic wacke	lithic wacke	lithic wacke
SiO <sub>2</sub>	64.59	62.92	53.08	70.99	55.20
TiO <sub>2</sub>	0.7	0.98	1.29	0.96	1.37
Al <sub>2</sub> O <sub>3</sub>	16.16	14.20	14.60	12.39	18.73
Fe <sub>2</sub> O <sub>3T</sub>	7.13	8.13	11.97	10.31	10.80
MgO	2.03	1.34	4.97	0.04	1.73
CaO	0.57	2.39	2.31	0.04	1.52
Na <sub>2</sub> O	3.89	2.55	6.00	--	4.70
K <sub>2</sub> O	1.86	3.47	0.11	3.27	2.08
MnO	0.07	0.05	0.21	0.02	0.08
P <sub>2</sub> O <sub>5</sub>	0.18	0.24	0.18	0.04	0.34
LOI	2.73	4.23	5.73	1.70	3.58
TOTAL	99.91	100.50	100.45	99.76	100.13

Table 1 Continued.

sample	WF - 12		TC - 9		WF - 2		WFT - 2		WF - 11	
	lithic wacke		lithic wacke		lithic wacke		lithic wacke		lithic wacke	
Rb	62.8		90.9		4.7		102.0		67.2	
Ba	498.		691.		79.		727.		528.	
Cs	2.9		5.3		0.8		3.4		4.2	
Sr	238.		188.		166.		64.		213.	
Pb	19.5		10.6		15.9		22.6		7.2	
Th	5.8		5.2		2.7		5.0		8.8	
U	2.74		1.62		0.69		4.19		2.08	
Sc	14.5		15.1		33.1		9.8		19.1	
V	106.		113.		236.		97.		90.	
Cr	212.0		37.9		294.8		88.0		42.8	
Co	20.		19.		35.		3.		28.	
Ni	64.		31.		58.		--		32.	

Table 1 Continued.

sample	WF - 12		TC - 9		WF - 2		WFT - 2		WF - 11	
	quartz wacke		quartz wacke		quartz wacke		quartz wacke		quartz wacke	
Y	24.7		15.5		8.9		13.3		21.9	
Zr	87.3		96.8		43.3		94.6		125.6	
Nb	6.2		3.6		2.2		7.6		4.7	
Hf	2.6		2.9		1.1		2.1		3.7	
Ta	0.3		0.38		0.20		0.28		0.50	
La	19.3		18.5		11.3		17.7		17.8	
Ce	39.2		42.0		25.7		31.4		33.6	
Sm	3.9		3.1		2.2		2.9		3.5	
Eu	0.66		0.80		0.41		0.62		0.81	
Tb	0.66		0.54		0.40		0.51		0.56	
Yb	2.72		1.31		0.70		1.06		1.87	
Lu	0.40		0.18		0.82		0.16		0.34	



Table 1 Continued.

sample	MW - E	MW - F	MW - B	HWY 87-1	WF - 15
sediment type	matrix-rich quartz wacke	matrix-rich quartz wacke	matrix-rich quartz wacke	pelite	pelite
SiO <sub>2</sub>	61.27	64.59	61.6	62.40	65.03
TiO <sub>2</sub>	0.75	0.67	0.7	0.68	0.66
Al <sub>2</sub> O <sub>3</sub>	18.14	16.96	16.17	16.39	15.84
FeO <sub>2-3T</sub>	8.81	7.48	7.49	7.1	7.46
MgO	1.93	2.02	2.18	1.36	1.74
CaO	0.14	0.27	1.26	1.98	1.09
Na <sub>2</sub> O	2.11	1.88	3.95	2.06	4.29
K <sub>2</sub> O	2.47	2.93	3.01	2.87	2.26
MnO	0.10	0.17	0.07	0.12	0.09
P <sub>2</sub> O <sub>5</sub>	0.09	0.12	0.23	0.13	0.16
LOI	3.00	3.11	3.55	5.32	2.5
TOTAL	98.81	100.20	100.21	100.50	101.12

Table 1 Continued.

sample	MW - E	MW - F	MW - B	HWY 87-1	WF - 15
	matrix-rich quartz wacke	matrix-rich quartz wacke	matrix-rich quartz wacke	pelite	pelite
Rb	122.8	101.1	105.4	109.4	81.6
Ba	865.	847.	1092.	579.	658.
Cs	--	5.66	4.92	6.9	6.0
Sr	254.	318.	253.	163.	204.
Pb	22.5	24.7	18.7	23.0	49.5
Th	14.0	11.9	7.1	8.8	10.1
U	--	--	--	2.10	2.65
Sc	--	14.41	17.85	17.9	21.3
V	55.	69.	91.	53.	105.
Cr	76.	105.	104.	75.	82.
Co	33.9	17.39	17.42	17.9	23.4
Ni	--	38.	--	38.	38.

Table 1 Continued.

sample	MW - E	MW - F	MW - B	HWY 87-1	WF - 15
sediment type	matrix-rich quartz wacke	matrix-rich quartz wacke	matrix-rich quartz wacke	pelite	pelite
Y	33.4	24.4	30.8	29.7	27.2
Zr	150.6	162.8	147.4	170.2	134.5
Nb	11.7	12.2	11.5	12.9	10.0
Hf	--	3.89	4.4	3.9	4.9
Ta	--	0.82	0.9	0.86	0.8
La	--	32.6	31.9	32.5	40.1
Ce	--	75.0	69.9	70.5	91.4
Sm	--	6.4	6.5	5.9	7.1
Eu	--	1.22	1.26	1.28	1.59
Tb	--	0.68	0.76	0.80	0.82
Yb	--	2.43	2.45	2.65	2.59
Lu	--	0.32	0.32	0.37	0.37

Table 1 Continued.

sample	WF - 16	WF - 3
sediment type	pelite	pelite
SiO <sub>2</sub>	58.31	56.13
TiO <sub>2</sub>	1.17	0.79
Al <sub>2</sub> O <sub>3</sub>	19.77	21.09
FeO <sub>2-3T</sub>	9.64	9.00
MgO	2.08	2.77
CaO	0.58	0.23
Na <sub>2</sub> O	2.81	1.18
K <sub>2</sub> O	2.26	3.81
MnO	0.06	0.05
P <sub>2</sub> O <sub>5</sub>	0.25	0.13
LOI	3.35	4.17
TOTAL	100.28	99.35

Table 1 Continued.

sample	WF - 16	WF - 3
sediment type	pelite	pelite
Rb	70.3	191.4
Ba	551.	111.
Cs	4.2	11.8
Sr	276.	93.
Pb	26.8	51.3
Th	9.3	13.3
U	2.21	3.40
Sc	21.6	33.9
V	135.	142.
Cr	41.7	186.1
Co	26.	33.
Ni	39.	66.

Table 1 Continued.

sample	WF - 16	WF - 3
sediment type	pelite	pelite
Y	35.4	47.0
Zr	228.3	146.7
Nb	18.6	10.3
Hf	6.1	5.3
Ta	1.10	0.83
La	34.2	44.7
Ce	83.3	95.5
Sm	7.0	8.0
Eu	1.75	1.82
Tb	1.05	1.10
Yb	3.31	3.97
Lu	0.50	0.55

Table 2. Modal compositions (%) of sedimentary samples which are used in provenance interpretation.

sample	MTO - 18	TC - 17	TC - 5	TC - 13	MTO - 19
sediment type	quartz wacke	quartz wacke	quartz wacke	quartz wacke	quartz wacke
matrix	23.	31.	25.	31.	52.
monocrystal-line quartz (Qm)	28.	28.	41.	24.	24.
polycrystal-line fine quartz (Qpf)	3.	1.	4.	14.	7.
polycrystal-line coarse quartz (Qpc)	32.	21.	18.	12.	4.
feldspar (fld)	1.	3.	1.	3.	5.
volcanic rock fragment (VRF)	6.	5.	5.	4.	5.
sedimentary rock fragment (SRF)	8.	10.	4.	12.	2.

77 63 50 35  
 1 1 3 5  
 16 9 16 7

0.07 0.8 0.11 0.10

0.10 0.10  
 →

Table 2 Continued. Modal compositions (%) of sedimentary samples which are used in provenance interpretations.

sample	*JBS - 17 AA	WF - 12 SW	WF - 11 SW	TC - 9 SW	WF - 2
sediment type	quartz arenite	lithic wacke	lithic wacke	lithic wacke	lithic wacke
matrix	4.	52.	67.	45.	3.
Om	82.	8.	1.	4.	3.
Qpf	1.	1.	1.	6.	3.
Qpc	1.	1.	1.	6.	3.
f1d	0.	12.	14.	4.	3.
Vrf	4.	17.	9.	20.	84.
SRF	8.	10.	9.	15.	3.

\*JBS - 17 has not been chemically analyzed

Handwritten notes: 8, 12, 14, 18, 25, 35, 44, 48, 54, 57, 64, 68, 72, 75, 78, 82, 85, 88, 92, 95, 98, 100, 105, 110, 115, 120, 125, 130, 135, 140, 145, 150, 155, 160, 165, 170, 175, 180, 185, 190, 195, 200, 205, 210, 215, 220, 225, 230, 235, 240, 245, 250, 255, 260, 265, 270, 275, 280, 285, 290, 295, 300, 305, 310, 315, 320, 325, 330, 335, 340, 345, 350, 355, 360, 365, 370, 375, 380, 385, 390, 395, 400, 405, 410, 415, 420, 425, 430, 435, 440, 445, 450, 455, 460, 465, 470, 475, 480, 485, 490, 495, 500, 505, 510, 515, 520, 525, 530, 535, 540, 545, 550, 555, 560, 565, 570, 575, 580, 585, 590, 595, 600, 605, 610, 615, 620, 625, 630, 635, 640, 645, 650, 655, 660, 665, 670, 675, 680, 685, 690, 695, 700, 705, 710, 715, 720, 725, 730, 735, 740, 745, 750, 755, 760, 765, 770, 775, 780, 785, 790, 795, 800, 805, 810, 815, 820, 825, 830, 835, 840, 845, 850, 855, 860, 865, 870, 875, 880, 885, 890, 895, 900, 905, 910, 915, 920, 925, 930, 935, 940, 945, 950, 955, 960, 965, 970, 975, 980, 985, 990, 995, 1000.



0 R 22 27 21 15 (18) 45 55 70 45  
 2 2 1 10 15 15 16 15  
 3 3 2 20 15 14 10 40

Table 2 Continued

sample	MW - E GW	MW - B GW	MW - F GW	WFT-2 GW
sediment type	matrix rich quartz wacke	matrix rich quartz wacke	matrix rich quartz wacke	lithic wacke
matrix	75.	71.	77.	67.
Qm	17.	25	14.	13.
Qpf	0.	0.	3.	1.
Qpc	5.	2.	4.	1.
fld	1.	1.	0.	2.
VRF	1.	1.	1.	10.
SRF	1.	1.	2.	6.

0 R 22 27 21 15 (18) 45 55 70 45  
 2 2 1 10 15 15 16 15  
 3 3 2 20 15 14 10 40

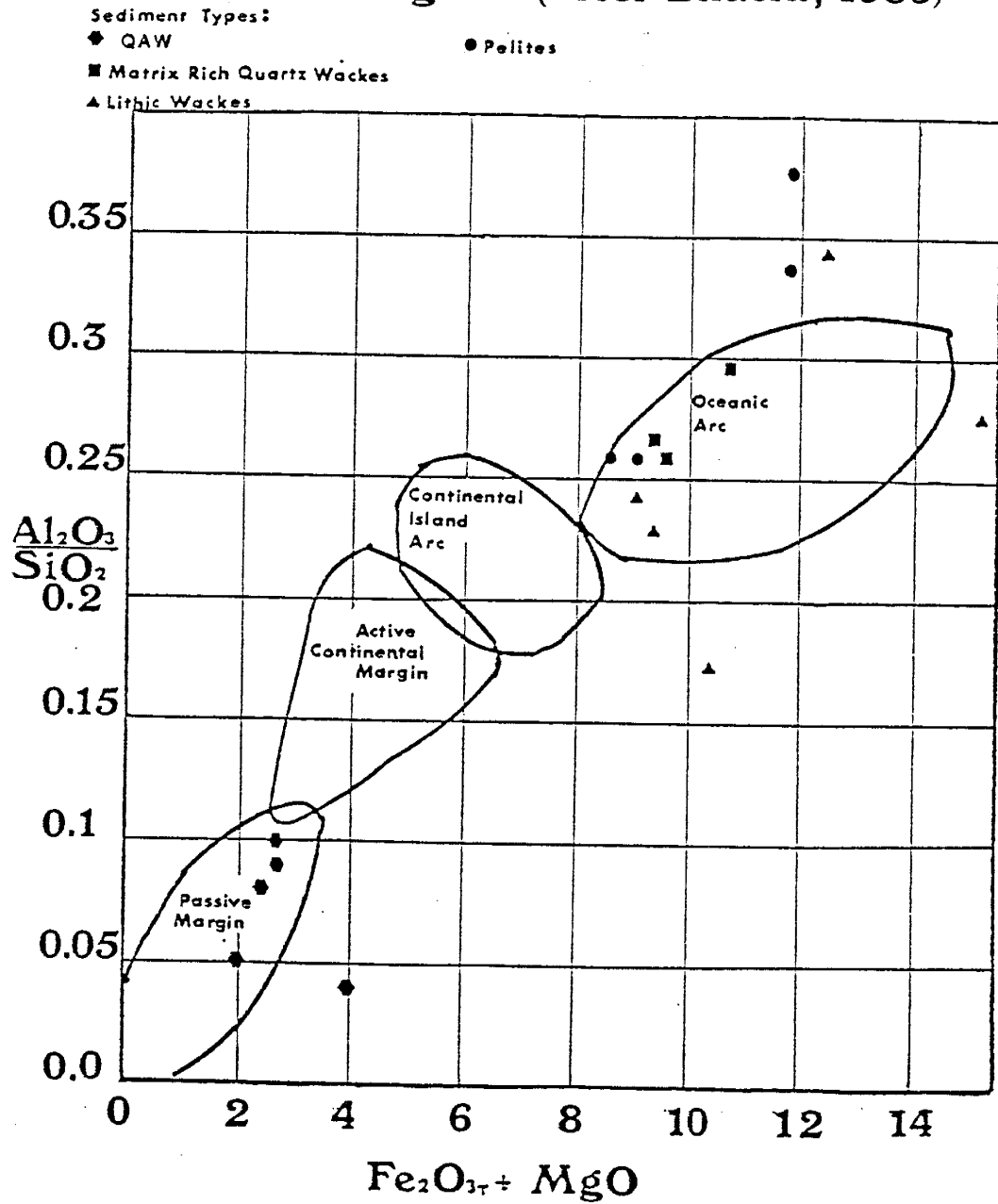
## Geochemistry of the Metasediments

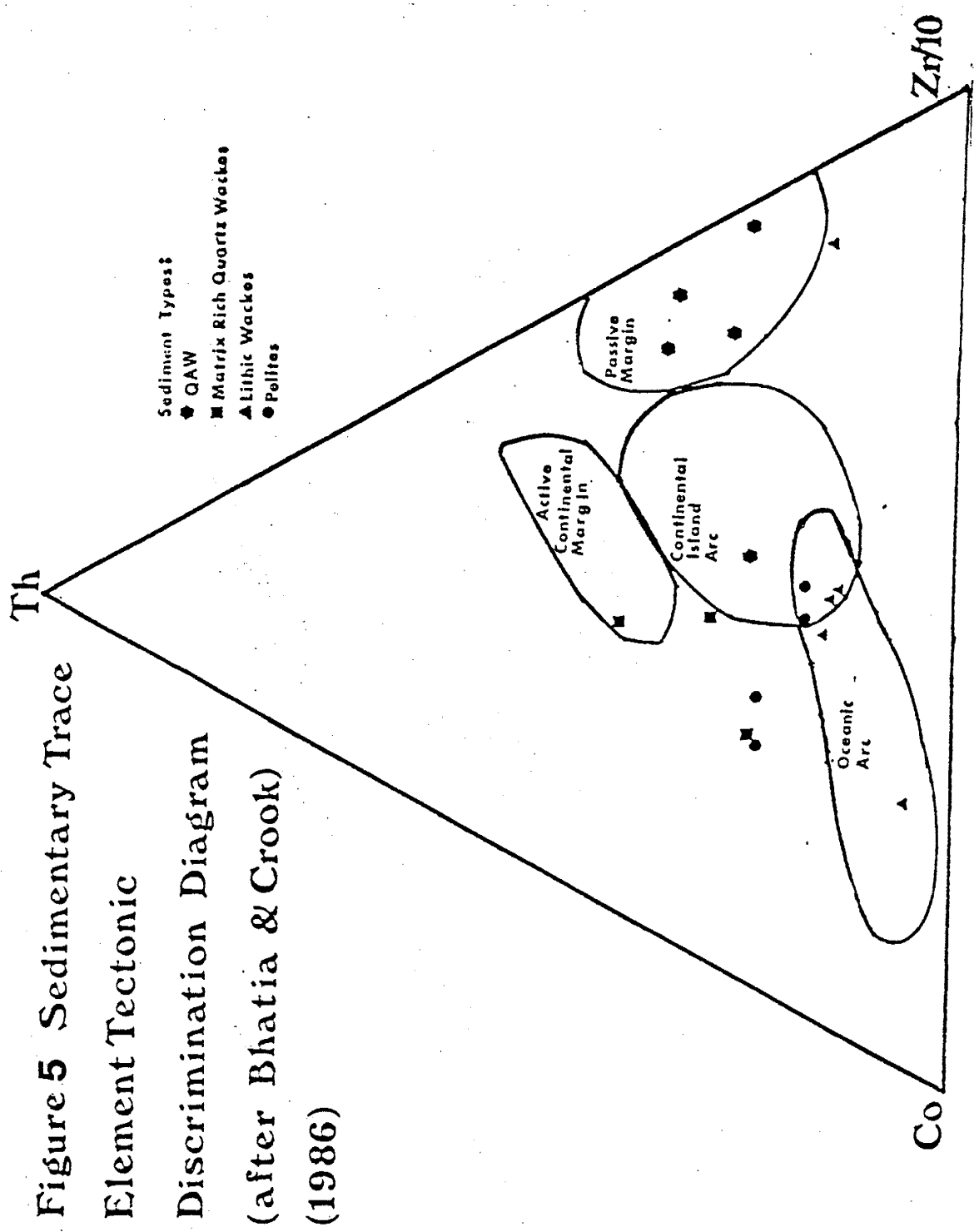
Geochemical results from Alder sandstone groups are plotted on tectonic discriminant diagrams (Figures 4-9). Figure 4 is the  $Al_2O_3/SiO_2$  vs  $Fe_2O_3t + MgO$  diagram (Bhatia, 1983). Results show two populations of sediment types. The QAW are chemically similar to passive margin sediments while the lithic wackes and matrix-rich quartz wackes are chemically similar to oceanic arc sediments. Although the diagram is only intended for sandstones, it shows that the pelitic samples have chemical affinities to arc type sandstones.

Figure 5 is a ternary Th-Co-Zr/10 diagram (Bhatia and Crook, 1986). Once again, the diagram shows two groups of sandstone types which roughly correspond with passive margin and oceanic arc type sandstones. For the most part, QAW plot in the passive margin field while the lithic wackes and the matrix-rich quartz wackes plot in or near the oceanic arc field; however, there are two exceptions to these tendencies. The quartz wacke, TC-17, plots closer to the oceanic arc group of sediments, and the lithic wacke, WFT-2, plots closer to the passive margin groups.

TC-17 comes from a sediment which occurs between two volcanic units in the upper Telephone Canyon member, and WFT-2 comes from the Oneida member on the northwestern limb of the syncline. The field occurrences of these samples suggest that extensive mixing and/or reworking of detritus may have been significant in these sediments. Variable amounts of mixing of the passive margin-oceanic arc end members may explain the anomolous positions of TC-17 and WFT-2 on the Th-Co-Zr/10 diagram. Figure 5 shows that relative to typical oceanic

Figure 4 Sedimentary Major Element Tectonic Discrimination Diagram (after Bhatia, 1983)





arc sandstones, the matrix-rich quartz wackes and the pelites have similar Co abundances and higher Th abundances.

Three other trace element tectonic discrimination diagrams for sediments also suggest the mixing of passive margin and oceanic arc sediment end-members. The Th-Sc-Zr/10 ternary diagram (Bhatia and Crook, 1986); (Figure 6) shows that although the QAW tend to plot separately from the lithic wackes and the matrix-rich quartz wackes, the groupings are not as well defined, as in Figures 4 and 5. The Ti/Zr vs La/Sc diagram (Bhatia and Crook, 1986); (Figure 7) shows that the Alder sedimentary samples plot roughly in a hyperbolic pattern which, on a ratio-ratio diagram, may indicate end-member mixing (Langmuir, et. al, 1978). A way to test this proposition is to plot a companion element-element diagram which has one of the ratios in Figure 7 on one axis and the ratio of the two denominators on the other axis. An example of such a companion diagram is shown in Figure 8. If the samples in the ratio-ratio diagram plot linearly in the companion diagram, there is strong evidence for the chemical mixing of sediment end members (Langmuir, et. al, 1978). It can be seen from the La/Sc vs Zr/Sc diagram that the pattern defined by the Alder samples is roughly linear; therefore, it seems likely that the distribution of data in the tectonic discriminant diagram represents variable mixing of passive margin and oceanic arc sediments.

The  $K_2O/Na_2O$  vs  $SiO_2$  diagram (Roser and Korsch, 1986); (Figure 9) may also demonstrate a variable amount of mixing between passive margin and oceanic arc sediment types. It should be noted that some of the samples appear to have lost  $Na_2O$ , and these samples (WFT-2 and MTO-19) could not be plotted on the diagram. The most chemically

Figure 6. Th-Sc-Zr/10 diagram for tectonic settings of sandstones (after Bhatia and Crook, 1986).

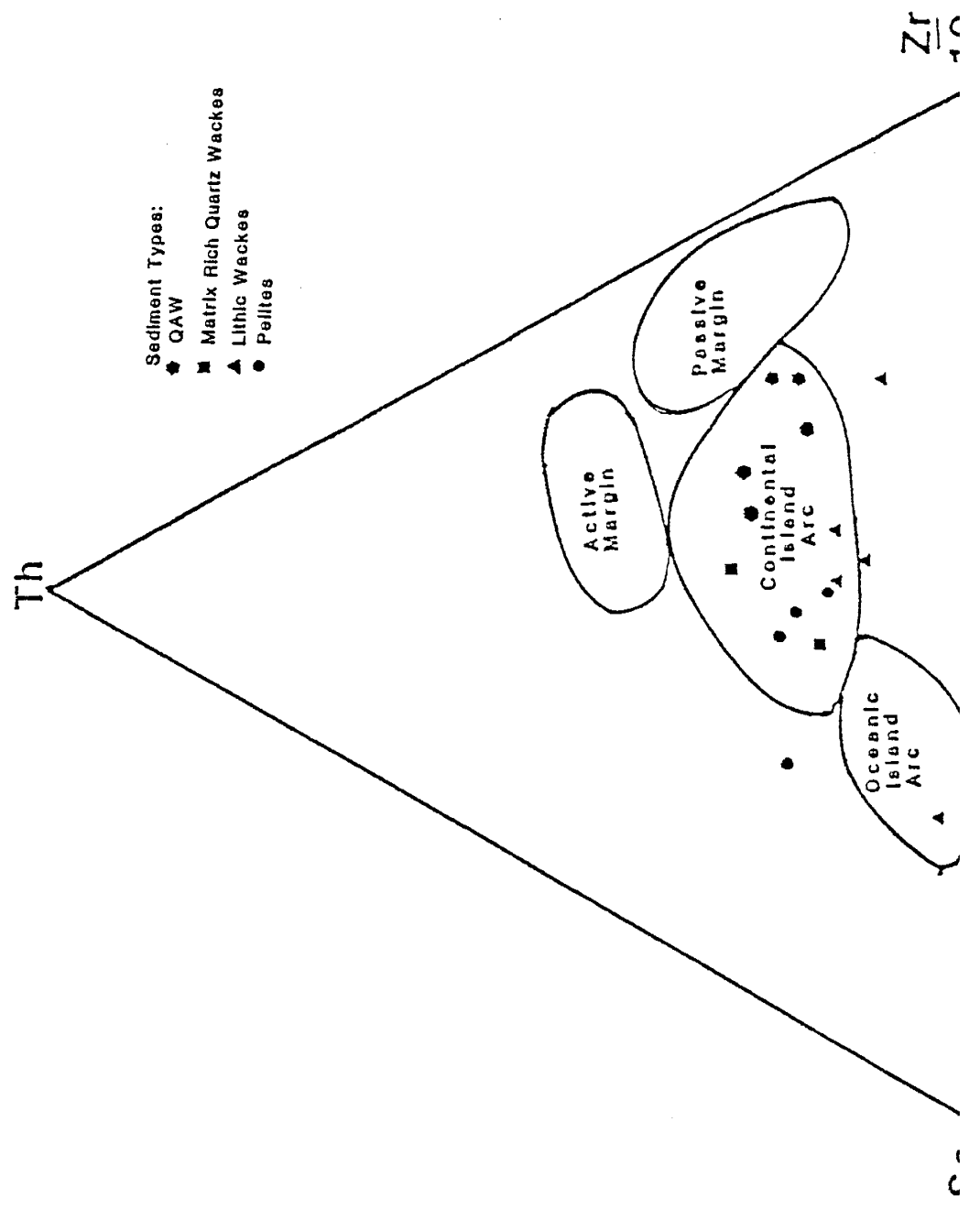


Figure 7. La/Sc vs Ti/Zr tectonic discrimination diagram for sediment  
The diagram shows the distribution of Alder sediment types.

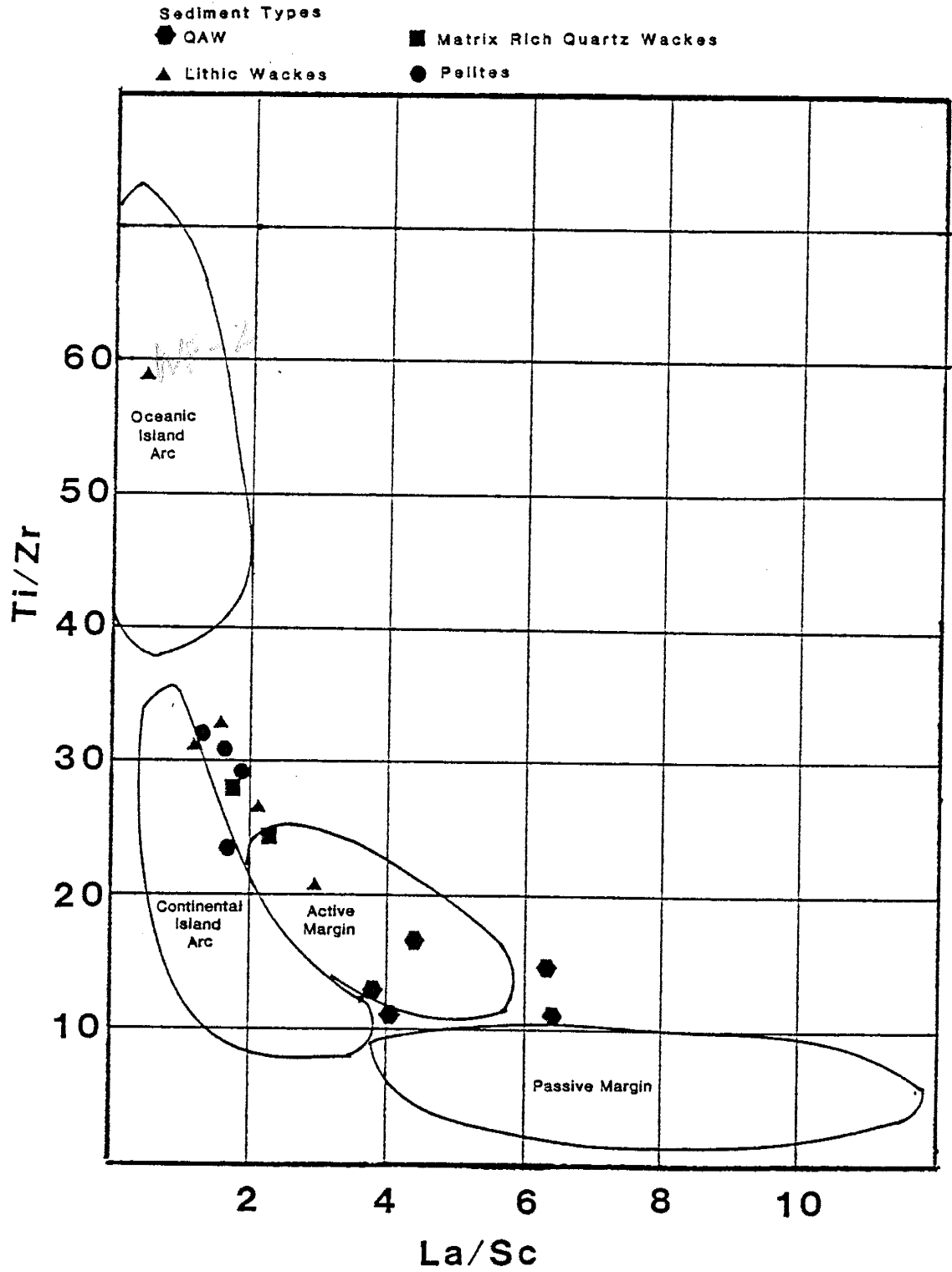


Figure 8. La/Sc vs Zr/Sc diagram which shows the distribution of Alder sedimentary samples. The figure is a "companion" diagram to the La/Sc vs Zr/Ti diagram (figure 9) (Langmuir et. al., 1978). Linear distributions on companion diagrams provide evidence for end-member mixing. An approximated best fit line has been drawn through the distribution of Alder samples.

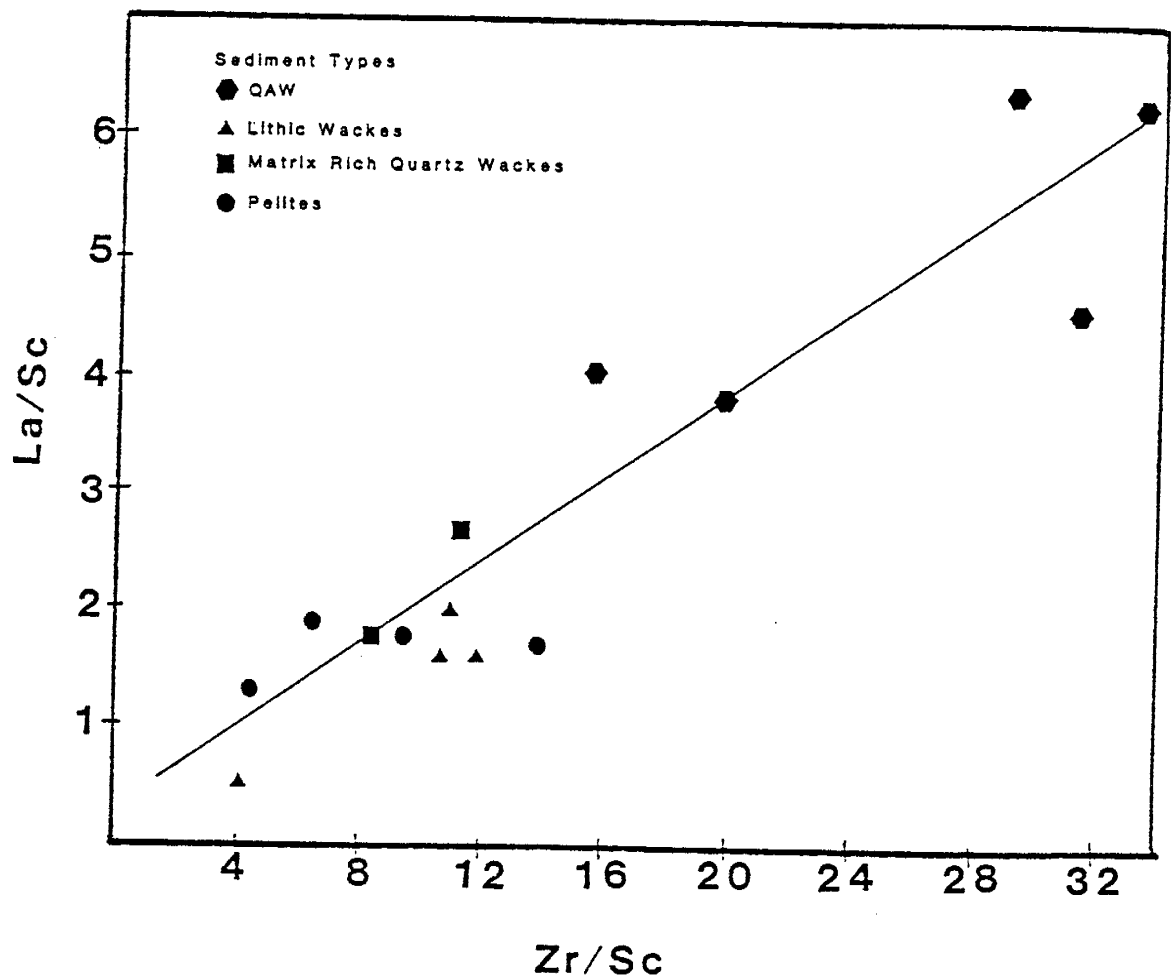




Figure 9.  $K_2O/Na_2O$  vs  $SiO_2$  diagram for tectonic settings of mudstones and sandstones (after Roser and Korsch, 1986).

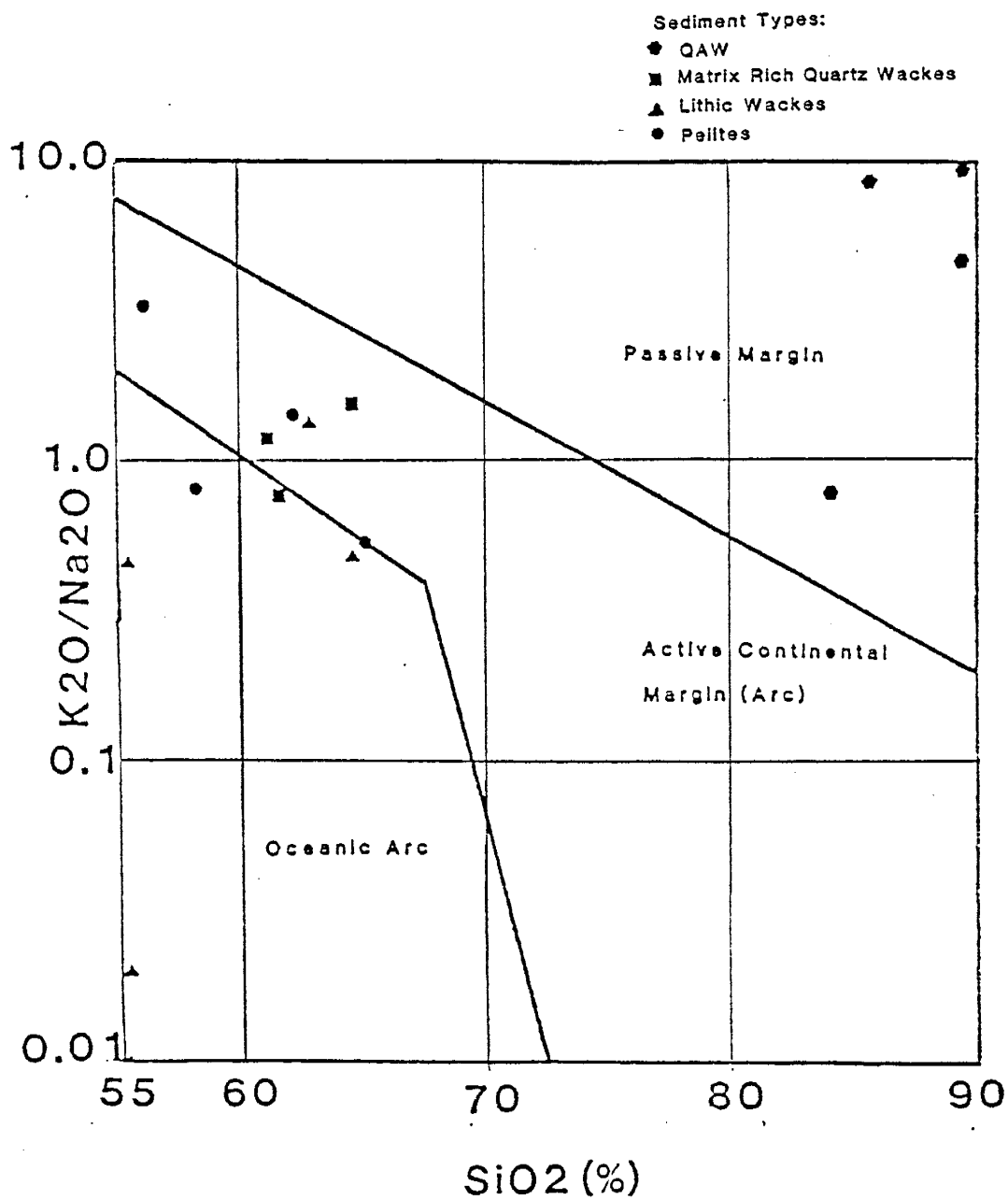
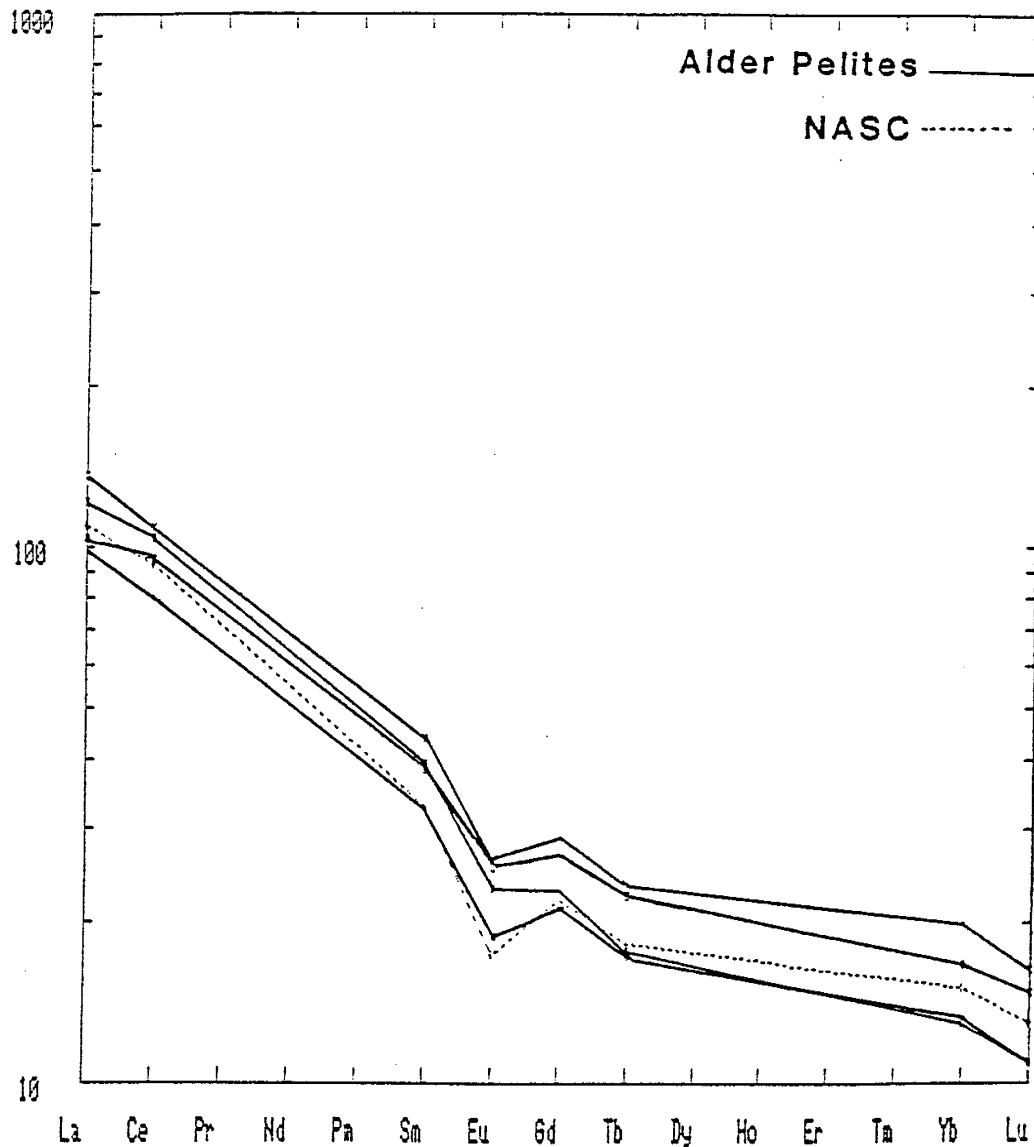


Figure 10. Chondrite normalized REE patterns for Alder pelites and NA



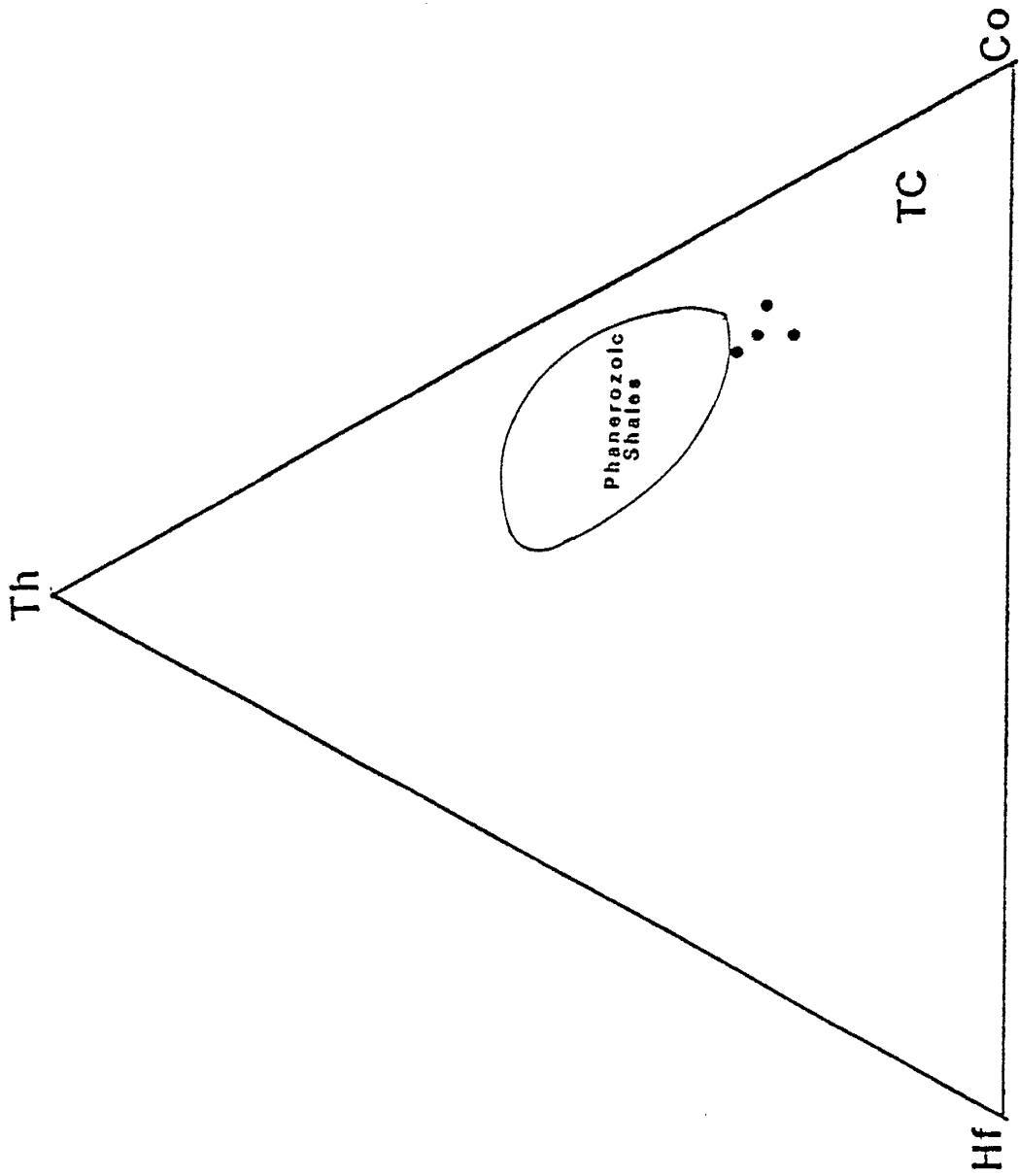


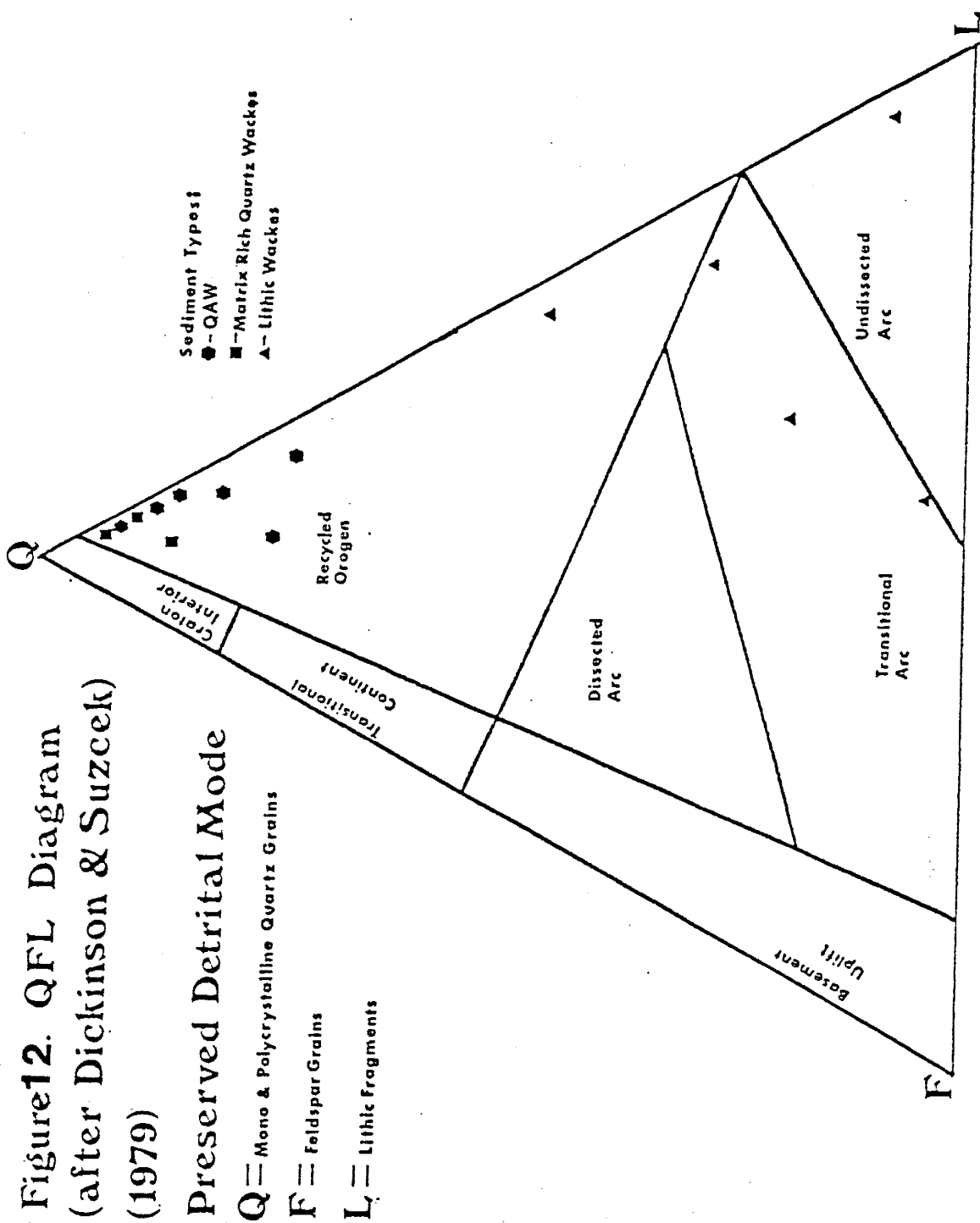
Figure 11. Th-Hf-Co diagram for pelites (after Taylor and McLennan, 1985). TC represents the composition of total crust.

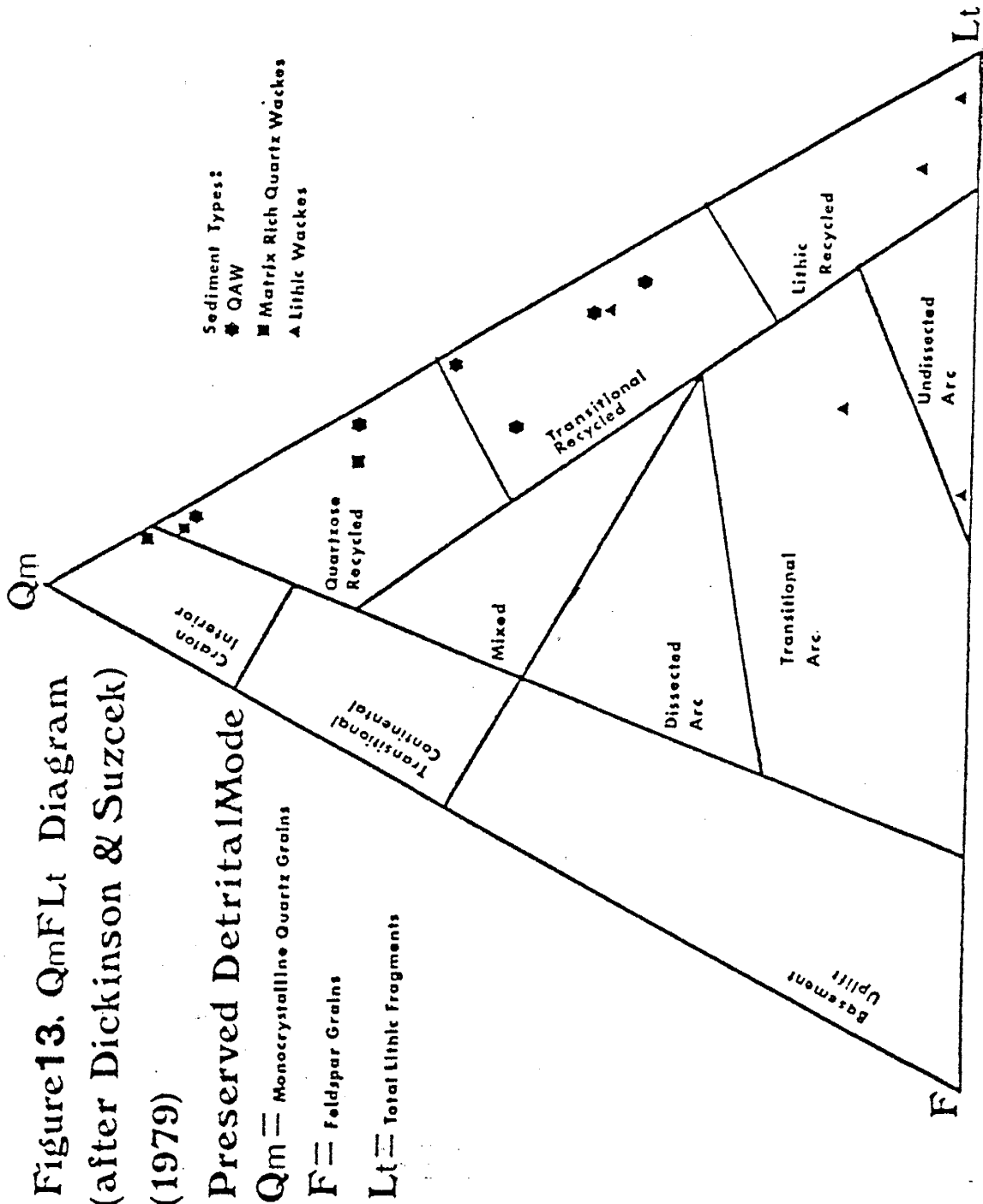
immature sediment is WF-2. This sample plots clearly as an oceanic arc type in all of the tectonic discriminant diagrams and it appears that the sediment has not received any input from the mature (passive margin) sediment end member.

The chondrite normalized REE patterns for the pelites are shown in Figure 10. The pattern of NASC is also shown in the Figure (dashed line). It is seen that the patterns of the pelites are very similar to that of NASC which suggests that the slates represent material which had been suspended in the basin. The ternary pelite diagram (Figure 11) of Taylor and McLennan, (1985) show some distinctions between the Alder pelites and Phanerozoic shales. The plots of the Alder pelites lie between the plot of total crust and the field of Phanerozoic shales. This suggests that relative to Phanerozoic shales, the Alder pelites have an increased input from a mafic source.

#### Provenance of the Metasediments

The interpretation of provenance is based on QFL and QmFLt diagrams after Dickinson and Suzcek (1979). The different sediment types which are defined at the beginning of this section are distinguished on these diagrams. The QFL diagram (Figure 12) shows that the QAW and matrix-rich quartz wackes plot as recycled orogen sediments while the lithic wackes tend to plot as arc sediments. In the QmFLt diagram (Figure 13), the QAW plot in quartzose recycled and transitional recycled fields. The matrix-rich quartz wackes plot in the quartzose recycled field and the lithic wackes plot in arc or lithic recycled fields.



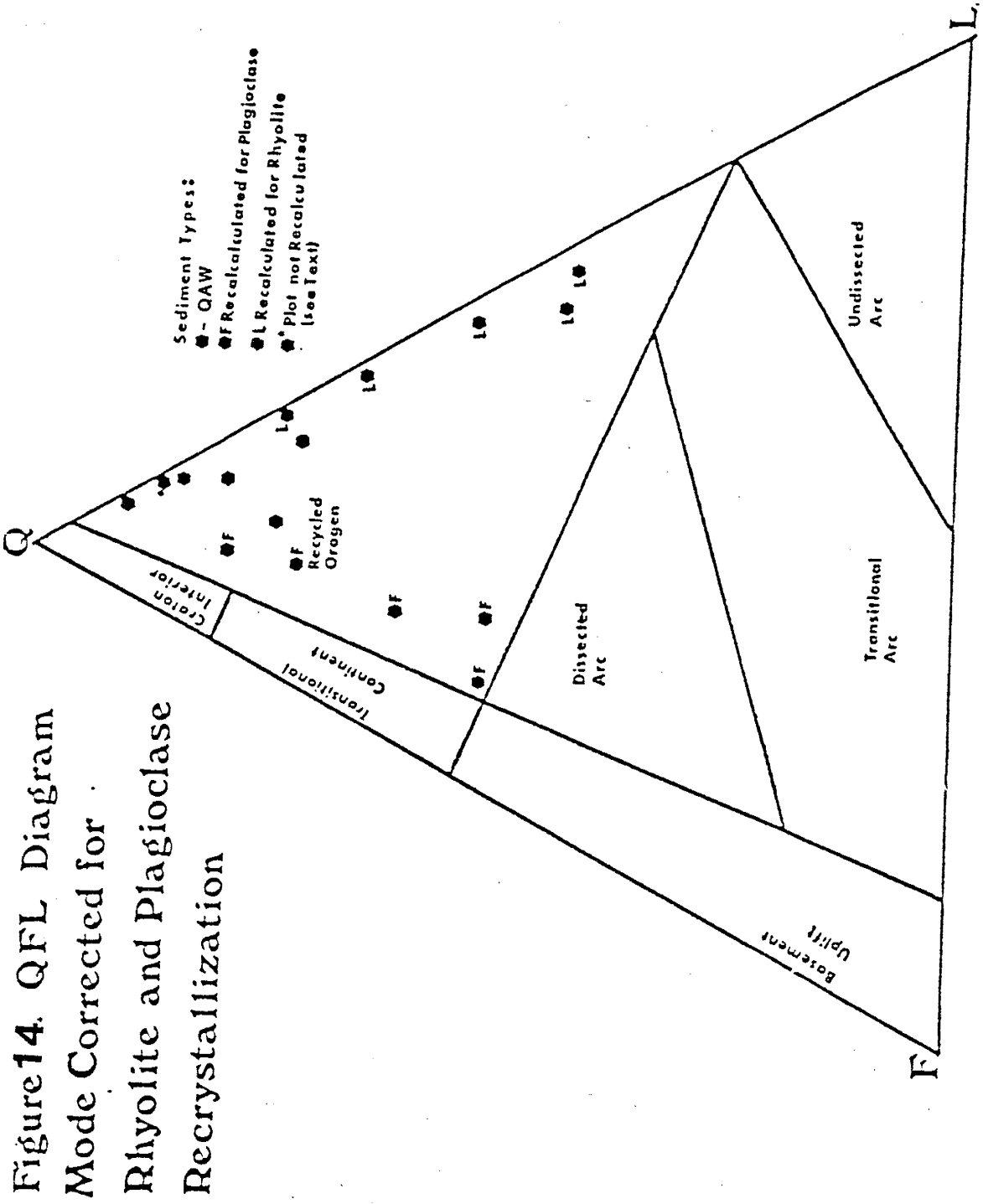


The interpretation of these diagrams can be affected by the recrystallization of detrital components into matrix. Because of the uncertainties related to the amount of secondary matrix in sandstones, Dickinson and Suzcek (1979) limit the use of these provenance diagrams to rocks which contain no more than 25% matrix. The applications of this restriction in this study prohibits the analysis of the lithic wacke and matrix-rich quartz wacke populations (Table 2). Reed and Condie (1987) describe a method which uses geochemical constraints to evaluate the potential effects of matrix recrystallization in a sandstone. The method is discussed in Appendix E.

Of the six rock types or mineral grains which are used in the matrix recalculation (Appendix E), the greatest change of provenance occurs when either plagioclase or rhyolite rock fragments is assumed to have recrystallized to matrix. Figures 14-19 show the degree to which the provenance interpretation of each representative sandstone group can change from the recrystallization of either plagioclase grains or rhyolite rock fragments into matrix.

Figure 14 is a QFL diagram which shows the preserved mode and both of the adjusted modes for the QAW group of sandstones. It is seen from the Figure that even if All of the  $Al_2O_3$  in the matrix is attributed to the recrystallization of either plagioclase or rhyolite, the QAW still plot in the recycled orogen field.

Figure 15 is a  $QmFL_c$  diagram for the preserved and adjusted modes of the QAW. In cases where the provenance interpretation of the preserved mode is different from that of either of the adjusted modes, triangular fields of uncertainty (dashed lines) are drawn around the respective plots. It is assumed that the provenance field which





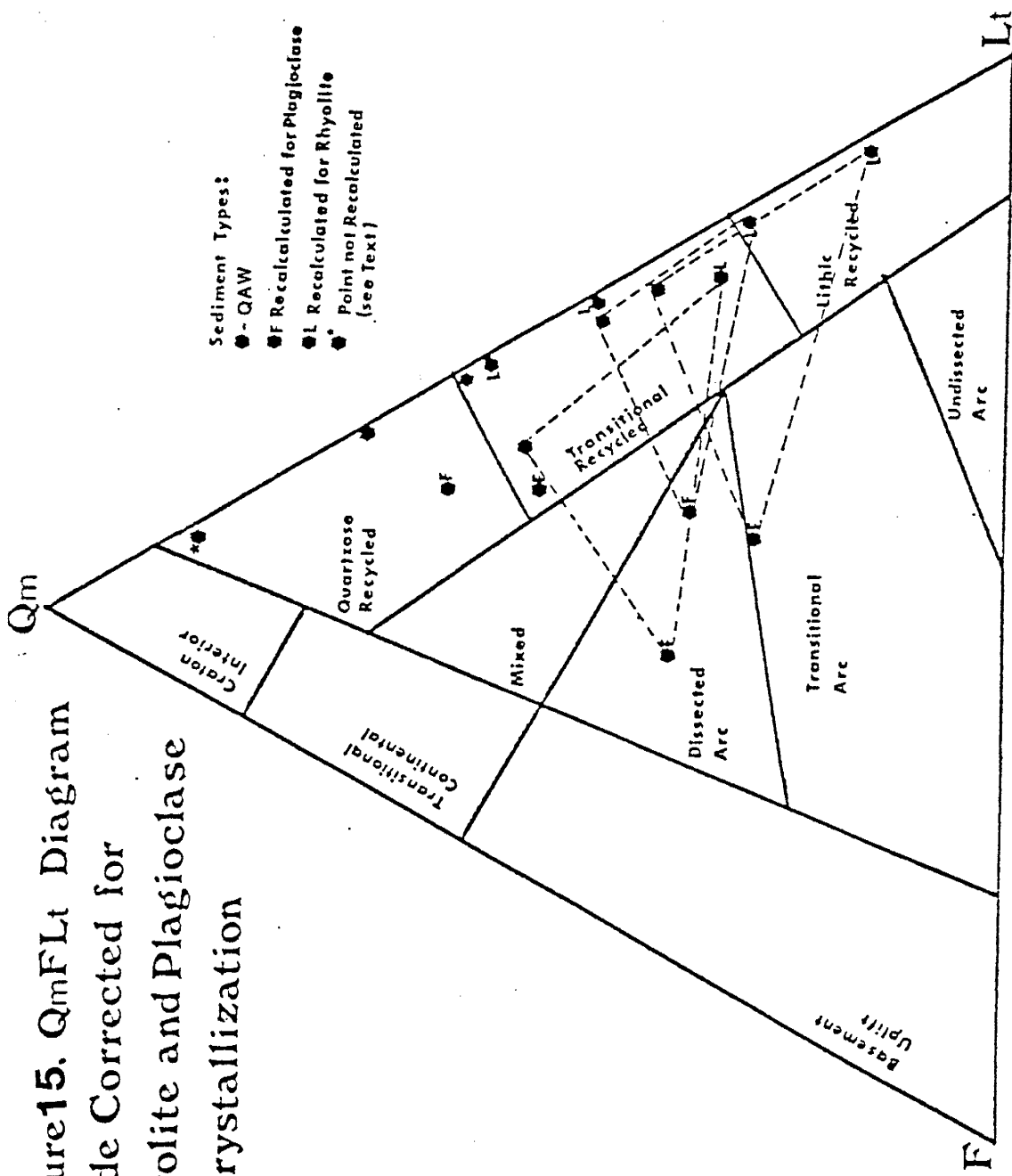


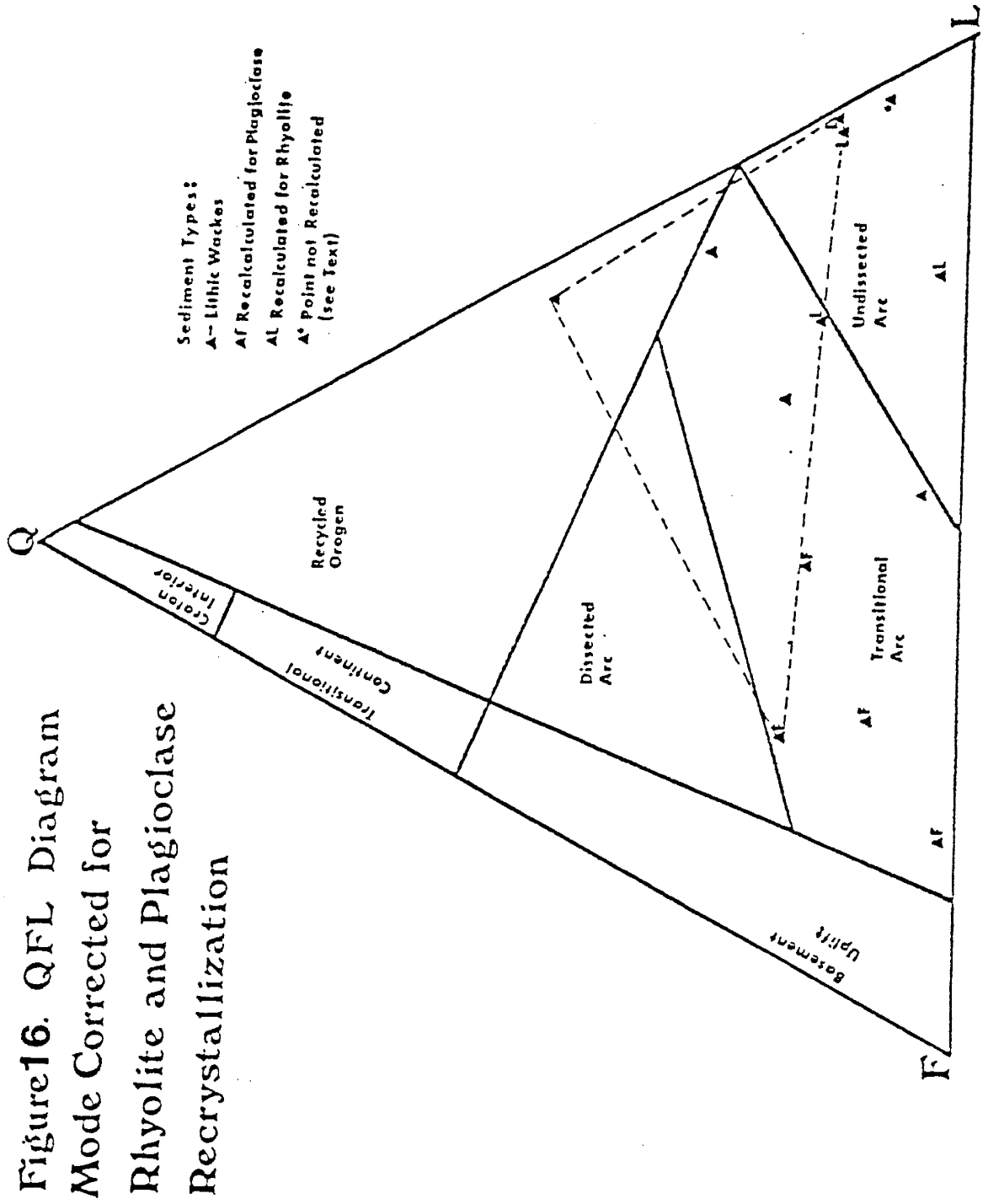
Figure 15. QmFLt Diagram Mode Corrected for Rhyolite and Plagioclase Recrystallization

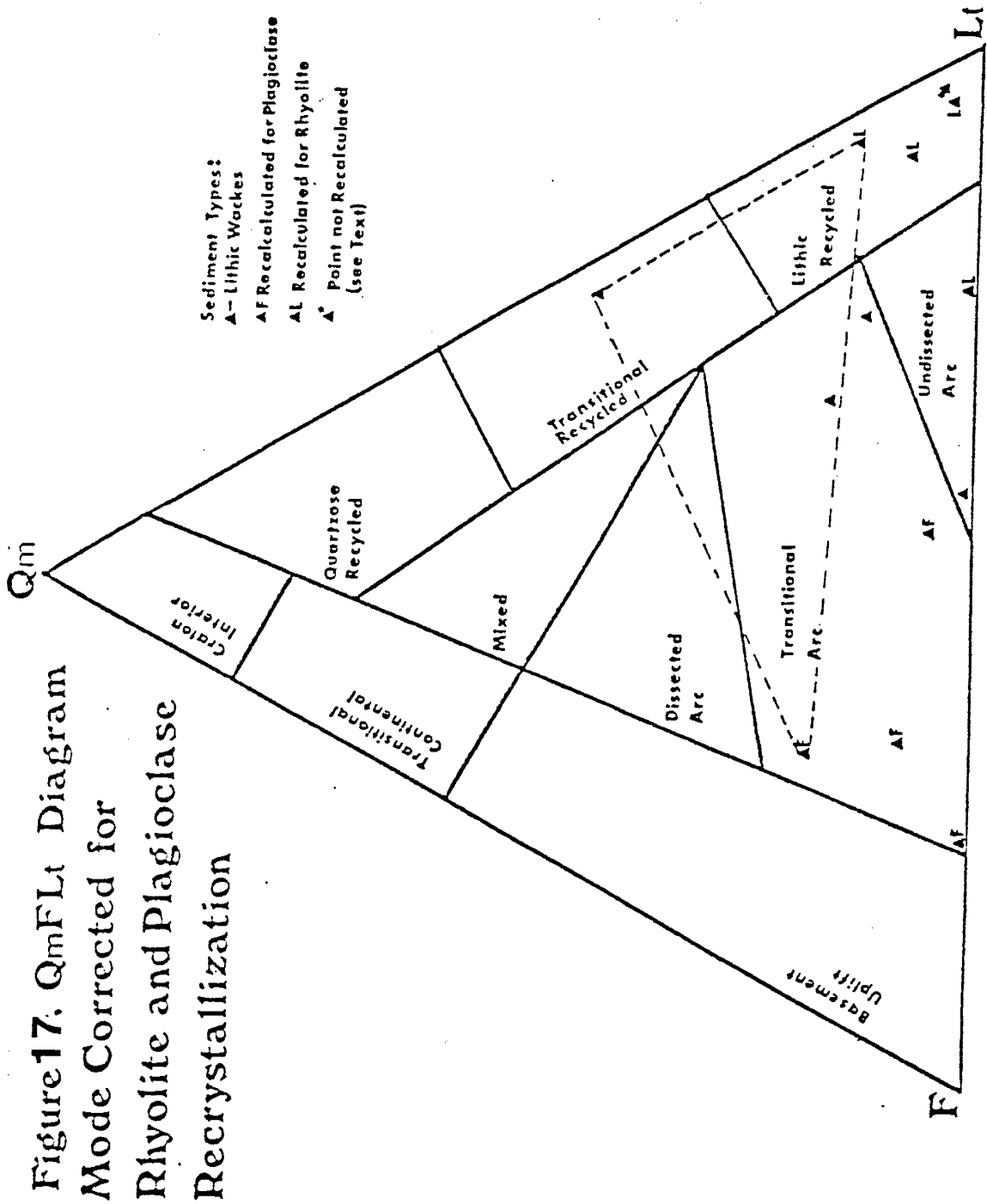
covers the largest proportion of the triangular area of uncertainty has the greatest probability of being the actual provenance type for the specific sample.

In this diagram, the most significant changes in interpretation occur when the maximum amount of allowable plagioclase is assumed to have recrystallized into matrix. Since the largest proportion of the areas of uncertainty cover the transitional recycled provenance field, this is the most probable provenance for the three questionable samples. In addition, the variations to arc related provenances are not considered to be valid because Figure 14 provides strong evidence that the sediments are representative of recycled orogen sediments, and this type of sandstone typically plots in one of the three recycled fields on the  $QmFL_t$  diagram.

It should be noticed that sample JBS-1 in Figures 14 and 15 is not recalculated. The sample has not been chemically analyzed; therefore, the mode cannot be adjusted. Table 2 shows that JBS-1 has less than 5% matrix. As a result, recalculation of the mode of JBS-1 would not significantly change the plots of the sample in Figures 14 and 15.

Figures 16 and 17 show the preserved and adjusted modes of the lithic wackes on the QFL and the  $QmFL_t$  diagrams, respectively. Figure 16 shows that the sandstones appear to be representative of undissected arc and/or transitional arc sediments. The one sample (WFT-2; Table 2) which has a varying interpretation upon modal recalculation has characteristics similar to both the QAW and the lithic wacke sediment types. It is grouped with the lithic wackes because it has approximately 10% modal volcanic lithic fragments, and

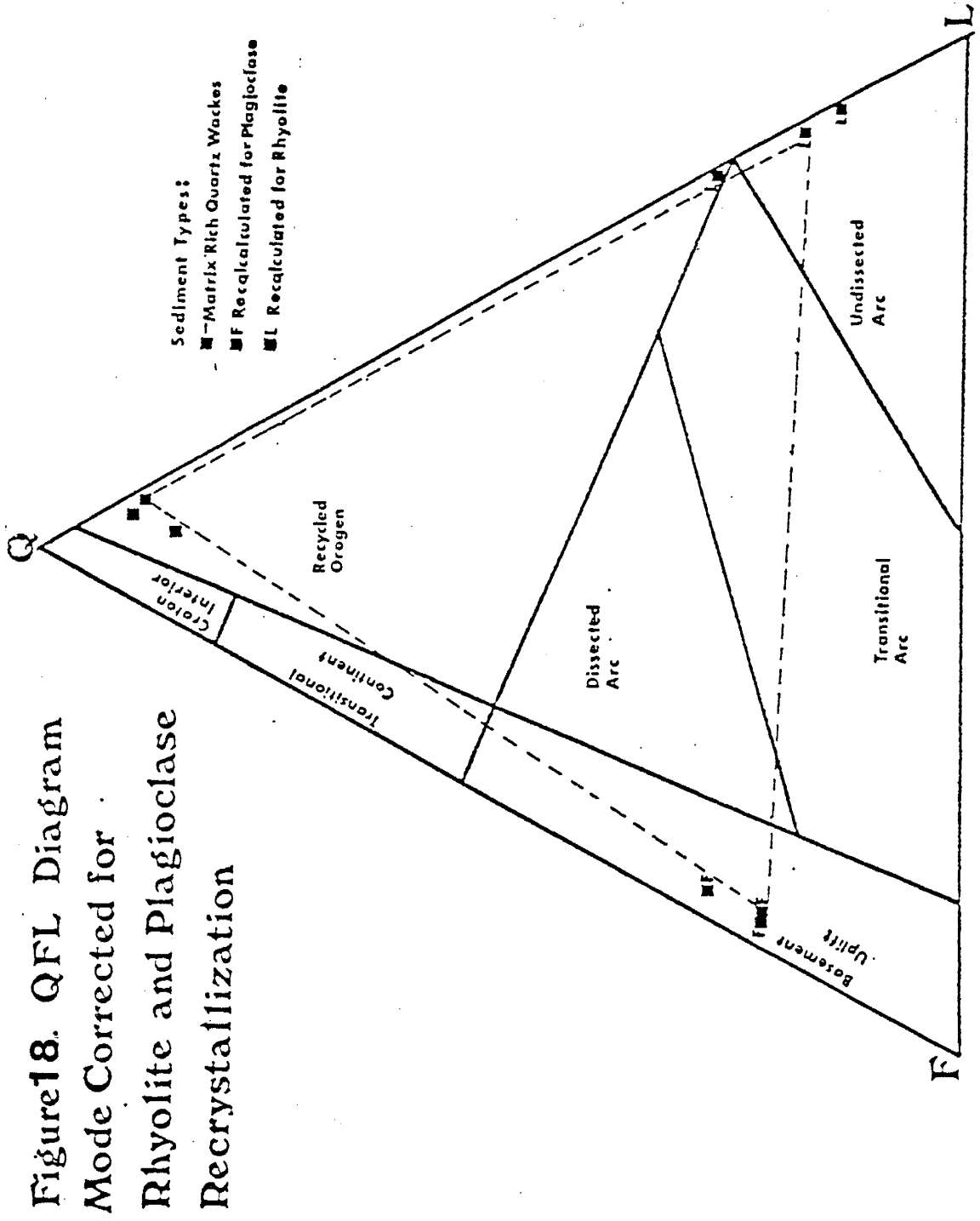


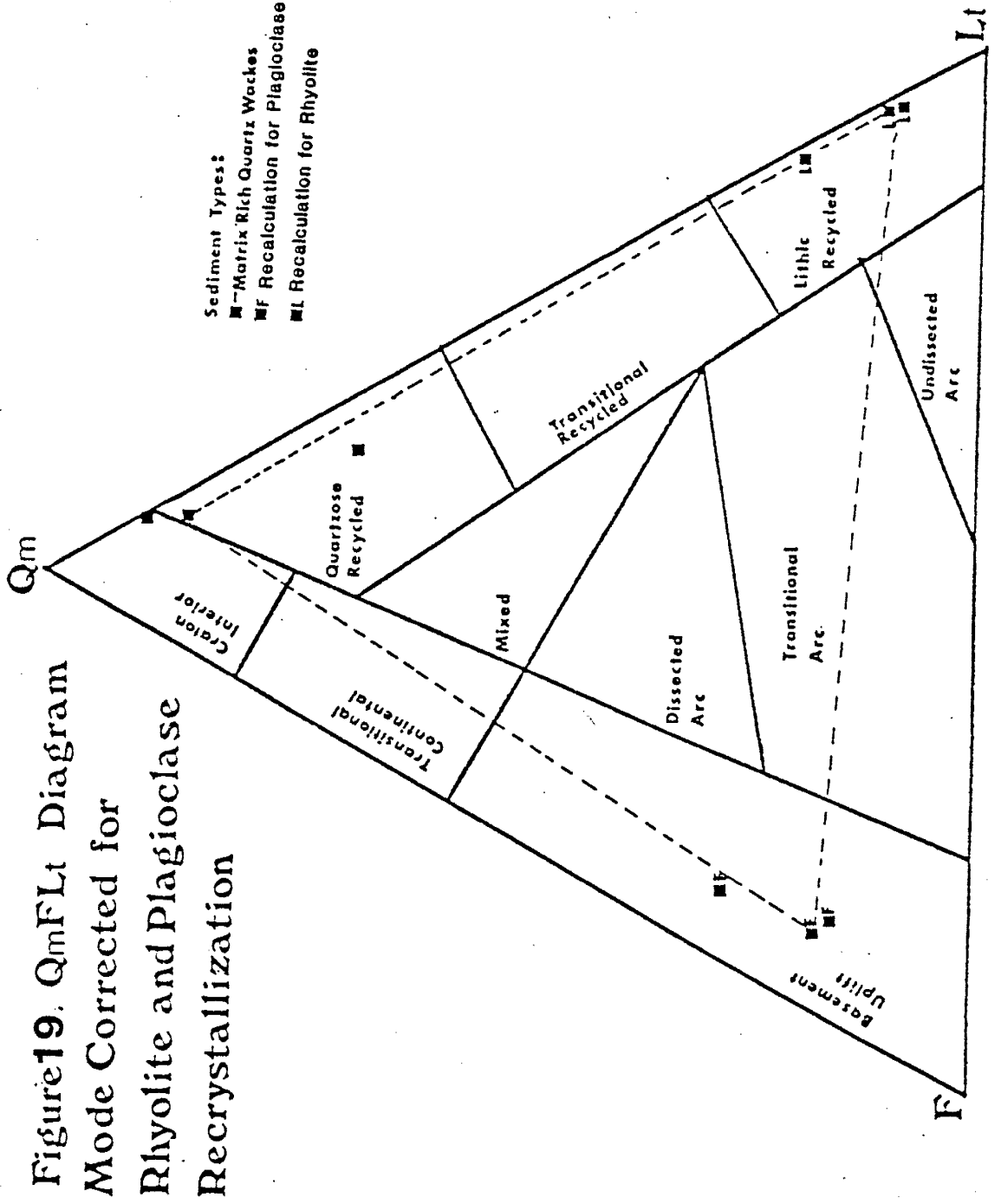


because it has more than 60% matrix; however, it is dissimilar to the other lithic wackes because it only contains approximately 1% plagioclase and because it has slightly more modal quartz. The Figure shows that a large proportion of the field of uncertainty of this sample falls in the transitional arc field; therefore, it seems probable that the sediment is related to the other lithic wackes with respect to provenance. Similar patterns can be seen in the  $QmFL_t$  diagram (Figure 17) for the lithic wackes. The adjusted modes fall dominantly in the transitional arc and undissected arc fields. Some adjusted modes plot as lithic recycled sediments.

Once again, in Figures 16 and 17, one of the samples (WF-2; Tables 1 and 2) is not adjusted for plagioclase or rhyolite recrystallization. In this case, the mode cannot be adjusted because all of the  $Al_2O_3$  in the whole rock is used up by the preserved mode. This may be the result of incorrect estimations of rock or mineral compositions. In any case, the sample has less than 10% matrix; therefore, lithic recycled is probably an accurate provenance assessment.

Finally, Figures 18 and 19 are the respective QFL and  $QmFL_t$  diagrams for the matrix-rich quartz wacke group. Both Figures show considerable uncertainty with respect to provenance assessment for all three of the samples. Subequal proportions of the areas of uncertainty are covered by recycled and arc related fields; therefore, one type of provenance cannot be quantitatively favored over the other.





## Lithofacies and Environmental Interpretation of Metasediments

The identification of ancient sedimentary environments is difficult without biotic evidence because similar sedimentary structures can be produced in different environments and ancient basin slope depositional systems often display a variety of facies types and facies associations which do not have modern analogues (Mutti, 1985; Heckel, 1972; Anderton, 1976; Shanmugam, Damuth and Miola, 1985).

The distinct nature of the respective rock types on the northwest and southeast limbs of the Alder syncline is discussed in the section on the Precambrian Geology. Since the stratigraphic relationships of these sections is ambiguous (see section on interpretation of the structure and stratigraphy), the limbs are considered separately in terms of lithologic facies and environmental interpretation.

### The southeastern limb

Primary sedimentary structures are well preserved in the Horse Camp and Telephone Canyon members on the southeast limb of the syncline (Figures 2 and 3). It appears that shearing has obliterated the primary structures in the southeastern exposures of the East Fork member, and primary structures are not observed in the Oneida member. The Telephone Canyon member and the Horse Camp member have dramatically different sedimentary structures. In general, the southern stratigraphic succession shows a fining upwards trend in the sedimentary lithologies. Volcanic cycles which are represented by flows and pyroclastic rocks occur intermittently within the sequence; however, the cycles seem to have dissipated in intensity with time.



At least two volcanic episodes can be observed on the Southeastern limb.

The Horse Camp member grades from coarse conglomerates to sericite rich slates over a short lateral distance (3-4m). The sediments occasionally show well defined grading and the coarse layers are typically more quartz rich. The coarsest grains are up to one centimeter in diameter, and they are subrounded to rounded. The percentage of quartz varies in these beds from 50 to 90%, while fine grained and slaty sediments have less than 10% quartz. The fine to medium grained sediments often show horizontal bedding in which the grain size is consistent throughout the bed. Matrix-supported poorly sorted conglomerates and breccias are also present in this sequence of sediments. The clasts in these rocks are elongated mafic and felsic volcanics ( $\leq 5\text{cm}$ ) and red jasper ( $\leq 1\text{cm}$ ), and the matrix is dominantly sericite.

The sedimentary rocks of the Horse Camp member are similar to those found in channel levee turbidite deposits of a lower slope or scarp environment. This conclusion is based on a comparison of structures, lithologies, and bedforms of this member with the lithofacies of Mutti and Ricci Lucci (1978). While making a distinction between upper slope and outer shelf deposits is problematical, the lower slope environment has characteristic lithofacies associations (Mutti, and Ricci Lucci, 1978, and Stanley, and Unrug, 1972).

The characteristics of the Horse Camp sediments which resemble submarine channel deposits are as follows: 1) the deposits vary from conglomerate to mudstones (slates); 2) sorting is consistently poor;

and 3) mineralogical compositions and textures are extremely variable (Shanmugam, Damuth, and Miola, 1985; Stanley and Unrug, 1972). It has been noted that the Horse Camp member predominantly shows graded bedding and horizontal bedding structures. The basin-slope is the only environment in which graded bedding and horizontal bedding are commonly occurring primary structures (Heckel, 1972).

Mutti and Ricci Lucci (1978) state that the A, B, G and F lithofacies of their turbidite classification is a typical association on the lower slope. The A, B and F facies characterize submarine channel deposits near the base of the slope while the G facies represents fine grained hemipelagic (terrigenous) sediments which are also deposited in the distal basin and the upper slope.

The Horse Camp member contains gradations of lithologies which are similar to the A-B facies transition. Pelitic slates of the Horse Camp member may represent the G facies, and conglomeratic units may represent the pebbly mudstones of the F facies. Quartzites probably represent resedimentation of shelf deposits as this process produces very little modification of original detritus (Ricci Lucci, 1985).

The slates and phyllites Oneida deposits may be equivalent to hemipelagic sediments of the G facies. In support of this comparison, the Oneida member lacks primary sedimentary structures, and similarly, the G facies commonly contains only vague indications of stratification (Mutti and Ricci Lucci, 1978). The upper slope environment is comprised almost entirely of this hemipelagic pelitic sedimentation (Mutti and Ricci Lucci, 1978). As a result, the Oneida member may represent the transition to upper slope deposition.

The Telephone Canyon sandstones are typically silt sized to medium grained. The sediments are composed mostly of quartz (65% to >95%), but they also include feldspar, red jasper, volcanic rock fragments, and sedimentary lithic fragments. The member shows small scale planar cross-bedding, symmetrical ripple marks, soft sediment deformation, horizontal bedding, and parallel lamination.

Occasionally, herringbone cross-bedding can be observed. Where structurally corrected, the cross-bedding shows dominantly southwest paleocurrent directions with occasional west and northeast directions (Appendix F). Quartz arenites become more important within the Telephone Canyon member to the northeast where the succession is correlated with Houden Formation in Tonto Basin (Conway and Silver, 1987). The sedimentary rocks in the upper Telephone Canyon member are interbedded with volcanics.

The Telephone Canyon member sediments contain many of the primary structures which are commonly observed in the marine pro-delta environment. For instance, the Telephone Canyon sediments typically show horizontal bedding. Although this feature is not exclusive to any one environment, it does seem to eliminate the beach, tidal, and fluvial environments (Heckel, 1972). Unlike the basin-slope sediments, the Telephone Canyon sediments contain very little graded bedding while cross bedding is very common. The presence of cross-bedding and symmetrical ripple marks also seems to exclude estuarine-lagoonal and distal marine (below wave base) environments (Heckel, 1972). By the process of elimination, a shallow marine pro-delta environment is the most likely site of deposition for the Telephone Canyon sediments.

The Telephone Canyon member contains sediments and primary structures which are similar to facies described in the Jura Quartzite (Anderton, 1976). This is a tidal-shelf sediment which is associated with a narrow funnel-shaped basin. The Telephone Canyon member shows stratigraphic alternations which are similar to Anderton's (1976) laminated and rippled subfacies of the fine facies of the Jura Quartzite. As a result, this terminology is used to describe the Telephone Canyon member. The laminated and rippled subfacies of the Telephone Canyon member are composed of very fine to medium sand interbedded with silt and clay. The laminated subfacies shows parallel laminations, small scale planar cross-bedding, and occasional ripple marks. Lower surfaces of beds are often erosional. The rippled subfacies has symmetrical ripple marks, planar cross-bedding, lenticular bedding, occasional parallel laminations, and load structures. The parallel laminations of fine sand and silt interbeds in these subfacies vary from graded to ungraded. They are similar to laminated sand and graded rhythmites in storm-sand layers of shelfal mud (Reineck and Singh, 1972; and Soegaard and Ericksson, 1984).

The laminated and rippled subfacies are indicative of shallow marine environments which are affected by storm and subordinate tidal activity. The laminated subfacies represents a proximal shelf environment. In conjunction with this association, the subfacies is more common at the top of the Telephone Canyon member. The rippled subfacies represents a distal shallow marine environment. Current directions which are obtained from cross-beds indicate that the Telephone Canyon sediments are derived from the northeast (Appendix F). As mentioned previously, coarser and more mature quartzose

lithologies are more common to the northeast within the Telephone Canyon member which also agrees with this direction of distribution. These facts suggest that the shelf sloped to the southwest.

#### The northwestern limb

The northwestern limb is composed mainly of volcanics and volcanoclastic sediments. The only quartzose rocks are sparse interbeds (2-3m thick) of graded quartz wackes within the Oneida member and within the two volcanoclastic-sedimentary units which have been mapped by Conway in the Lion Mountain Quadrangle.

Poorly sorted volcanoclastics dominate ( $\approx 90\%$ ) in the Oneida member on the northwestern limb. Volcanic breccias contain clasts that vary in size and lithology and resemble clasts in the breccias of the Horse Camp member in the Southern Area. Most clasts appear to be felsic volcanics; however, mafic volcanics, red jasper, and intraformational rip up clasts are also present. The clasts are elongated and up to 10 cm in length. These rocks grade from cobble-sized conglomerates and breccias to phyllitic sediments, and it is likely that they are water-laid. Beds of graded accretionary lapilli tuffs also occur in the section. The rocks are highly foliated with a matrix of sericite, quartz, and minor feldspar. Volcanoclastic rocks occasionally grade into thin (2-3m) quartz-rich beds (80-85% quartz). These beds contain large quartz grains ( $\leq 1\text{cm}$ ) similar to quartz grains in the Horse Camp member of the Southern Area. The sediments in the Oneida member are similar to the F and A lithofacies; therefore, the unit resembles inner fan deposits.

The lower thirds of the aforementioned volcanoclastic-sedimentary units are chloritized and are poorly bedded to massive. This rock type is identified as the crystal Lithic Tuff member in Ludwig's stratigraphy (1974). Higher in the members, the sediments contain up to 30% sericite. These sediments contain detritus ranging from pebble-sized to silt sized. The sericite-rich rocks are moderately to poorly sorted and show graded and lenticular bedding. Graded beds show complete Bouma sequences (Bouma, 1962). Conglomerate layers contain mafic to felsic volcanic rock fragments, and purple intraformational slate-siltstone clasts. Sericite rich sediments (matrix rich quartz wackes) contain up to 25% monocrystalline quartz grains ( $\leq 5$ mm in size).

Graded quartz wackes and plane parallel beds in the volcanoclastic-sedimentary units of the Northern Area resemble the C turbidite facies (Mutti and Ricci Lucci, 1978). This facies represents turbidites in the classical sense of the Bouma sequence (1962). Complete Bouma sequences are observable in the volcanoclastic-sedimentary units of the northern sequence. The C facies is believed to be associated primarily with deposits from an outer zone in a submarine fan.

Purple to maroon slates (West Fork member, East Fork member, and an unnamed unit) are interpreted to be distal plain sediments in the northwestern limb because they are in conformable contact below the volcanoclastic-sedimentary units which resemble outer submarine fan deposits. It is proposed that the relationship between the slates and the volcanoclastic-sedimentary units represents the original progradation of turbidite fan detritus, over distal plain sediments in

the basin of deposition. If this interpretation is correct, the stratigraphic record shows that volcanic flow and pyroclastic material (Cornucopia member) was also deposited in the distal plain environment.

#### IGNEOUS ROCKS

A diverse suite of igneous rock types is present in the Alder Group. Volcanic members contain varying proportions of mafic to intermediate flows, pyroclastic tuffs, breccias, and ash flows. Although felsic volcanics are rare in the Alder Group, they are the dominant rock types in the Red Rock Group. Hypabyssal bodies include mafic to intermediate dikes and sills and the felsic Pine Mountain Porphyry.

#### Pyroclastic Rocks

Volcanic breccias and volcanoclastics are very common in the Alder Group. Typically, they are poorly sorted and comprise a sericite rich matrix with minor amounts of quartz, feldspar, and rock fragments; however, some breccias contain a chlorite rich matrix. Felsic volcanics, mafic volcanoclastics, red jasper, and intra-formational rip-up clasts are the most common rock types in the breccias. Clasts are typically elongated and range in size up to 10 cm in length. Sediments vary rapidly from breccias to mudstones over short distances (3-5m) and the breccias occasionally show graded bedding. The volcanic breccias appear to be relatively less resistant

to deformation as the matrix of these rocks is typically highly foliated. Elongated clasts have been attributed to shearing in the units (Karlstrom and Conway, 1986). The volcanic breccias described above can be found in the Mt. Ord, Cornucopia, and the upper Telephone Canyon members on the southeastern limb of the syncline and in the Oneida member on the northwestern limb. The breccias compose ~90% of the Oneida member on the northwestern limb.

The matrix of a volcanic breccia which is found on the flank of Mt. Ord contains subhedral to euhedral hornblende phenocrysts (after pyroxene). The breccia contains up to 60% clasts of mafic volcanics, sediments, and felsic volcanics. Sedimentary clasts are polycrystalline, coarse grained quartzose fragments. This breccia and associated volcanics lie to the southeast of the Pine Mountain Porphyry on the flank of Mt. Ord, and they have not been mapped by Ludwig. The geologic map (plate I) shows where these rocks have been observed in this study.

Tuffs and tuffaceous sediments vary from slates to fine-grained rocks. These rocks are often chloritized; however, sericite-rich tuffs can also be observed. These tuffs and tuffaceous sediments are often interbedded with volcanic breccias and volcanic flows in the Mt. Ord, Cornucopia, and upper Telephone Canyon members on the southeastern limb and in the Oneida, East Fork, and Crystal Lithic Tuff members on the northwestern limb of the syncline.

Ash flow tuffs are present in the Mt. Ord member and in the Cornucopia member. These rocks are dense, massive, and blue-green. They contain glass shards and broken phenocrysts of feldspar and



quartz. Silicified squashed pumice fragments can be observed in an ash flow unit in the Mt. Ord member.

#### Mafic Igneous Rocks

Mafic igneous rocks occur as volcanics, dikes, and sills in the Alder Group. Volcanic flows in the Alder succession are typically mafic in composition. Fresh surfaces of the mafic flows are black, green, and blue-green, and weathered surfaces are typically brown. The flows are aphanitic to porphyritic, and porphyritic flows contain <10% phenocrysts of quartz, feldspar, and hornblende (after pyroxene). Phenocrysts are typically  $\leq 1$ mm in size; however, mafic flows southeast of the Pine Mountain Porphyry on the flank of Mt. Ord contain phenocrysts of hornblende (after pyroxene) which are up to 8mm in size. Mafic volcanics are typically massive; however, pillow flows can be observed in the Cornucopia member in McFarland Canyon on the northwest limb of the syncline.

Mafic dikes and sills which mainly intrude the Red Rock Group and the Telephone Canyon member are lithologically similar to mafic flows. These hypabyssal bodies are massive and are typically more resistant to weathering than the country rocks. Intrusive relationships such as discordant contacts and bake zones can be observed in the Telephone Canyon member on the southeastern limb of the syncline.

## Intermediate and Felsic Igneous Rocks

Intermediate igneous rocks also occur as volcanics and hypabyssal bodies in the Alder Group. Approximately 30% of the volcanic flows which have been analyzed in the Alder succession are intermediate in chemical composition (see next section). An andesitic dike (TC-16) which intrudes the Telephone Canyon member has been sampled and analyzed. The andesite appears to be associated with the mafic intrusives in the Telephone Canyon member and the Red Rock Group. Intermediate igneous rocks are green to blue-green on fresh surfaces and contain <15% phenocrysts of quartz and feldspar.

Felsic extrusive rocks are only found in the ~1000m thick Red Rock Group. One rhyolitic sample (MW-C) which has been taken from the outer northwestern exposures of the Alder section in the Lion Mt. Quadrangle has many geochemical similarities to the Red Rock Rhyolite (RRR). The contacts of this rock can not be observed; therefore, it is assumed that the unit is an intrusive which is related to the RRR extrusion. Most of the observed exposures of the RRR in the central part of the Proterozoic section are variably jointed and/or sheared, and light colored (clay) alteration zones are common. In outcrops of fresh exposures, four different rock types have been observed. Flowbanded volcanics are laminated in red and black. The bands are often contorted; however, in some outcrops, the bands persist for 3-5m. Welded lithic tuffs are massive and have preserved black flattened pumice fragments in a dense red to white matrix. Massive aphanitic flows are also present and volcanic breccias contain ≤5cm aphanitic felsic volcanic clasts which are lithologically similar to

matrix. Ludwig (1974) also describes spherulitic pyroclastics in the Red Rock Rhyolite.

The Pine Mountain (PMP) which is a felsic hypabyssal rock intrudes at various intervals of the Alder section; however, large bodies of the rock are located near the southeastern boundary of the Slate Creek shear zone and near the contact of the Oneida and East Fork members on the northwestern limb of the syncline (Figure 2). Near the southeastern boundary of the Slate Creek shear zone, the rock is highly foliated, and it is pink on fresh surfaces and white on weathered surfaces. It appears to have been altered to clay minerals in some areas. Near the contact of the Oneida and East Fork members on the northwestern limb of the syncline, the PMP is massive and white to green on fresh surfaces. Weathered surfaces are brown. The PMP contains  $\leq 10\%$  phenocrysts of quartz and feldspar ( $< 5$  mm in size).

### Geochemistry of Igneous Rocks

#### Introduction

Twenty one igneous rocks have been geochemically analyzed for major and trace elements. Various factors may affect the geochemical interpretation of the igneous rocks in the Alder sequence. One of these factors is alteration. The igneous rocks on the average seem to be high in volatile losses on ignition (LOI). Despite the high LOI, the high field strength elements (HFSE) and the heavy rare earth elements (HREE) appear to have been immobile in highly altered rocks (Appendix I); therefore, these elements are considered to be the most significant ones in geochemical interpretations. Tables 3, 6, and 7

show the chemical compositions of the analyzed igneous rock samples. In this study, samples are considered altered if: 1) they have an LOI greater than 5%, or 2) they plot outside of the  $\text{CaO}/\text{Al}_2\text{O}_3\text{-SiO}_2/100\text{-MgO}/10$  alteration screen (Davis, et al., 1979). This screen with the plots of the Alder samples is shown in Figure 20. Altered rocks are denoted by special symbols (Figure 21) in the modeling and tectono-magmatic diagrams, and Appendix I discusses some of the effects and the geochemical trends of alteration processes.

Another factor which may affect or hinder the geochemical interpretation of igneous rocks from the Alder sequence is sampling bias. One-half of the rocks that lie to the northwest of the Red Rock Rhyolite are extremely altered. This alteration which may have been caused by primary hydrothermal activity is discussed in the section which pertains to the discussion of stratigraphy and in Appendix I. There is limited accessibility to the unaltered half of rocks on the northwestern limb of the syncline because these rocks are located within the Mazatzal Wilderness area. As a result, very few rocks on the northwestern limb of the syncline have been chemically analyzed.

#### Igneous Rock Classification

The igneous rocks are classified using the scheme of Winchester and Floyd (1977) in Figure 22. This scheme is based on high field strength element (HFSE) ratios. The HFSE are considered to be among the most immobile trace elements (Pearce and Cann, 1973); therefore, the diagram should be a reliable indicator of igneous rock protolith. When the diagram is compared to a conventional silica-based classification scheme after Winchester and Floyd (1977) in Figure 23,

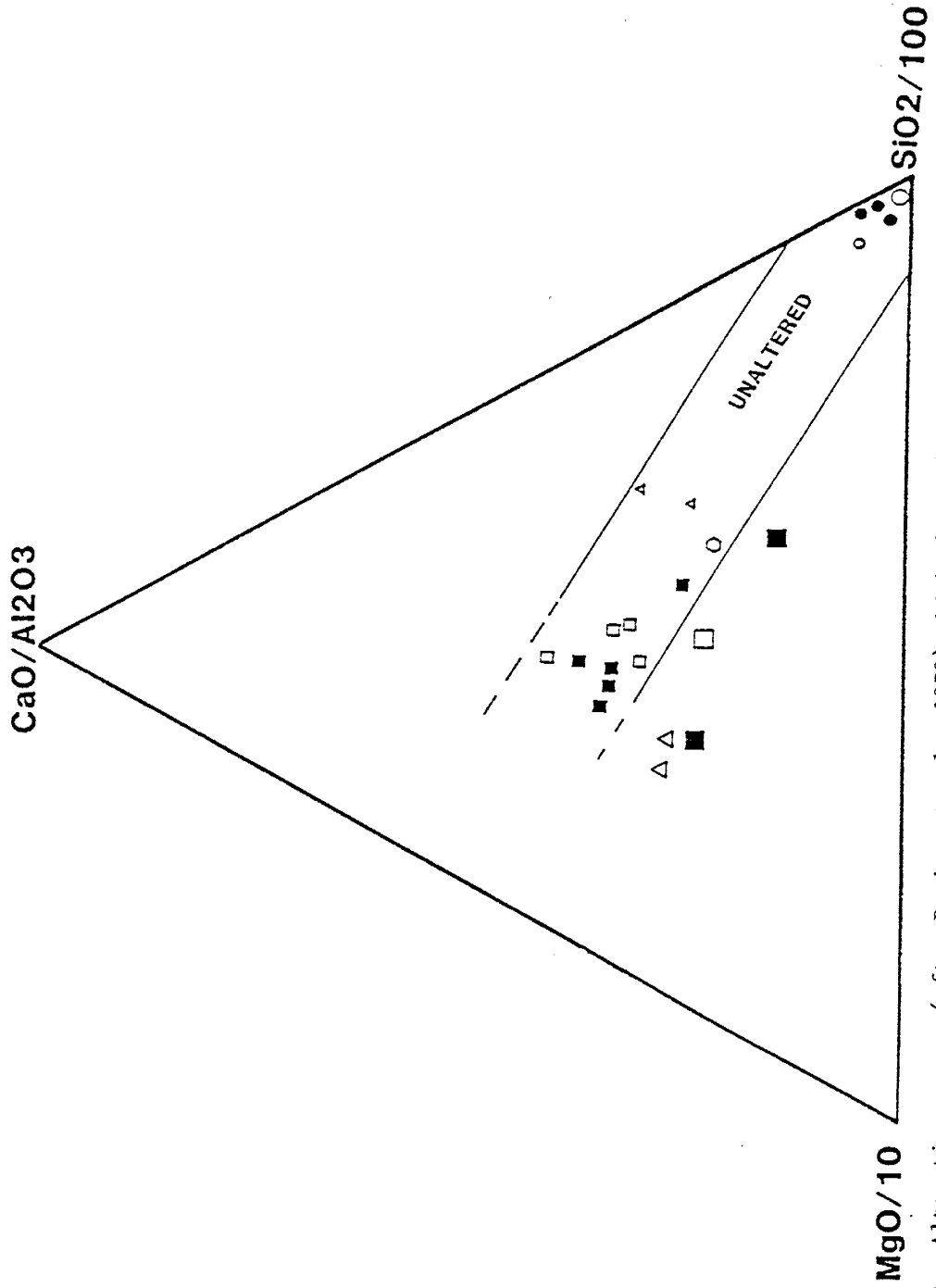
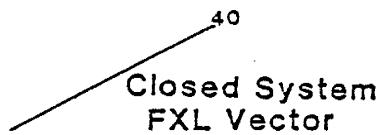
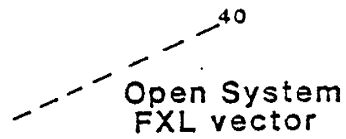
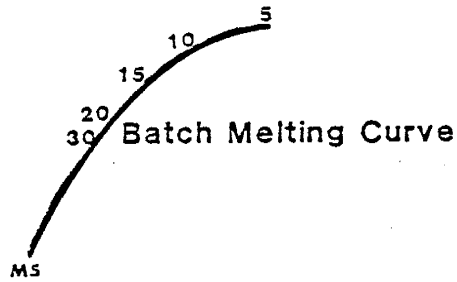


Figure 20. Alteration screen (after Davis, et. al., 1979) which shows the distribution of Alder and Red Rock igneous samples. Symbols are explained in figure 21.

Figure 21. Symbols used in a geochemical diagram for igneous rocks. The classification of igneous rocks is based on the Zr/TiO<sub>2</sub> vs Nb/Y diagram (figure 22) (see text for explanation of source types and altered samples).

Rock Type	Unaltered Samples		Altered Samples	
	derived from a high garnet source	derived from a low garnet source	derived from a high garnet source	derived from a low garnet source
Basalt	□	■	□	■
Andesite	△	▲	△	▲
Dacite	○	●	○	●
Rhyodacite-Rhyolite	○	●	○	●



MS = calculated mantle source (table 5a)

Table 3 . Chemical compositions of mafic igneous rocks. Major elements are in %, and trace elements are in ppm.

sample	TB - 5	HMTN - 2	MTO - 16	MTO - 4	TC - 21
field occurrence	volcanic	volcanic	volcanic	volcanic	volcanic
altered unaltered	unaltered	unaltered	unaltered	unaltered	unaltered
symbol in modeling diagram	■	□	□	■	■
SiO <sub>2</sub>	49.40	47.80	47.84	50.40	46.88
TiO <sub>2</sub>	0.90	0.69	0.81	1.20	1.30
Al <sub>2</sub> O <sub>3</sub>	13.10	16.41	17.24	18.14	18.72
FeO <sub>2-3T</sub>	13.00	11.61	14.35	13.10	11.77
MgO	10.10	5.25	5.85	3.98	5.57
CaO	7.30	1.43	7.93	4.69	9.89
Na <sub>2</sub> O	1.82	1.18	2.38	5.83	2.07
K <sub>2</sub> O	0.46	0.59	0.22	1.52	0.04
MnO	0.20	0.16	0.23	0.17	0.16
P <sub>2</sub> O <sub>5</sub>	0.16	0.18	0.15	0.24	0.22
LOI	3.52	4.21	3.57	1.18	3.52
TOTAL	99.96	99.51	100.57	100.45	100.14

Table 3 Continued.

sample	TB - 5	HMTN - 2	MTO - 16	MTO - 4	TC - 21
Rb	11.9	12.4	7.1	43.0	3.5
Ba	322.	181.	156.	979.	75.
Cs	3.3	0.83	0.37	12.3	0.1
Sr	301.	580.	263.	605.	476.
Pb	6.4	11.1	10.8	14.0	14.6
Th	1.7	0.9	0.9	2.4	1.3
U	0.45	--	--	0.86	0.71
Sc	42.4	32.8	31.1	33.6	27.8
V	--	264.	312.	229.	237.
Cr	51.0	48.2	20.7	40.0	131.5
Co	51.	29.	29.	34.	43.
Ni	76.	36.	14.	6.	65.



Table 3 Continued.

sample	TB - 5	HMTN - 2	MTO - 16	MTO - 4	TC - 21
Y	21.7	15.4	15.4	26.6	22.0
Zr	77.0	61.4	51.7	123.	91.2
Nb	5.0	2.1	2.2	7.3	4.6
Hf	2.1	1.17	1.08	2.6	2.7
Ta	0.25	0.17	0.17	0.42	0.19
La	10.0	13.46	5.58	14.0	10.7
Ce	24.0	28.9	11.7	32.1	26.7
Sm	3.5	3.88	2.2	4.7	3.9
Eu	1.20	1.18	0.70	1.45	1.49
Tb	0.71	0.45	0.32	0.94	0.61
Yb	2.20	1.70	1.31	3.16	2.12
Lu	0.35	0.2	0.20	0.46	0.32



Table 3 Continued.

sample	TB - 9	TC - 3	TC - 2	TC - 18	WF - A	TC - 7
Rb	22.9	9.3	10.4	27.1	11.4	99.9
Ba	538.	394.	466.	829.	452.	565.
Cs	6.5	0.4	1.4	0.6	2.1	5.5
Sr	544.	478.	427.	1221.	241.	149.
Pb	13.0	13.2	12.8	16.7	39.7	24.6
Th	1.8	1.7	1.5	3.7	3.3	4.2
U	--	--	0.78	1.71	1.59	1.74
Sc	30.1	35.5	42.1	23.3	26.7	22.5
V	211.	334.	356.	213.	285.	294.
Cr	173.3	63.7	125.2	161.5	19.2	7.3
Co	31.	50.	46.	30.	41.	69.
Ni	39.	66.	41.	62.	54.	54.

Table 3 Continued.

sample	TB - 9	TC - 3	TC - 2	TC - 18	WF - A	TC - 7
<u>Y</u>	11.7	21.8	27.6	16.7	29.9	38.1
<u>Zr</u>	102.4	130.1	125.5	136.4	150.1	173.0
<u>Nb</u>	6.1	6.7	6.5	6.4	8.5	12.0
<u>Hf</u>	1.7	2.8	3.4	3.5	3.8	4.2
<u>Ta</u>	0.23	0.30	0.29	0.28	0.43	0.59
<u>La</u>	10.2	15.5	19.0	33.8	24.8	18.7
<u>Ce</u>	22.7	37.0	39.4	80.8	61.7	50.1
<u>Sm</u>	2.8	4.6	5.3	7.6	6.5	7.3
<u>Eu</u>	0.99	1.75	1.80	2.09	1.88	2.23
<u>Tb</u>	0.58	0.81	0.86	0.79	0.91	1.21
<u>Yb</u>	1.80	2.40	2.76	2.19	2.60	3.58
<u>Lu</u>	0.27	0.38	0.43	0.31	0.41	0.51

Table 3 Continued.

sample	TB - 1
field occurrence	volcanic
altered unaltered	altered
symbol in modeling diagram	<input type="checkbox"/>
SiO <sub>2</sub>	56.12
TiO <sub>2</sub>	1.23
Al <sub>2</sub> O <sub>3</sub>	14.66
Fe <sub>2</sub> O <sub>3T</sub>	9.75
MgO	5.42
CaO	4.92
Na <sub>2</sub> O	5.55
K <sub>2</sub> O	0.26
MnO	0.16
P <sub>2</sub> O <sub>5</sub>	0.36
LOI	2.03
TOTAL	100.46

Table 3 Continued.

sample	TB - 1
Rb	5.0
Ba	183.
Cs	--
Sr	534.
Pb	9.9
Th	3.4
U	1.24
Sc	25.9
V	184.
Cr	155.5
Co	80.
Ni	68.
Y	16.5
Zr	156.4
Nb	9.0
Hr	3.4
Ta	0.55
La	27.1
Ce	60.7
Sm	6.1
Eu	2.00
Tb	0.77
Yb	1.68
Lu	0.30

discrepancies are seen for some of the samples. These discrepancies may be attributed to a combination of alteration and/or crustal contamination.

From the  $Zr/TiO_2$  vs  $Nb/Y$  diagram, it is seen that the igneous rocks are subalkaline in character. The igneous rocks show mixed calc-alkaline and tholeiitic affinities when the data are plotted on the Jensen diagram (Figure 24); however, it is noted that the mafic and intermediate hypabyssal bodies are tholeiitic while the Alder volcanics, the Red Rock Rhyolite, and the Pine Mountain Porphyry are calc-alkaline. The mafic rocks seem to be evolved as they straddle the subalkaline basalt-basaltic andesite boundary on the  $Zr/TiO_2$  vs  $Nb/Y$  diagram. There seems to be a paucity of intermediate samples in the Alder section of the Mazatzal Mountains. The data suggest that there is a bimodal distribution of igneous samples; however, this may be the result of sampling bias. Noll (1988) indicates that intermediate igneous rocks dominate in the Alder Group of Tonto Basin.

Five felsic samples have been analyzed (Table 7). The samples of the Red Rock Group classify as rhyolites, and the two samples of the Pine Mountain Porphyry intrusive are rhyodacites (Figure 22). One of the porphyry samples appears to be altered. The chemical affects of this alteration are similar to those which are observed in Proterozoic felsic volcanics from Sweden (Baker and de Groot, 1983) (Appendix I).

#### Tectono-Magmatic Diagrams for Mafic Rocks

Immobile trace elements have been used to characterize the volcanics from specific tectonic settings (Pearce and Cann, 1973). This approach is used in this section to compare the Alder mafic rocks

Figure 22.  $Zr/TiO_2$  vs  $Nb/Y$  diagram for the classification of volcanic rocks (after Winchester and Floyd, 1977). Symbols are explained in figure 21.

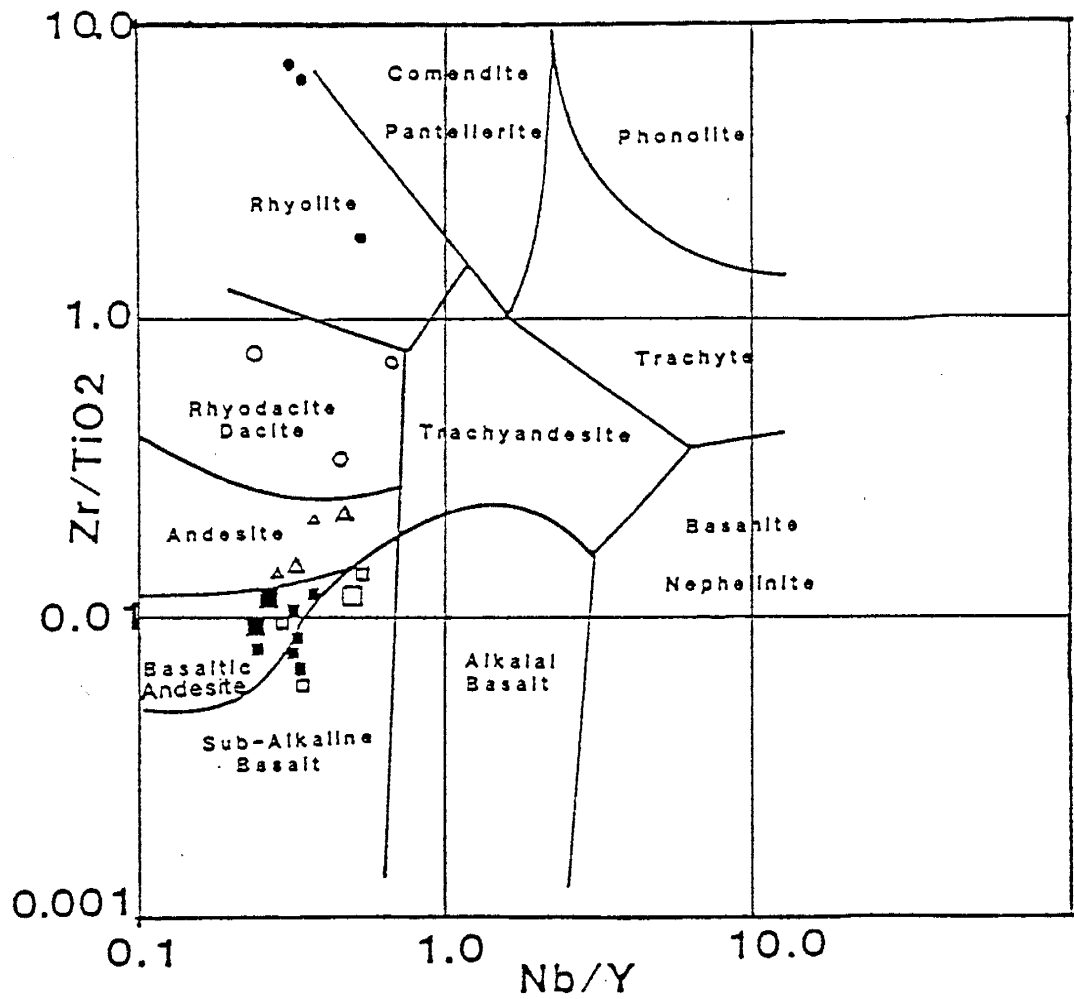


Figure 23. SiO<sub>2</sub> vs Nb/Y diagram for the classification of volcanic rocks (after Winchester and Floyd, 1977). Symbols are explained in figure 21.

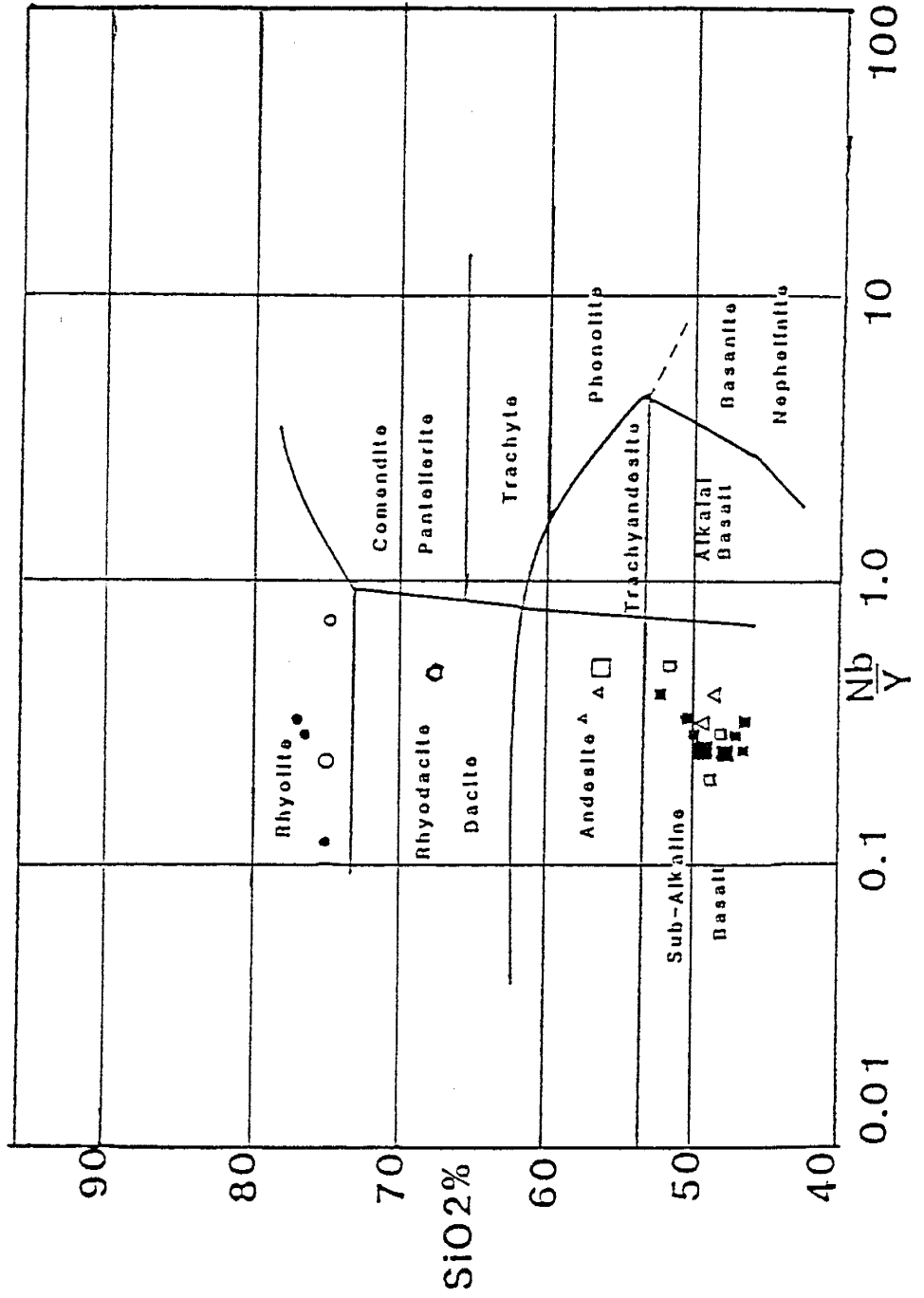
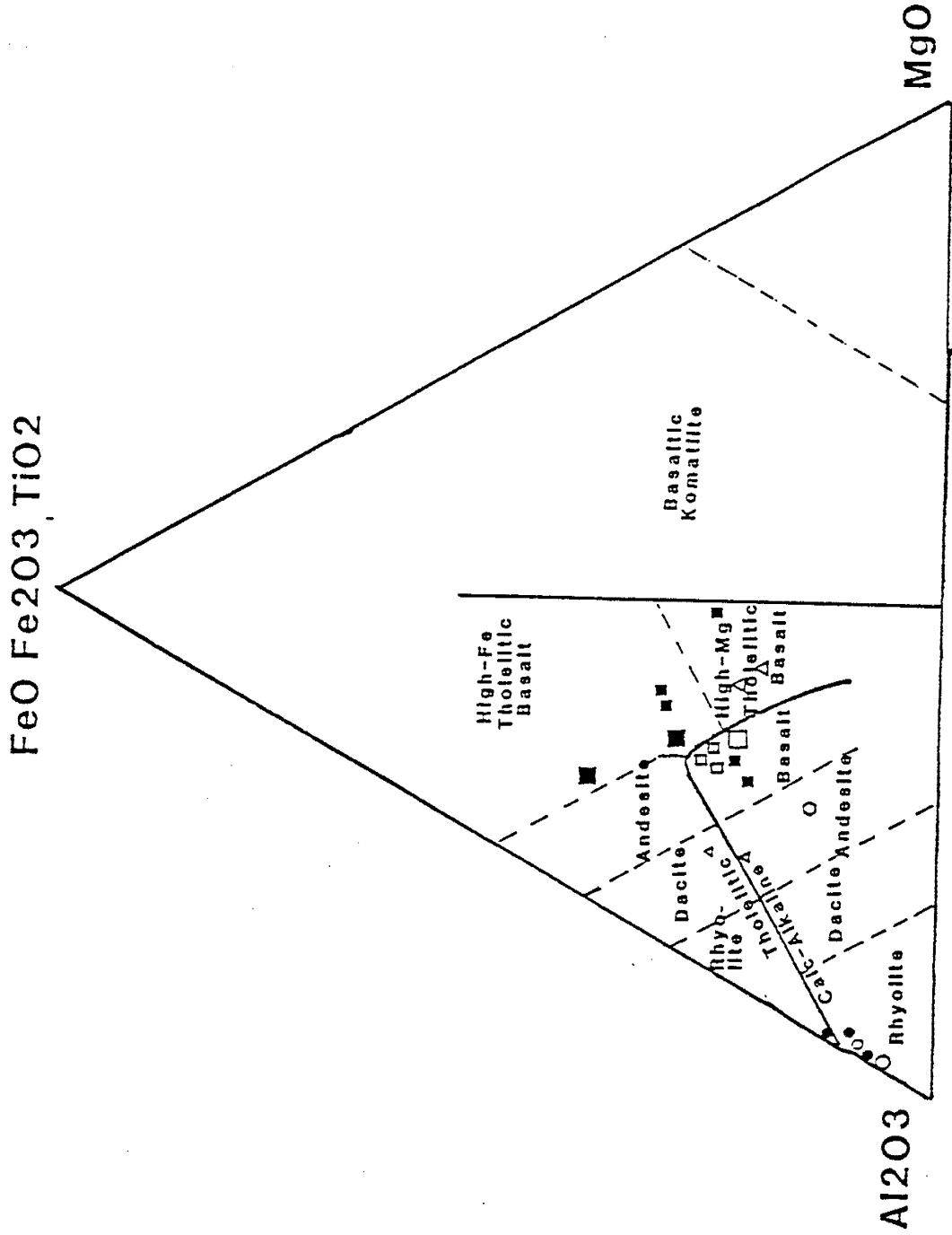




Figure 24. Jensen cation plot for the classification of igneous rocks (Jensen, 1976). Symbols are explained in figure 21.



to volcanics which are typical of modern tectonic settings. The mafic dikes and sills appear to be chemically distinct from the mafic volcanics. The older mafic volcanics are geochemically similar to continental arc basalts. In all of the discriminant diagrams which are presented below, fields which represent the distribution of the intrusive samples are shown in order to demonstrate the geochemical distinctiveness of these rocks.

Some of the mafic samples have significantly lower Y and HREE abundances. It is proposed (next section) that these trends result from low degrees of batch melting (BM) of a mantle source which has a higher proportion of garnet. These samples are designated by special symbols (Figure 21) in geochemical diagrams, and in future discussion, the mantle source of these samples is referred to as the high garnet source.

The Ti/Zr vs Zr/Y diagram (Figure 25) shows that the dikes, sills, and the samples which are derived by low degrees of BM of a high garnet source have higher Zr/Y ratios. In fact, the latter samples plot on the extreme outer margin of the diagram. In general, the intrusives plot in the active continental margin field while the volcanics tend to plot in the fields of overlap of continental island arc basalts and active continental margin basalts.

The distinction between the intrusives and the volcanics can be seen in various tectono-magmatic diagrams which are based on relative incompatible element abundances. The  $TiO_2$  vs Zr diagram (Pharoah and Pearce, 1984) (Figure 26) shows that the intrusives plot as within plate basalts while the volcanics appear to be arc related. The

Figure 25. Ti/Zr vs Zr/Y diagram (Condie; personal communication) which shows the distribution of the Alder mafic samples. Symbols are explained in figure 21.

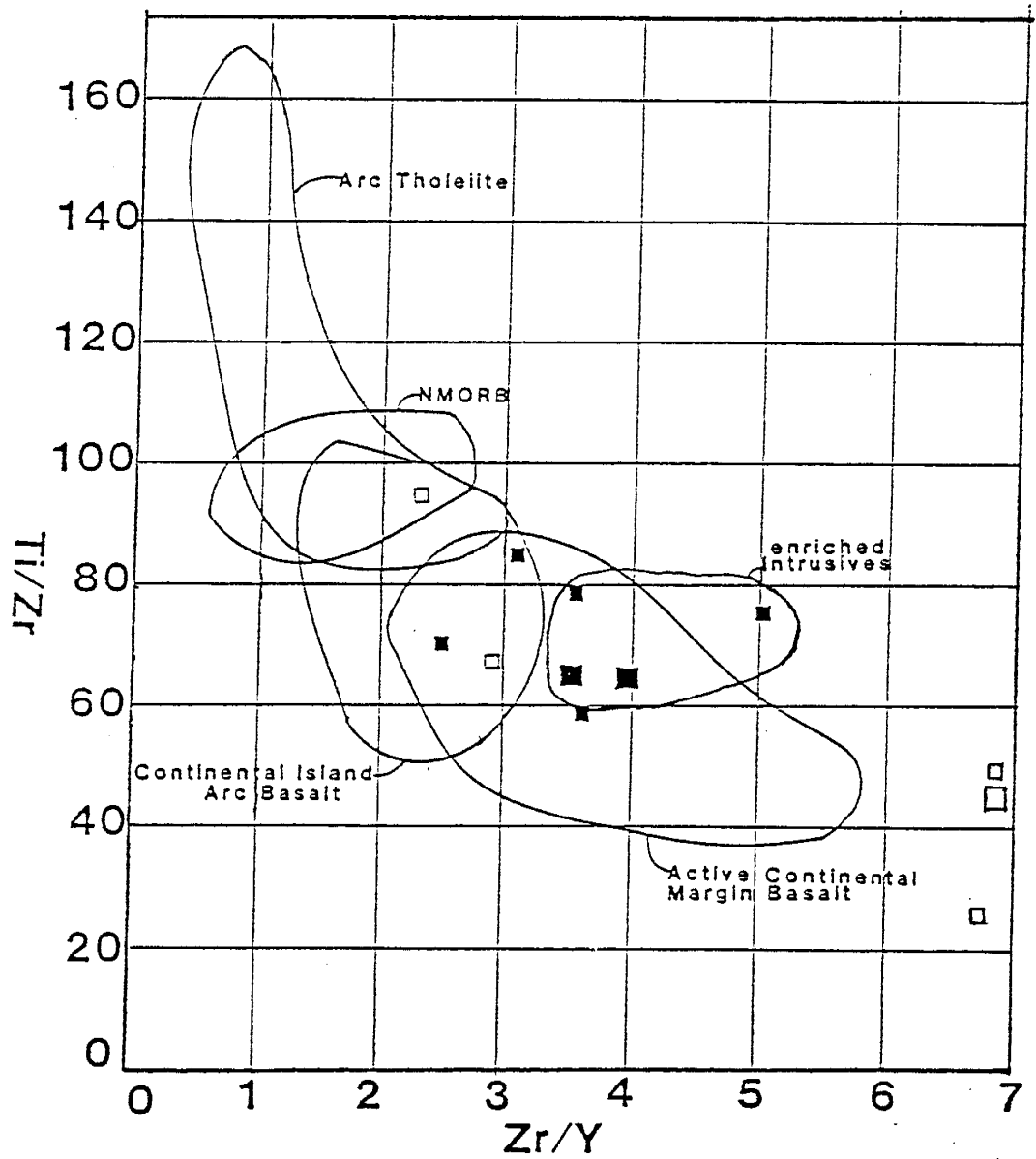


Figure 26. Zr vs  $\text{TiO}_2$  discriminant diagram (Pharoah and Pearce, 1984) which shows the distribution of Alder igneous samples of all compositions. Symbols are explained in figure 2L.

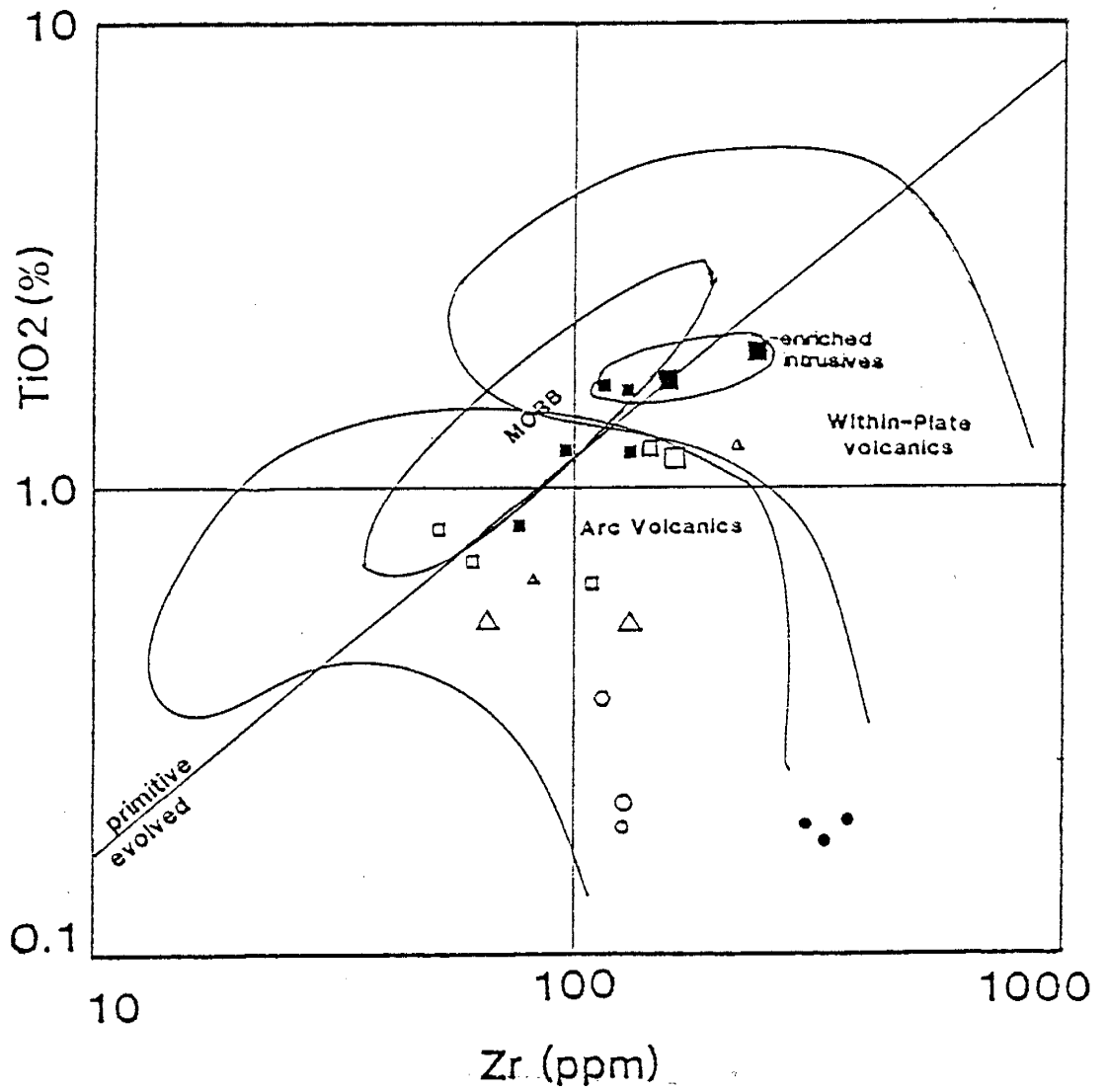


diagram accommodates volcanics of all compositions; therefore, all of the Alder igneous samples are plotted in Figure 26.

The Th vs Hf diagram (Wood et al., 1979) (Figure 27) also shows that the intrusives are more similar to within plate basalts. It should be noted that the high Th abundances of some of the samples may be attributed to alteration (Appendix I); however, even if the Th abundances of the altered samples are changed, the Hf abundances are higher than those characteristic of arc related basalts. The older volcanics, once again, plot in the field of overlap of arc related and within plate related basalts.

Another diagram which is very effective in distinguishing within plate volcanics is Ti-Zr-Y diagram (Pearce and Cann, 1973). This diagram (Figure 28) also shows the enriched tendencies of the intrusives. Once again, the samples which are related by low degrees of BM to the high garnet source are displaced from the other samples with respect to Y abundances. The majority of the volcanics plot in the field of overlap of arc basalts and MORB.

The V vs  $TiO_2$  diagram (Shervais, 1982) (Figure 29) shows that the intrusives plot at higher Ti/V ratios than the older volcanics. The intrusives plot in a field which is characteristic of continental rift basalts. These samples plot predominantly in the primitive field in Figure 26, and similarly, they have high V abundances ( $\sim 300$  ppm); therefore, it is unlikely that very much magnetite has fractionated from the parent liquids of these samples. This suggests that the high Ti/V ratios of the intrusives indicate less oxidizing conditions than those which are seen in arc magmas.

Figure 27. Th vs Hf tectonic discrimination diagram (Wood, et. al., 1979) which shows the distribution of Alder mafic samples. Symbols are explained in figure 21.

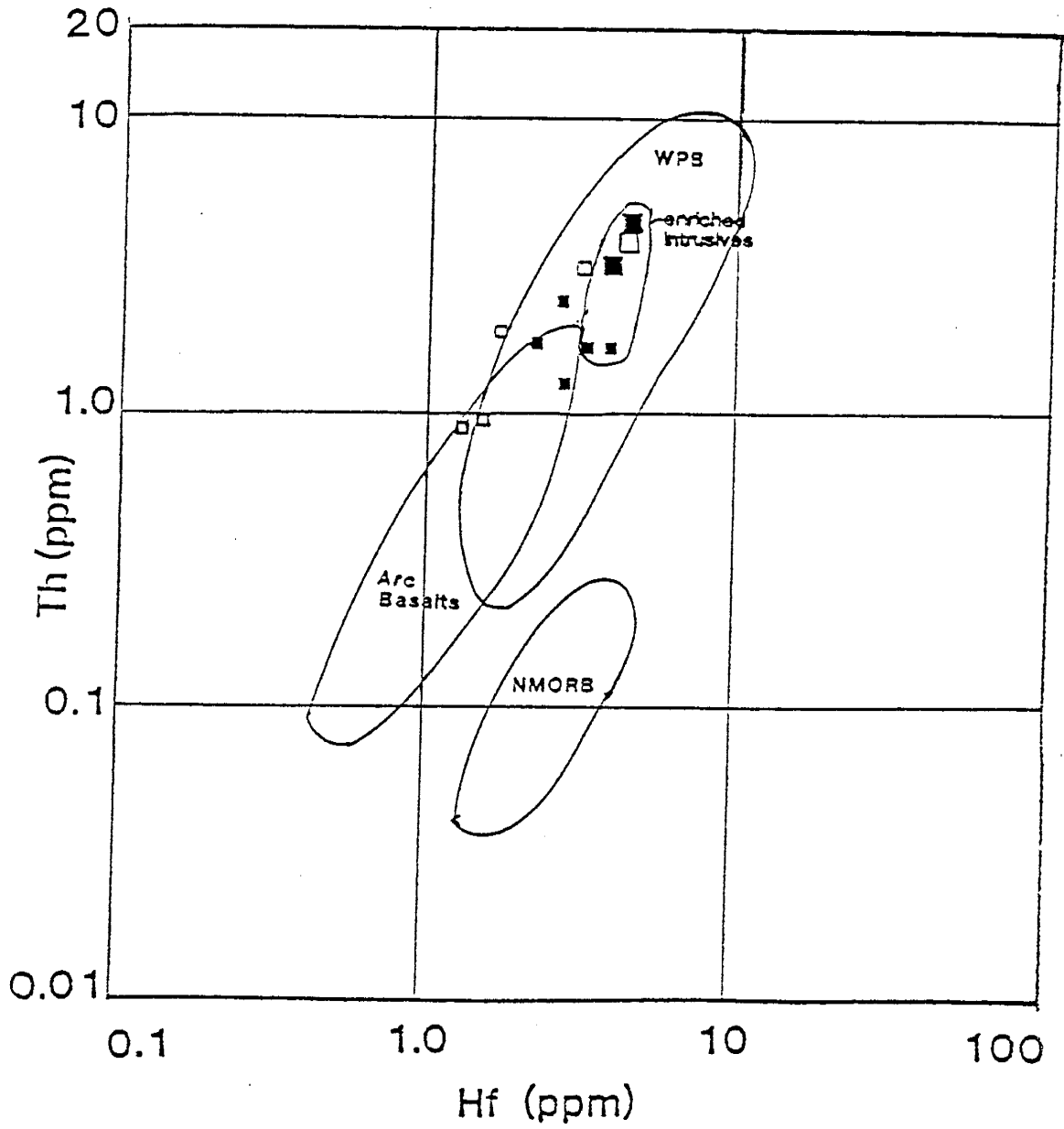


Figure 28. Ti-Zr-Y\*3 tectonic discrimination diagram (Pearce and Cann, 1973) which shows the distribution of Alder mafic samples. Symbols are explained in figure 21.

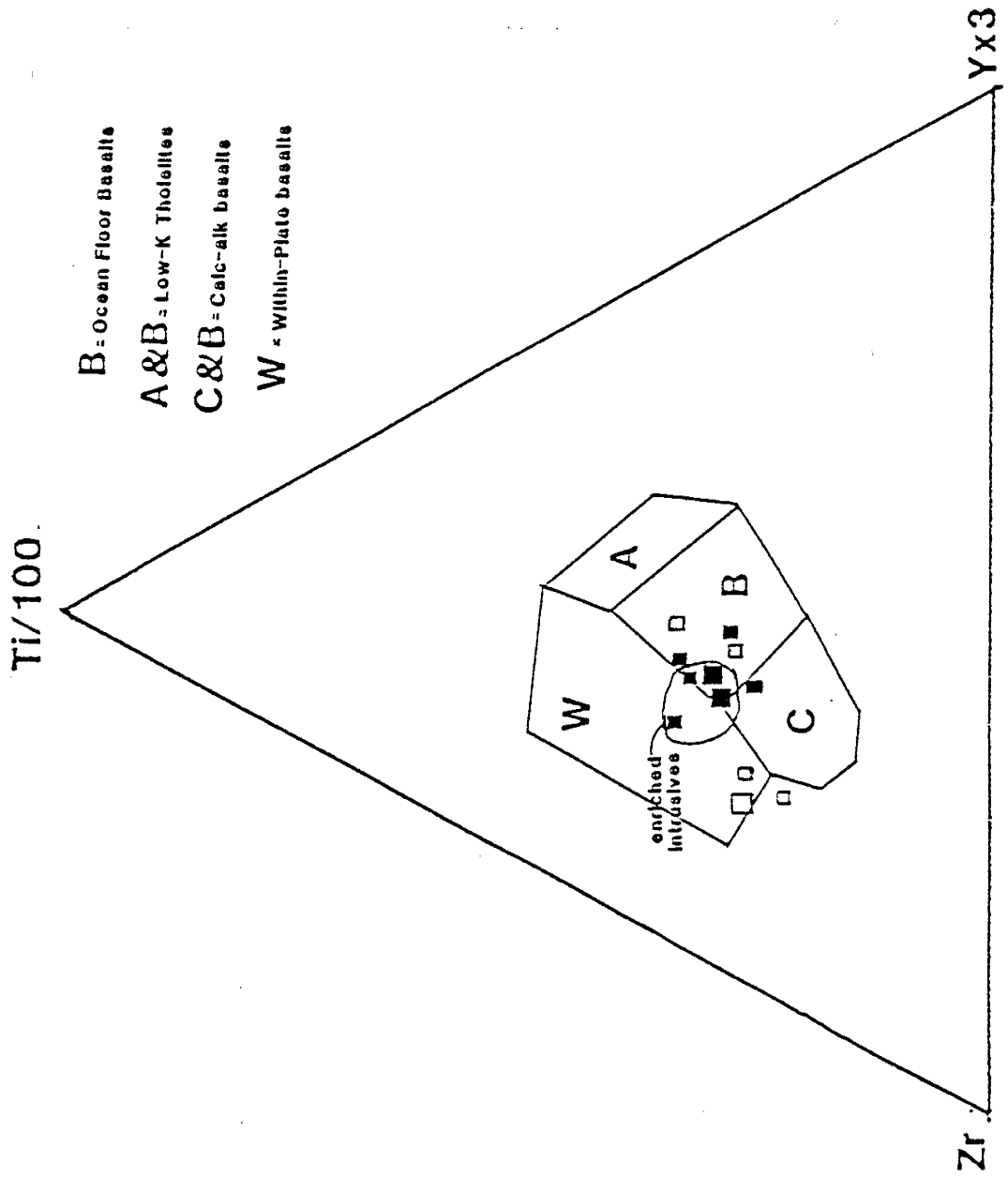
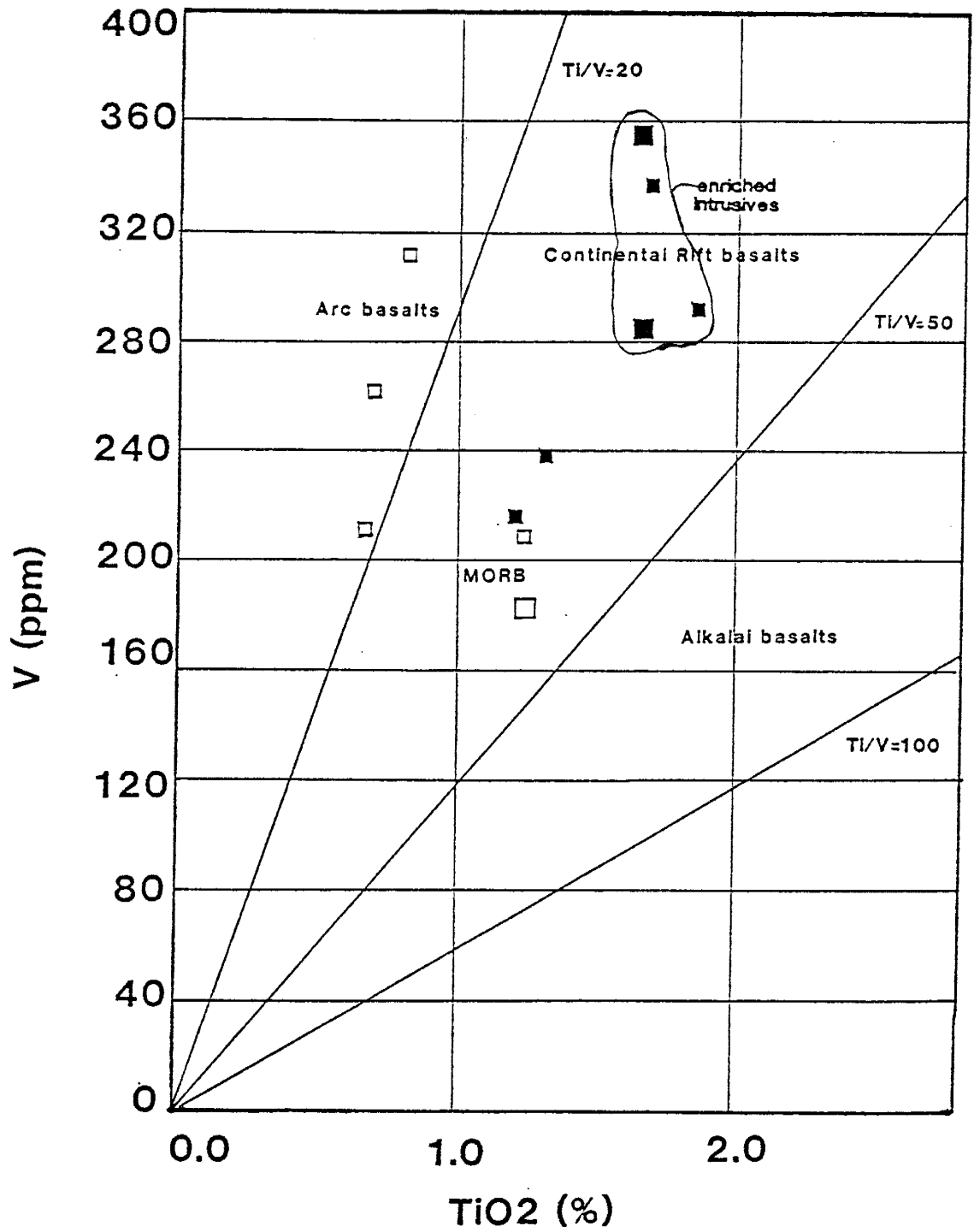


Figure 29. V vs TiO<sub>2</sub> tectonic discrimination diagram (Shervais, 1982) which shows the distribution of Alder mafic samples. Symbols are explained in figure 21.





Another indicator of tectonic setting is the MORB normalized diagram (Pearce, 1983) (Figures 30-32). On MORB normalized diagrams, the most mobile elements (Sr, K, Rb and Ba) are placed on the left of the diagram. The rest of the elements are placed in order of decreasing incompatibility, with respect to a garnet lherzolite mineralogy, from left to right. The patterns in these diagrams result from normalizing the abundances of the elements in a sample to those in average MORB. It is found that the rocks which are derived from tectonic settings other than MOR have relative enrichments compared to MORB which show up as humps or spikes in these patterns. These "enrichments" are the result of the interaction of processes and/or source types which are unique to each tectonic setting. It is noted that fractional crystallization (FXL) and partial melting variations typically affect the level but not the shapes of these patterns.

By comparing the patterns in Figure 30 to those of the Alder mafics in Figures 31 and 32, it can be seen that the Alder igneous rocks are similar to volcanics erupted at active continental margins and/or continental island arcs. The high normalized LIL/HFS element ratios of the Alder patterns are diagnostic of convergent plate boundaries (Pearce, 1983). Positive Ce and Sm anomalies, which may reflect crustal contamination (see later section), appear to be related to subduction zone components. These anomalies may reflect the melting of subducted sediments (Pearce, 1983; and James, 1981). Basalts which are derived from mantle sources which have a within plate component have normalized Nb-Ta/Zr-Hf ratios which are greater than 1 (see the WPB pattern in Figure 31).

Figure 10. MORB normalized diagram (Pearce, 1983) which shows the patterns of typical basalts from different tectonic settings.

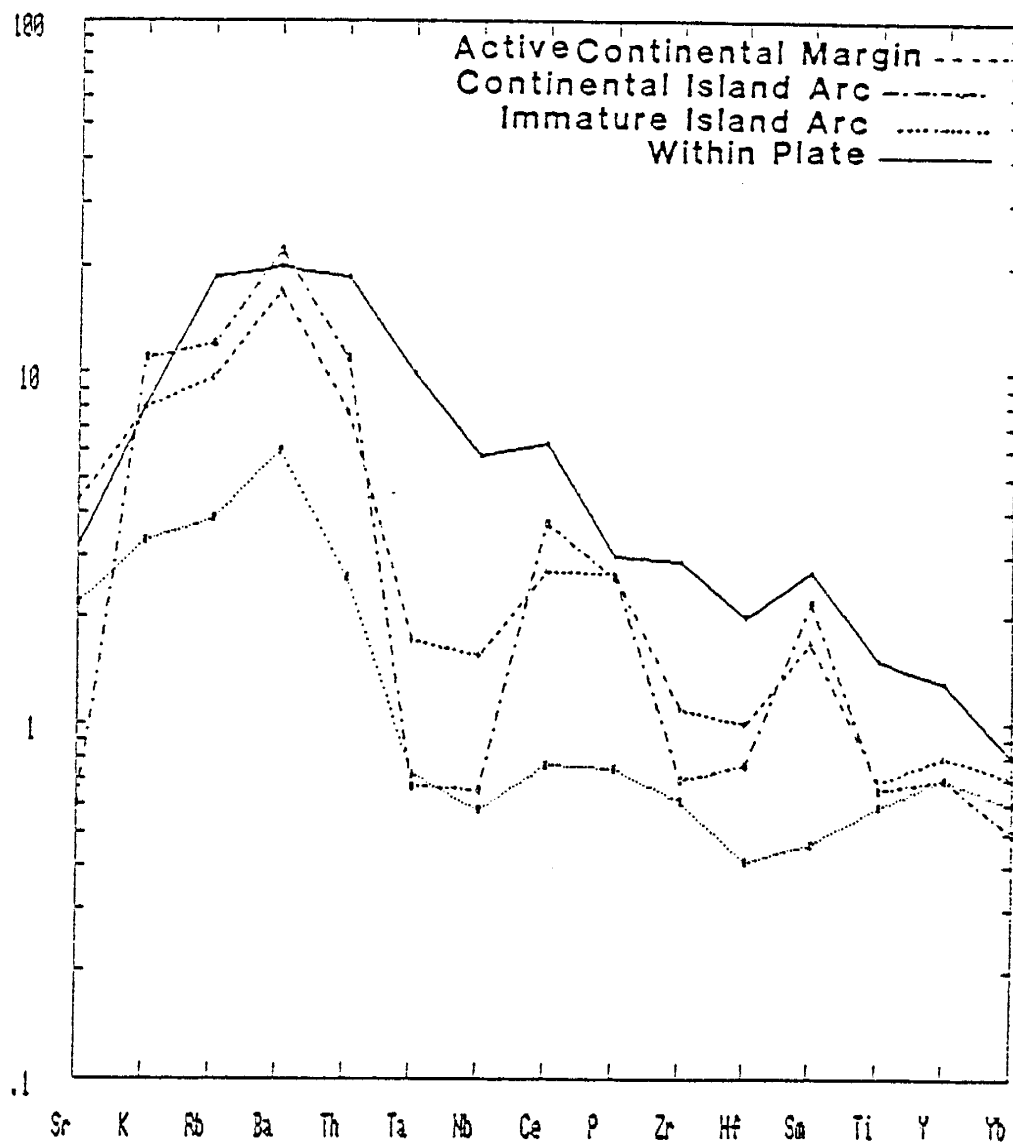


Figure 31. MORB normalized diagram (Pearce, 1983) which shows the patterns of four of the Alder volcanics. The pattern of the average of the four enriched intrusives (figure 32) is also shown.

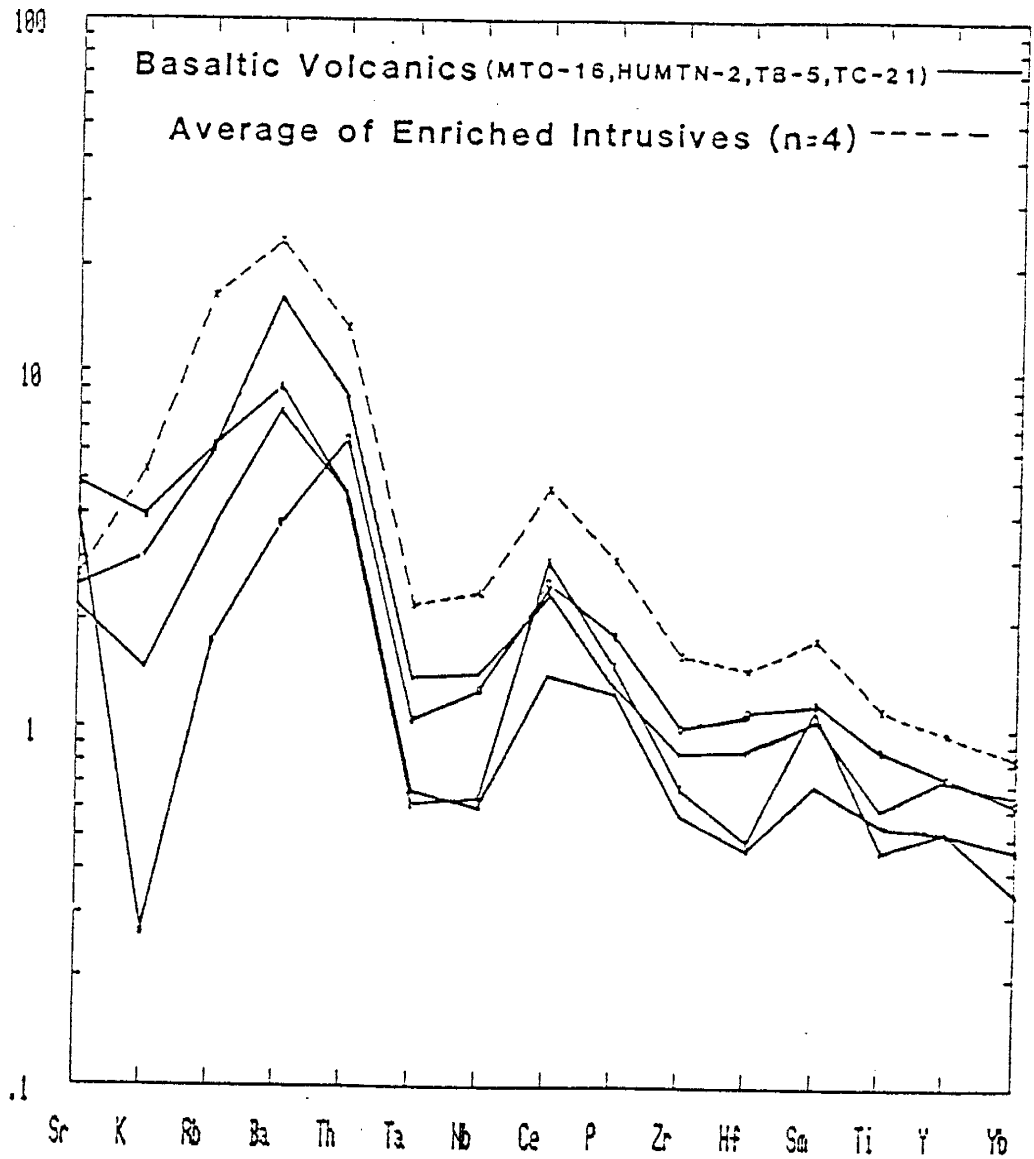


Figure 32. MORB normalized diagram (Pearce, 1983) which shows the patterns of the four enriched intrusive samples. The pattern of the average of the four volcanics in figure 31 is also shown.

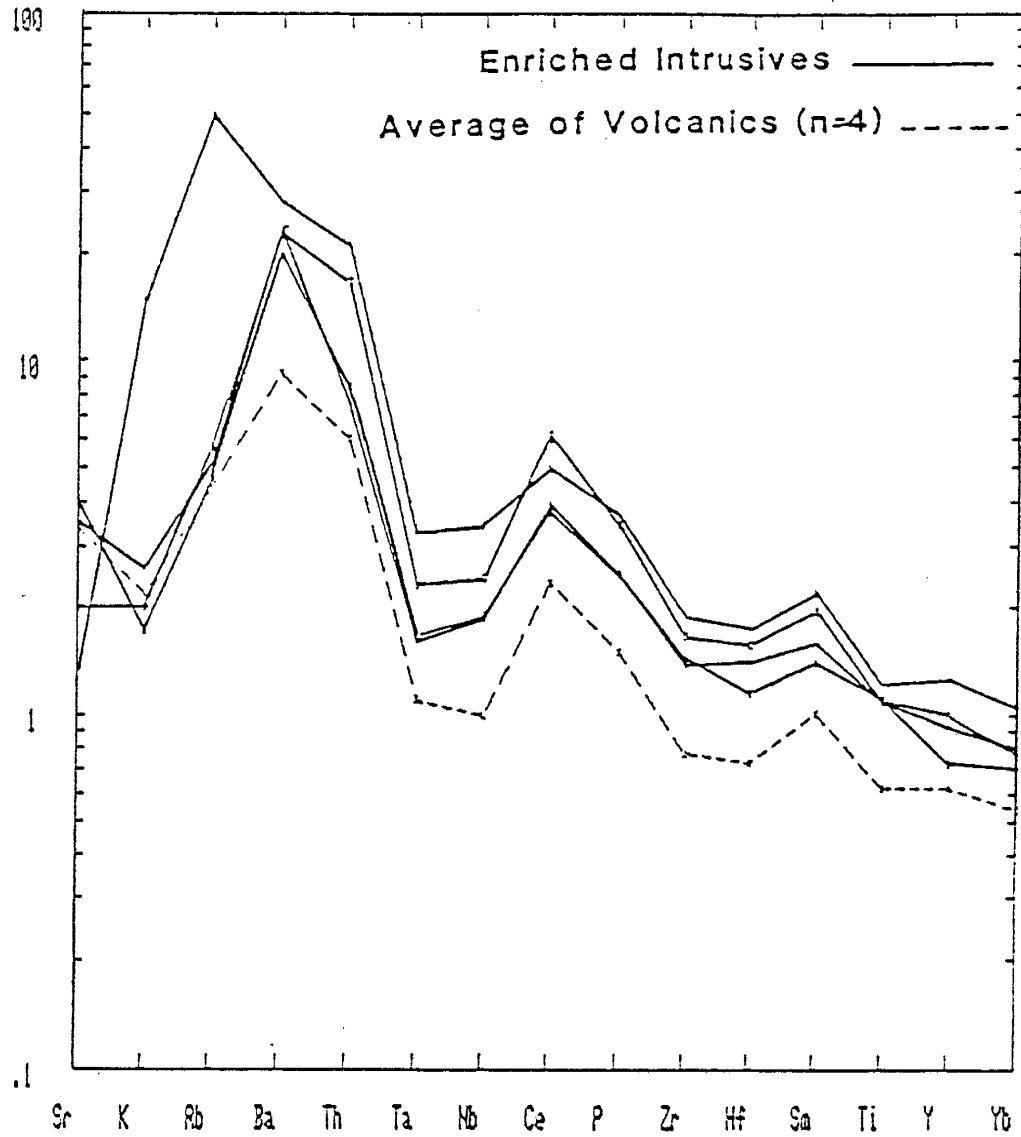
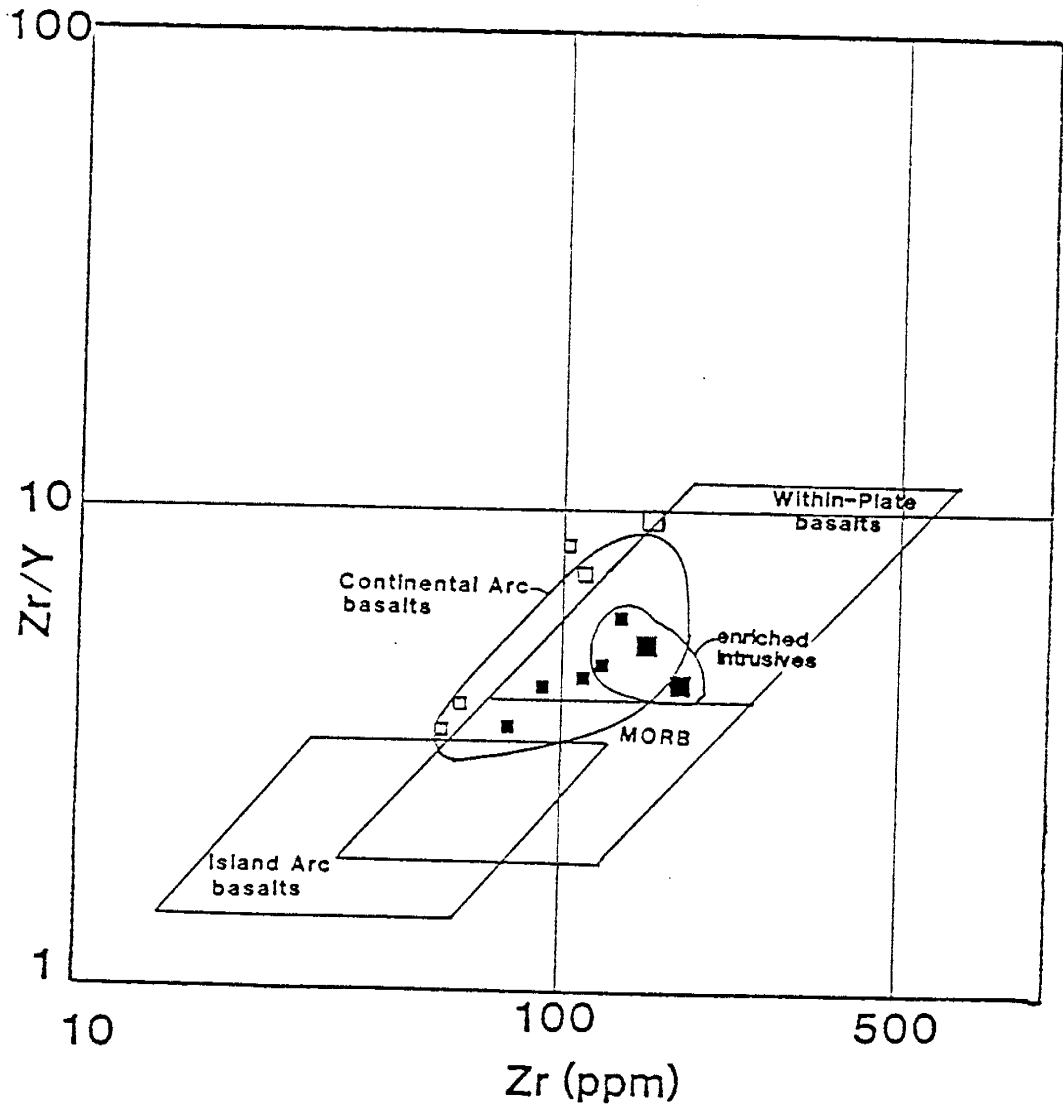


Figure 33. Zr/Y vs Zr tectonic discrimination diagram (Pearce, 1983) which shows the distribution of Alder mafic samples. Symbols are explained in figure 21.



In Figure 31, the MORB normalized patterns for the older volcanics are shown while the patterns of the intrusives are shown in Figure 32. It is interesting that the older volcanics are more like basalts from continental island arcs while the intrusives are more similar to basalts from active margins.

The Zr/Y vs Zr diagram (Pearce and Norry, 1979) is very sensitive to within plate enrichment in the source of basalts (Figure 33). The Alder basalts plot in the field of overlap of within plate basalts and continental arc basalts. It is noted that the intrusives and the samples which are related to the high garnet source by low degrees of BM have higher Zr/Y ratios; however, the intrusives also tend to have higher Zr values.

#### Mantle Source

Petrogenetic modeling of the mafic rocks is used to constrain the chemical composition and the mineralogy of the mantle source. In an effort to determine if garnet was a residual phase in the mantle source during melting, the basalts are plotted on various graphs that use elements which are compatible with garnet (Figures 34 and 35). Batch melting curves for enriched, depleted, and primordial mantle are also drawn on the graphs. The batch melting curves are calculated by assuming a typical garnet lherzolite mineralogy (Table 4b). The element abundances for undepleted mantle (Table 4a) are after Wood (1979). The abundances of enriched and depleted mantle are taken from Condie (personal communication). It has been mentioned that Figure 22 suggests that the mafics are relatively evolved. The evolved nature of the basalts is also borne out by the Magnesium numbers and the Ni

Figure 34. Y vs Hf diagram which compares primordial (undepleted) mantle and enriched mantle as likely sources for the mafic igneous rocks. Symbols are explained in figure 21.

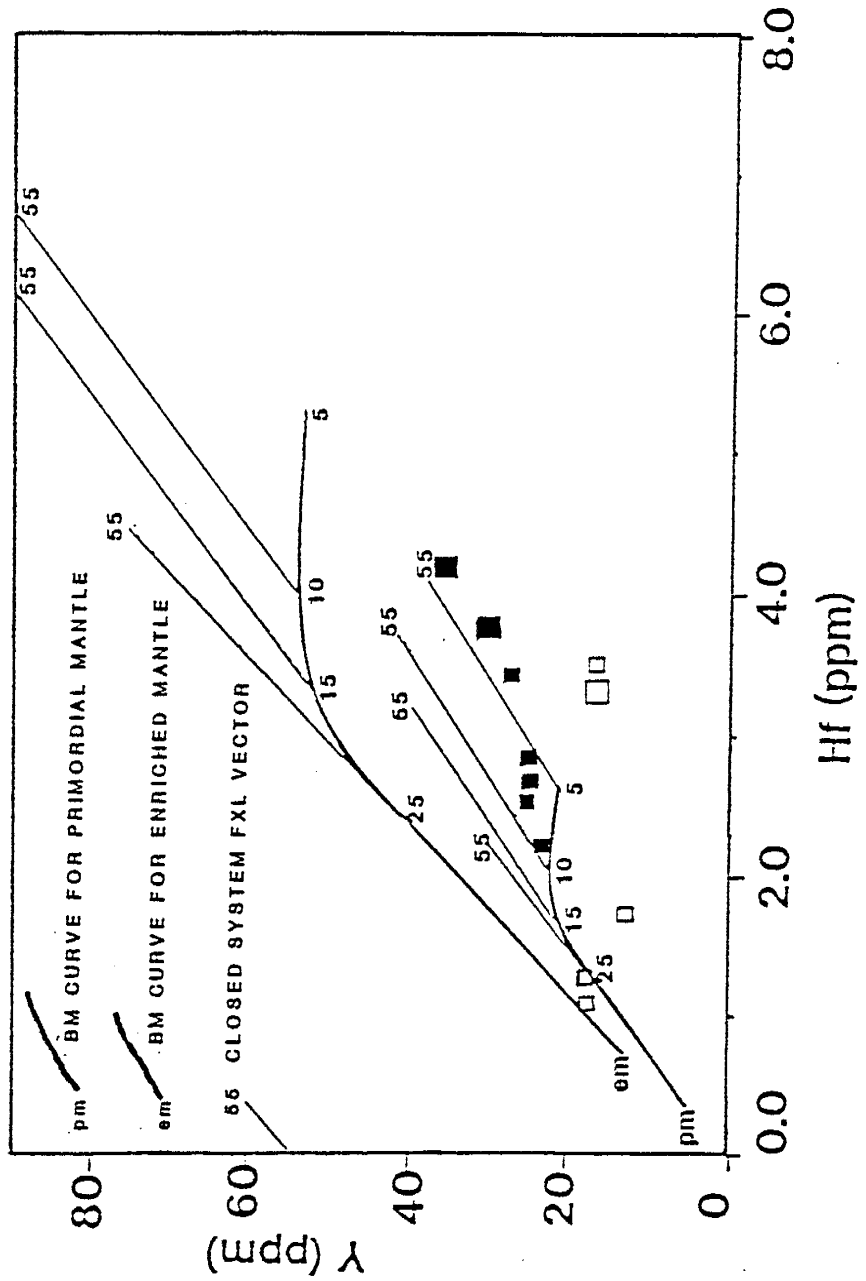


Figure 35. Nb vs Yb diagram which compares primordial (undepleted) mantle and depleted mantle as likely sources for the mafic igneous rocks. Symbols are explained in figure 21.

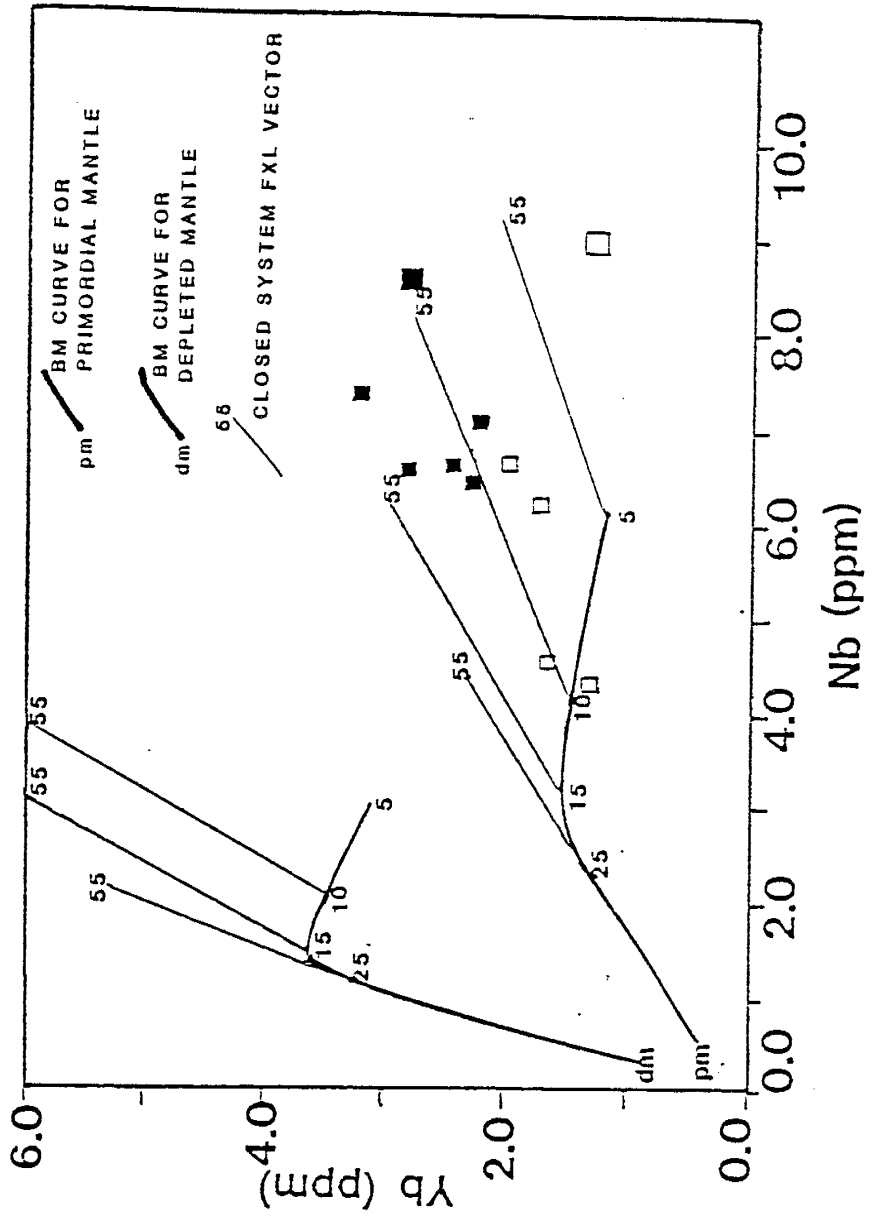




Table 4a. Mantle source types used in figures 34 and 35, and compared with calculated mantle source (Table 5a) in petrogenetic models.

element	primordial mantle (Wood)	depleted mantle	enriched mantle
Th	0.10	0.02	0.50
Nb	0.62	0.31	3.0
La	0.70	0.30	4.0
Hf	0.36	0.34	0.70
Zr	11.0	9.0	40.0
Sm	0.39	0.6	1.0
Ti	1526.0	1180.0	3000.0
Y	0.38	0.87	0.55
Yb	4.90	4.0	12.0

Table 4b. Modal and melting proportions used for batch melting curves of mantle sources in figures 34 and 35.

mineral	mode	melt
olivine	0.60	0.05
clinopyroxene	0.20	0.45
orthopyroxene	0.15	0.05
garnet	0.05	0.45

contents of the unaltered rocks which range from 41 to 55 and 14 to 66, respectively (Table 3). Since the mafics are evolved, 55% closed system fractional crystallization vectors which use a 4:1 ratio of olivine and clinopyroxene are also plotted on the diagrams in order to relate the samples to the batch melting curves.

Figures 34 and 35 are graphs of Y vs Hf and Nb vs Yb, respectively. The diagrams show that with respect to the HFSE and the HREE, the most likely source for the mafic rocks is most similar to undepleted mantle. It can be seen that the undepleted batch melting curve and the FXL vectors cover the spread of basalts when garnet is present in the residue during melting. The batch melting curves of depleted, undepleted, and enriched mantles are too enriched in Y and Yb if garnet is not present in the residue during melting. There is a significant spread of samples along the trends of the FXL vectors, (especially in Figure 34), and some of the samples lie very close to the batch melting curve. It is doubtful that basalts with such low Ni contents could be so closely related to the mantle batch melting curve. These rocks are not even the least evolved of those which are analyzed. The spread along the trends of the FXL vectors may be explained by a variable amount of garnet in the mantle residue during batch melting. Since it appears that most of the samples are related by similar degrees of batch melting, a variable proportion of garnet in the residue can best be explained by a variable amount of garnet in the mode of the mantle source. The batch melting curve which is calculated by assuming a mode with 5% garnet (Table 4b) seems to satisfactorily explain the distribution of most of the basalts. The samples which appear to relate to a source with a higher proportion of

garnet are indicated by open symbols (Figure 21) in geochemical diagrams.

From the information gathered in Figures 34 and 35, a specific mantle source composition is calculated from one of the Alder mafic samples. The sample which is used to calculate the source composition is MT0-16 (Table 3). In order to calculate the source composition, a primary mantle melt must first be calculated from MT0-16. Grove and Baker (1984); and Green and Ringwood (1972) have determined that the calc-alkaline fractionation trend results from the early shallow level FXL of an assemblage which is dominated by olivine and clinopyroxene; plagioclase crystallizes in reduced proportions. The low Ni contents of the mafic samples suggest that a high proportion of olivine and clinopyroxene FXL has occurred; therefore, an assemblage which involves the shallow level FXL of olivine, clinopyroxene, and plagioclase (Table 5b) is assumed to simulate the evolution of primary melts to the mafic samples. Table 5a shows the chemical composition of the primary mantle melt which is calculated from MT0-16 by assuming 35% closed system FXL of the crystallization assemblage at 1170°C.

This melt is then used to calculate the source composition by solving for "Co" in the batch melting equation (Appendix H). In the calculation, many different values for F are tested in the equation. The value of F which gives the closest match with respect to the HREE and the HFSE abundances of the calculated source composition and the primordial mantle composition is considered to be the best estimate of the degree of mantle BM which is needed to derive the parent liquid of MT0-16. MT0-16 appears to be one of the samples which relates to a mantle source which has more than 5% garnet. As a result, the source

Table 5a. Results of mantle source calculation (see text for explanation)

element	Cl for mantle source calculation; calculated by FXL (table 5b) from MTO-16	Co-calculated mantle source at 1250°C (F = 0.3)	undepleted mantle (table 4a)
Th	0.59	0.19	0.096
La	4.0	1.2	0.7
Ce	9.3	2.8	---
Sm	1.58	0.49	0.36
Eu	0.57	0.18	---
Tb	0.31	0.11	---
Yb	0.90	0.37	0.38
Lu	0.12	0.05	---
Ti	3347.0	1107.0	1526.0
Y	10.7	3.9	4.9
Zr	34.1	10.7	11.0
Nb	2.7	0.9	0.62
Hf	0.75	0.25	0.36
Ta	0.08	0.03	---
Ni	524.0	1890.0	2000.0

Table 5b. Mafic FXL assemblage; used to calculate C1 (table 5a; F = 0.65)  
from MTO-16 at 1170°C

mineral	proportion
olivine	0.6
clinopyroxene	0.3
plagioclase	0.1

Table 5c. Modal and melting proportions of mantle source; used in  
petrogenetic modeling. Table also shows mode of the mantle residue  
after 30% BM.

mineral	high garnet		low garnet			
	mode	melt	residue	mode	melt	residue
olivine	0.6	0.05	0.81	0.6	0.05	0.78
clinopyroxene	0.15	0.45	0.03	0.2	0.45	0.07
orthopyroxene	0.10	0.05	0.13	0.15	0.05	0.15
garnet	0.15	0.45	0.03	0.05	0.45	-

is calculated by assuming a mode with 15% garnet. Table 5c shows the two modes which are used to model the samples designated by open and closed symbols in geochemical diagrams. In future discussion these two modes are referred to as the high garnet source and the low garnet source, respectively. Table 5c also shows the modes of the mantle residue after 30% BM of the high garnet and the low garnet sources.

Table 5a shows the calculated mantle source. 30% BM is needed to derive the mantle melt from the calculated source. The Ni content of a typical mantle ( $\approx 2000$  ppm) is derived in the calculation by assuming that melting has occurred at  $1250^{\circ}\text{C}$ . It should be noted that Th and the LREE are enriched, relative to primordial mantle, in the calculated source. These enrichments could be the result of crustal contamination and/or a subduction zone component. These two possibilities are evaluated in the discussion pertaining to the modeling of intermediate rocks.

Figures 36 through 39 show batch melting curves which are calculated from the source composition and the low garnet mode from Table 5. Vectors which represent 40% open and closed system FXL of the assemblage in Table 5b are also projected from different proportions of the BM curves. It can be seen that the basalts can be modeled satisfactorily by different degrees of BM followed by closed system FXL on the Zr/Y vs Zr diagram (Figure 36) and the Zr vs Ni diagram (Figure 37). It should be noted that the samples which are geochemically modeled with a high garnet source plot very close to the batch melting curve in Figure 36, yet the evolved nature of these samples is clearly shown in Figure 37.

Figure 36. Zr/Y vs Zr diagram which shows the distribution of mafic samples and the petrogenetic model for the samples which relate to the low garnet source (table 5c). See text for explanation. Symbols are explained in figure 21.

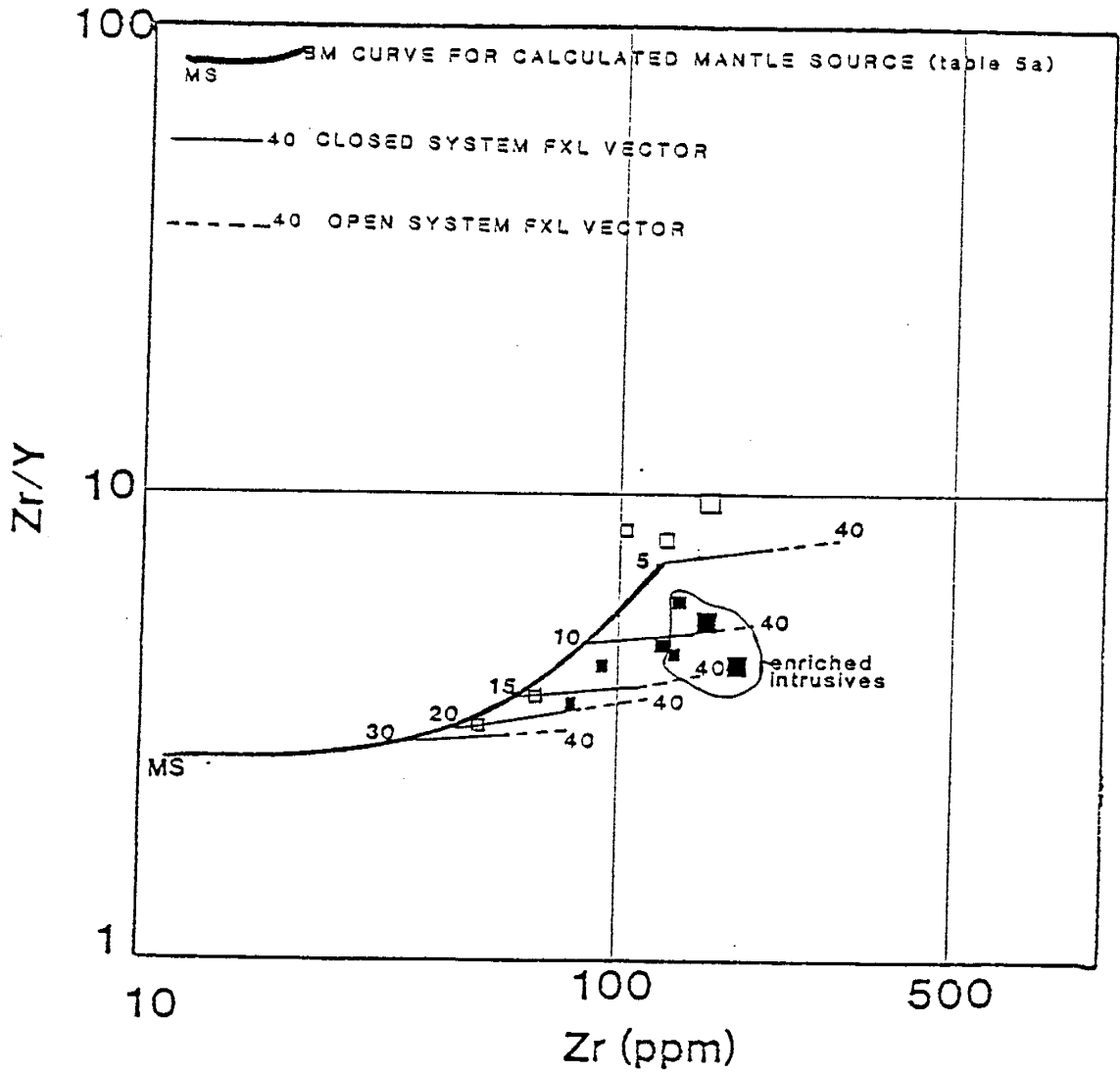


Figure 37. Zr vs Ni diagram which shows the distribution of mafic samples and the petrogenetic model for the samples which relate to the low garnet source (table 5c). See text for explanation. Symbols are explained in figure 21.

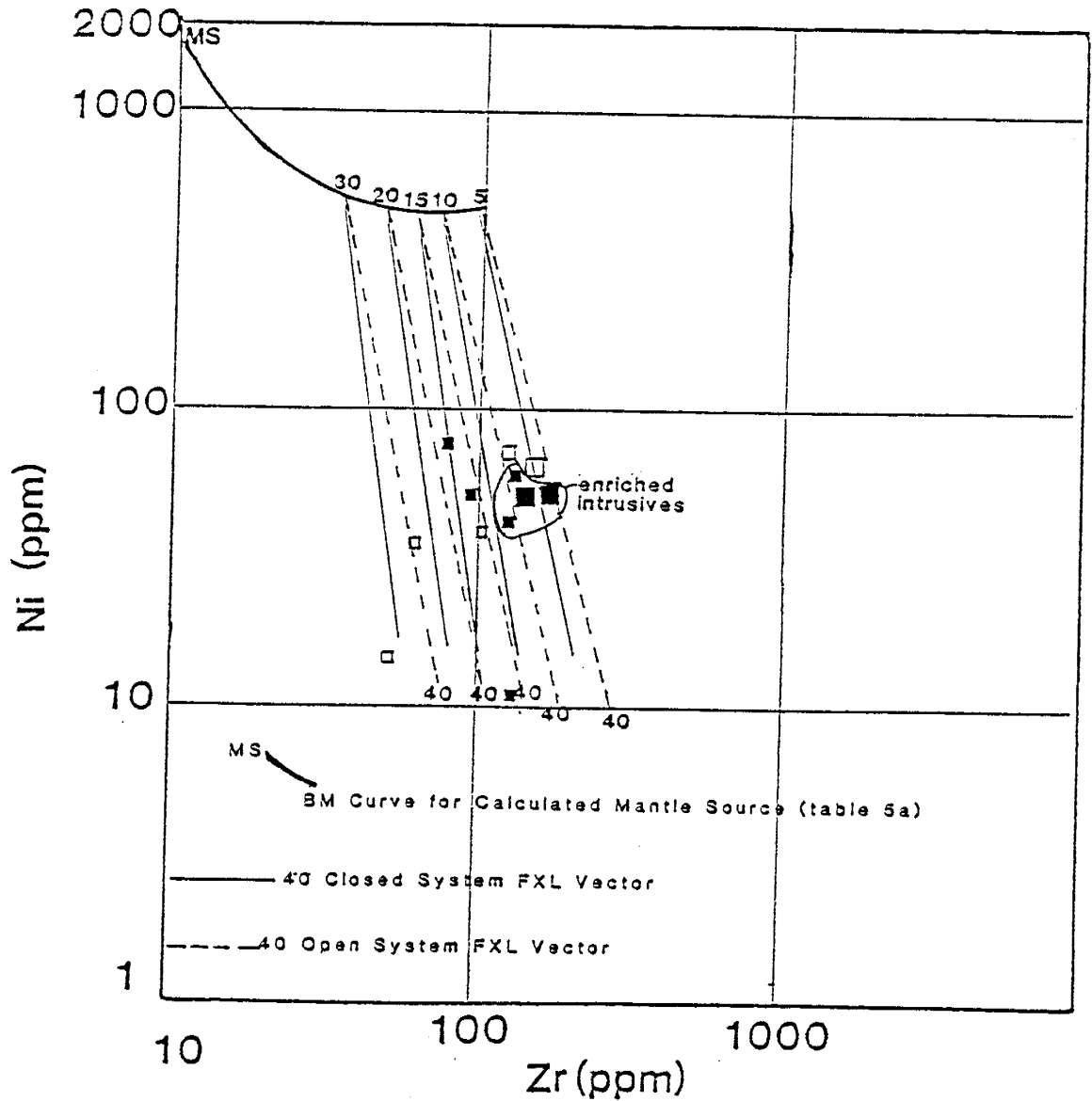




Figure 38. Zr vs  $TiO_2$  diagram which shows the distribution of mafic samples and the petrogenetic model for the samples which relate to the low garnet source (table 5c). See text for explanation. Symbols are explained in figure 21.

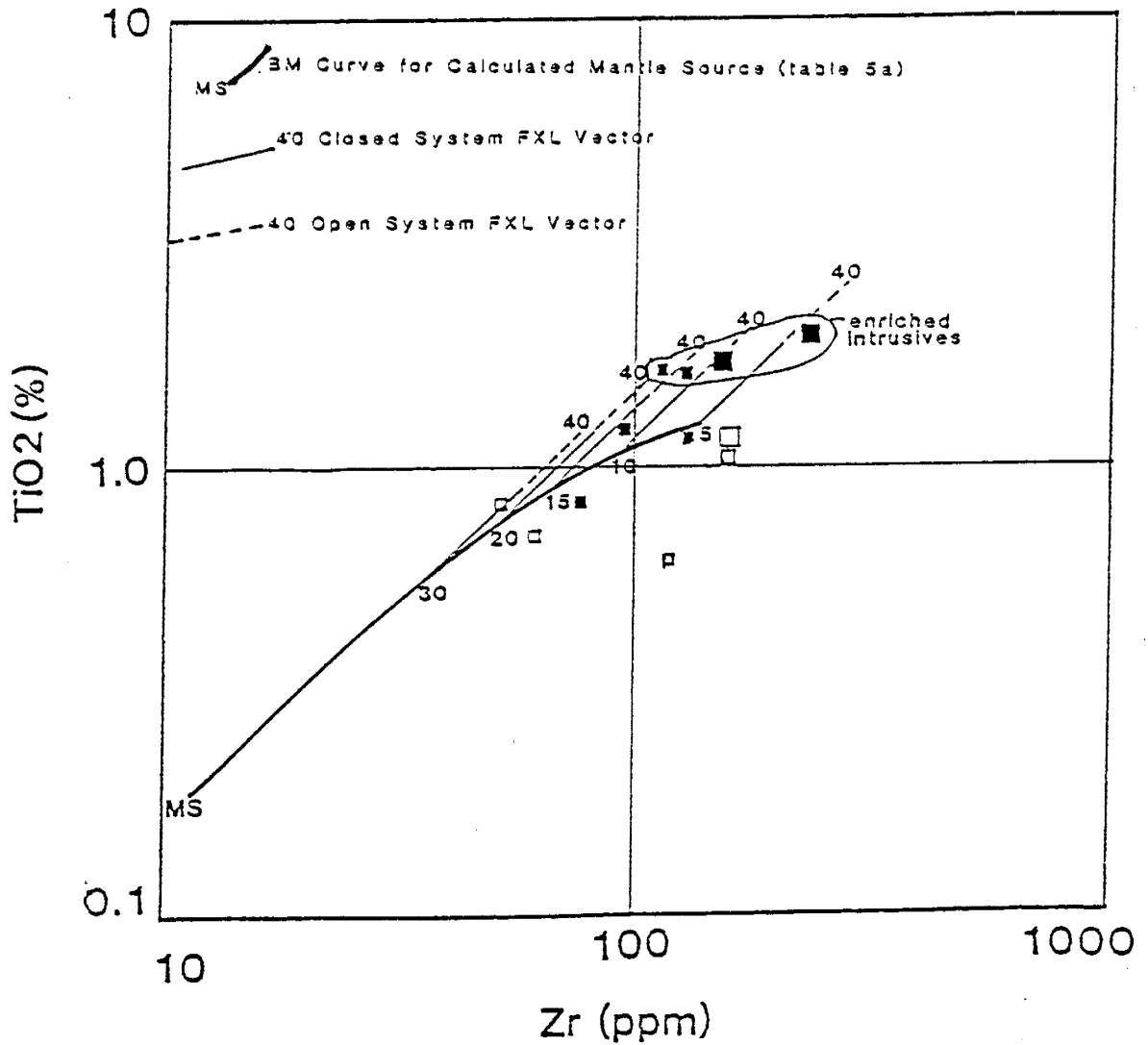
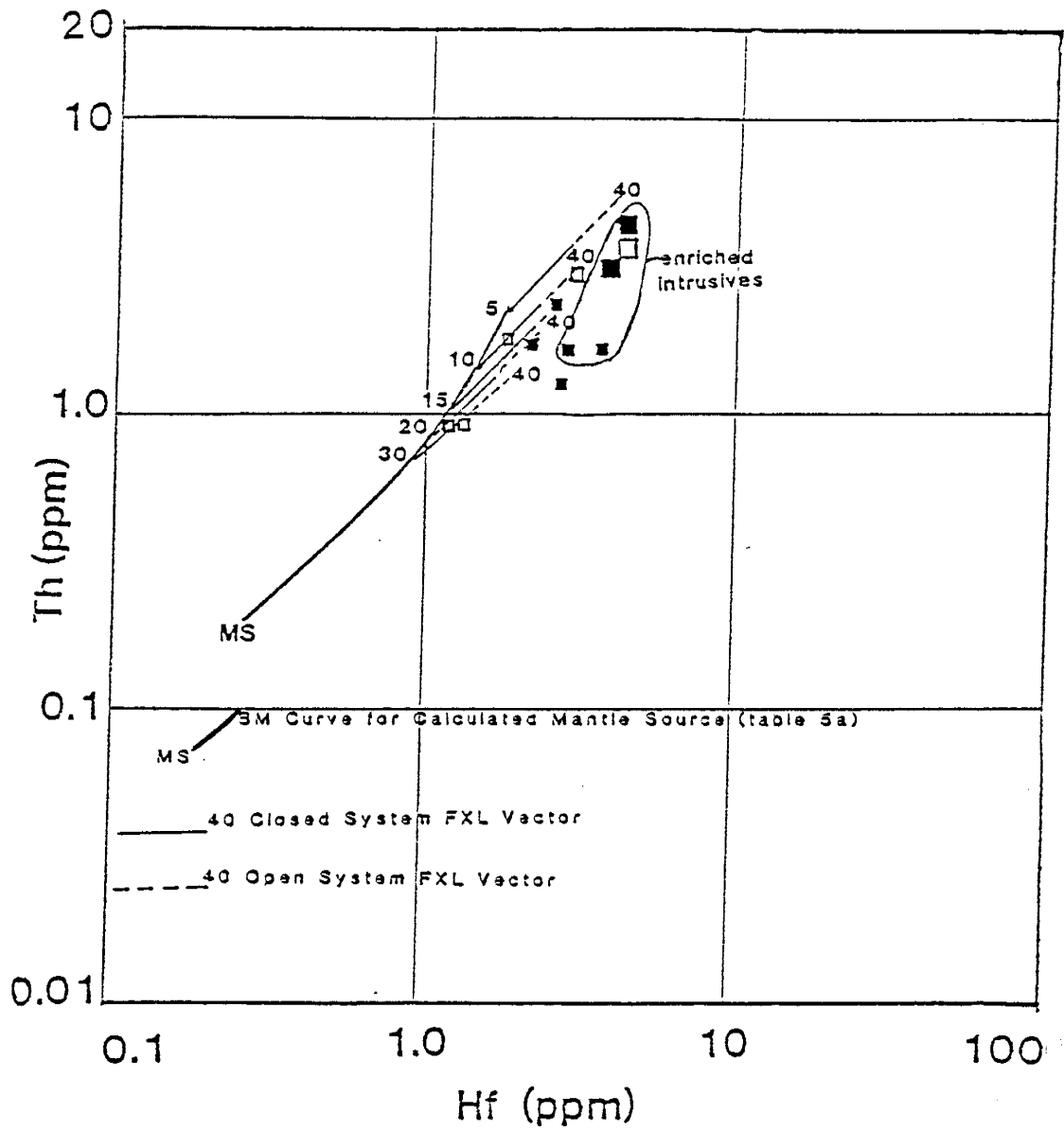


Figure 39. Th vs Hf diagram which shows the distribution of mafic samples and the petrogenetic model for the samples which relate to the low garnet source (table 5c). See text for explanation. Symbols are explained in figure 21.



The fields which represent the distribution of the intrusives cannot be modeled by closed FXL from the calculated batch melting curves on the Zr vs TiO<sub>2</sub> diagram (Figure 38) and the Th vs Hf diagram (Figure 39). Some of the samples on the Zr vs TiO<sub>2</sub> diagram plot below the batch melting curve. These samples plot in the evolved field (Figure 26) which indicates that they have been affected by magnetite fractionation.

The dikes and sills may be enriched by open system FXL. The model of O'Hara (1977) shows that volcanics can be enriched in incompatible element abundances and essentially unchanged in compatible element abundances relative to parent magmas if the volcanics represent a small fraction ( $\leq 30\%$ ) of the original magma. In order to test open system FXL in explaining the chemical variability of the basalts, open system FXL vectors are drawn from the batch melting curves in Figures (36-39). The part of the trajectories which are enriched relative to the closed system vectors are indicated as dashed lines in the diagrams. The open system model uses the same FXL assemblage and the same F value (Table 5), and it assumes that 30% of the magma has leaked from the chamber to form the basalts.

This model effectively explains the enrichment of the intrusives on the Zr vs TiO<sub>2</sub> (Figure 38); however, the Th vs Hf diagram (Figure 39) shows that open system effects cannot explain the range of Hf abundances. The range of Th abundances in the intrusives may be due to alteration (Appendix I). These diagrams suggest that the dikes and sills are not enriched by open system FXL.

Table 6. Chemical compositions of intermediate igneous rocks. Major elements are in %, and trace elements are in ppm.

sample	TC - 16	MTO - 14	MTO - B	WF - 5	MW - D
field occurrence	intrusive	volcanic	volcanic	volcanic	volcanic
altered unaltered	unaltered	unaltered	altered	altered	unaltered
symbol in modeling diagram	△	△	△	△	○
SiO <sub>2</sub>	56.43	61.79	48.48	48.75	66.95
TiO <sub>2</sub>	1.22	0.61	0.51	0.51	0.36
Al <sub>2</sub> O <sub>3</sub>	15.56	15.15	15.24	13.74	13.49
FeO <sup>2 3T</sup>	8.72	8.63	9.66	9.57	3.85
MgO	2.47	2.10	8.45	6.83	3.71
CaO	4.22	5.78	7.52	8.21	3.82
Na <sub>2</sub> O	4.57	2.48	2.56	2.25	0.84
K <sub>2</sub> O	3.12	0.77	0.23	0.52	4.10
MnO	0.13	0.11	0.11	0.15	0.05
P <sub>2</sub> O <sub>5</sub>	0.45	0.18	0.23	0.30	0.14
LOI	3.21	2.25	5.91	9.44	2.3
TOTAL	100.10	99.85	98.90	100.27	100.04

Table 6. Chemical compositions of intermediate igneous rocks. Major elements are in %, and trace elements are in ppm.

sample	TC - 16	MTO - 14	MTO - B	WF - 5	MW - D
Rb	98.1	21.8	6.1	15.5	74.0
Ba	874.	438.	1734.	--	440.
Cs	11.1	1.5	3.5	0.6	0.87
Sr	465.	248.	683.	589.	91.
Pb	22.9	8.7	44.0	19.3	14.0
Th	10.6	2.6	2.7	4.5	8.9
U	4.40	1.13	0.69	1.07	1.93
Sc	19.6	25.3	29.9	26.2	9.56
V	151.	102.	219.	196.	92.
Cr	16.2	16.5	351.0	361.6	16.6
Co	21.	14.	49.	38.	7.
Ni	21.	7.	188.	128.	7.

Table 6 Continued.

sample	TC - 16	MTO - 14	MTO - B	WF - 5	MW - D
Y	35.8	22.2	10.1	16.0	18.9
Zr	276.8	74.6	69.3	122.5	122.3
Nb	15.5	6.7	5.0	6.4	9.0
Hf	6.2	1.7	1.6	2.0	2.81
Ta	0.89	0.40	0.17	0.25	0.45
La	55.9	13.3	40.3	82.8	25.4
Ce	126.0	30.6	85.9	127.2	53.6
Sm	10.3	3.9	5.8	7.6	3.9
Eu	2.47	1.20	1.41	1.95	0.86
Tb	1.13	0.70	0.56	0.74	0.38
Yb	3.12	2.58	1.81	2.04	1.06
Lu	0.45	0.38	0.28	0.30	0.18

Table 7. Chemical compositions of felsic igneous rocks. Major elements are in %, and trace elements are in ppm.

sample	TC - 25	TC - 24	MW - C	WF - 1	MTO - 8
field occurrence	volcanic	volcanic	volcanic	volcanic	volcanic
altered unaltered	unaltered	unaltered	unaltered	unaltered	altered
symbol in modeling diagram	●	●	●	○	○
SiO <sub>2</sub>	76.97	76.61	75.99	74.62	75.04
TiO <sub>2</sub>	0.19	0.18	0.18	0.19	0.20
Al <sub>2</sub> O <sub>3</sub>	12.04	12.19	11.76	13.95	16.41
FeO <sub>2-3T</sub>	1.63	2.18	2.14	1.84	1.45
MgO	--	--	0.08	0.16	--
CaO	0.57	0.26	0.29	0.58	--
Na <sub>2</sub> O	5.67	3.32	4.37	2.48	0.33
K <sub>2</sub> O	1.94	5.11	4.52	4.52	3.68
MnO	0.01	0.03	0.01	0.05	--
P <sub>2</sub> O <sub>5</sub>	0.01	0.01	0.04	0.05	0.07
LOI	0.85	0.61	3.18	2.07	2.93
TOTAL	99.88	100.50	102.56	100.51	100.11

Table 7. Chemical compositions of felsic igneous rocks. Major elements are in %, and trace elements are in ppm.

sample	TC - 25	TC - 24	MW - C	WF - 1	MTO - 8
Rb	33.1	120.6	79.3	116.9	181.9
Ba	393.	968.	1297.	946.	933.
Cs	0.4	1.5	1.53	1.7	10.1
Sr	66.	65.	97.	81.	65.
Pb	32.3	13.5	24.3	21.8	18.8
Th	12.2	14.6	10.8	16.2	7.4
U	5.60	3.55	--	6.3	2.40
Sc	2.8	2.3	4.55	3.2	5.1
V	1.	3.	4.	8.	10.
Cr	3.6	9.3	7.5	--	--
Co	0.	0.	1.	2.	0.
Ni	--	--	--	--	--



Table 7 continued.

sample	TC - 25	TC - 24	MW - C	WF - 1	MTO - 8
Y	49.5	63.9	62.9	19.0	24.8
Zr	315.7	325.3	342.8	140.3	148.8
Nb	16.9	18.5	10.6	12.7	5.8
Hf	8.2	8.5	8.71	3.8	3.8
Ta	1.30	1.40	0.51	1.10	0.70
La	70.1	110.9	64.3	44.0	7.9
Ce	146.4	173.3	122.6	85.2	20.9
Sm	11.4	18.2	12.4	5.7	2.2
Eu	2.10	2.55	2.45	1.00	0.6
Tb	1.70	2.25	1.89	0.55	0.45
Yb	5.50	5.78	5.52	2.17	1.95
Lu	0.80	0.89	0.85	0.26	0.31

### Tectono-Magmatic Diagrams for Intermediate and Felsic Rocks

There are not many tectonic discriminant diagrams for evolved rocks. Some of those which are available are presented in this section. Others are summarized in Tables 8 and 9. It is difficult to draw conclusions from the small number of analyzed intermediate samples; however, when the data are compared to the geochemical trends of the mafic samples, some interesting similarities are seen. Discriminant diagrams suggest that the Red Rock Rhyolite (RRR) is derived by crustal melting in a rift environment and that the Pine Mountain Porphyry (PMP) intrusive is a residual liquid of fractionating arc derived magma.

Discriminant diagrams show dramatic geochemical differences between the two andesitic samples. The intrusive, TC-16, is enriched in incompatible elements relative to the volcanic, MTO-14. The  $\text{TiO}_2$  vs Zr diagram (Figure 26) shows that TC-16 is related to a rift setting while MTO-14 is related to an arc setting. Table 8 shows the results of other discriminant diagrams for the two samples. The relative enrichment of TC-16 can be seen in all of the diagrams. These diagrams may represent the same enrichment process which is observed in the mafic intrusives (Figures 25-39).

Most tectono-magmatic diagrams for rhyolites show a clear distinction between the samples of the RRR and those of the PMP. Figure 40 is a diagram which is devised by Condie (personal communication). The diagram shows that the three samples of the RRR (TC-24, TC-25, and MW-C) plot as rift related rhyolites. Conversely, the two PMP samples (MTO-8 and WF-1) plot as differentiates of arc derived magmas. The  $\text{TiO}_2$  vs Zr diagram (Figure 40) also suggests that

Table 8. Various tectono-magmatic diagrams for andesites and where the samples, TC-16 and MTO-14, plot in these diagrams.

diagram	reference	fields of tectonic setting	
		continental island arc	active continental margin
Zr/Y vs Ti/V	Bailey, 1981	MTO - 14	TC - 16
La/Yb vs Sc/Ni	Bailey, 1981	MTO - 14	TC - 16
La/Yb vs Th	Bailey, 1981	MTO - 14	TC - 16
La/Yb vs Th/Yb	Bailey, 1981	MTO - 14	TC - 16

Table 9. Various tectono-magmatic diagrams for felsic rocks and where the Pine Mountain Porphyry samples (PMP) and the Red Rock Rhyolite samples (RRR) plot in these diagrams.

diagram	reference	fields of tectonic setting	
		arc-related	rift-related
HF vs Zr	Condie (pers. comm.)	PMP	RRR
Y vs Zr	Condie (pers. comm.)	PMP	RRR
La/Yb vs Yb	Condie, 1986	PMP	RRR
V vs Zr	Condie (pers. comm.)	PMP	RRR
Ta vs Yb	Pearce, et. al, 1984	PMP	RRR
Nb vs Y	Pearce, et. al, 1984	PMP	RRR

Figure 40.  $TiO_2$  vs Zr tectonic discrimination diagram for felsic rocks (Condie; personal communication). The five analyzed felsic samples from the Mazatzal Mountains are shown.

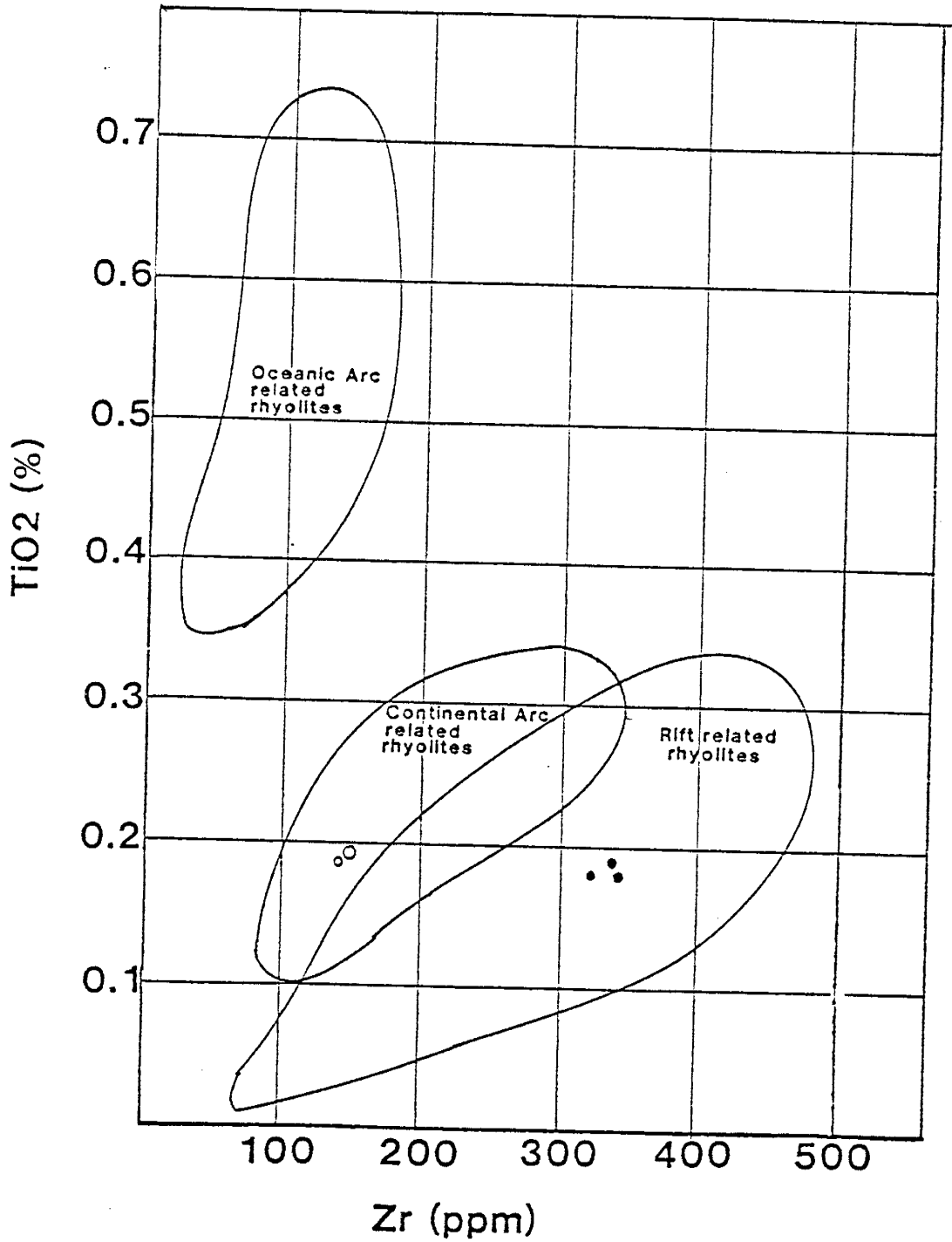


Figure 4L MORB normalized patterns for the five analyzed felsic samples from the Mazatzal Mountains (see text for explanation).

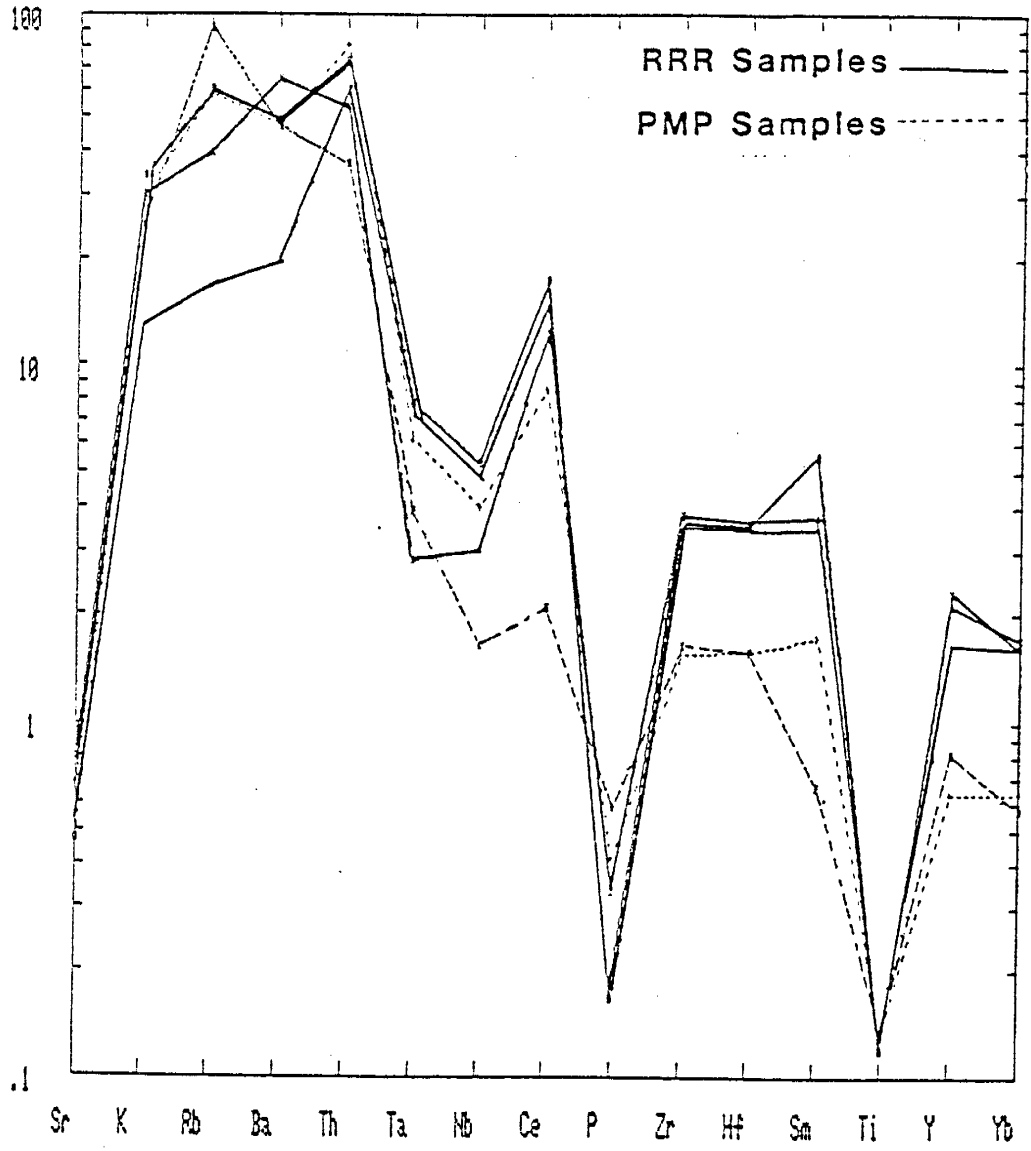
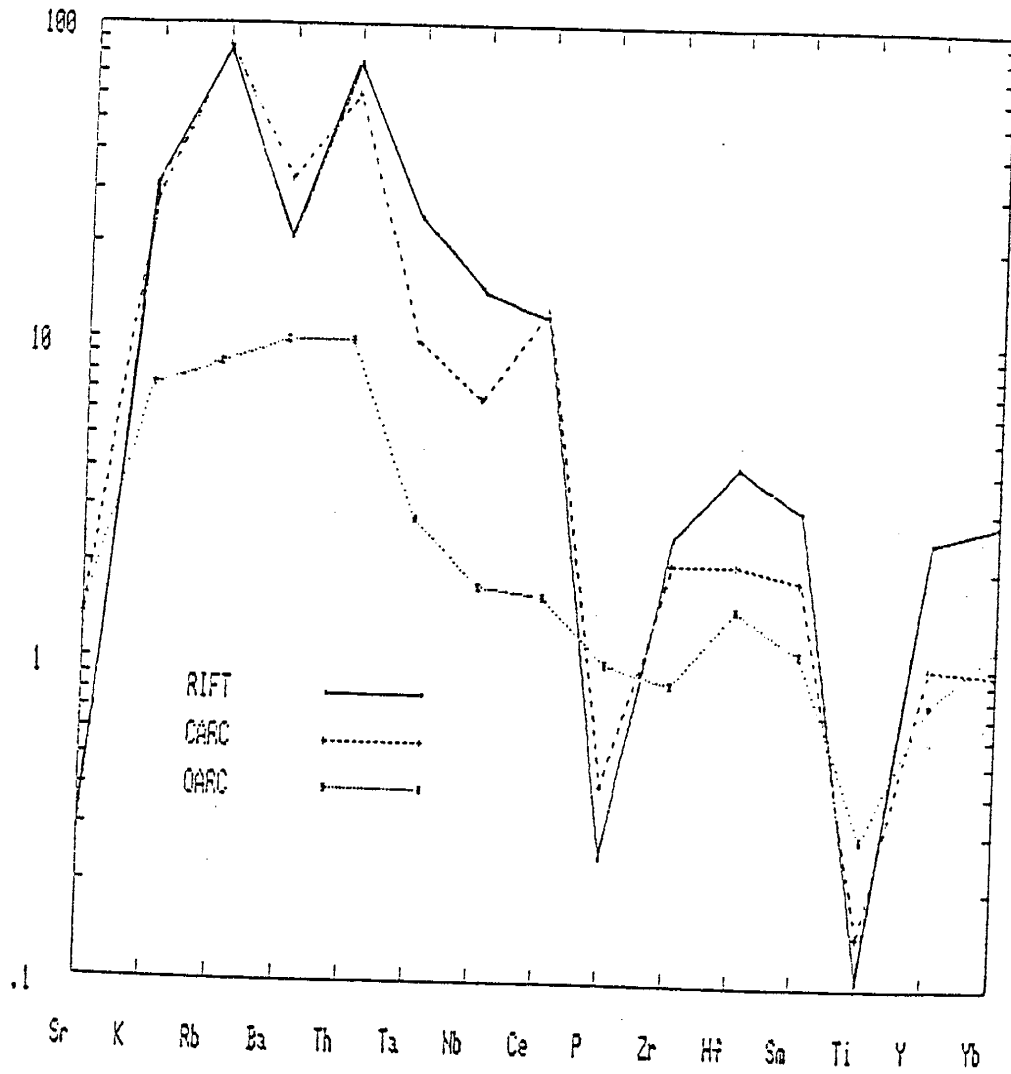


Figure 42. MORB normalized patterns of typical felsic rocks from different modern tectonic settings (Condie; personal communication).



the PMP are related to a continental arc as opposed to an oceanic arc. The results of other felsic tectonic discrimination diagrams are shown in Table 9.

The MORB normalized diagram for rhyolites (Figure 41) suggests that the RRR have patterns which are similar to rhyolites which form in continental arcs (Figure 42). The negative Ta-Nb anomalies are the most notable similarities with this type of rhyolite. The PMP sample (WF-1) is also similar to continental arc rhyolites. The sample (MT0-8) appears to be highly altered (Appendix I); however, it also shows a well-defined Ta-Nb anomaly.

#### Fractional Crystallization Models

In this section, intermediate and felsic rocks are tested as derivatives from associated basalts by FXL. It is difficult to model the evolved samples because: 1) only eight evolved samples have been analyzed; and 2) the samples show a wide variability in trace element abundances. In order to minimize the problems associated with a paucity of data, the geochemical models for the evolved samples are constrained by petrologic major element mixing calculations. These calculations limit the number of potential FXL models for the intermediate and felsic samples because a major element mixing model that yields a sum of squared residuals which is close to or less than 0.1 is statistically valid and because one that yields a much higher sum is clearly not plausible as a petrogenetic model (Bryan, et.al., 1969; and Wright and Doherty, 1970). It is found that many mafic samples cannot be related to the different intermediate samples by major element mixing (Appendix G). This may be a function of the



chemical variability of intermediate and/or mafic rocks in the Alder Group. Similarly, the relative trace element abundances of mafic and intermediate rocks limit the number of potential parent samples for the different intermediate samples. For instance, only two mafic samples have lower incompatible element abundances than the andesite, MTO-14. As a result, these are the only samples which can be considered as viable parent liquids for MTO-14.

Two of the three intermediate samples which are analyzed can be approximately related to specific mafic samples by FXL. These two mafic-intermediate pairs are: MTO-16, MTO-14; and TC-18, TC-16. Three facts which support the parent daughter association of these pairs are as follows: 1) in both cases, the basalt and the related sample are collected in the same part of the section; 2) trace element concentrations in the respective basalt and andesite pairs can be petrogenetically modeled as parent and daughter liquids; and 3) major element mixing calculations provide a good fit between the respective basalts and andesites as indicated by the small sum of squared residuals in the matches (Appendix G).

Apparently, the association between the basaltic andesite, TC-18, and the andesite, TC-16, represents the best parent-daughter relationship because the mode which is derived by major element mixing can be used directly in petrogenetic modeling with trace elements. The mode which is calculated for the other pair requires some modification with respect to the proportions of phases. The mafic and felsic mineral compositions which are used in major element mixing models and the four successful parent-daughter calculations in this study are shown in Appendix G.

Table 10a. Parameters and results of a geochemical model used to derive a liquid which is similar to TC - 16 (see text for explanation).

element	TC-18 - Co	TC-16	calculated daughter liquid using closed FXL (F = 0.7) Cl <sub>a</sub>	calculated daughter liquid using open FXL (F=0.7; L=0.25) Cl <sub>b</sub>
Th	3.7	10.6	5.2	7.8
La	33.8	55.9	46.5	67.0
Ce	80.8	126.0	111.5	162.0
Sm	7.55	10.28	10.29	14.62
Eu	2.09	2.47	2.68	3.48
Tb	0.79	1.13	1.07	1.50
Yb	2.19	3.12	2.93	4.05
Lu	0.31	0.45	0.42	0.58
Tl	6714.0	7314.0	7036.0	7324.0
Y	16.7	35.8	22.7	32.0
Zr	136.4	276.8	192.4	289.8
Nb	6.4	15.5	9.0	13.4
Hf	3.50	6.20	4.83	7.03
Ta	0.28	0.89	0.39	0.58
Ni	62.0	21.0	21.0	13.5

Table 10b. FXL assemblage used to calculate Cla and Cib.

mineral	proportion
olivine	0.11
clinopyroxene	0.23
orthopyroxene	0.61
magnetite	0.05

\*The assemblage has been determined from a major element mixing calculation which has used TC - 18 and TC - 16 as parent and daughter liquids, respectively.

TC-18 can be related by FXL to a parent liquid which is derived by 5-10% BM of the mantle source which contains a high proportion of garnet. A daughter liquid which is similar to TC-16 with respect to trace element abundances can be calculated from TC-18 by open system FXL. Tables 10a and 10b show the mode of the crystallization assemblage, the proportion of residual liquid (F), and the assumed amount of leakage from the residual liquid in the magma chamber. The Tables also show the calculated compositions of the open and closed system daughter liquids and the composition of TC-16. The "F" value of 0.7 is assumed in the models because: 1) this value gives a good approximate match of the nickel contents of TC-16 and the calculated daughter; and 2) a minimum of 30% FXL is needed to derive an andesite from a basaltic liquid (Condie, personal communication).

The open and closed system models for TC-16 are compared in Table 10a. From the Table, it can be seen that the calculated daughter liquid is too low, relative to TC-16, in the LREE abundances and in Th abundance. The enrichments of these elements in TC-16 may be attributed to alteration, crustal contamination, or subduction zone enrichment. This is addressed more thoroughly in the discussion at the end of this section. It is emphasized that the open system model provides a good fit between the calculated daughter and TC-16 with respect to the HFSE and HREE abundances. It is apparent that open system FXL is required for the model because: 1) the daughter liquid of closed system FXL is too depleted in HFSE and HREE abundances; and 2) a maximum of only 30% FXL is allowed by the relative Ni contents.

The other petrogenetically related basalt-andesite pair (MT0-16; MT0-14) is collected from the Slate Creek shear zone from the Mt. Ord

member. Both samples represent volcanics. MT0-16 can be related to a 30% batch melt of the mantle source with a high garnet mode. A daughter liquid which is similar to MT0-14 can be calculated from MT0-16 by open system FXL. The parameters and the results of the model are shown in Tables 11a and 11b. The closed system FXL model is also presented. Once again, the Ni contents of the two samples limit the amount of FXL to 30%. The mode which is calculated from the petrologic mixing calculation using MT0-16 and MT0-14 as parent and daughter liquids, respectively, appears to be too high in magnetite. Because of the small sum of squared residuals (Appendix G), the phases in the calculated mode are probably representative of the original assemblage. As a result, the FXL mode which is used to calculate Cla and Clb in Table 11a is determined by varying the proportion of phases which are indicated by the major element mixing calculation which uses MT0-16 and MT0-14. Compared to the closed system FXL model, the open system model provides a better match with respect to HFSE and HREE abundances. Once again, the calculated liquid is too depleted in Th and LREE abundances.

One sample (MW-D) of dacitic composition is analyzed in this study. MW-D is one of two unaltered igneous samples which have been analyzed northwest of the Red Rock Rhyolite sequence. The dacite cannot be related by FXL to any of the analyzed samples. Major element mixing calculations which use many different combinations of mineral phases and parent samples are entirely unsuccessful in producing realistic FXL modes. Similarly, the trace element abundances of MW-D can not be related to those of any one sample by FXL. As a result, a mafic parent for MW-D is calculated by 20% BM of

Table 11a. Parameters and results of a geochemical model used to derive a liquid which is similar to MTO - 14 (see text for explanation).

element	MTO-16 = Co	MTO-14	calculated daughter liquid using closed FXL (F = 0.7) Cl <sub>a</sub>	calculated daughter liquid using open FXL (F=0.7; L=0.5) Cl <sub>b</sub>
Th	0.90	2.60	1.3	1.4
La	5.6	13.3	7.7	8.5
Ce	14.1	30.6	19.6	21.7
Sm	2.30	3.89	3.21	3.56
Eu	0.82	1.20	1.07	1.17
Tb	0.44	0.70	0.61	0.68
Yb	1.27	2.38	1.76	1.94
Lu	0.17	0.33	0.24	0.26
Tl	4856.0	3657.0	3981.0	3810.0
Y	15.4	22.2	21.4	23.7
Zr	51.7	74.6	73.2	81.7
Nb	5.2	6.7	7.3	8.1
Hf	1.00	1.70	1.40	1.55
Ta	0.18	0.40	0.25	0.18
Ni	15.0	7.0	5.9	5.2

Table 11b. FXL assemblage used to calculate Cl<sub>a</sub> and Cl<sub>b</sub>.

Mineral	proportion
olivine	0.22
clinopyroxene	0.07
plagioclase	0.61
magnetite	0.10

\*The phases in the assemblage have been determined from a major element mixing calculation which has used MTO - 16 and MTO - 14 as parent and daughter liquids, respectively. The proportion of phases have been determined by finding a best match of Cl with MTO - 14.

the high garnet mantle source. A daughter liquid which is similar to MW-D can be calculated by 70% closed system FXL of the parental liquid. This is the minimum amount of FXL which is required to derive a dacitic liquid from a mafic parent (Condie, personal communication). The mode which is used in the FXL model for MW-D is a typical mafic to dacitic assemblage (Condie, personal communication).

The parameters and results of the MW-D model are shown in Table 12a and 12b. It can be seen that 70% closed system FXL results in an approximate match between the calculated daughter liquid and MW-D with respect to HFSE; however, the calculated element abundances are high for the most part; therefore, open system FXL can not be considered in the model for MW-D. From Table 12a, it is seen that the calculated daughter liquid (C1) does not provide a very good match with MW-D. Once again, the actual sample is dramatically enriched in LREE and Th abundances relative to the calculated liquid.

Two samples of the Pine Mt. Porphyry intrusive have been analyzed in this study. The samples appear to be rhyodacitic in Figure 22. One of the samples (MT0-8) appears to be highly altered (Appendix I), and as a result, the geochemical modeling concentrates on the relatively unaltered sample (WF-1). The rhyodacites are modeled only by FXL because discriminant diagrams (last section) suggest that the samples are differentiation products of arc magmas.

Tables 13a and 13b show the modeling parameters for the rhyodacites. The phases for the crystallization assemblage are derived from a major element mixing calculation between MT0-14 and WF-1 (Appendix G). MT0-14 is too depleted in incompatible trace element abundances to be the parent for WF-1; however, the sum of the squared



Table 12a. Parameters and results of a geochemical model used to derive a liquid which is similar to MW - D (see text for explanation).

element	20% batch melt of high garnet mantle source = Co	MW-D	calculated daughter liquid closed FXL (F = 0.3) = Cl
Th	0.85	8.90	2.6
La	5.8	25.4	14.3
Ce	13.4	53.6	27.6
Sm	2.05	3.89	4.11
Eu	0.63	0.86	1.04
Tb	0.26	0.38	0.55
Yb	0.66	1.06	1.47
Lu	0.08	0.18	0.19
Tl	4212.0	2158.0	2678.0
Y	10.4	18.9	26.8
Zr	46.0	122.3	146.7
Nb	3.9	9.0	12.2
Hf	0.98	2.81	2.89
Ta	0.13	0.45	0.40
Ni	509.0	7.0	10.6

Table 12b. FXL assemblage used to calculate Cl.

mineral	proportion
olivine	0.05
clinopyroxene	0.25
plagioclase	0.63
magnetite	0.05
apatite	0.02

\*An FXL assemblage could not be calculated from major element mixing calculations; therefore, the mode is based on a typical basalt to dacite FXL assemblage (Condie; personal communication). Apatite is added to lower the MREE abundances in Cl.

Table 13a. Parameters and results of a geochemical model used to derive a liquid which is similar to WF - 1 (see text for explanation).

element	Co - Cl Table 10a	WF-1	calculated daughter liquid using closed FXL (F=0.4) = Cl
Th	2.6	16.20	5.5
La	14.3	44.0	27.1
Ce	27.6	85.2	48.9
Sm	4.11	5.70	5.75
Eu	1.04	1.00	0.83
Tb	0.55	0.55	0.59
Yb	1.47	2.17	1.98
Lu	0.19	0.26	0.26
Ti	2678.0	1139.0	1204.0
Y	26.8	19.0	21.8
Zr	146.7	140.3	129.6
Nb	12.2	12.2	16.2
Hf	2.89	3.80	4.10
Ta	0.4	1.10	0.65

Table 13b. FXL assemblage used to calculate Cl\*.

mineral	proportion
orthopyroxene	0.10
clinopyroxene	0.20
plagioclase	0.547
biotite	0.05
quartz	0.05
zircon	0.001
apatite	0.003

\*The major phases in the assemblage have been determined from a major element mixing calculation. Zircon and apatite have been added to lower the Zr and MREE abundances in Cl.

residuals in the mixing calculation is very low which suggests that MT0-14 is chemically similar, with respect to major elements to the parent of WF-1. In batch melting, liquids which are derived by different degrees of melting have similar major element abundances. The calculated mixing mode has 30% quartz (Appendix G). This seems to be unrealistically high, and it is attributed to silica enrichment in MT0-14 (Appendix I). It is once again assumed that a good match in the mixing calculation constrains the phases but not the proportion of phases in the crystallization assemblage.

The rhyodacites can be related by closed system FXL to the daughter liquid which is calculated in the MW-D model (C1 in Table 12a). A daughter liquid (C1 in Table 13a) which is similar to WF-1 is calculated from the parent liquid by 60% closed system FXL. This is the minimum amount of fractionation which is necessary for a dacitic liquid to evolve to one of felsic composition (Condie, personal communication).

The proportion of phases in the crystallization assemblage of Table 13b results in the best match for the trace element abundances of WF-1 and the calculated daughter liquid (C1). Table 13a shows a good fit between the HFSE and the HREE abundances of the calculated daughter liquid and WF-1; however, it can be seen that the models for the rhyodacites work very poorly with respect to Th and LREE abundances.

Most geochemical tectonic discriminant diagrams which are discussed in the previous section suggest that the RRR is related to partial crustal melting in a rift environment; however, the MORB normalized patterns of the RRR resemble those which are seen in

rhyolites from continental arcs. As a result, both FXL and partial melting are considered in the petrogenetic modeling of the RRR.

Major element mixing calculations (Appendix G) are used in an attempt to constrain an FXL assemblage and an assemblage of mineral phases in the lower crust. Appendix G shows and discusses the results of a mixing calculation which involves the lower crustal composition of Weaver and Tarney (1984) and one of the RRR samples (TC-25). It can be observed from the small sum of squared residuals that a composition which is very close to that of the approximated lower crust can be calculated from the major element mixing of the phases (in Appendix G) with TC-25. The phases in the residue are those which are typically found in granulite rocks.

This phase assemblage is used in trace element petrogenetic modeling of the RRR by partial melting of the lower crust. In Table 14a, the trace element composition of Weaver and Tarney's lower crust is used as "Co" in a batch melting calculation. A best match between the trace element abundances of a 10% batch melt of lower crust and TC-25 is obtained by using the source mode in Table 14b. This mode is derived by varying the proportions of phases which are calculated from the major element mixing calculation. Minor proportions of zircon and allanite are added to the mode in order to obtain a better match for the zirconium and LREE abundances. Table 14a shows the trace element abundances of both the calculated daughter liquid and the sample TC-25.

The partial melting model works very well with respect to most of the elements; however, it is slightly high in Th and HF abundances. This may be due to uncertainties in the lower crust composition.

Table 14a. Parameters and results of a geochemical model involving batch melting of lower crust to generate the Red Rock Rhyolite (see text for explanation).

element	Weaver and Tarney (1984) lower crust composition = Co	TG - 25	10% batch melt of lower crust = Cl
Th	6.00	12.2	20.85
La	29.0	70.1	70.1
Ce	61.0	146.4	163.2
Sm	4.9	11.40	16.74
Eu	1.29	2.10	1.23
Tb	0.65	1.70	1.12
Yb	1.50	5.50	5.42
Lu	0.24	0.80	0.88
Tl	5396.0	1139.0	1278.0
Y	15.0	49.5	48.9
Zr	181.0	315.7	309.2
Nb	10.0	16.9	15.8
Hf	5.80	8.20	14.79

Table 14b. Modal and melting proportions of lower crust used to calculate Cl in table 12a.\*

mineral	proportion	melt
orthopyroxene	0.05	0.02
clinopyroxene	0.02	0.02
plagioclase	0.62	0.42
biotite	0.05	0.11
quartz	0.18	0.42
ilmenite	0.08	0.01
zircon	0.00035	0.001
allanite	0.00005	0.000

\*Phases in the mode of the source have been determined by major element mixing calculations. Zircon and allanite have been added to lower the Zr and LREE abundances of Cl.



Taylor and McLennan (1984) have estimated the Th and Hf abundances of the lower crust as 1.06 and 2.1, respectively. As a result, the actual Th and Hf abundances of a 10% batch melt of lower crust could be much lower than those which are listed in Table 14a.

A parent liquid is needed to evaluate the possibility that FXL processes have generated the RRR. It has already been mentioned that there is a paucity of analyzed intermediate samples in the study. There appears to be a significant compositional gap between all of the intermediate rocks and the samples of the RRR (Figures 22 and 26). Geochemical similarities have been observed between the RRR samples which are taken from the Tonto Basin and the Mazatzal Mountains, respectively. (Reed, Noll, and Condie, 1987). Dacites in Tonto Basin have trace element abundances which may be related to those of the RRR by FXL; however, there is apparently still a minor compositional gap between these dacites and the RRR samples (Noll, 1988). Regardless of this fact, one of the dacitic samples from Tonto Basin (WCRD-1; Appendix G) has been chosen to test FXL processes in the petrogenetic modeling of the RRR.

Major element mixing calculations are unsuccessful in relating the RRR sample, TC-25, to WCRD-1 (Appendix G). It is noted that the major element concentrations of the RRR samples from Tonto Basin, when substituted in these mixing calculations, have results which are almost identical to calculations which use the major element abundances of the RRR samples from the Mazatzal Mountains.

Since major element mixing calculations are unsuccessful in approximating the major element concentrations of WCRD-1, a crystallization mode is estimated by matching the trace element

abundances of the RRR with those of a daughter liquid which is derived by FXL from WCRD-1.

Tables 15a and 15b shows the comparison of the trace element abundances of the RRR and a daughter liquid which is derived by 60% closed system FXL. The trace element abundances of WCRD-1 and the crystallization mode are also shown in the Tables. It should be noted that the daughter liquid is enriched relative to the RRR, with respect to Hf, Th, and the HREE abundances; therefore, both open system FXL and higher degrees of closed system FXL are not allowed. The addition of sphene to the FXL mode may result in a better match since sphene is compatible with respect to Hf, Th, and the HREE; however, sphene is also compatible with respect to Ta, and the Ta concentration in the daughter liquid is lower than in the RRR.

The major phases of the mode which results from the best fit of trace elements in the FXL model are used in a major element mixing calculation between TC-25 and WCRD-1 (Appendix G). It is noted that the squared residuals of the calculated parent with WCRD-1 is high (0.39), and that the mode requires negative proportions of quartz and clinopyroxene.

Table 15a. Parameters and results of a petrogenetic model used to derive a liquid which is similar to the Red Rock Rhyolite by FXL (see text for explanation).

element	WCRD-1 - Co	TC-25	Calculated daughter liquid using closed system FXL ( $F = 0.4$ ) = Cl
Th	8.60	12.20	16.4
La	55.0	70.1	87.3
Ce	117.4	146.4	186.7
Sm	11.20	11.40	15.38
Eu	2.70	2.10	2.14
Tb	2.02	1.70	2.10
Yb	5.40	5.50	7.37
Lu	0.85	0.80	1.17
Ti	4856.0	1139.0	1211.0
Y	59.0	49.5	50.7
Zr	379.7	315.7	301.7
Nb	19.5	16.9	20.8
Hf	10.20	8.20	13.07
Ta	1.14	1.30	0.74

Table 15b. FXL assemblage used to calculate CL in table 13a.\*

mineral	proportion
orthopyroxene	0.05
clinopyroxene	0.25
plagioclase	0.509
biotite	0.10
quartz	0.05
ilmenite	0.04
zircon	0.0008
allanite	0.00005

\*FXL assemblage has been determined by varying the proportion of phases of a typical dacite to rhyolite FXL assemblage (Condie, personal communication) in order to obtain a good match between Cl and TC-25.

## DISCUSSION

## Interpretation of the Metasedimentary Rocks

The QAW appear to have been recycled from passive margin sediments (Figures 4, 5, 14 and 15), and the lithic wackes were probably derived from an arc source (Figures 4, 5 16 and 17); therefore, it is probable that different sources have supplied material into the Alder basin.

The provenance of the matrix-rich quartz wackes is dubious; however, the sediments are chemically similar to oceanic arc sediments. Because of the proximity to the Slate Creek shear zone (Figure 3), the rocks which have been taken from the southeastern limb of the syncline are considerable more deformed than those from which the matrix-rich quartz wackes have been taken. As a result, it seems improbable that diagenetic or metamorphic processes would have affected the matrix-rich quartz wackes more than the other sandstones in the Alder sequence, and the paucity of large detrital components in the matrix-rich quartz wackes is assumed to be a primary characteristic. These sandstones appear to represent mid to outer turbidite fan deposits; therefore, it is plausible that the detritus has been extensively reworked as it was carried in the depositional basin. Extensive reworking of the sediments may have broken down the less resistant detrital components such as feldspar and volcanic rock fragments.

The Alder pelites have geochemical affinities to both Phanerozoic pelites and volcanic sediments (Figures 10 and 11). As a result, it

is proposed that they represent the deposition of silts and clays of a volcanic provenance. Because of the respective depositional histories of the matrix-rich quartz wackes and pelites, it is possible that the higher relative Th abundances of these rocks (Figures 5 and 6) reflect prolonged contact and reaction of the detritus with seawater. In support of this possibility, the residence times of Co, Sc, and Zr in seawater are nearly three orders of magnitude larger than that of Th (Holland, 1978).

Mature recycled orogen sediments and arc sediments can be associated either in a remnant ocean basin between converging land masses or in a backarc basin along an active continental margin. The distinction between these possibilities of tectonic setting is problematical. The Alder deposition may have occurred in a basin which was located between an advancing arc and a passive continental margin or it may have occurred in a continental margin back arc basin.

The chemical composition of sediments suggest that the Alder basin formed as an arc approached a cratonic margin. More specifically, sediments which are deposited in back arc basins of active continental margins plot within either the active continental margin field or the continental island arc field in Figures 4, 5, 6 and 7. The Alder sediments plot in two groups which seem to represent opposite end members of the chemical range of sediments. The Alder sediments that plot in the continental island arc and active margin fields in Figures 7 and 8, respectively, may reflect mixing of different sediment types within the Alder basin. The chemical signature of the Alder sediments may be diagnostic of tectonic settings which involve arc-continent collisions.

## Interpretation of the Mafic Igneous Rocks

The igneous rocks from the Alder and Red Rock Groups appear to represent a bimodal suite. The Alder volcanics range in composition from basalts to dacites but are dominated by mafic rocks which are basaltic andesite in chemical composition (Figure 22). Dikes and sills, which appear to be the youngest rock types in the Alder and Red Rock Groups, range from basalt to andesite in composition.

The mafic to andesitic dikes and sills in the Alder and Red Rock Groups are chemically distinct from Alder volcanics. The intrusives are tholeiitic while the volcanics are calc-alkaline, and the former are enriched in incompatible elements. These trends suggest that the hypabyssal rocks represent a change from dominantly calc-alkaline to tholeiitic fractionation with time. The calc-alkaline trend has been attributed to high oxygen fugacity (magnetite fractionation) in parent magmas (Osborn, 1959). In conjunction with this hypothesis, the V vs  $TiO_2$  diagram (Figure 29) suggests that the oxygen fugacities in the parent magmas decreased as the fractionation trends changed from calc-alkaline to tholeiitic. Also, the intrusives tend to have chemical similarities to both within plate basalts and continental arc basalts, while the older mafic volcanics are geochemically similar to continental arc basalts.

The mafic rocks can be related by shallow fractional crystallization of olivine, plagioclase, and clinopyroxene to primary liquids which were derived by variable degrees of batch melting of a mantle source. With respect to HFSE and HREE, the source is similar to primordial mantle; however, it is enriched with respect to Th and

the LREE. This could be the result of either alteration (Appendix I) or crustal contamination (see next section).

The mineralogic composition of the mantle source was probably that of a garnet lherzolite. A wide range of Y and HREE abundances in the mafic samples suggests that the amount of garnet in the source was variable. Similar explanations for Y and HREE abundances of igneous rocks are invoked in other Proterozoic terranes in the Southwest (Condie and Nuter, 1981). The mafic intrusives and the Alder volcanics cannot be related to the same source by different degrees of batch melting or open or closed fractional crystallization; therefore, it is possible that some process enriched the intrusives or the source of the intrusives in incompatible elements. This could explain the within-plate tendencies of the intrusives.

#### Interpretation of the Intermediate and Felsic Igneous Rocks

Most of the evolved samples can be related by open or closed system fractional crystallization to mafic parents which are derived by different degrees of batch melting of a mineralogically heterogeneous garnet lherzolite source. Because of the limited data, it cannot be determined if the distinctions between the different petrogenetic models for the intermediate samples are significant; however, in light of the mafic geochemistry, some distinctions are worth mentioning.

Evidence has been presented which suggests that the fractionation trends of magmas changed from calc-alkaline to tholeiitic with time and that oxygen fugacity decreased as this change occurred (see previous section). The affect of these changes on major element



chemistry of the igneous rocks may be demonstrated by the results of major element mixing of mafic and intermediate samples. Such mixing calculations cannot relate the proposed parent sample of the volcanic, MTO-14, to the intrusive, TC-16, and the proposed parent of TC-16 cannot be related to MTO-14 (Appendix G). Similarly, the oldest igneous sample, (MW-D), shows the strongest calc-alkaline affinities, and this sample cannot be related to any potential parent sample by major element mixing. The proportion of magnetite which fractionates from a magma is a function of oxygen fugacity (Grove and Kinzler, 1986; Osborn, 1959; and Shervais, 1982), and magnetite fractionation ( $O_2$  fugacity) has been invoked to play a major role in the development of the calc-alkaline trend (Osborn, 1959). In conjunction with this, the petrogenetic models for the two andesitic samples (Tables 10 and 11) show that the proportion of magnetite appears to have decreased in the fractionating magma as the trend changed from calc-alkaline to tholeiitic.

The mafic geochemistry also shows that incompatible element enrichment may have occurred in the magmas or the source of the magmas throughout the history of Alder-Red Rock volcanism. In conjunction with this possibility, the oldest sample, (MW-D), appears to be derived from a relatively depleted mantle source, and the youngest intermediate sample, (TC-16), is relatively enriched in incompatible elements. As mentioned previously, more data are needed to verify the distinctions which are seen in the petrogenetic models for the different intermediate rocks.

All of the petrogenetic fractional crystallization models for evolved rocks show that the samples have been affected by a relative

enrichment of the LREE and Th which cannot be explained by fractional crystallization. The associated basalts also show a minor amount of enrichment in these elements (Table 5a). These enrichments may be the result of one or more of the following: 1) a subduction zone component; 2) crustal contamination; or 3) alteration.

These same enrichments occur in highly altered basalts (Appendix I). However, the modeled evolved rocks plot within the unaltered screen (Davis, et al., 1979), and they have relatively low LOI; therefore, secondary alteration does not seem to be likely. Distinguishing between the other two alternatives is problematical. Estimates of the composition of the upper continental crust (Taylor and McLennan, 1984) have been used to test the possibility of crustal contamination. The Th value of MW-D exceeds that of the upper crust; and thus, crustal contamination is improbable. Some researchers propose that the contamination of a magma can result from mixing with sialic partial melts (Thompson, et al., 1982; James, 1981; and Pearce, 1983). Sialic partial melts could have much higher La/Yb ratios and Th abundances than the upper crust. This type of contamination can have a significant effect on Ba, Rb, Th, K, Sr, and LREE abundances and a negligible effect on the HFSE and the HREE abundances (Thompson et al., 1982). Isotopic data are needed before it can be determined whether or not the enrichments in Alder volcanics are due to contamination by sialic partial melts.

The results of this study favor a partial melting origin for the RRR for the following reasons: 1) there seems to be a significant compositional gap between the rhyolites and potential parent samples (especially in the Mazatzal Mountains); 2) major element mixing

calculations work well for partial melting models (Appendix G); 3) these same calculations do not give workable modes for FXL models; and 4) most geochemical discriminant diagrams (last section) suggest that the rhyolite is derived from partial melting of the crust.

#### Interpretation of the Structure and Stratigraphy

The respective successions of rock which lie to the northwest and the southeast of the Red Rock Rhyolite are dramatically different, and it seems unlikely that facies changes within the depositional basin can explain these differences. As a result, it seems unlikely that the simple structural interpretation proposed by Ludwig (1974) is correct. An alternative interpretation of the structure and stratigraphy of the Alder and Red Rock Groups in the central Mazatzal Mountains is proposed in this section. More detailed structural work is needed to verify this alternative interpretation.

Since the southeastern contact of the RRR with the Alder Group appears to be conformable (Ludwig, 1974; and Conway, 1976), it is inferred that the northwestern exposure of the RRR is in fault contact with the Alder Group, and it is proposed that this northeast-southwest trending fault separates an older sequence (the Northern Succession) to the northwest from a younger sequence (the Southern Succession) to the southeast (Figures 43 and 44). The evidence that the Northern Succession is older is as follows: 1) the Northern Succession only contains immature sediments which appear to have been derived from an arc while the Southern Succession contains an appreciable proportion (~40%) of mature and submature sediments which appear to have been

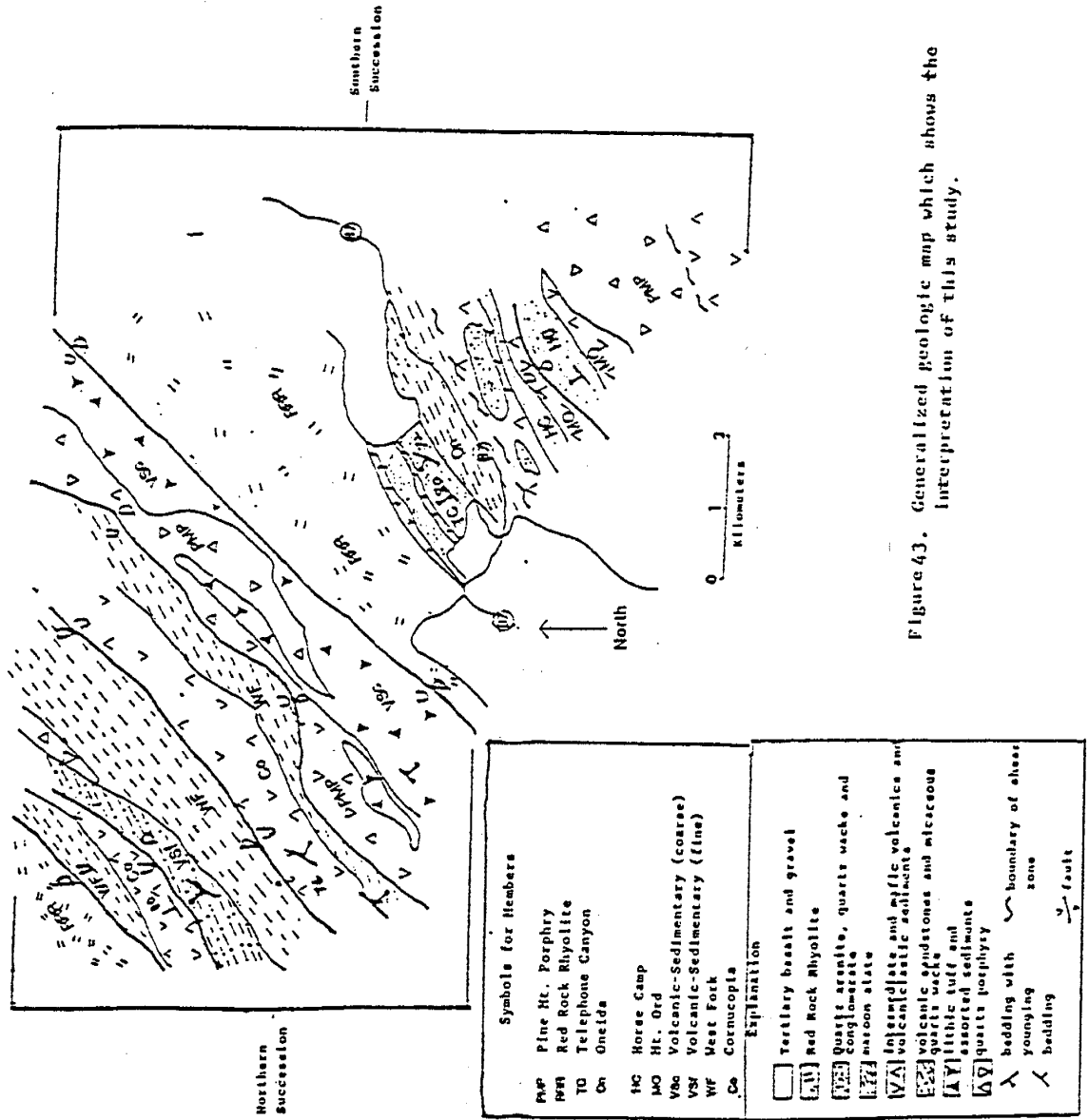
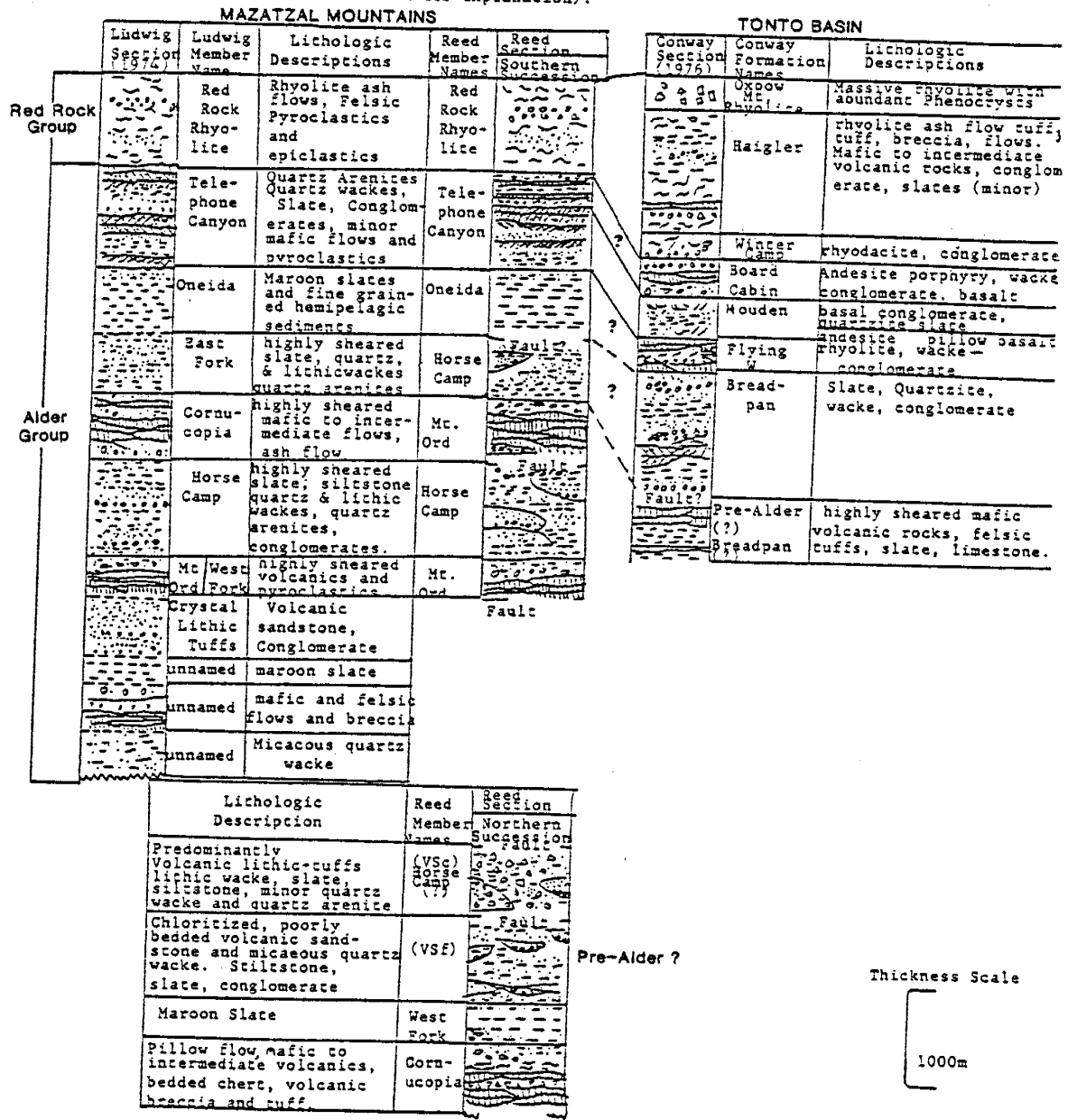


Figure 43. Generalized geologic map which shows the interpretation of this study.

Figure 44. Different stratigraphic columns of the Alder and Red Rock Groups in the Mazatzal Mountains and proposed correlations with Tonto Basin (see text for explanation).



derived from a recycled orogen; 2) jasper beds are found only in the Northern Succession, and jasper is a common clast in the sedimentary rocks of the Southern Succession; 3) northern sediments appear to represent outer fan deposits of turbidite systems while southern sediments are similar to slope and shelf sediments; 4) the effects of hydrothermal activity can be visibly observed in the depositional history of the Northern Succession but not in that of the Southern Succession; 5) the sandstone sample WF-2, which is taken from a unit assumed to be one of the oldest members in the sequence (see below) appears, chemically, to be the most immature sandstone in the study; and 6) igneous geochemistry suggests both that the mantle source has been chemically enriched with time and that the fractionation of magmas has changed from calc-alkaline to tholeiitic with time, and the only unaltered volcanic sample (MW-D) from the Northern Succession is strongly calc-alkaline and appears to be related to a relatively depleted source.

Jasper beds are found only in the Cornucopia member in the Northern Succession. This unit also contains volcanics and volcanoclastics that are contaminated by carbonate. Areas of less intense contamination are typically chloritized. The contaminated sediments may have been mistaken for clastic limestones by Ludwig. Evidence shows that the carbonate alteration occurred at the time the rocks were deposited. More specifically, some coarse interbeds contain both altered and unaltered rock fragments, and carbonate laminations are interbedded with purple slate laminations. The occurrence of red jasper beds farther down section suggests that carbonate contamination may be attributed to hydrothermal alteration.

In Ludwig's stratigraphy, the sediment represented by WF-2 was inferred to be part of the middle of the Alder Group (East Fork member; Figure 44); however, in the stratigraphy proposed in this study, the sample is inferred to have been collected from the oldest unit in the Alder Group. The chemical immaturity of this sample suggests that mature sediments were not mixed with arc sediments at the time of its deposition (see discussion of sediments). If the unit containing WF-2 occupied the stratigraphic position designated by Ludwig, mature sediments would have been mixing with arc sediments in the basin of deposition and the sediment would not have its immature chemical signature.

Stratigraphic repetitions in the areas which lie on both sides of the Red Rock Rhyolite are attributed to faulting or folding (Figure 43 and Plate I). The one fold (Plate I) which is mapped in the area northwest of the Red Rock Rhyolite is inferred from stratigraphic repetition and reversed younging directions. The stratigraphic interpretation of this study is shown in the middle columns of Figure 44. Ludwig's stratigraphic member names are applied to units which best typify his lithologic descriptions. Two Horse Camp and Mt. Ord member names are present in the stratigraphic column of the Southern Succession because it is inferred that a fault (Figure 43 & Plate I) has caused a repetition of the stratigraphy proposed by Ludwig. In two locations in the area northwest of the Red Rock Rhyolite (Copper Camp and the Squaw Flat Spring), the chloritized volcanic sandstone unit (the Crystal Lithic Tuff member in Ludwig's stratigraphy) is found to lie in conformable contact below the micaceous quartz wacke unit. As a result, these two rock types are considered to be part of

one fine grained volcanoclastic-sedimentary (VSF) unit in the stratigraphic column of the Northern Succession. Three sequences of maroon slates and phyllites in the Northern Succession are inferred to be repetitions of the same unit and are collectively referred to as the West Fork member. The latter unit lies conformably beneath the chloritized volcanic sandstones near the junction of the Squaw Flat Spring and McFarland Canyon. The contact is characterized by immature, clast-rich sandstones and conglomerates interbedded with slates.

A coarse grained volcanoclastic-sedimentary unit (VSC) in the stratigraphic column of the Northern Succession was correlated as the Oneida member in Ludwig's stratigraphy. Both the northwestern and southeastern contacts of the unit are believed to be faults. The unit is inferred to be younger than the rest of the Northern Succession because: 1) the sequence has occasional interbeds (1-2m thick) of mature sediments; and 2) the unit is similar to inner fan deposits while the other sediments are similar to outer fan deposits. The unit has some similarities to the unit which is identified as the Horse Camp member in the stratigraphic column of the Southern Succession, and a possible correlation is indicated in the stratigraphic column.

Figure 44 also shows possible correlation with the Alder Group and the Red Rock Group in Tonto Basin. Correlations indicated by a question mark represent correlations proposed in this study. Other correlations are those which have been made by Conway and Silver (1986). The Horse Camp member is similar to the descriptions of the upper and lower Breadpan Formation from Tonto Basin which were made by Gastil (1958). The Oneida member is in the same stratigraphic



position as the Flying W Formation in Tonto Basin. If this correlation is correct, the Oneida member must represent a relatively distal facies since it is composed of fine grained and pelitic sediments while the Flying W is composed of volcanics and conglomerates. Volcanics which were not identified by Ludwig (1974) occur at the top of the Telephone Canyon member. These may be equivalent to the volcanics of the Board Cabin Formation in Tonto Basin.

## SUMMARY AND CONCLUSIONS

## Evolution of the Alder Basin of Deposition

As Ludwig (1974) proposed, it appears that the sedimentary lithofacies of the Alder Group represent a change from deep water to shallow water deposition. The fan-slope-shelf association which is observed in the Horse Camp, Oneida, and Telephone Canyon members of the Southern Succession indicates the progradation of a shelf within the Alder basin of deposition. Cross-bedding in quartz arenites and quartz wackes suggest that the shelf prograded from the northeast. The Northern Succession contains sediments which are similar to outer fan-distal basin deposits. This could indicate (previous section) that the Northern Succession represents an older sequence of rocks. Basins which are affected by strong marginal tectonic uplift are: 1) areally restricted; 2) composed of relatively small volumes ( $\leq 20\%$ ) of coarse grained sediments; and 3) often rapidly infilled with nearshore deposits. As discussed below, the Alder sedimentary record suggests that these three characteristics typify the basin of deposition.

The coarsening of volcanic and cratonic deposits to the southwest and northeast, respectively, suggests that the two types of detritus were derived from opposite source directions. The basin of deposition must have been areally restricted since the volcanic and cratonic sediments are interlayered. In the Alder section, only 10-15% of the sedimentary sequences are comprised of coarse grained lithologies. Two facts which suggest the basin was rapidly infilled with nearshore deposits are the Alder sedimentary record does not show vertical

cyclicality of lithofacies and a transition from deep-water to shallow-water lithofacies is recorded in only approximately 800 m of the Southern Succession. In the Southern Succession, the transition from inner fan (Horse Camp member) to shelf (Telephone Canyon member) facies is recorded by only approximately 800m of slope sedimentation (Oneida member). Vertical cyclicality is a common feature of many turbidite systems. Cyclic facies are absent only in cases where vertical accretion rate largely exceeds the rate of small scale sea level variations. Such conditions are commonly associated with phases of rapid tectonic uplift and abundance of sediment supply (Mutti, 1985). In conclusion, it is proposed that the Alder Group represents the rapid infilling of a small basin which was affected by strong marginal tectonic uplift.

#### Proposed Tectonic Setting

The geochemistry of Alder igneous rocks suggests that the volcanics and hypabyssal bodies are related to one of the following: 1) a continental island arc; 2) a continental margin arc; or 3) an incipient back arc rift along an active continental margin. Mature recycled orogen sediments indicate that the Alder basin of deposition was associated with a continental margin. The chemical composition of the sediments indicate that there were variable degrees of mixing between two sediment types derived from diverse provenances. This seems to imply that the provenances evolved independently as in an arc-continent collision, and in support of this assumption, no modern sediments from back arc basins of active continental margins have the

chemical signature of the Alder sediments (Bhatia, 1983; and Bhatia and Crook, 1986). On the contrary, back-arc basin sediments commonly plot either in the continental island arc field or in the active margin field in Figures 4-7. Also, Dickinson and Yarborough (1976) show that it is improbable for mature sediments to be deposited in back arc basins which form from the rifting of active margins, and when back arc basins do receive mature sediments, the sediments are typically derived from craton-interior provenances and not from recycled orogen provenances (Karig and Moore, 1975). As a result, it is possible that the Alder basin resulted from the collision of an arc with a cratonic margin. It is proposed that a collision formed a foreland thrust belt along the margin of the Alder basin. This explains the data (last section) which suggest that the basin was small and that it was affected by strong, marginal tectonic uplift. The foreland thrust belt would also explain the presence of recycled passive-margin sediments in the Alder sequence. Since ophiolite sequences are absent in the Alder stratigraphy, the deposition of the Alder Group may have occurred on submerged continental crust which was located between an exposed craton and an arc.

Paleocurrent analysis (Appendix F) suggests that the recycled orogen sediments were derived from the northeast; therefore, an arc may have collided with a passive margin to the northeast of the study area. Other evidence for a collision occurring to the northeast are as follows: 1) the Houden Formation quartzites in Tonto Basin apparently have a greater proportion of herringbone cross-bedding (Noll, 1988) than the correlative Telephone Canyon member sediments from the Mazatzal Mountains; and 2) quartz arenites are more common to

the northeast within the Telephone Canyon member. These facts suggest that relatively shallow water deposition occurred to the northeast of the Mazatzal Mountain Area, which in turn suggests that the late Alder shelf sloped to the southwest away from the proposed direction of the foreland thrust belt. Also, the lithic wacke group and the quartz wacke group from Tonto Basin are not as chemically distinct as they are in the Mazatzal Mountains (Noll, 1988). This may indicate that mixing of sediments was more thorough to the northeast, and if so the basin of deposition was probably narrower to the northeast.

It appears that the overlying Red Rock Rhyolite (RRR) erupted to the northeast of the Mazatzal Mountains because it thickens in this direction (Ludwig 1974; and Conway and Silver, 1986). It is proposed that the event responsible for partial melting of the lower crust and for the subsequent eruption of the RRR was the collision of an arc with a continent to the northeast of the study area.

The transition from calc-alkaline to tholeiitic fractionation and the enrichment in incompatible element abundances of fractionating magmas also may be attributed to this melting event. The data which supports this are as follows: 1) the tholeiitic and enriched mafic and intermediate hypabyssal rocks appear to be closely related to the RRR extrusion; and 2) volcanics from the Alder Group in Tonto Basin to the northeast have tholeiitic tendencies and are enriched in incompatible elements relative to the Mazatzal Mountain Alder volcanics (Noll, 1988). In conjunction with the latter point, a mafic sample (HUMMTN-2) which has been collected by K.C. Condie along strike to the southwest on Humboldt Mountain is geochemically similar to the

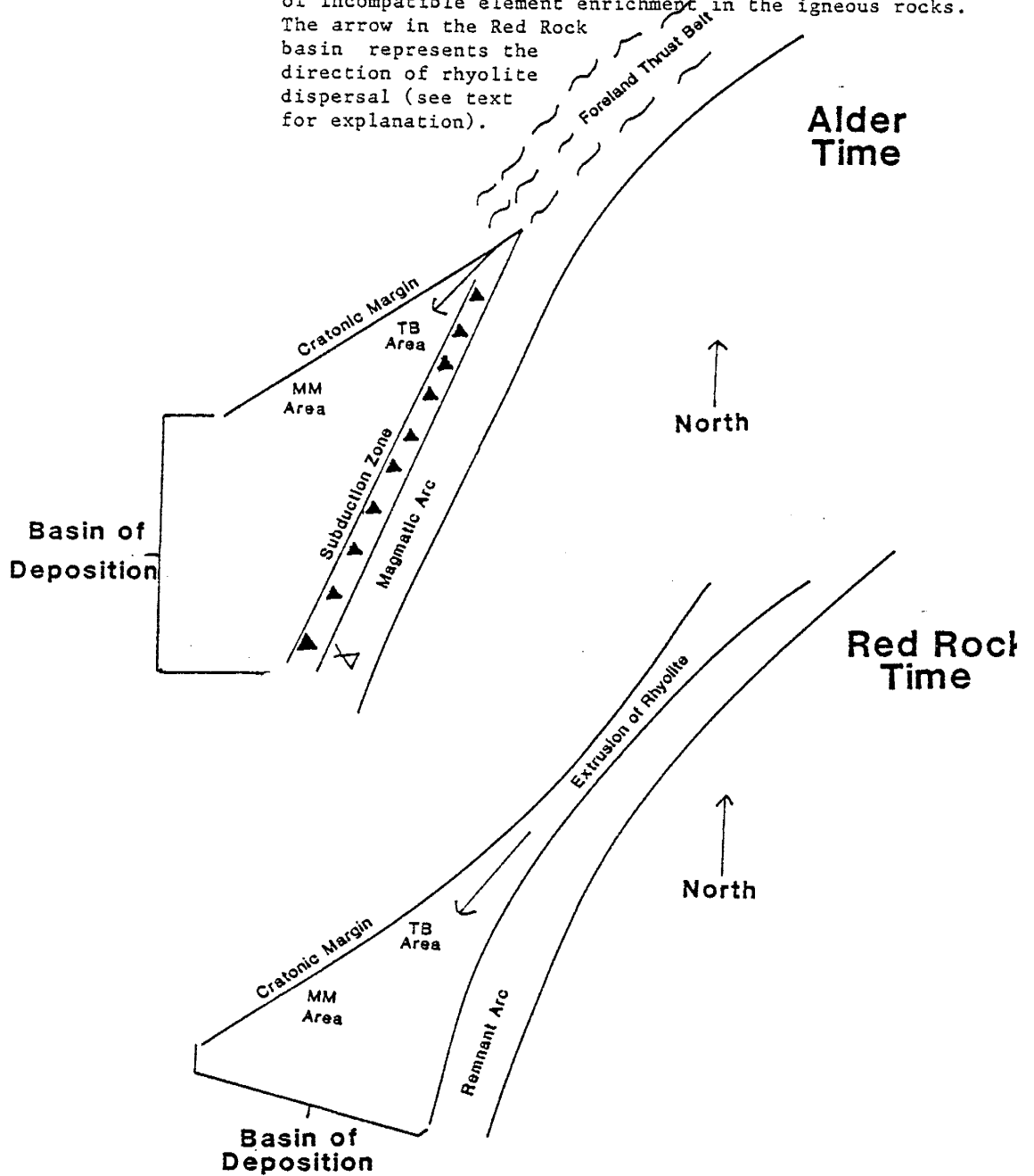
most depleted sample (MT0-16) which has been analyzed in the Mazatzal Mountains.

It is plausible that the arc-continent collision resulted in a decrease in the rate of subduction beneath the island arc. This would have caused a decrease in the rate of devolatilization from subducted crust; consequently, both  $H_2O$  pressure and oxygen fugacity would have decreased in the arc magmas. The reduction of oxygen fugacity may explain the transition from calc-alkaline to tholeiitic fractionation (Osborn, 1959). Lower  $H_2O$  pressure would have resulted in lower degrees of partial melting of the mantle source because the mantle solidus is raised to higher temperatures as  $H_2O$  pressure decreases (Green and Ringwood, 1972.)

Lower degrees of mantle partial melting can explain some but not all of the incompatible element enrichment in the intrusive rocks (see Mantle Source section). The apparent enrichment in LREE and Th in mafic and intermediate igneous rocks may have resulted from contamination of arc magmas with sialic melts (Thompson, et. al., 1982). Sialic melts could have been derived from subducted sediments (Pearce, 1983; and James, 1981); however, it seems likely that the proposed lower crustal melting associated with the arc-continent collision to the northeast could have provided the contaminant of the arc magmas. The enrichment of HFSE and HREE in the hypabyssal rocks may be the result of the extreme contamination of the arc magmas with sialic melts.

Figure 45 shows schematic maps of the proposed tectonic settings during Alder and Red Rock times, respectively. In Alder time, a foreland thrust belt results from the collision of the island arc and

Figure 45. Schematic diagrams in map view which show the proposed tectonic settings of the Alder and Red Rock basins of deposition. The basins of depositions are represented by the open triangular areas which are bracketed. The relative positions of the Tonto Basin (TB) and the Mazatzal (MM) areas in the basins are shown. The tectonic setting of the Alder basin (upper diagram) is adapted from Dickinson and Suzcek (1979). The arrow in the Alder basin represents both the direction of sediment dispersal and the direction of incompatible element enrichment in the igneous rocks. The arrow in the Red Rock basin represents the direction of rhyolite dispersal (see text for explanation).



the continent to the northeast. The vector which points to the southwest in the basin of the deposition represents the direction of sediment dispersal and of progressive incompatible element enrichment in the igneous rocks. The Figure shows that the collision occurred between an island arc and a craton; however, the data could also be explained by the collision of an active continental margin with a passive cratonic margin similarly, the arc may have been located to the north of the Alder basin and the passive margin may have been located to the south; however, the coarsening of volcanoclastic detritus to the southwest in the Cornucopia member suggests that the arc was located to the south of the basin. In Red Rock time, partial melting has occurred in the lower crust of the foreland thrust belt, and the rhyolite associated with this event is erupted into the basin to the southwest. This eruption may have obliterated the tectonic evidence of the suture between the arc and the continent. The southwest pointing vector in the lower Figure represents the direction of movement of the rhyolitic material into the basin of deposition.

Shearing in the Proterozoic rocks of the Mazatzal Mountains was probably the result of the Mazatzal Orogeny. Both the association of the Pine Mountain Porphyry (PMP) with heavily sheared areas of the Alder sequence and the highly foliated nature of the PMP suggest that the rock intruded syntectonically. It is proposed that the PMP crystallized from arc magma which was fractionating in a dormant magma chamber after extrusion of the RRR and that this magma was intruded into a higher level of the crust that underwent intense shearing during the Mazatzal orogeny.



## Scope for Future Studies

There is a considerable amount of evidence which disputes the simple structural interpretation proposed by Ludwig (1974). The structure must be fully understood before the stratigraphy of the Alder and Red Rock Groups can be determined. The interpretation of the Proterozoic stratigraphy is fundamental to the geochemical and sedimentologic interpretation of the Proterozoic succession. As a result, more structural work is needed in the area.

This study has proposed many trends in the igneous geochemistry. More chemical analyses are needed to verify the proposed trends. It would be interesting to analyze the intrusives in the Red Rock Rhyolite because clearly, these would be the youngest igneous rocks in the Proterozoic succession of the central Mazatzal Mountains. Similarly, more chemical analyses are needed of the igneous rocks in the Northern Succession. Although many of the rocks appear to be highly altered, some information may be obtained from the analysis of HFSE and HREE.

Finally, results of this study also suggest that the geochemical signature of the Alder sediments may be characteristic of an arc-continent collision. Young sediments from this type of setting must be chemically analyzed in order to verify this claim.

## Appendix A.

## Instrumental Neutron Activation Analysis (INAA)

Rock powders at  $\leq 200$  mesh (250-300 mg) have been sealed in polyethelene vials and have been irradiated at the core research reactor at the Sandia National Laboratories, Albuquerque, N.M. The rock powders have been prepared from hand specimens by successively grinding each sample in a jaw crusher, a high speed rotary ceramic disc grinder, and an automatic agate mortar and pestle. After each specimen is broken up by the jaw crusher, the pieces were analyzed under a  $10^X$  magnification scope, and the visibly altered pieces were removed from the sample. The  $\leq 200$  mesh powder was divided into three portions which were used for major and trace element analysis by XRF and trace element analysis by INAA.

Trace elements Cs, Sc, Hf, Ta, Cr, Co, Ar, U, Th, and REE were analyzed by INAA. Quality of NAA data is determined by intensity, stability, and homogeneity of the thermal neutron flux. The Sandia reactor has a moderate intensity and homogeneity with a thermal neutron flux of about  $5 \times 10^{11} \text{ cm}^{-2} \text{ sec}^{-1}$ . Minor variations in flux stability have little effect on final results if samples are compared to reference standards that are simultaneously irradiated with the samples. Reference standards have been used to calibrate the NAA analyses. Check standards which were used in part of the NAA runs (Appendix C) are BCR-1, An-G, W-2, DR-N.

Irradiation time also plays an important role in INAA. Longer irradiation time results in higher degrees of accuracy. The Sandia irradiation time is approximately 10000 seconds.

Counts were made at 7 and 40 days using a liquid nitrogen cooled, coaxial intrinsic Ge detector. Data were channeled and analyzed with a Nuclear Data 6600 multichannel analyzer and a LSI-11 computer. Analytical methods are similar to those described by Gibson and Jagam (1980).

## Appendix B.

## X-Ray Fluorescent Spectrometry (XRF)

XRF analysis follows the methods of Norrish and Hutton (1969); and Norrish and Chappel (1977). Analyses for major elements ( $\text{SiO}_2$ ,  $\text{TiO}_2$ ,  $\text{Al}_2\text{O}_3$ ,  $\text{Fe}_2\text{O}_3$ ,  $\text{MgO}$ ,  $\text{CaO}$ ,  $\text{Na}_2\text{O}$ ,  $\text{K}_2\text{O}$ ,  $\text{MnO}$ , and  $\text{P}_2\text{O}_5$ ) have been made by using fused disks which were comprised of  $\sim 0.5$  g of sample powder and  $\sim 2.7$ g of lithium borate flux. The sample and flux were fused in a platinum cubicle to  $\approx 900^\circ\text{C}$  for 5 to 15 minutes. The molten sample is then quenched to a glass disk by pressing in a platen and mold.

Trace elements (Ba, V, Zr, Rb, Sr, Y, Nb, Cr, and Ni) have been analyzed by using pressed powder pellets with a boric acid backing. Pellets were pressed under a pressure of 10 tons/in<sup>2</sup> for 30 seconds. Several drops of polyvinyl alcohol were added to the sample in order to increase adhesion.

Calibration curves for both major and trace element analysis using XRF have been calculated from USGS and in-house standards. Analyses were performed on a Rigaku 3064 XRF spectrometer with an associated PDP-11 computer and in-house software at the New Mexico Bureau of Mines and Mineral Resources.

## Appendix C.

## Accuracy and Precision of Geochemical Data

Accuracy and precision are determined by analyzing international and in-house rock standards. Root mean square percent error is calculated by the equation:

$$\text{RMS error} = \sqrt{\frac{\sum_{i=1}^n \left( \frac{r_i - m_i}{m_i} \right)^2}{n}} \times 100$$

where  $r$  is the recommended value,  $m$  is the measured value, and  $n$  is the number of analyses considered for that element. Precision is appraised by the average of 1 sigma deviations which are expressed as a percentage of the mean (coefficient of variation).

Unfortunately, there is some uncertainty with respect to the accuracy and precision of the NAA data which has been obtained before the spring of 1985 because standards were not run as unknowns. It is assumed that reference standards (Appendix A), which have been used to compensate for variations of the thermal neutron flux, have minimized the error associated with the early analyses; however, the lack of quantified accuracy and precision for this data may lead to some doubt regarding the geochemical significance of the compositional variations which are seen in the igneous rock samples.

Table C-1 shows which samples have been analyzed by NAA before check standards were used and which samples have been analyzed with standard control on accuracy and precision.

Table C - 1. Period of time in which NAA was acquired for each sample. Samples which were run after the spring of 1985 have better analytical certainty.

Igneous Rocks	
Samples analyzed before Spring 1985	Samples analyzed after Spring 1985
WF - 1	WF - A
MTO - 4	MTO - B
TB - 9	TC - 2
MTO - 8	TC - 18
TC - 25	TC - 21
TC - 24	MW - C
TC - 7	MW - D
MTO - 16	MTO - 16
TC - 3	
TB - 1	
MTO - 14	
TC - 16	
HUMMTN - 2	

Sedimentary Rocks	
Sediments analyzed before Spring 1985	Sediments analyzed after Spring 1985
HWY 87 - 1	WF - 3
WF - 11	WF - 16
TC - 17	WF - 15
WF - 2	WF - 12
	MW - F
	MTO - 19
	MW - B
	TC - 9
	TC - 5
	TC - 13
	MTO - 18
	WFT - 2

Even with the uncertainties regarding the early NAA data, some points can be made which substantiate the proposed compositional variation of the igneous rocks. Firstly, relatively enriched mafic samples have higher abundances of the trace elements which have been determined by XRF. Secondly, enriched samples have been analyzed in NAA runs before and after check standards were used. Thirdly, the "depleted" mafic sample, MTO-16, has been analyzed before and after checks standards were used, and good precision has been calculated for these analyses. The two analyses of MTO-16 and the coefficient of variation are shown in Table C-2. Finally, the enriched samples have the same occurrences in the field (intrusives), and it seems unlikely that analytical variations would have selectively affected this group of rocks.

Table C-3 shows the standards which are used to compute accuracy and precision and the number of analyses of each element which are run for each standard. Table C-4 shows the accuracy and precision of the geochemical data. It can be seen from Table C-4 that the major element data appear to be analytically reliable for the most part. The elements MgO, MnO, and P<sub>2</sub>O<sub>5</sub> have high associated errors because some of the standards have concentrations which are near the detectability limit. The analytical data appear reliable for all of the trace elements except Cr.

Table C-2. Precision of the analyses of MTO - 16 which were acquired before and after the spring of 1985, respectively.

Element	NAA data acquired before spring 1985	NAA data acquired after spring 1985	Coefficients of variations (%)
Cs	0.5	0.37	14.8
Sc	36.2	31.1	7.6
Co	30.2	29.3	1.5
Hf	1.0	1.08	3.9
Ta	0.12	0.17	17.2
La	6.1	5.58	4.5
Ce	14.1	11.7	9.3
Sm	2.3	2.22	1.8
Eu	0.82	0.70	7.9
Tb	0.44	0.32	15.8
Yb	1.27	1.31	1.6
Lu	0.17	0.20	8.1



Table C-3. Standards used in computing accuracy and precision. Numbers indicate the number of times a particular standard was run for a specific element.

	BLCR	LOSP	HI-31	STM-1	DR-N	AN-G	W-2	G-2	BCR
SiO <sub>2</sub>	5	4	4	1					2
TiO <sub>2</sub>	5	4	4	1					2
Al <sub>2</sub> O <sub>3</sub>	5	4	4	1					2
Fe <sub>2</sub> O <sub>3</sub>	5	4	4	1					2
MgO	5	4	4	1					2
CaO	5	4	4	1					2
Na <sub>2</sub> O	5	4	4	1					2
K <sub>2</sub> O	5	4	4	1					2
MnO	5	4	4	1					2
P <sub>2</sub> O <sub>5</sub>	5	4	4	1					2
Rb	4	4	3					1	
Ba			2					1	3
Cs					2	4	2	1	2
Sr	4	3	3					1	
Th	4	3	3					1	
U					2	4	2	1	2
Sc					2	4	2	1	2
Cr			2				1		3
Co					2	4	2	1	2
Ni			2		1	1			3
Y	5	4	3					1	
Zr	4	3	3					1	
Nb	5	4	3					1	
Hf					2	4	2	1	2

Table C-3 Continued.

Ta					2	4	2	1	2
La					2	4	2	1	2
Ce					2	4	2	1	2
Sm					2	4	2	1	2
Eu					2	4	2	1	2
Tb					2	4	2	1	2
Yb					2	4	2	1	2
Lu					2	4	2	1	2
V			2					1	3

Table C-4. Summary of precision and accuracy of chemical data. Values calculated are based on analyses of standards listed in table C-3.

	n	rms % error	average 1 sigma as % of mean
SiO <sub>2</sub>	16	1.01	0.60
TiO <sub>2</sub>	16	3.70	1.12
Al <sub>2</sub> O <sub>3</sub>	16	2.58	0.61
Fe <sub>2</sub> O <sub>3</sub> T	16	3.22	2.34
MgO	16	49.34	5.27
CaO	16	3.56	0.59
Na <sub>2</sub> O	16	4.47	4.15
K <sub>2</sub> O	16	3.30	0.77
MnO	16	23.78	4.06
P <sub>2</sub> O <sub>5</sub>	16	33.64	5.04
Rb	12	3.07	0.40
Ba	6	8.05	0.24
Cs	11	7.24	5.16
Sr	11	2.72	1.48
Th	11	11.61	4.14
U	10	3.38	3.67
Sc	11	6.82	4.70
Cr	6	48.66	35.35
Co	11	6.81	4.05
Ni	7	4.99	2.59
Y	13	6.98	4.42
Zr	11	6.37	2.38
Nb	13	16.39	11.17
Hf	11	13.17	8.52
Ta	11	22.18	12.27

Table C-4. Continued.

	n	rms % error	average 1 sigma as % of mean
La	10	10.38	5.83
Ce	11	8.49	5.88
Sm	10	10.71	3.47
Eu	11	11.53	8.85
Tb	11	12.28	7.58
Yb	11	0.54	2.81
Lu	10	17.59	6.13
V	6	7.55	3.26

## Appendix D.

## Parameters and Constraints of Modal Analysis

As part of the petrographic examination of the sedimentary lithologies, point counts have been conducted in order to determine the framework modes of the different samples in thin section. The grain types which were identified in the point counts are: 1) potassium feldspar, 2) plagioclase feldspar; 3) silty-sandy sedimentary rock fragments, 4) pelitic rock fragments, 5) volcanic rock fragments, 6) monocrystalline quartz grains, 7) polycrystalline fine grained quartzose rock fragments, 8) polycrystalline coarse grained quartzose rock fragments, and 9) opaque grains.

The thin sections have been stained in order to distinguish potassium feldspar from plagioclase feldspar. The silty-sandy and volcanic rock fragments are sometimes difficult to distinguish. Silty-sandy refers to the terminology of Dickinson (1970). These rock fragments have an abundance of quartz with a minor proportion of interstitial clay (sericite). Volcanic rock fragments are distinguished from silty-sandy types by: 1) the presence of subhedral to euhedral microphenocrysts of feldspar laths in an anhedral mosaic under crossed nicols (sometimes carlsbad twinning can be seen in these laths); 2) internal relief between different phenocryst types within the grain under plain light; and 3) an appreciable proportion of chlorite. Microprobe work suggests that these distinctions are chemically valid as grains which were identified as silty-sandy rock fragments have on the average 80-90% silica while grains which were identified as volcanic rock fragments have 68-76% silica. Pelitic

rock fragments are entirely sericitized in thin section; however, the outlines of the original rock fragments are still visible in plain light.

When distinguishing monocrystalline from polycrystalline quartz, care was taken to distinguish true polycrystalline quartz from polygonized quartz. In polygonized quartz grains, the difference in extinction position between adjacent subgrains is small (a few to several degrees) (Bond and DeVay, 1980). As a result, quartz grains with changes of several degrees or less in extinction position across internal grain boundaries are classified as monocrystalline.

Only quartz grains which are 0.05 mm or larger have been counted because, with decreasing grain size, the ratio of monocrystalline to polycrystalline quartz increasingly becomes a function of the degree to which polycrystalline quartz has disintegrated during weathering and transport (Bond and DeVay, 1980). A polycrystalline quartz rock fragment is considered coarse grained if a single subgrain exceeds 0.1 mm; otherwise, the fragment is considered to be a polycrystalline fine grained quartzose rock fragment.

Any grain which is smaller than 0.05 mm is considered to be matrix. A minimum of 400 points have been counted in each thin section.

## Appendix E.

Geochemical Method for Determining the Amount of Possible  
Recrystallization of Specific Detrital Components in Matrix Rich  
Sandstones

This appendix discusses a geochemical approach to constrain sandstone matrix composition in terms of specific compositions of detrital rock and mineral fragments. The method involves recalculation of the proportions of detrital components as constrained by major-element contents of sandstones. To employ the method, it is necessary to have major-element analyses of sandstones, and of rock and mineral fragments in the sandstones. Rock and mineral fragment compositions can be determined directly with an electron probe or estimated from published analyses of appropriate rocks and minerals.

The geochemical calculation determines the upper limit of the amount of a specific detrital component present in an original sediment before recrystallization. The calculation uses the ratio:

$d = S/R \times 100\%$  where:

$d$  = % of a rock or mineral fragment that has recrystallized into matrix;

$R$  = % of a specific major element in a rock or mineral fragment; and  $S$  = % of a specific major element in the matrix of the whole rock.

There are five steps to the geochemical calculation which are as follows: 1) determine the controlling element (the element which gives the smallest  $S/R$  ratio for a specific rock or mineral type); 2) calculate the contributions of the controlling element from the preserved detrital grains; 3) subtract this contribution from the

whole rock concentration of the controlling element; 4) divide the excess controlling element by the amount in the rock or mineral type and multiply by 100%; and 5) add this percentage of rock or mineral type to the preserved detrital mode and calculate a new mode.

An example calculation is shown below in order to help clarify the procedure. Table E-1 shows the chemical and modal compositions of the sample, TC-13, which are taken from Tables 1 and 2, respectively. Table E-2 shows typical compositions, which have been reported in the literature, of various rock and mineral types. The composition of the silty-sandy rock fragment have been estimated from microprobe analysis. The example calculation which is presented in this section assumes that only plagioclase has recrystallized to matrix.

Step 1 of the geochemical calculation involves determining the controlling element. It is found that CaO results in the lowest S/R ratio for plagioclase and TC-13 ( $S/R = 0.14/4.5 = 0.03$ ). One of the problems with controlling elements is the fact that they are typically the most mobile elements during metamorphism and/or alteration.  $Al_2O_3$  is typically immobile (Bhatia, 1983); therefore, it is used in steps 2-5 to constrain the amount of plagioclase recrystallization. For comparison, the S/R ratio of aluminum in plagioclase and TC-13 is 0.36 ( $8.41/23.5$ ). Step 2 is the determination of  $Al_2O_3$  contributions from the preserved mode in the sediments. Table E-3 shows this determination. The compositions of the rock fragments and mineral grains are taken from Table E-2. Microprobe work has shown that volcanic rock fragments are typically rhyolitic in composition.

The total  $Al_2O_3$  in the preserved mode is subtracted from the whole rock concentration in order to derive the concentration of  $Al_2O_3$



Table E-1. Modal and chemical compositions of TC - 13 which are used to correct for plagioclase recrystallization.

	chemical composition of TC-13 (%)	modal composition of TC-13 (%)
SiO <sub>2</sub>	84.26	potassium feldspar (KF) 0.0
TiO <sub>2</sub>	0.23	plagioclase feldspar (plg) 2.56
Al <sub>2</sub> O <sub>3</sub>	8.41	sedimentary rock fragment (SRF) 11.50
FeO <sub>2.3T</sub>	2.49	volcanic rock fragment (VRF) 3.80
MgO	0.24	pelitic rock fragment (PRF) 0.28
CaO	0.14	monocrystalline quartz (Qm) 24.22
Na <sub>2</sub> O	2.21	polycrystalline fine quartz (QPF) 13.96
K <sub>2</sub> O	1.74	polycrystalline coarse quartz (QPC) 10.54

Table E-2. Chemical compositions of rock and mineral fragments used in geochemical matrix calculations.

element	K	P(An <sub>2</sub> O)	And	CAB	Rhy	PRF	SRF
SiO <sub>2</sub>	64.5	62.5	57.9	51.6	74.4	61.5	85.90
TiO <sub>2</sub>	0.0	0.0	0.9	1.0	0.2	0.8	0.21
Al <sub>2</sub> O <sub>3</sub>	20.0	23.5	17.0	17.4	13.7	17.0	7.32
Fe <sub>2</sub> O <sub>3T</sub>	0.0	0.0	7.8	10.1	1.6	6.7	2.57
MgO	0.0	0.0	3.4	6.8	0.3	2.5	0.12
CaO	0.3	4.5	6.8	9.7	1.1	1.8	0.20
Na <sub>2</sub> O	3.0	8.8	3.5	2.7	3.6	1.8	0.84
K <sub>2</sub> O	12.0	0.6	1.6	1.2	4.7	3.5	1.57

Fe<sub>2</sub>O<sub>3T</sub>, total Fe as Fe<sub>2</sub>O<sub>3</sub>; K, K-feldspar; P, plagioclase; AND, andesite; CAB, calc-alkaline basalt; Rhy, rhyolite; PRF, pelitic rock fragment; SRF, sedimentary rock fragment. References: Deer, et al., (1963); Le Maitre (1976); Ewart (1979); Shaw (1956); Condie (1985).

Table E-3. The determination of contributions of  $Al_2O_3$  from the preserved detrital grains and the determination of the amount of  $Al_2O_3$  in the matrix of TC-13.

component	mode	$Al_2O_3$ % in component	contribution of $Al_2O_3$ to whole rock (%)
plg	0.026	23.5	0.61
SRF	0.115	7.32	0.84
VRF	0.038	13.7	0.52
PRF	0.003	17.0	+0.05

Total  $Al_2O_3$  in detrital components - (2.02)

$Al_2O_3$  in whole rock + 8.41

$Al_2O_3$  in matrix 6.39

in the matrix (step 3). The calculated  $\text{Al}_2\text{O}_3$  concentration in the matrix is divided by the  $\text{Al}_2\text{O}_3$  which is used by plagioclase in order to calculate the maximum proportion of plagioclase which may have recrystallized to matrix. This calculation is shown below:

$$\text{excess } \text{Al}_2\text{O}_3 \text{ in matrix (S)} = 6.39\%$$

$$\text{Al}_2\text{O}_3 \text{ in plagioclase (R)} = 23.5\%$$

maximum proportion of recrystallized plagioclase

$$(d) = S/R = 6.39/23.5 = 0.272 \times 100\% = 27.2\%$$

$$\begin{aligned} \text{maximum possible amount of original plagioclase in the sediment} \\ = 27.2 + 2.56 = 29.76. \end{aligned}$$

The affect of this calculation on the relative modal abundances is shown below:

preserved mode in TC-13:	Recalculated mode for plagioclase recrystallization
Q = 72.9 Om = 36.2	Q = 5.18 Qm = 25.8
F = 3.8 F = 3.8	F = 31.6 F = 31.6
L = 23.3 Lt = 60.0	L = 16.6 Lt = 42.6

Modes for all of the sediment samples (except JBS-1) in Table 4 have been calculated by assuming the recrystallization of each type of rock fragment or mineral grain in Table E-2. It is found that the greatest change in detrital interpretation of provenance occurs when either rhyolite or plagioclase is assumed to have recrystallized to matrix.

## Appendix F.

## Paleocurrent Directions

This appendix discusses the method by which paleocurrent directions are determined from cross-bedding in tilted beds. It also shows the results of this analysis. The strikes and dips of the cross-bedding and the bedding are taken from quartz arenites and quartz wackes of the Telephone Canyon member in Telephone Canyon and Gold Tooth Spring Canyon (see geologic map).

The restoration of original cross-bedding is calculated on a Wulff net. Figure F-1 shows an example of how this restoration is performed, and Table F-1 shows the results of the paleocurrent analysis.

The first cross-bed in Table F-1 is in a bed which strikes N38E and dips  $64^\circ$  to the west. This bed is plotted on the Wulff net as plane 1. The pole to the cross-bedding ( $P_1$ ) is also plotted in the Figure. In order to restore the tilted bed to the horizontal position, the strike of the bed (plane 1) is aligned along the north-south axis, and the plane is "rotated"  $64^\circ$  to the primitive circle. When this is done,  $P_1$  moves along a small circle to  $P_2$  which is indicated by the arrow in Figure F-1.  $P_2$  is the pole to the restored cross-bedding. The original cross-bedding plane is determined by rotating  $P_2$  along a great circle to the east-west axis, and the great circle which is  $90^\circ$  from  $P_2$  when it is in this position represents the original cross-bedding plane (plane 2). The original dispersal direction is parallel to the dip of plane 2; and this is indicated by an arrow in Figure F-1.

The results in Table F-1 indicate a dominantly southwestern dispersal direction. Two of the measurements indicate a northwesterly dispersal, and one measurement which has been taken from a herringbone cross-bed indicates a northeasterly dispersal. Since the majority of measurements indicate southwesterly dispersal, it is inferred that the source of the quartz arenites and quartz wackes was to the northeast.

Figure F-1. Outline of a Wulff net which shows the restoration of the first bedding-cross-bedding pair in Table F-1 (see text for explanation).

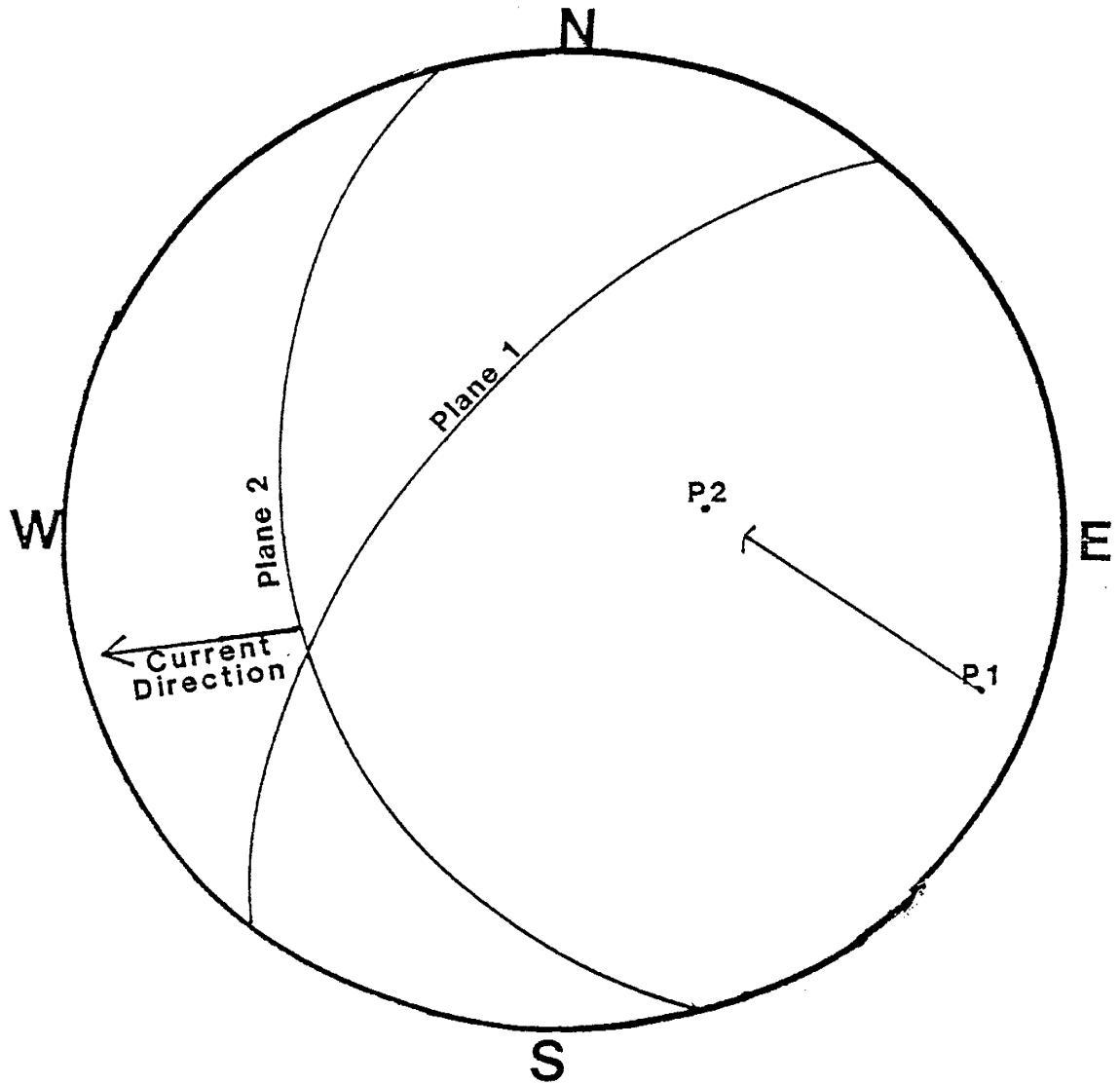


Table F-1. Strikes and dips of unrestored cross-bedding and bedding, and dispersal direction indicated by restored cross-bedding.

<u>unrestored cross-bedding</u>	<u>strike and dip of bedding</u>	<u>dispersal direction</u>	<u>dip angle of cross-bedding</u>
N 20°E 78°W	N 38°E 64°W	S 75°W	30°
W 50°E 60°W	N 38°E 64°W	N 60°E	14°
N 14°E 74°W	N 38°E 64°W	S 58°W	33°
N 40°E 42°W	N 65°E 60°W	S 15°W	36°
N 46°E 72°W	N 65°E 60°W	S 52°W	20°
N 36°E 58°W	N 65°E 60°W	N 84°W	30°
N 17°E 70°W	N 54°E 66°W	S 77°W	37°
N 34°E 74°W	N 59°E 80°W	S 44°W	22°
N 53°E 88°W	N 59°E 80°W	N 58°W	10°
N 44°E 75°W	N 67°E 82°W	S 52°W	32°
N 50°E 84°W	N 67°E 82°W	S 46°W	12°



## Appendix G.

## Petrologic Major Element Modal Mixing Calculations

The calculation of a least squares approximation of the major element abundances of an assumed parent liquid or a source rock follows the procedures described in Bryan, et al., (1969); and Wright and Doherty (1970). The calculations were performed by using the computer program, MIXFRAC which has been written by Michael Knoper. Major element mixing calculations result in statistically valid and unique solutions.

In this study, major element mixing calculations which involve assumed compositions of parent liquids, daughter liquids, and mineral phases are considered to be petrogenetically valid if the sum of squared residuals is less than or close to 0.1. It is very difficult to find mixing solutions which meet the stated criterion and which give workable FXL or BM modes. More specifically, only certain combinations of mafic and evolved samples can be petrogenetically related by major element modal mixing. This is demonstrated below, and it is assumed that these limitations reflect the chemical variability which is demonstrated in the igneous rocks.

Table G-1 shows the compositions of the mineral phases which are used to relate mafic samples to intermediate samples. Two mafic-intermediate sample pairs result in major element mixing calculations which meet the previously stated restriction for the sum of squared residuals. Both of the calculated modes include plagioclase, olivene, clinopyroxene, and magnetite. Various compositions for amphibole and the phases mentioned above have been used in these calculations which

involve different combinations of mafic and intermediate samples. None of the combinations involving amphibole have been successful in meeting the requirements for a good petrogenetic relationship. As a result, amphibole has not been considered as a mineral phase in geochemical models.

The least squares approximation of the major elements of TC-18 by mixing of those of TC-16 and some of the mineral phases in Table G-1 results in the mode and sum of squared residuals which is shown in the following Table.

	TC - 16	TC - 18	Component	Proportion
SiO <sub>2</sub>	58.24	53.20	TC- 16	0.55
TiO <sub>2</sub>	1.26	1.14	epx	0.10
Al <sub>2</sub> O <sub>3</sub>	16.06	17.51	plg	0.27
FeO <sub>2 3T</sub>	9.00	9.06	oliv	0.05
MnO	0.13	0.12	Mgt	0.02
MgO	2.55	4.94		
CaO	4.36	8.35	sum of squared residuals = 0.12	
Na <sub>2</sub> O	4.72	3.61		
K <sub>2</sub> O	3.22	0.39		
P <sub>2</sub> O <sub>5</sub>	0.46	0.39		

The mode from this calculation is used directly in a petrogenetic model with the respective trace element abundances.

The relationship between MTO-16, MTO-14, and the phases in Table G-1 is shown below.

	MTO - 14	MTO - 16	Component	Proportion
SiO <sub>2</sub>	63.31	49.32	MTO- 14	0.41
TiO <sub>2</sub>	0.63	0.84	cpx	0.01
Al <sub>2</sub> O <sub>3</sub>	15.52	17.77	plg	0.36
Fe <sub>2</sub> O <sub>3</sub> T	8.84	14.79	oliv	0.13
MnO	0.11	0.24	Mgt	0.09
MgO	2.15	6.03		
CaO	5.92	8.18		
Na <sub>2</sub> O	2.54	2.45	sum of squared residuals = 0.14	
K <sub>2</sub> O	0.79	0.23		
P <sub>2</sub> O <sub>5</sub>	0.18	0.15		

The mode from this calculation appears to be too high in magnetite. This may result from the fact that MTO-14 has been enriched in silica (Appendix I). The mode which is used in the trace element modeling of these samples is adjusted from the phases which are calculated above.

In order to further demonstrate the chemical variability of the igneous rocks and to show the significance of the mafic-intermediate pairs which are related above, the samples MTO-16 and TC-18 have been related to TC-16 and MTO-14, respectively. The results of these calculations are shown below.

MTO-16 and TC-16		TC-18 and MTO-14	
Component	Proportion	Component	Proportion
TC-16	0.41	MTO-14	0.52
cpx	0.08	cpx	0.31
plg	0.35	plg	0.30
oliv	0.10	oliv	0.09
mgt	0.09	mgt	0.02

sum of squared residuals = 1.9

sum of squared residuals = 3.9.

It can be seen that the sums of squared residuals of these calculations are too high for these relationships to be statistically valid petrogenetic models. The results suggest that TC-16 and MTO-14 can not be related by FXL to MTO-16 and TC-18, respectively.

The composition of the mineral phases which have resulted in successful mixing calculations for felsic and intermediate samples are shown in Table G-2. An acceptable least squares approximation of the major elements of MTO-14 has been obtained by mixing with those of the Pine Mt. Porphyry sample, WF-1, and the phases listed in Table G-2. The results of this calculation are shown on the following page.

	WF - 1	MTO -14	Component	Proportion
SiO <sub>2</sub>	75.77	63.32	WF - 1	0.04
TiO <sub>2</sub>	0.19	0.63	opx	0.06
Al <sub>2</sub> O <sub>3</sub>	14.17	15.52	plg	0.49
FeO <sub>2 3T</sub>	1.87	8.84	cpx	0.01
MnO	0.05	0.11	biot	0.06
MgO	0.20	2.15	mgt	0.07
CaO	0.59	5.92	qtz	0.28
Na <sub>2</sub> O	2.52	2.54		
K <sub>2</sub> O	4.59	0.79	sum of squared residuals = 0.04	
P <sub>2</sub> O <sub>5</sub>	0.05	0.18		

The mode is very high in quartz, and the relationship calls for a high degree of FXL to generate WF-1. Both of these results may be caused by silica enrichment in MTO-14. The low sum of squared residuals suggests that WF-1 is related to a parent liquid which is similar in chemistry to MTO-14. The mode which is used in trace element modeling of WF-1 is constrained by the phases in the assemblage which is shown above.

One of the Red Rock Rhyolite samples, MW-C, is used in petrologic mixing calculations which test both partial melting and fractional crystallization, respectively.

The partial melting calculation uses the lower crust composition of Weaver and Tarney (1984), and the mafic mineral compositions for the residual phases in the lower crust. The results of the calculation are shown below.

	MW - C	Lower Crust	Component	Proportion
SiO <sub>2</sub>	76.51	59.03	MW - C	0.31
TiO <sub>2</sub>	0.18	0.90	opx	0.05
Al <sub>2</sub> O <sub>3</sub>	11.84	17.15	plg	0.44
Fe <sub>2</sub> O <sub>3T</sub>	2.15	6.88	cpz	0.01
MnO	0.00	0.12	biot	0.08
MgO	0.08	3.39	mgt	0.05
CaO	0.29	5.88	qtz	0.05
Na <sub>2</sub> O	4.40	3.99		
K <sub>2</sub> O	4.55	2.39		
P <sub>2</sub> O <sub>5</sub>	0.00	0.27		
			sum of squared residuals =	0.16

The composition of biotite which has been used in the least squares approximation above is taken from Table G-2. It is likely that the composition of biotite in the lower crust would actually be more mafic. As a result, the Red Rock calculation has also been performed with a typical phlogopite composition (Best, 1982) substituted for the felsic biotite. The sum of the squared residuals after this change is made is 0.08.

Petrologic mixing has been unsuccessful in relating the Red Rock Rhyolite to any analyzed sample by typical assemblages of mineral phases. In modeling the Red Rock Rhyolite by FXL, a mode has been determined by deriving a daughter liquid with similar trace element abundances to those of the Red Rock Rhyolite from a dacitic parent (WCRD-1) from Tonto Basin. The assemblage of phases in this mode and the two samples do not provide a statistically valid petrogenetic mixing calculation. The results of this calculation using the mineral compositions of Table G-2 are shown below.

	MW - C	WCRD-1	Component	Proportion
SiO <sub>2</sub>	76.51	66.02	MW - C	0.86
TiO <sub>2</sub>	0.18	0.82	opx	0.03
Al <sub>2</sub> O <sub>3</sub>	11.84	15.64	plg	0.19
Fe <sub>2</sub> O <sub>3T</sub>	2.15	5.95	cpx	-0.03
MnO	0.08	0.21	biot	0.01
MgO	0.08	0.27	mgt	0.04
CaO	0.29	1.92	qtz	-0.11
Na <sub>2</sub> O	4.40	5.05		
K <sub>2</sub> O	4.55	3.90	sum of squared residuals =	0.39
P <sub>2</sub> O <sub>5</sub>	0.00	0.22		

The comparison of petrologic mixing calculations involving batch melting and FXL processes for the generation of the Red Rock Rhyolite suggests that the former process is the most likely origin for this rock type.



Petrologic mixing has been unsuccessful in relating the Red Rock Rhyolite to any analyzed sample by typical assemblages of mineral phases. In modeling the Red Rock Rhyolite by FXL, a mode has been determined by deriving a daughter liquid with similar trace element abundances to those of the Red Rock Rhyolite from a dacitic parent (WCRD-1) from Tonto Basin. The assemblage of phases in this mode and the two samples do not provide a statistically valid petrogenetic mixing calculation. The results of this calculation using the mineral compositions of Table G-2 are shown below.

	MW - C	WCRD-1	Component	Proportion
SiO <sub>2</sub>	76.51	66.02	MW - C	0.86
TiO <sub>2</sub>	0.18	0.82	opx	0.03
Al <sub>2</sub> O <sub>3</sub>	11.84	15.64	plg	0.19
Fe <sub>2</sub> O <sub>3T</sub>	2.15	5.95	cpx	-0.03
MnO	0.08	0.21	biot	0.01
MgO	0.08	0.27	mgt	0.04
CaO	0.29	1.92	qtz	-0.11
Na <sub>2</sub> O	4.40	5.05		
K <sub>2</sub> O	4.55	3.90	sum of squared residuals = 0.39	
P <sub>2</sub> O <sub>5</sub>	0.00	0.22		

The comparison of petrologic mixing calculations involving batch melting and FXL processes for the generation of the Red Rock Rhyolite suggests that the former process is the most likely origin for this rock type.

Table G-1. Compositions of mafic mineral phases used in major element mixing calculations.

element	clinopyroxene	plagioclase	olivine	orthopyroxene	magnetite
SiO <sub>2</sub>	53.82	50.19	36.17	50.46	0.17
TiO <sub>2</sub>	0.45	0.00	0.00	0.50	7.91
Al <sub>2</sub> O <sub>3</sub>	1.74	30.79	0.00	0.53	3.14
Fe <sub>2</sub> O <sub>3T</sub>	9.09	0.80	28.59	25.60	81.90
MnO	0.00	0.00	0.45	1.20	0.47
MgO	16.91	0.00	34.57	16.87	6.42
CaO	17.73	15.13	0.22	4.70	0.00
Na <sub>2</sub> O	0.26	3.05	0.00	0.15	0.00
K <sub>2</sub> O	0.00	0.04	0.00	0.00	0.00
P <sub>2</sub> O <sub>5</sub>	0.00	0.00	0.00	0.00	0.00

References: Luhr and Carmichael (1985); and Kay and Kay (1985).

Table G-2. Compositions of felsic mineral phases used in major element mixing calculations.

element	clinopyroxene	plagioclase	ortho-pyroxene	biotite	magnetite
SiO <sub>2</sub>	50.46	54.81	50.96	38.00	0.85
TiO <sub>2</sub>	0.50	0.00	0.67	4.66	4.98
Al <sub>2</sub> O <sub>3</sub>	0.53	28.40	3.95	14.03	1.51
FeO <sub>2-3T</sub>	25.60	0.60	10.95	16.36	90.71
MnO	1.20	0.00	0.32	0.98	0.99
MgO	16.87	0.06	14.30	16.37	0.91
CaO	4.70	11.03	18.72	0.06	0.06
Na <sub>2</sub> O	0.15	4.83	0.13	0.90	0.00
K <sub>2</sub> O	0.00	0.26	0.01	8.62	0.00
P <sub>2</sub> O <sub>5</sub>	0.00	0.00	0.00	0.00	0.00

References: Frey, et al., (1984); and Grove and Donnelly-Nolan (1986).

## Appendix H.

## Trace Element Geochemical Modeling

The petrogenetic modeling of trace element abundances uses published mineral-liquid distribution coefficients (kd's) and empirical equations which relate parent and daughter element concentrations to the bulk distribution coefficients. As mentioned in the text, the mineral phases which are used in trace element modeling are largely constrained by petrologic major element mixing calculations (Appendix G).

The geochemical modeling equations are as follows:

fractional crystallization -  $C_0/C_1 = F^{(D-1)}$

batch melting -  $C_0/C_1 = D + F(1-P)$

open system fractional crystallization (O'Hara, 1977) -

$$C_1/C_0 = \frac{X[1+q((C_0/C_1) - 1) + Y] (1-X)^{D-1}}{1-(1-X-Y) (1-X)^{D-1}}$$

$$D = \sum m_i K_i$$

$$P = \sum p_i K_i$$

where:

$C_0$  = initial concentration of an element

$C_1$  = instantaneous concentration of an element

$F$  = fraction of melt

$D$  = bulk distribution coefficient

$P$  = bulk distribution coefficient for melting

$K_d$  = distribution coefficient for an element (solid liquid)

$M_i$  = mass fraction of a mineral in a rock

$p_i$  = mass fraction of a mineral entering a melt

$x$  = mass fraction of cumulate formed from the magma in each cycle

$Y$  = mass fraction of the original liquid before this

fractionation which is extracted as a lava flow at the end  
of each cycle.

$Z$  = mass of parental magma added in each cycle (expressed as an  
absolute quantity relative to the initial size of the magma  
chamber)

$C_0$  = concentration of element in material digested by the magma  
chamber

$q$  = fraction of the total cumulate  $X$ , fraction, which has been  
precipitated in order to provide the energy necessary to  
digest a mass fraction,  $Q$ , of a previously erupted basalt.  
It has been assumed that  $Q = qX$  and that  $(1 - q) X$   
represents fractionation caused by conductive and other  
energy losses.

$C_0$  and  $C_1$  calculations involving these equations were performed by  
using a versatile computer petrogenetic modeling program (MODULUS)  
which has been written by Michael Knoper.

## Appendix I.

## Alteration

Analyzed samples are considered altered if: 1) they plot outside of the  $\text{CaO}/\text{Al}_2\text{O}_3$ - $\text{MgO}/10$ - $\text{SiO}_2/100$  alteration screen of Davis, et. al., (1979), or 2) they have LOI greater than 5%. Altered samples are denoted by special symbols in geochemical diagrams

It is noted that many of the lithologies in the northern section appear to be hydrothermally altered. Geochemical trends support this assumption. Two samples which seem to be hydrothermally altered are WF-5 and MTO-B.

WF-5 is taken from the area of carbonate alteration in the northern succession, and MTO-B is taken from an area of maximum deformation in the shear zone of the southern succession. The samples are difficult to classify. In Figure 23, the samples plot as subalkaline basalts, and in Figure 22, they plot as andesites. The latter classification scheme is considered to be more reliable; therefore, it is assumed that the samples are andesitic.

Of the two unaltered andesites which are analyzed, the sample, MTO-14, is most similar to MTO-B and WF-5. As a result, the chemical composition of MTO-14 is compared with the compositions of the two altered andesites in Table I-1. Common geochemical trends of hydrothermal alteration are also shown in Table I-1. It can be seen that silica is often lost during hydrothermal alteration, and this may explain the classification of MTO-B and WF-5 as subalkaline basalts in Figure 22. Other trends which may be attributed to hydrothermal alteration of the two samples are enrichments in MgO, Ba, LREE, Th,

Ni, and Cr. The HFSE and HREE do not appear to be affected greatly by the alteration.

Other trends of alteration may have also affected some of the other mafic samples. Two of the "enriched" intrusive samples appear to be altered (TC-7 and WF-A). These samples have LOI greater than 7%, and they plot outside of the  $\text{CaO}/\text{Al}_2\text{O}_3$  -  $\text{MgO}/10$  -  $\text{SiO}_2/100$  alteration screen. CIPW normative calculations for TC - 7 show that the sample has 20% quartz.

When these samples are compared to the unaltered intrusive samples (TC-2 and TC-3; Table 3), it is observed that the altered samples may have been enriched in  $\text{Fe}_2\text{O}_3\text{T}$ ,  $\text{K}_2\text{O}$ ,  $\text{MnO}$ ,  $\text{P}_2\text{O}_5$ ,  $\text{H}_2\text{O}$ , Rb, Th, and Ba and depleted in  $\text{MgO}$ ,  $\text{CaO}$ ,  $\text{Na}_2\text{O}$ , and Sr. The altered and unaltered intrusives are very similar with respect to the HFSE and the REE abundances. This is a good indication that the HFSE have been relatively immobile.

An altered sample (TB-1) which has been collected by Kent Condie in the shear zone of the southern succession is very similar with respect to HFSE, REE, Th, Cr, Ni, and Co to the the sample, TC-18. The most notable distinction between the two samples is the respective silica abundances. On the  $\text{SiO}_2$  vs Nb/Y diagram (Figure 22), TB-1 classifies as an andesite while TC-18 classifies as a subalkaline basalt; however, on the  $\text{Zr}/\text{TiO}_2$  vs Nb/Y diagram (Figure 21), both samples classify as subalkaline basalts. As a result, it seems that TB-1 has been silicified as it has been altered. Other geochemical distinctions between the two samples which may be attributed to alteration of TB-1 are lower CaO,  $\text{K}_2\text{O}$ , Rb, Ba, and Sr abundances; and higher  $\text{Na}_2\text{O}$  abundance in TB-1. Of course, it can not be determined

whether or not TB-1 and TC-18 are actually representative of identical mafic liquids; therefore, the only trend which can be definitively associated with the alteration of TB-1 is silification.

Enrichments in  $\text{SiO}_2$ , LREE, and Th are attributed to the alteration of mafic rocks. The enrichments discussed above are also attributed to crustal contamination. It may seem unwarranted to invoke crustal contamination when the same enrichments appear to result from alteration.

One point which strongly suggests that crustal contamination has affected the Alder magmas is that the evolved samples seem to have been enriched in Th and LREE relative to the mafic samples. It doesn't seem plausible that alteration would have selectively enriched the evolved igneous samples. Since MW-D, WF-1, TC-16, and MTO-14 do not appear altered, the enrichment of the LREE and Th in these samples is attributed to crustal contamination.

WF-1 and MTO-14 also appear to be enriched in silica (Figures 21 and 22).

The two samples of the Pine Mt. Porphyry intrusive which have been analyzed are very similar in Zr,  $\text{TiO}_2$ , Y, Hf, Ta, and HREE abundances; however, the samples have significantly different  $\text{Na}_2\text{O}$ , Th, LREE, and Nb abundances. The sample, MTO-8, is taken from the northern boundary of the shear zone. The rock here is highly foliated and friable. It appears that the lithology has undergone some clay alteration. The geochemical differences between the two samples is similar to differences seen in unaltered and altered Proterozoic felsic volcanics studied in Sweden (Baker and de Groot, 1983). These latter rocks are believed to have been altered from the interaction with sea water in a



hydrothermal sub-sea floor system. Table I-2 shows comparison of the two samples; the third column summarizes the geochemical differences of the two samples; and the fourth column shows the alteration trends which are observed in the felsic volcanics of Sweden.

It can be seen that there are many similarities to the geochemical trends of alteration which are observed in Sweden. The alteration process in the Swedish Proterozoic felsic volcanics is not fully understood, but it appears to be two-stage in some cases, with alkali feldspar altering first to a kaolinite or illite group clay mineral conserving  $K_2O$  and losing  $Na_2O$ . The second stage involves the development of Mg-chlorite from the clay. It appears that the Pine Mt. Porphyry sample, MTO-8, has only undergone the first stage of this alteration since chlorite is not apparent in the sample, and the MgO abundance is relatively similar in the two samples, but  $Na_2O$  is much lower in MTO-8.

The depletion of LREE's in MTO-8 is remarkable as is the surprising apparent depletion in Nb. In conclusion, it appears that there is a significant amount of evidence which suggests that some of the lithologies of the Alder rocks in the Mazatzal Mountains have been hydrothermally altered.

Table I-1. Possible effects of hydrothermal alteration on the andesitic samples, MTO-B and WF-5.

	MTO-B	WF-5	MTO-14	Comparison of altered samples with MTO-14	geochemical trends of hydrothermal alteration
SiO <sub>2</sub>	48.48	48.75	61.79	-SiO <sub>2</sub>	-SiO <sub>2</sub>
TiO <sub>2</sub>	0.51	0.51	0.61	no change	no change
Al <sub>2</sub> O <sub>3</sub>	15.24	13.74	15.15	no change	----
Fe <sub>2</sub> O <sub>3</sub>	9.66	9.57	8.63	no change	+Fe <sub>2</sub> O <sub>3</sub>
MgO	8.45	6.83	2.1	+MgO	variable
CaO	7.52	8.21	5.78	+CaO (?)	variable
Na <sub>2</sub> O	2.56	2.25	2.48	no change	----
K <sub>2</sub> O	0.23	0.52	0.77	-K <sub>2</sub> O (?)	+K <sub>2</sub> O
MnO	0.11	0.15	0.11	no change	+MnO
P <sub>2</sub> O <sub>5</sub>	0.23	0.30	0.18	no change	no change
LOI	5.91	9.44	2.25	+H <sub>2</sub> O	+H <sub>2</sub> O
TOTAL	98.90	100.27	99.85		

Table I-1 Continued:

	MTO-B	WF-5	MTO-14	Comparison of altered samples with MTO-14	geochemical trends of hydrothermal alteration
Rb	6.1	8.3	21.8	-Rb(?)	+Rb
Ba	1734.2	--	437.7	+Ba	+Ba
Cs	3.5	2.1	1.5	+Cs (?)	+Cs
Sr	689.2	589.2	247.5	+Sr (?)	+Sr
Pb	44.0	19.3	8.7	+Pb (?)	---
Th	2.7	4.5	2.6	no change	no change
U	0.69	1.07	1.13	no change	+U
Sc	29.9	26.2	25.3	no change	no change
Cr	351.0	361.6	16.5	+Cr	+Cr
V	219.1	196.3	102.2	+V	---
Ni	188.0	128.2	6.7	+Ni	+Ni
Y	16.2	16.0	22.2	no change	no change
Zr	69.3	122.5	74.6	no change	no change
Nb	5.0	6.4	6.7	no change	no change
Hf	1.6	2.0	1.7	no change	no change
Ta	0.17	0.25	0.40	-Ta (?)	no change
La	40.3	62.8	13.3	+La	+La
Ce	85.99	127.2	30.6	+Ce	+Ce
Sm	5.84	7.6	3.89	+Sm	+Sm
Eu	1.41	1.95	1.20	no change	no change
Tb	0.56	0.74	0.70	no change	no change
Yb	1.81	2.04	2.58	no change	no change
Lu	0.28	0.30	0.38	no change	no change

References: Michard, et al., (1983); Menzies (1979); Hellman and Henderson (1977); Floyd (1977); and Condie (1979).

Table I-2. Alteration trends of the Pine Mt. Porphyry intrusive which are similar to those seen in hydrothermally altered Proterozoic felsic rocks from Sweden.

	WF - 1	MTO - 8	comparison of MTO-8 to WF-1	geochemical trends of hydrothermal alteration of Proterozoic felsic rocks
SiO <sub>2</sub>	unaltered 74.62	altered 75.04	no change	no change
TiO <sub>2</sub>	0.19	0.20	no change	no change
Al <sub>2</sub> O <sub>3</sub>	13.95	16.41	no change	no change
Fe <sub>2</sub> O <sub>3T</sub>	1.84	1.45	-Fe <sub>2</sub> O <sub>3</sub> (?)	-Fe <sub>2</sub> O <sub>3</sub>
MgO	0.16	--	no change	+MgO
CaO	0.58	--	-CaO (?)	-CaO (?)
Na <sub>2</sub> O	2.48	0.33	-Na <sub>2</sub> O	-Na <sub>2</sub> O
K <sub>2</sub> O	4.52	3.68	-K <sub>2</sub> O (?)	no change
P <sub>2</sub> O <sub>5</sub>	0.05	0.07	no change	no change
LOI	2.07	2.93		
TOTAL	100.51	100.11		

	WF - 1	MTO - 8	comparison of MIO-8 to WF1-	geochemical trends of hydro- thermal alteration of Proterozoic felsic rocks
Rb	116.9	181.8	+Rb (?)	no change
Ba	946.3	no change		
Cs	1.7	10.1	+Cs	no change
Sr	81.2	65.2	-Sr (?)	-Sr
Pb	21.8	18.8	no change	no change
Th	16.2	7.4	-Th	-Th (?)
U	6.30	2.40	-U	-U (?)
Sc	3.2	5.1	+Sc (?)	no change
V	8.25	10.4	no change	
Cr	--	--	--	
Co	--	--	--	
Ni	--	--	--	
Y	19.0	24.8	+Y (?)	-Y
Zr	140.3	148.8	no change	no change
Nb	12.7	5.8	-Nb	no change
Hf	3.8	3.8	no change	no change
Ta	1.1	0.7	-Ta (?)	no change
La	44.0	7.9	-La	-La
Ce	85.2	20.9	-Ce	-Ce
Sm	5.70	2.18	-Sm	-Sm
Eu	1.00	0.60	-Eu	-Eu
Tb	0.55	0.45	-Tb (?)	-TB
Yb	2.17	1.95	-Yb(?)	-Yb
Lu	0.26	0.31	no change	no change

Reference: Baker and DeGroot (1983).

## REFERENCES

- Anderton, R., 1976, Tidal-shelf sedimentation: An example from the Scottish Dalradian: *Sedimentology*, V. 23, p. 429-458.
- Bailey, J.C., 1981, Geochemical criteria for a refined tectonic discrimination of orogenic andesites. *Chemical Geology*, V. 32, p. 139-154.
- Baker, J.H., and de Groot, P.A., 1983, Proterozoic seawater-felsic volcanics interaction W. Bergslagen, Sweden. Evidence for high REE mobility and implications for 1.8 Ga seawater compositions. *Contrib. Mineral. Petrol.*, V. 82, p. 119-130.
- Best, M.G., 1982, Igneous and Metamorphic Petrology. New York: W.H. Freeman and Company, 630 p.
- Bhatia, M.K., 1983, Plate tectonics and the geochemical composition of sandstones. *Journal of Geology*, V. 91, p. 611-627.
- Bhatia, M.K., and Crook, K.W., 1986, Trace element characteristics of graywackes and tectonic setting discrimination of sedimentary basins *Contrib. Mineral. Petrol.*, V. 92, p. 181-193.
- Blatt, H.; Middleton, G.; and Murray R., 1972, Origin of Sedimentary Rocks: Prentice-Hall, Englewood Cliffs, 634p.
- Bond, G.C.; and Devay, J.C., 1980, Pre-Upper Devonian quartzose sandstones in the Shoo Fly Fm. Northern California: Petrology, provenance and implications for regional tectonics. *Jour. of Geology*, V. 88, p. 285-308.
- Bouma, A.H., 1962, Sedimentology of Some Flysch Deposits: Elsevier, Amsterdam, 108 p.
- Bruhn, R.L.; Stern, C.R.; and DeWit, M.J., 1978, Field and geochemical data bearing on the development of a Mesozoic volcano-tectonic rift zone and back-arc basin in southernmost South America. *Earth and Planetary Science Letters*, V. 41, p. 3d-46.
- Bryan, W.B., Finger, L.W.; and Chayes, F., 1968, Estimating proportions in petrographic mixing equations by least-square approximation. *Science*, V. 163, p. 926-927.
- Condie, K.C., 1986, Geochemistry and tectonic setting of Early Proterozoic supracrustal rocks in the Southwestern United States. *Jour. Petr.*, V. 26, p. 545-563.
- Condie, K.C., 1987, Early Proterozoic volcanic regimes in southwestern North America. In: Pharoah, T.C., Beckinsale, R.D., and Rickard, D. (eds.) *Geochemistry and Mineralization of Proterozoic Volcanic Suites*, Geological Society Special Publication No. 33, pp. 211-218.

- Condie, K.C. and DeMalas, J.P., 1985, The Pinal Schist: an early Proterozoic quartz-wacke association in southeastern Arizona. *Precambrian Research*, V. 27, p. 337-356.
- Condie, K.C.; Viljoen, M.J.; and Kable, E.J.D., 1977, Effects of alteration on element distributions in Archean tholeiites from the Barberton Greenstone Belt, South Africa. *Contr., Mineral. Petr.*, V. 64, p. 75-89.
- Condie, K.C., and Nuter, J.A., 1981, Geochemistry of the Dubois greenstone succession: An early Proterozoic bimodal volcanic association in west-central Colorado. *Precambrian Research*, V. 15, p. 131-155.
- Conway, C.M., 1973, Structure and evolution of a Precambrian rhyolite volcanic complex, Gila County, Arizona. *Geol. Soc. of America, Abstracts with Programs*, V.5, p.25-26.
- Conway, C.M., 1976, Petrology, Structure, and Evolution of a Precambrian Volcanic and Plutonic Complex, Tonto Basin, Arizona: California Institute of Technology, Pasadena, Ph.D. dissertation, 460 p.
- Conway, C.M., and Silver, L.T., 1987, 1700-1610 Ma. Proterozoic rocks in central to southeastern Arizona. *Ariz. Geol. Digest*, (in press).
- Cullers, R.L.; Chaudhuri, S.; Arnold, B.; Lee, M; and Wolf, C.W., 1975, Rare earth distributions in clay minerals and in the clay sized fraction of the Lower Permian Havensville and Eskridge Shales of Kansas and Oklahoma. *Geoc. Cosmo. Acta.*, V. 39, p. 1691-1703.
- Cullers, R.L.; Chaudhuri, S.; Kilbane, N.; and Koch, R., 1979, Rare earths in size fractions and sedimentary rocks of Pennsylvanian-Permian age from the mid-continent of the U.S.A. *Geocl. Cosmo. Acta.*, V. 43, p. 1285-1301.
- Davis, A.; Blackburn, W.H.; Brown, W.R.; and Ehmann, W.D., 1979, Trace element geochemistry and origin of late Precambrian-early Cambrian Catocin greenstones of the Appalachian Mountains. Univ. of California at Davis, Davis California (unpublished manuscript-submitted to *Chemical Geology*).
- Deer, W.A.; Howie, R.A.; and Zussman, J., 1963, Rock Forming Minerals: J. Wiley and Sons, New York, 435 p.
- Dickinson, W.R., 1970, Interpreting detrital modes of graywacke and arkose. *Jour. of Sed. Petr.*, Vol. 40, p. 695-707.
- Dickinson, W.R., and Yarborough, H., 1976, Plate Tectonics and Hydrocarbon Accumulation: AAPG, Tulsa, Okla., 251 p.
- Dickinson, W.R., and others, 1983, Provenance of North American Phanerozoic sandstones in relation to tectonic setting. *Geol. Soc. America Bull.*, V. 94, p. 222-235.

- Dickinson, W.R., and Seely, D.R., 1979, Structure and stratigraphy of forearc regions. *Am. Ass. of Petr. Geol. Bull.*, V. 63, p. 2-31.
- Dickinson, W.R. and Suczek, C.A., 1979, Plate tectonics and sandstone compositions. *Am. Ass. of Petr. Geol. Bull.*, V. 94, p. 222-235.
- Dickinson, W.R. and Valloni, R., 1980, Plate settings and provenances of sands in modern ocean basins. *Geology*, V. 8, p. 82-86.
- Ewart, A., 1979, A review of the mineralogy and chemistry of Tertiary-Recent dacitic, latitic, rhyolitic and related sialic rocks. In: Barker, F (ed.) Trondhjemites, Dacites, and Related Rocks: Elsevier, Amsterdam. pp. 13-119.
- Floyd, P.A., 1977, Rare earth element mobility and geochemical characteristics of spilitic rocks. *Nature*, V. 269, p. 135-137.
- Frey, F.A.; Gerlach, D.C.; Hickey, R.L.; Lopez-Escobar, L.; and Munizaga-Villavicencio, F., 1984, Petrogenesis of the Laguna del Maule volcanic complex, Chile (36°S). *Contrib. Mineral. Petrol.*, V. 88, p. 133-149.
- Gastil, G., 1958, Older Precambrian rocks of the Diamond Butte Quadrangle, Gila County Arizona. *Geol. Soc. of Am. Bull.*, V. 69, p. 1495,-1514.
- Gibson, I.L., and Jagam, P., 1980, Instrumental neutron activation analysis of rocks and minerals. In: Muecke, G.K. (ed.), Short Course in Neutron Activation Analysis in the Geosciences. Mineralogical Association of Canada, pp. 109-131.
- Green, T.H., 1972, Crystallization of calc-alkaline andesite under controlled high pressure hydrous conditions. *Contrib. Mineral. Petrol.*, V. 34, p. 150-166.
- Green, T.H., 1980, Island arc and continent-building magmatism-a review of petrogenic models based on experimental petrology and geochemistry. *Tectonophysics*, V. 63, p. 367-385.
- Green, T.H. and Ringwood, A.E., 1972, Genesis of the calc-alkaline igneous rock suite. *Contrib. Mineral. Petrol.*, V. 18, p. 105-162.
- Grove, T.L., and Baker, M.B., 1984, Phase equilibrium controls on the tholeiitic versus calc-alkaline differentiation trends. *Jour. of Geoph. Res.*, V. 89, p. 3253-3274.
- Grove, T.L., and Donnelly-Nolan, J.M., 1986, The evolution of young silicic lavas at Medicine Lake Volcano, California: Implications for the origin of compositional gaps in the calc-alkaline series lavas. *Contrib. Mineral. Petrol.*, V. 92, p. 281-302.
- Grove, T.L., and Kinzler, R.J., 1986, Petrogenesis of Andesites. *Am. Rev. Earth Planet. Sci.*, V. 14, p. 417-454.



- Harms, J.C.; Southard, J.B.; Walker, R.G. (eds.). In: Structures and Sequences in Clastic Rocks. Soc. Econ. Pal. Min.; short course no. 9; Tulsa, Okla., 249 p.
- Heckel, P.H., 1972, Recognition of ancient shallow marine environments. In: Rigby, K.J., and Hamblin, W.K. (eds.), Recognition of ancient sedimentary environments: Soc. of Econ. Pal. and Mineral. Tulsa, Okla. p. 226-250.
- Hellman, P.L., and Henderson, P. 1977, Are rare earth elements mobile during hydrothermal spilitization? *Nature*, V. 267, p. 38-40.
- Holland, H.D., 1978, The Chemistry of the Atmosphere and Oceans: Wiley and Sons, New York, 364 p.
- Ingersoll, R.V., and Graham, S.H., 1983, Recognition of the shelf-slope break along ancient, tectonically active continental margins: In, Stanley, D.J., and Moore, G.T. (eds.) *The Shelfbreak: Critical Interface on Continental Margins*. Soc. Econ. Pal. Min.; spec. publ. no 33; Tulsa, Okla., pp. 107-117.
- James, D.E., 1981, Role of subducted continental material in the genesis of calc-alkaline volcanics of the central Andes. *Geol. Soc. America*, Memoir 154, p. 769-790.
- Jensen, L.S., 1976, A new cation plot for classifying subalkalic volcanic rocks: Ontario Div. Mines Misc. paper 66, 22 p.
- Karig, D.E., and Moore, G.F., 1975, Tectonically controlled sedimentation in marginal basins. *Earth and Planetary Science Letters*, V.26, pp. 233-238.
- Karlstrom, K.E., and Conway, C.M., 1986, Deformational styles and contrasting lithostratigraphic sequences within an early Proterozoic orogenic belt, Central Arizona. In: Nations, J.D., Conway, C.M., and Gordon, A.S., (eds.), *Geology of Central and Northern Arizona*: Geology Dept., Northern Arizona University, Flagstaff, AZ., 176 p.
- Karlstrom, K.E., Bowring, S.A., and Conway, C.M., 1987, Early Proterozoic two Province boundary in central Arizona: *G.S.A. Bull* (in press).
- Kay, S.M., and Kay, R.W., 1985, Aleutian tholeiitic and calc-alkaline magma series I: The mafic phenocrysts. *Contrib. Mineral. Petrol*, V. 90, p. 276-290.
- Langmuir, C.H.; Vocke, Jr., R.D.; Hanson, G.N.; and Hart, S.R., 1978, A general mixing equation with applications to Icelandic Basalts. *Earth and Planetary Science Letters*, V.37, p. 380-392.
- Lemaitre, R.W., 1976, The chemical variability of some common igneous rocks. *Jour. Petrology*, V. 17, p. 589-637.

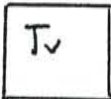



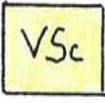







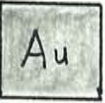

- Lopez-Escobar, L.; Frey, F.A.; and Vergara, M., 1977, Andesities and high-alumina basalts from the central-south Chile high Andes: Geochemical evidence bearing on their petrogenesis. *Contrib. Mineral. Petrol.*, V. 63, p. 199-228.
- Lucci, R.F., 1985, Influence of transport processes and basin geometry on sandstone composition. In: Zuffa, G.G. (ed.), Provenance of Arenites, pp. 50-65.
- Ludden, J.N., and Thompson, G., 1979, An evaluation of the behavior of the rare earth elements during the weathering of sea floor basalt. *Earth Planet. Sci. Lett.*, V. 43, p. 85-92.
- Ludwig, K.R., 1974, Precambrian geology of the central Mazatzal Mountains, Arizona: California Institute of Technology, Pasadena, California, Ph.D. Dissertation, 363 p.
- Luhr, J.R., and Carmichael, I.S.E., 1985, Jorullo volcano, Michoacan, Mexico (1759-1774): The earliest stages of fractionation in calc-alkaline magmas. *Contrib. Mineral. Petrol.*, V. 90, p. 142-161.
- Menzies, M.; Segfried, Jr., W.; and Blanchard, D., 1979, Experimental evidence of rare earth element immobility in greenstones. *Nature*, V. 282, p. 398-399.
- Michard, A.; Albarede, F.; Michard, G.; Minster, J.F.; and Charlou, J.L., 1983, Rare earth elements and uranium in high temperature solutions from the East Pacific Rise hydrothermal vent field (13°N). *Nature*, V. 303, p. 795-796.
- Mutti, E., 1985, Turbidite systems and their relations to depositional sequences. In: Zuffa, G.G. (ed.), Provenance of Arenites, pp. 65-93.
- Mutti, E., and Ricci Lucci, F., 1978, Turbidites of the northern Apennines: Introduction to facies analysis. *Internat. Geology Rev.* V. 10, p. 125-166.
- Noll, P.D., Jr., Geology and Geochemistry of Proterozoic Rocks from Tonto Basin, Arizona: New Mexico Institute of Mining and Technology, Socorro, New Mexico, M.S. Thesis, in preparation.
- Norrish, K., and Chappel, B.W., 1977, X-ray fluorescence. In: Zussman, J. (ed.), *Physical Methods in Determinative Mineralogy*, Academic Press, pp. 235-262.
- Norrish, K., and Hutton, J.T., 1969, An accurate x-ray spectrographic method for the analyses of a wide range of geological samples. *Geochem. Cosmochem. Acta.*, V. 33, p. 431-435.
- O'Hara, M.J. 1977, Geochemical evolution during fractional crystallization of a periodically refilled magma chamber. *Nature*, V. 266, p. 503-507.

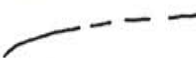




- Osborn, E.F., 1959, Role of oxygen pressure in the crystallization and differentiation of basaltic magma. *Am. Jour. Sci.*, V. 257, p. 609-647..
- Pearce, J.A., 1975, Basalt geochemistry used to investigate past tectonic environments on Cyprus. *Tectonophysics*, V. 25, p. 41-67.
- Pearce, J.A., 1983, in: Thorpe, R.S. (ed.), Andesities Orogenic Andesites, and Related Rocks: J.W. Wiley and Sons, New York. 724 p.
- Pearce, J.A., 1983, Role of the subcontinental lithosphere in magma genesis at active continental margins. In: Hawkesworth, C.J., and Norry, M.J. (eds.), Continental Basalts and Mantle Xenoliths: Cheshire, U.K., Shiva Press, Ltd. pp. 230-249.
- Pearce, J.A.; Harris, N.B.W.; and Tindle, A.G., 1984, Trace element discrimination diagrams for the tectonic interpretation of granitic rocks. *Tour of Petrol*, V. 25, p. 956-983.
- Pearce, J.A., and Norry, M.J., 1979, Petrogenetic implications of Ti, Zr, Y, and Nb variations in volcanic rocks. *Contr. Mineral. Petrol*, V. 69, p. 33-47.
- Pettijohn, F.J.; Potter, P.E.; and Siever, R., 1972, Sand and Sandstone: Springer-Verlag, New York, 618 p.
- Pharoah, T.C., and Pearce, J.A., 1984, Geochemical evidence for the geotectonic setting of early Proterozoic metavolcanic sequences in Lapland. *Precamb. Res.*, V. 25, p. 283-308.
- Powers, M.C., 1953, A new roundness scale for sedimentary particles. *Jour. of Sed. Petr.*, V. 23, p. 117-119.
- Puls, D.D. and Karlstrom, K.E., 1986, Proposed names for major thrusts in the northern Mazatzal Mountains, Central Arizona. *Geol. Soc. Am. Abst. Programs*, V. 18, p. 404.
- Reed, J.R., and Condie, K.C., 1988, Geochemical constraints on the composition of sandstone matrix and the interpretation of detrital modes. *Geologie en Mijnbouw*, V.66, p. 327-332.
- Reed, J.R.; Noll, Jr., P.D.; and Condie, K.C., 1987, Geochemistry and tectonic setting of 1700Ma supracrustal rocks from central Arizona. *Geol. Soc. Am. Abst. Programs*, V. 19, p. 533.
- Reineck, H.E., and Singh, I.B., 1972, Genesis of laminated sands and graded rythmites in storm sand layers of shelf mud. *Sedimatology*, V. 18, p. 123-128.
- Ronov, A.B.; Balashov, Y.A.; and Migdisov, A.A., 1967, Geochemistry of the rare earths in the sedimentary cycle. *Geochem. Int.*, V. 4, p. 1-17.

- Roser, B.P. and Korsch, R.J., 1986, Determination of tectonic setting of sandstone-mudstone suites using  $\text{SiO}_2$  content and  $\text{K}_2\text{O}/\text{Na}_2\text{O}$  ratio. *Jour. Geol.*, V. 94, p. 635-650.
- Saunders, A.D.; Tarney, J.; Stern, C.R.; and Dalziel, I.W.D., 1979, Geochemistry of Mesozoic marginal basin floor igneous rocks from southern Chile. *Geol. Soc. Am. Bull.*, V. 90, p. 237-258.
- Saunders, A.D., and Tarney, J., 1979, The geochemistry of basalts from a back-arc spreading center in the east Scotia Sea, *Geochem. Cosmo. Acta*. V. 43, p. 555-572.
- Shanmugam, G.; Damuth, J.E.; and Miola, R.J., 1985, Is the turbidite facies association scheme valid for interpreting ancient submarine fan environments. *Geology*, V. 13, 234-238.
- Shaw, D.M., 1956, Geochemistry of pelitic rocks. Part III: Major elements and general geochemistry. *Geol. Soc. America Bull.*, V. 67, 919-934.
- Shervais, J.W., 1982, Ti-V plots and the petrogenesis of modern and ophiolitic lavas. *Earth Planet. Sci. Lett.*, V. 59, p. 101-118.
- Silver, L.T., 1977, Chronostratigraphic elements of the Precambrian rocks of the southwestern and far western U.S.. *Geol. Soc. Am. Abst. Programs*, V. 9, p. 1176.
- Soegaard, K. and Eriksson, K., 1985, Evidence of tide, storm, and wave interaction on a Precambrian siliciclastic shelf; the 1700 m.y. Ortega Group, N.M.. *Jour. Sed. Petrol.*, V. 55, p. 672-684.
- Stanley, D.J. and Unrug, R., 1972, Submarine channel deposits, fluxoturbidites and other indicators of slope and base of slope environments in modern and ancient marine basins. In: Rigby, K.J., and Hamblin, W.K. (eds.), Recognition of Ancient Sedimentary Environments: Soc. of Econ. Paleon. and Minerals; Tulsa, Okla., pp. 287-335.
- Stern, C.R., 1980, Geochemistry of Chilean ophiolites: evidence for the compositional evolution of the mantle source of back-arc basin basalts. *Jour. of Geoph. Res.*, V. 85, p. 955-966.
- Taylor, S.R., and McLennan, S.M., 1985, The Continental Crust: Its Composition and Evolution: London, Blackwell Scientific Publications, 312 p.
- Thompson, R.N.; Dickin, A.P.; Gibson, I.L.; and Morrison, M.A., 1982, Elemental fingerprints of isotopic contamination of Hebridean Paleocene mantle-derived magmas by Archean sial. *Contrib. Mineral. Petrol.*, V. 79, p. 159-168.
- Weaver, B.L. and Larney, J., 1984, Empirical approach to estimating the composition of the continental crust. *Nature*, V. 310, p. 575-577.

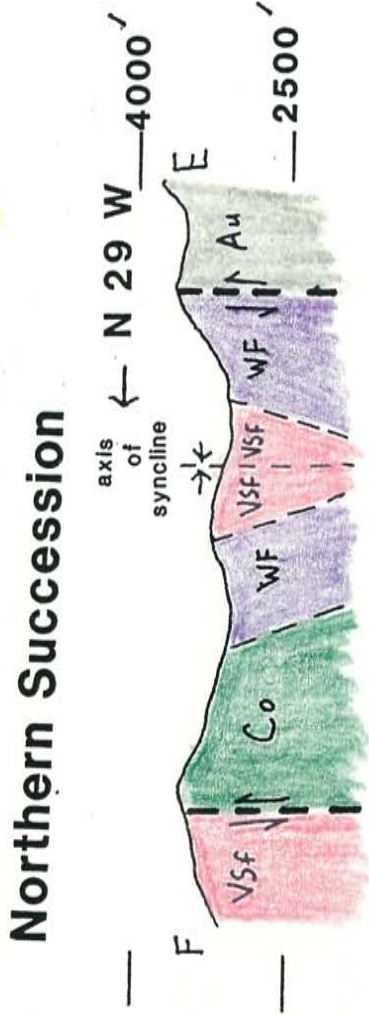
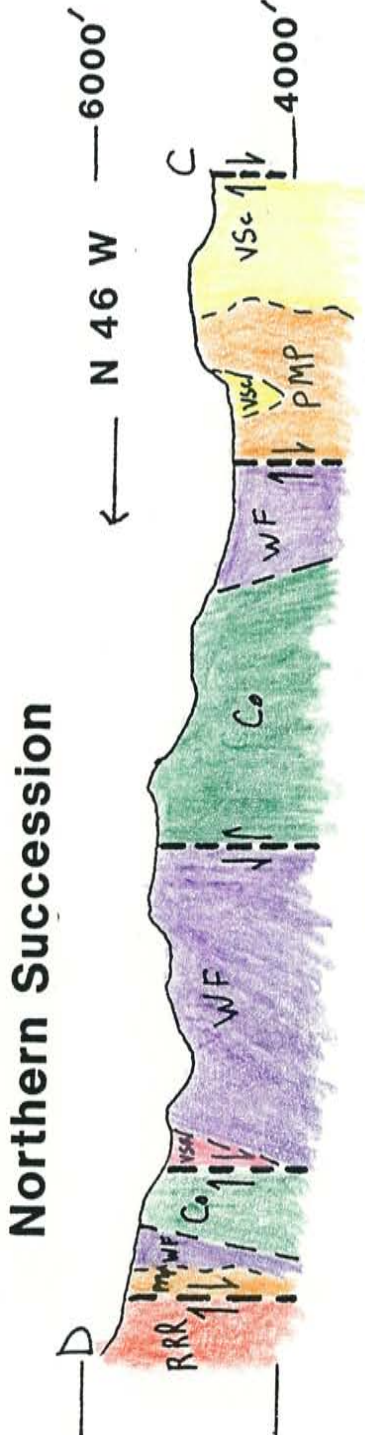
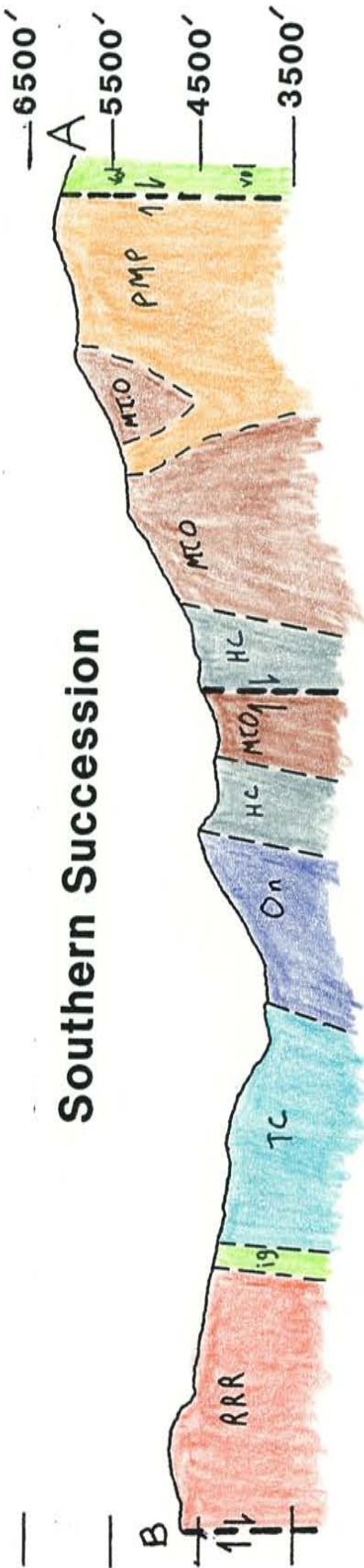
- Weaver, S.D.; Saunders, A.D.; Pankhurst, R.J.; and Larney, J., 1979, A geochemical study of magmatism associated with the initial stages of back-arc spreading. *Contrib. Mineral. Petrol.*, V. 68, p. 151-169.
- Wilson, E.D., 1929, Mazatzal revolution in Arizona. *Bull. Geol. Soc. Am.*, V. 50, p. 1113-1160.
- Winchester, J.A., and Floyd, P.A., 1977, Geochemical discrimination of different magma series and their differentiation products using immobile elements. *Chemical Geology*, V. 20, p. 325-343.
- Wood, D.A.; Joron, J.L.; and Freuil, M., 1979, A re-appraisal of the use of trace elements to classify and discriminate between magma series erupted in different tectonic settings. *Earth Planet. Sci. Lett.*, V. 45, p. 326-336.
- Wright, T.L., and Doherty, P.C., 1970, A linear programming and least squares computer method for solving petrologic mixing problems. *Bull. Geol. Soc. Am.*, V. 81, p. 1995-2008.

EXPLANATION OF GEOLOGIC MAP AND STRUCTURAL CROSS-SECTIONS\*

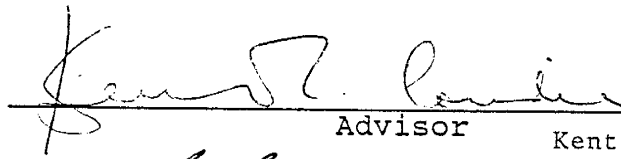
	Tertiary and Quaternary volcanics		Mt. Ord-Mafic to intermediate lavas, ash flow tuffs, tuffs, volcanic breccias.
Unconformity			Volcanics in the southeastern of the section near the summit Mt. Ord.
	Pine Mt. Porphyry-intrusive rhyodacite		dominantly strongly foliated v breccias and conglomerates with slates and coarse grained quar
	Red Rock Rhyolite-rhyolite ashflow tuffs, breccias, flow lavas, and agglomerates		poorly bedded chloritized fine coarse grained volcanoclastics grade upwards into sericite-rich quartz wackes, slates, and conglomerates
	mafic to intermediate volcanics at the top of the Telephone Canyon member, and mafic to intermediate dikes and sills		West Fork-fine grained chlorit tuffaceous sediments and coarse grained scour fills overlain by hemipelagic slates and phyllites
	Telephone Canyon-Quartzose and argillaceous sediments with minor volcanics and volcanoclastics		Cornucopia-hydrothermally altered mafic to intermediate volcanic pillow basalts, pyroclastics, minor jasper beds
	Oneida-hemipelagic slates and phyllites		poorly preserved, unmapped VSc Cornucopia, and West Fork memb
	Horse Camp-Quartzose sediments, conglomerates, and breccias		

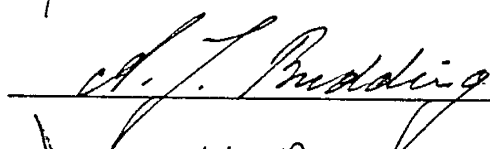
	Contact, dashed where approximated
	Fault contact, dashed where approximated
	Strike and dip of bedding
	Strike and dip of bedding; bedding tops determined by primary features.
	syncline axis

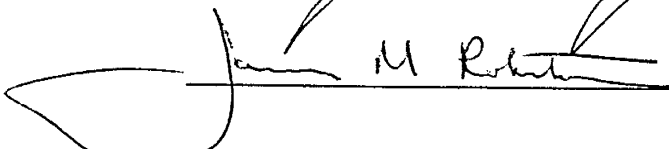
\*The geologic map east of longitude 111° 30' has been adapted from Ludwig (1974), and the mapping west of longitude 111° 30' has been adapted from Conway, C.M. (unpublished).



This thesis is accepted on behalf of the faculty of the Institute by the following committee:

  
\_\_\_\_\_  
Advisor                      Kent C. Condie

  
\_\_\_\_\_  
A.J. Budding

  
\_\_\_\_\_  
James M. Robertson

\_\_\_\_\_  
\_\_\_\_\_  
4-25-88  
\_\_\_\_\_  
Date



Beam size ~100µm

each analysis is composite of more than 1 grain  
average is best estimate of rock frag.

### Microprobe Summary TC-13

Whole chemical comp. of this rock TC-13

Elements analyzed: SiO<sub>2</sub>, Fe<sub>2</sub>O<sub>3</sub>, Na<sub>2</sub>O, CaO

8926 2.49 2.21 0.135

# of fragments analyzed: 7

Fragment #'s shown on pictures

Matrix avg. comp:

SiO<sub>2</sub> 68.22% 4.0 13.5  
FeO 2.12% 1.31  
Na<sub>2</sub>O 3.35% 3.10  
CaO 0.08% 0.11

Rock Fragment #1 S.D

SiO<sub>2</sub> 76.97% 3.6  
FeO 1.55% 2.3  
Na<sub>2</sub>O 6.40% 1.39  
CaO 0.08% 0.04

Rock Fragment #2 S.D

SiO<sub>2</sub> 79.29% 4.16  
FeO 1.71% 0.58  
Na<sub>2</sub>O 1.02% 0.35  
CaO 0.21% 0.26

\* Rock Fragment #5

SiO<sub>2</sub> 89.05% 2.17  
FeO 1.18% 0.26  
Na<sub>2</sub>O 1.55% 0.27  
CaO 0.02% 0.02

\* Rock Fragment #6

SiO<sub>2</sub> 86.1% 3.79  
FeO 1.63% 0.76  
Na<sub>2</sub>O 3.65% 1.11  
CaO 0.04% 0.01

\* Rock Fragment #7

SiO<sub>2</sub> 66.1% 8.88  
FeO 1.98% 2.22  
Na<sub>2</sub>O 7.17% 3.47  
CaO 0.11% 0.07

\* Rock Fragment #3 S.D

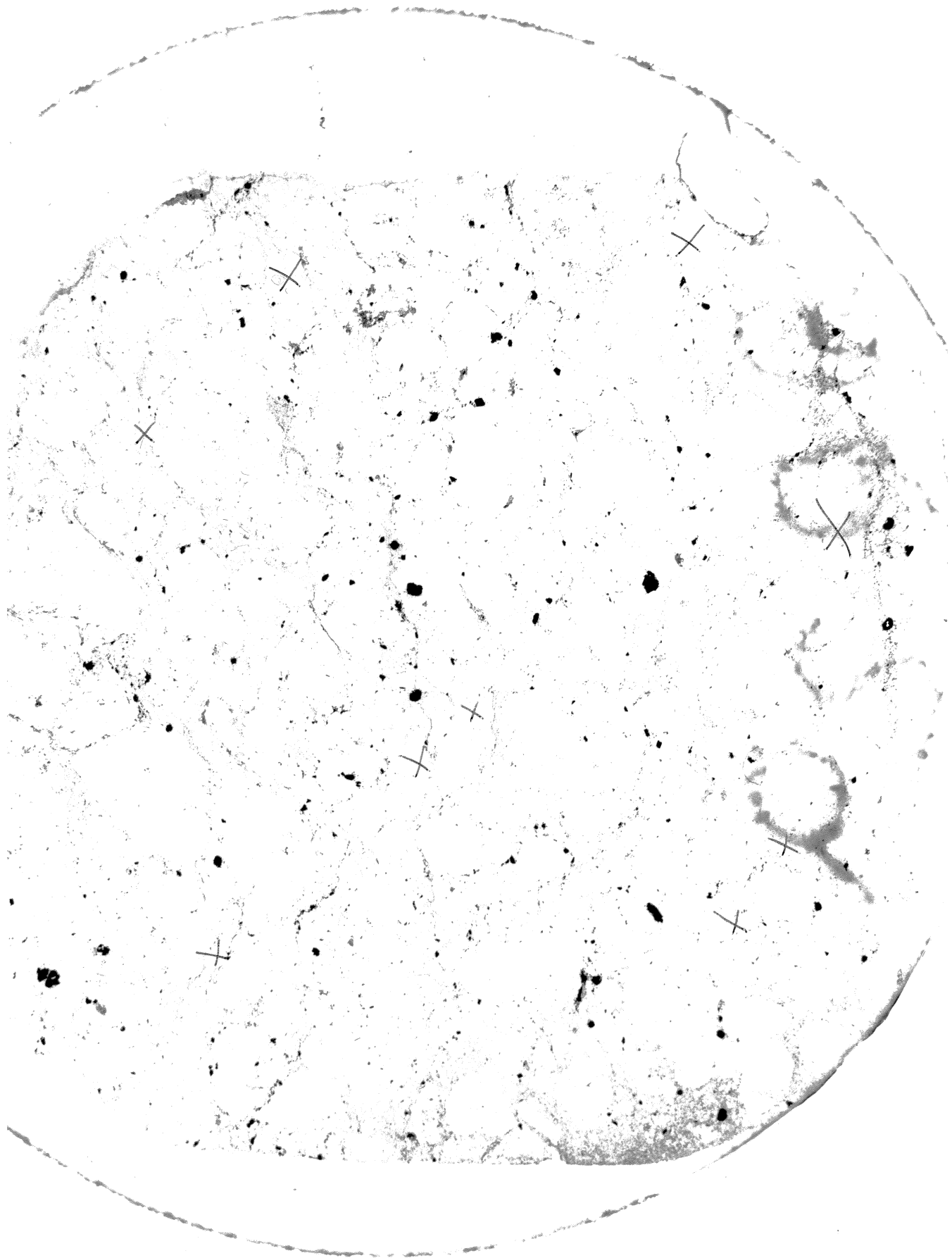
SiO<sub>2</sub> 86.61% 1.27  
FeO 0.73% 0.36  
Na<sub>2</sub>O 1.78% 0.30  
CaO 0.04% 0.02

\* Rock Fragment #4 S.D

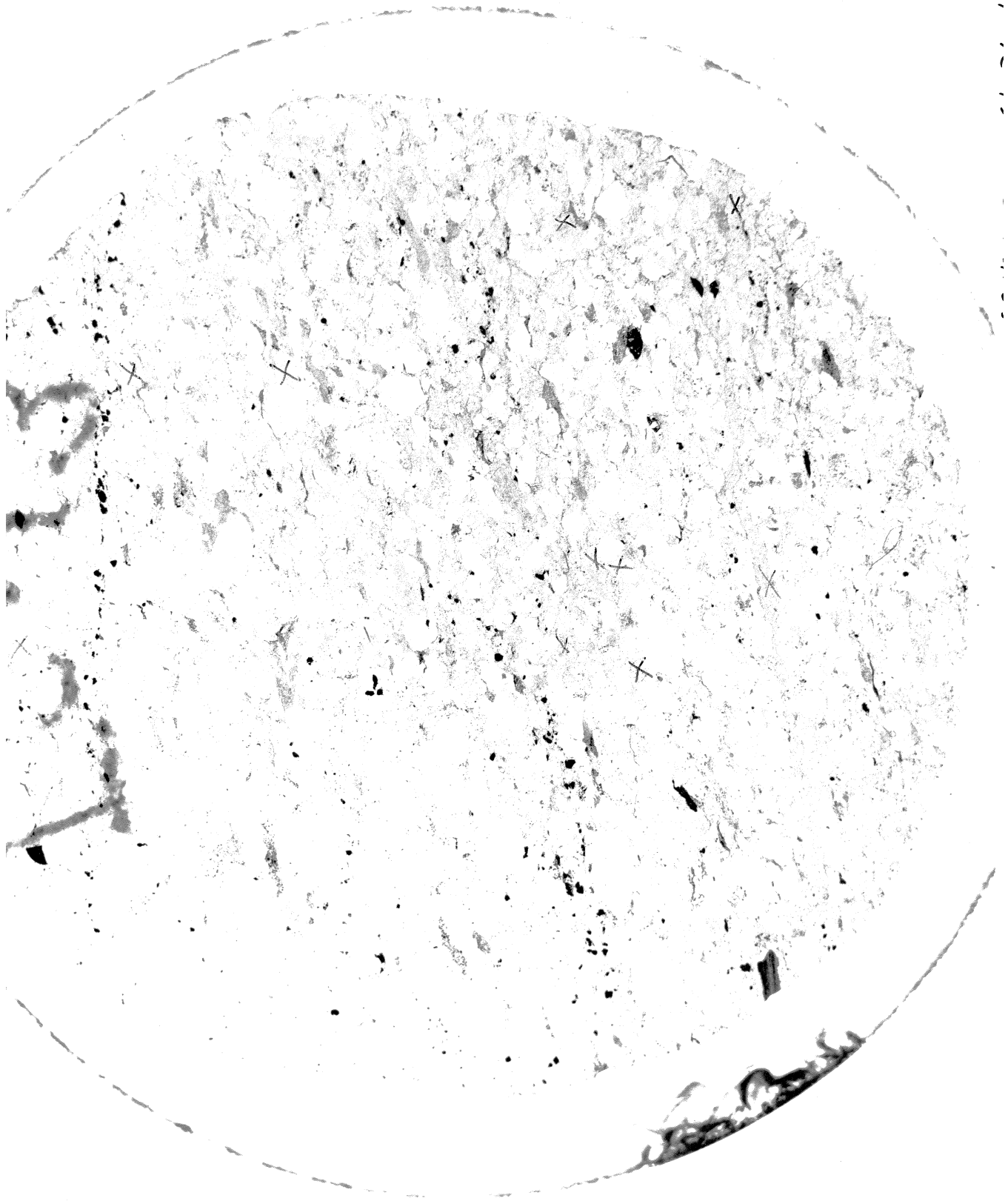
SiO<sub>2</sub> 88.5% 2.8  
FeO 0.77% 0.32  
Na<sub>2</sub>O 0.46% 0.33  
CaO 0.01% 0.00

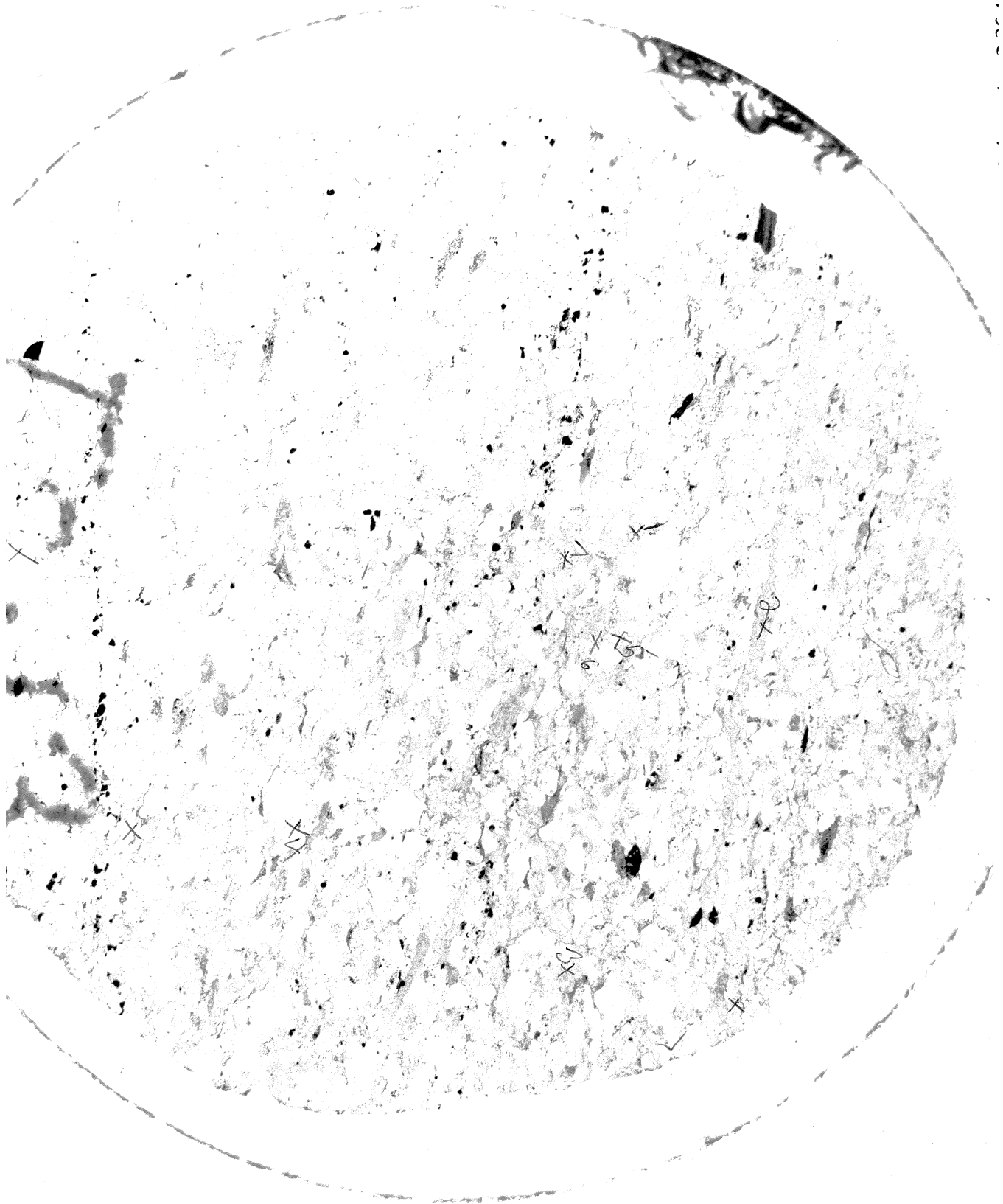
Conclusion: <sup>supposed</sup>

Of the seven fine grained fragments analyzed, one may have been matrix. One or two (#2, 4) may be rhyolite rock fragments. #s 3, 4, 5, 6 appear to be fine grained sedimentary fragments mostly polycrystalline quartz. This is reasonable since this is a T.S. of a recycled oxygen sediment. Fragments #s 3, 4, 5, 6 are most representative of the comp. of this rock.

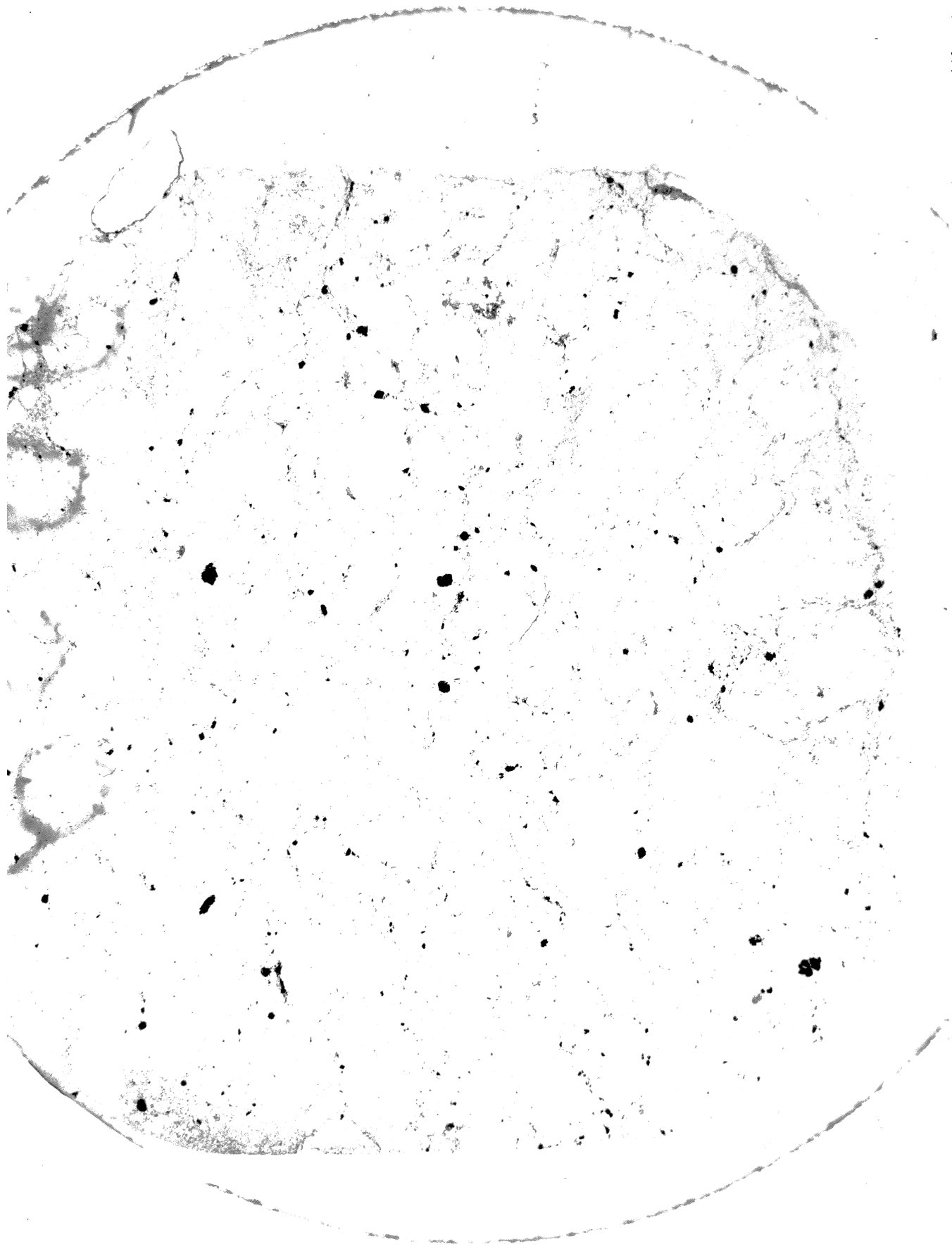


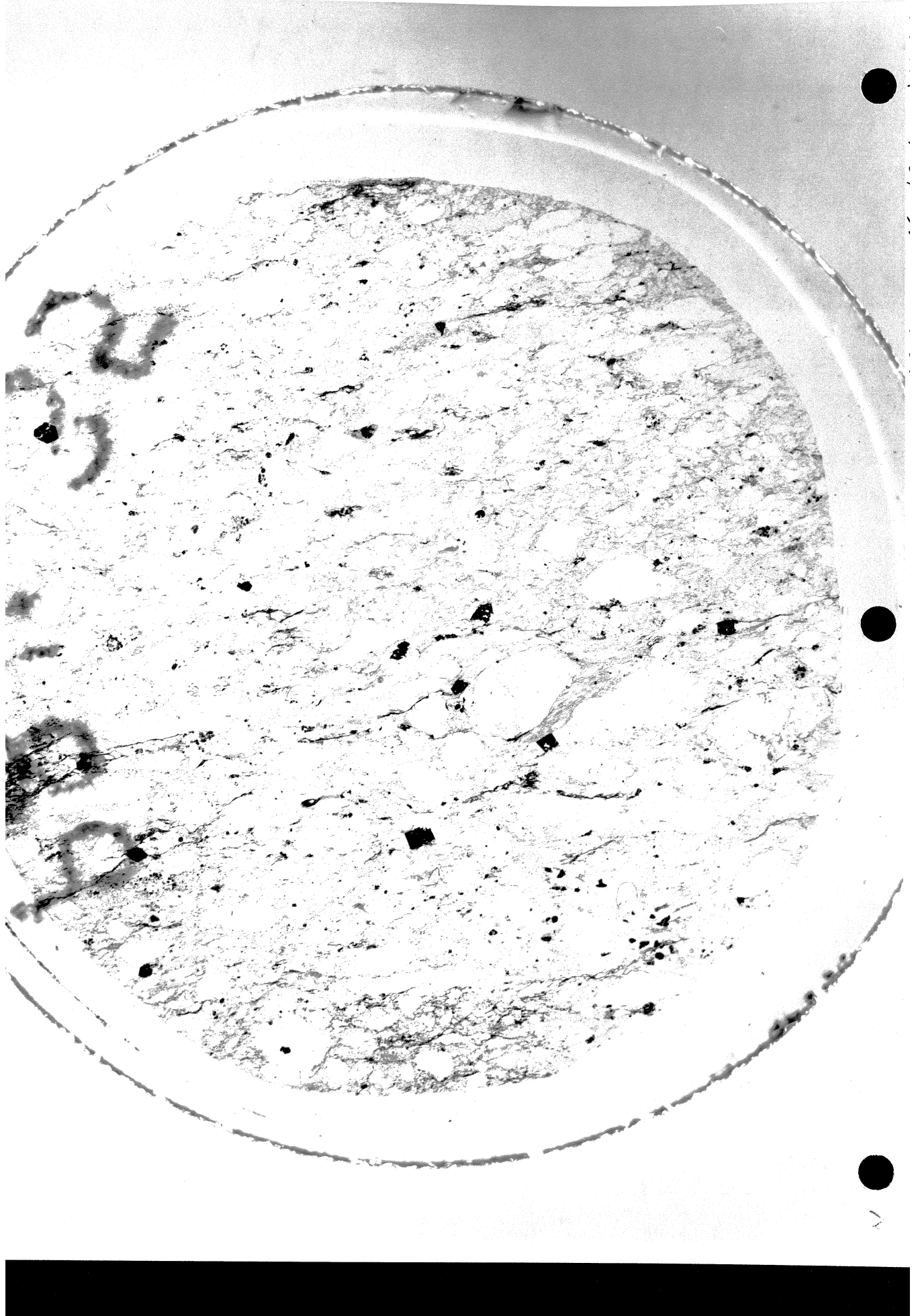


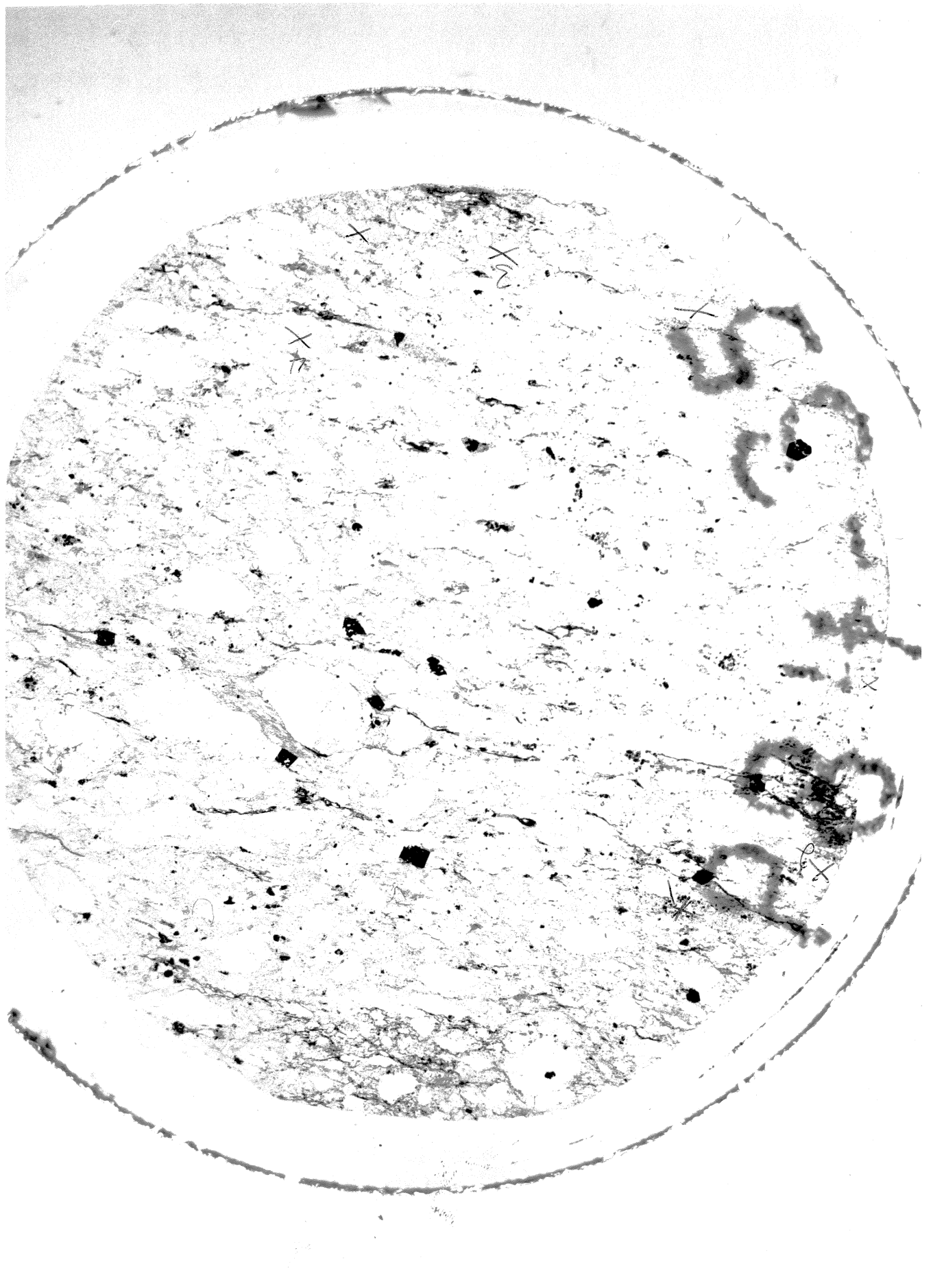




11 115







\*6 DO YOU WISH TO INITIALIZE THE SYSTEM

\*SAM MAXIMUM # OF POINTS 126  
28 MAY 1985 4:56 PM

#  
POINT 1 ( 1 )  
CR 40 SI 55884 NR 227 FE

COUNTS PERK/BG UNC WTX BRCDR WTX  
SIDE 55884 701 90.17 90.34  
FED 193 4 0.61 0.63  
NR2D 227 2 0.18 0.18  
CRD 40 1 0.04 0.04  
TOTAL 91.00 91.19

#  
POINT 2 ( 2 )  
CR 100 SI 30224 NR 4456 FE

COUNTS PERK/BG UNC WTX BRCDR WTX  
SIDE 30224 377 48.52 50.30  
FED 318 6 1.14 1.15  
NR2D 4456 44 6.20 6.17  
CRD 100 4 0.18 0.20  
TOTAL 56.05 57.84

#  
POINT 3 ( 3 )  
CR 120 SI 32365 NR 4991 FE

COUNTS PERK/BG UNC WTX BRCDR WTX  
SIDE 32365 404 51.94 54.00  
FED 475 9 1.80 1.82  
NR2D 4991 49 6.96 6.98  
CRD 120 4 0.23 0.25  
TOTAL 60.93 63.06

#  
POINT 4 ( 4 )  
CR 83 SI 21118 NR 2362 FE

COUNTS PERK/BG UNC WTX BRCDR WTX  
SIDE 21118 263 33.81 35.15  
FED 830 17 3.28 3.31  
NR2D 2362 23 3.21 3.40  
CRD 83 3 0.14 0.15  
TOTAL 40.45 42.02

#RVE  
COUNTS PERK/BG UNC WTX BRCDR WTX  
SIDE 28779 359 46.16 47.20  
FED 862 18 3.42 3.46  
NR2D 1225 12 1.60 1.59  
CRD 82 3 0.14 0.15  
TOTAL 51.32 52.50

#RVE  
COUNTS PERK/BG UNC WTX BRCDR WTX  
SIDE 28779 359 46.16 47.20  
FED 862 18 3.42 3.46  
NR2D 1225 12 1.60 1.59  
CRD 82 3 0.14 0.15  
TOTAL 51.32 52.50

#RVE  
COUNTS PERK/BG UNC WTX BRCDR WTX  
SIDE 28779 359 46.16 47.20  
FED 862 18 3.42 3.46  
NR2D 1225 12 1.60 1.59  
CRD 82 3 0.14 0.15  
TOTAL 51.32 52.50

✓  
111  
MTH



POINT 7 ( 2) SI 60202 NR 200 FE

SIDE	COUNTS	PEAK/BG	UNC	WT%	BRCORR	WT%	SD
FED	146	3	0.41	0.42	0.05		
NR2D	200	1	0.14	0.14	0.02		
CRD	31	1	0.01	0.02*	0.01		
TOTAL			96.67	96.80			

POINT 8 ( 3) SI 60533 NR 160 FE 64 BC 12882

SIDE	COUNTS	PEAK/BG	UNC	WT%	BRCORR	WT%	SD
FED	64	1	0.07	0.07*	0.03		
NR2D	160	1	0.08	0.08	0.01		
CRD	27	1	0.00	0.01*	0.00		
TOTAL			96.80	96.83			

POINT 9 ( 4) SI 60608 NR 99 FE 180 BC 12891

SIDE	COUNTS	PEAK/BG	UNC	WT%	BRCORR	WT%	SD
FED	180	3	0.55	0.56	0.01		
NR2D	99	0	0.00	0.00*	-0.01		
CRD	29	1	0.01	0.01*	0.01		
TOTAL			97.33	97.41			

POINT 10 ( 5) SI 58266 NR 162 FE

SIDE	COUNTS	PEAK/BG	UNC	WT%	BRCORR	WT%	SD
FED	370	7	1.35	1.37	0.01		
NR2D	162	1	0.09	0.09	0.01		
CRD	40	1	0.04	0.04	0.01		
TOTAL			94.50	94.81			

SIDE	WT%	SD	SF
FED	94.58	3.03	
NR2D	0.66	0.49	
CRD	0.07	0.05	
TOTAL	95.31	0.01	

*Area #1*

POINT 11 ( 1) SI 47415 NR 4052 FE 272 BC 12882

SIDE	COUNTS	PEAK/BG	UNC	WT%	BRCORR	WT%	SD
FED	272	5	0.93	0.95	0.07		
NR2D	4052	39	5.58	5.56	0.10		
CRD	76	3	0.12	0.13	0.02		
TOTAL			82.15	83.87			

POINT 12 ( 2) SI 51152 NR 3476 FE

NR2D	3476	34	0.98	4.76	0.98	0.00
CRD	77	3	0.13	0.14	0.14	0.16
TOTAL		3	86.75	88.16		

#

POINT 13 ( 3)

CR 78 SI 49333 NR 3706 FE 106 BC 12914

COUNTS PERK/BG UNC WTX BRCDRR WTX SD

SID2	49333	611	78.54	80.01	0.37
FED	106	2	0.24	0.25	0.04
NR2D	3706	36	5.08	5.04	0.09
CRD	78	3	0.13	0.14	0.02
TOTAL		3	84.00	85.44	

#

POINT 14 ( 4)

CR 76 SI 49378 NR 3773 FE 121 BC 12909

COUNTS PERK/BG UNC WTX BRCDRR WTX SD

SID2	49378	611	78.64	80.15	0.37
FED	121	2	0.30	0.31	0.05
NR2D	3773	37	5.18	5.14	0.09
CRD	76	3	0.12	0.13	0.02
TOTAL		3	84.25	85.74	

#

POINT 15 ( 5)

CR 87 SI 49589 NR 3843

COUNTS PERK/BG UNC WTX BRCDRR WTX SD

SID2	49589	614	78.96	80.47	0.37
FED	96	2	0.20	0.20	0.04
NR2D	3843	37	5.28	5.23	0.06
CRD	87	3	0.15	0.16	0.02
TOTAL		3	84.58	86.07	

#RVE

SID2	80.15	2.01		
FED	0.42	0.30		
NR2D	5.14	0.29		
CRD	0.14	0.01		
TOTAL	85.84			

*Handwritten signature*

#

POINT 16 ( 1)

CR 59 SI 52873 NR 1850 FE 374 BC 12923

COUNTS PERK/BG UNC WTX BRCDRR WTX SD

SID2	52873	654	84.13	85.10	0.39
FED	374	7	1.36	1.38	0.08
NR2D	1850	18	2.46	2.49	0.06
CRD	59	2	0.08	0.09	0.02
TOTAL		3	88.03	89.06	

#

POINT 17 ( 2)

CR 61 SI 54729 NR 1061 FE 364 BC 12923

COUNTS PERK/BG UNC WTX BRCDRR WTX SD

SID2	54729	677	87.06	87.71	0.40
FED	364	7	1.31	1.34	0.08
NR2D	1061	10	1.35	1.37	0.04
CRD	61	2	0.09	0.09	0.02
TOTAL		3	89.81	90.51	

#

POINT 18 ( 3)

CR 70 SI 50986 NR 2640 FE 133 BC 12923

COUNTS PERK/BG UNC WTX BRCDRR WTX SD

SID2	50986	631	81.12	82.22	0.38
FED	133	2	0.35	0.36	0.05
NR2D	2640	25	3.58	3.57	0.07
CRD	70	2	0.11	0.12	0.02
TOTAL		3	85.16	86.27	

#

POINT 19 ( 4)

CR 62 SI 53281 NR 2549 FE 249 BC 12923

NR2D	2549	25	3.45	3.46	0.07
CRD	62	2	0.09	0.10	0.02
3		TOTAL	89.15	90.34	

#

POINT 20 ( 5)

CR 57 SI 38164 NR 1047 FE 510 BC 12927

SIDE	38164	472	60.67	61.42	0.32
FED	510	10	1.92	1.95	0.09
NR2D	1047	10	1.33	1.37	0.04
CRD	57	2	0.08	0.08	0.02
3		TOTAL	64.01	64.82	

#

POINT 21 ( 6)

CR 73 SI 53728 NR 2411 FE 185 BC 12927

SIDE	53728	664	85.46	86.52	0.39
FED	185	3	0.57	0.58	0.06
NR2D	2411	23	3.25	3.25	0.07
CRD	73	2	0.12	0.12	0.02
3		TOTAL	89.40	90.48	

#RVE

SIDE	81.48	10.00			
FED	1.08	0.58			
NR2D	2.58	1.01			
CRD	0.10	0.01			
3		TOTAL	85.24		

*Orla #3*

#

POINT 22 ( 1)

CR 42 SI 52005 NR 479 FE 680 BC 12927

SIDE	52005	643	82.71	83.36	0.38
FED	688	14	2.66	2.70	0.11
NR2D	479	4	0.53	0.55	0.03
CRD	42	1	0.04	0.04	0.01
3		TOTAL	85.95	86.66	

#

POINT 23 ( 2)

CR 46 SI 54687 NR 827 FE 601 BC 12931

SIDE	54687	676	86.96	87.70	0.40
FED	601	12	2.30	2.34	0.10
NR2D	827	8	1.02	1.05	0.04
CRD	46	1	0.05	0.05	0.01
3		TOTAL	90.34	91.14	

#

POINT 24 ( 3)

CR 47 SI 50821 NR 1676 FE 769 BC 12927

SIDE	50821	628	80.83	82.02	0.39
FED	769	16	3.00	3.04	0.12
NR2D	1676	16	2.22	2.28	0.05
CRD	47	1	0.05	0.06	0.01
3		TOTAL	86.10	87.40	

FED	769	16	3.00	3.04	0.12
NR2D	1676	16	2.22	2.28	0.05
CRD	47	1	0.05	0.06	0.01
TOTAL			86.10	87.40	

POINT 25 ( 4)  
 CR 50 SI 45372 NR 1489 FE 1206 BC 12110

SIDE	45372	560	72.08	73.48	0.36
FED	1206	25	4.81	4.87	0.15
NR2D	1489	14	1.95	2.06	0.05
CRD	50	1	0.06	0.06	0.01
TOTAL			78.91	80.47	

POINT 26 ( 5)  
 CR 48 SI 48644 NR 474 FE 1361 BC 11900

SIDE	48644	601	77.29	78.41	0.37
FED	1361	28	5.46	5.52	0.16
NR2D	474	4	0.52	0.56	0.03
CRD	48	1	0.06	0.06	0.01
TOTAL			83.33	84.54	

POINT 27 ( 6)  
 CR 63 SI 43692 NR 3636 FE 874 BC 12833

SIDE	43692	540	69.44	71.38	0.35
FED	874	18	3.44	3.48	0.12
NR2D	3636	35	4.98	5.12	0.09
CRD	63	2	0.09	0.10	0.02
TOTAL			77.95	80.08	

#RVE

SIDE	79.39	6.19	SF
FED	3.66	1.26	
NR2D	1.94	1.72	
CRD	0.06	0.01	
TOTAL	85.05		

#

#4



N

